An Observational Review of Submarine Hydrothermal System Geochemistry and an Evaluation of Vented Products as an Unconventional Mineral Resource

Michael Anthony Metford Saunders

Abstract:

In the context of reducing the environmental impact of the exploration of submarine hydrothermal systems – this work evaluates the observed relationships between element abundances in hydrothermal fluids; chimneys; deposit surfaces; and core sections. This is conducted for up to 31 elements, including ‘critical metals’, across a meta-analysis of 26 submarine hydrothermal systems distributed globally.

The work also revaluates the mechanism of copper enrichment in submarine hydrothermal systems between 50 and 200°C; and investigates hydrothermal fluids as an unconventional mineral resource in their own right.

CONTENTS **I**

List of Figures

Introduction:

Literature Review:

Meta-Analysis Section

Figure 41: Distribution of bromine average Chimney and Surface deposit abundance with fluid barium concentration. Chimney data (black) seem to follow the exponential curve (black line), $y = 0.0003e^{(0.0579x)}$, with an R^2 value of 0.9861.

The distribution of surface data (red) is less obvious. Following an exponential trend, $y = 0.0018e^{0.0305x}$, the R^2 value is 0.5151; however, a linear fit following y = 0.0003x, has a R^2 of 0.8864. Both lines of best fit are dashed red.

Figure 42: Distribution of calcium average Chimney, Core and Surface deposit abundance with fluid calcium concentration. Chimney data (black) is fit to the line y = 0.051x, with an R^2 value of 0.3693. Core data (blue) is fit to the line y = 0.084x, with an R^2 value of 0.6205. Surface data (red) is fit to the line y = 0.0184x, with an R^2 value of 0.5845.

Figure 43: Distribution of cadmium average Chimney and Surface deposit abundance with fluid cadmium concentration. Chimney data (black) is fit to the line y = 9.5313x, with an R^2 value of 0.557. No surface trend is observed.

Figure 44: Distribution of copper average Chimney, Core and Surface deposit abundance with fluid copper concentration. Chimney data (black) is fit to the line y = 6.7573x, with an R^2 value of 0.1451. Identifying Beebe, the supercritical venting system, as a high fluid concentration anomaly – the trend indicated by the dashed line is increased to y = 41.108x, with an R^2 value of 0.3077.

No trends in Core or Surface data.

Figure 48: Distribution of iron average Chimney, Core and Surface deposit abundance with fluid iron concentration. Chimney data (black) is fit to the line y = 0.9146x, with an R^2 value of 0.6145. No trends in Core or Surface data

Figure 49: Distribution of Zinc average Chimney, Core and Surface deposit abundance with fluid iron concentration. Chimney data (black) is fit to the line y = 10.071x, with an R^2 value of 0.2524. Identifying Lucky Strike as an anomaly, the dashed line represents a reviewed relationship as y = 36.483x, with an R^2 value of 0.8168.

Experimental Section:

Figure 50: (A) Density Separation of Chalcopyrite, where regions **i** and **ii** have less than, and equal density to the sodium meta-tungstate respectively (B), and region **iii** is the chalcopyrite concentrate (C).

Figure 51: Cross section diagram of the autoclaves used for high temperature experiments.

Figure 52: (Left) Scanning Electron Microscopy image of reacted grain, showing spot (EBSD) analysis locations where potential copper uptake is observed. (Right) grain under optical microscopy (OM)

Figure 53: Highly reacted pyrrhotite grain in PO4 experiment, showing multiple successive reaction rims.

Figure 54: Interpretation of EBSD electron emission data from PO4 analysis: showing unaltered pyrrhotite; intermediate phases; chalcopyrite reference, without observed chalcopyrite; bornite reference with a cluster of observations; and two distinct minerals with higher copper concentrations.

Figure 55: SEM analyses on PO5 mineral product. Very fine mineralisation seen in strait of crescent of grain

Figure 56: PO6 (grain 1) mineral product shown under (left), Scanning Electron Microscope; and (right), Optical Microscopy

Figure 57: PO6 (grain 2) mineral product shown under (left), Scanning Electron Microscopy; and (right), Optical Microscopy

Figure 58: PO7 mineral product shown under (left), Scanning Electron Microscopy; and (right) Optical Microscopy

Figure 59: Interpretation of EBSD electron emission data from PO6 and PO7 analyses: showing intermediate phases; chalcopyrite reference, without observed chalcopyrite; bornite reference within a cluster of observations.

Figure 60: PO8 mineral product grain 1, shown under (left), Scanning Electron Microscopy; and (right) Optical Microscopy

Figure 61: PO8 mineral product grain 2, shown under (left), Scanning Electron Microscopy; and (right) Optical Microscopy

Figure 62: Interpretation of EBSD electron emission data from PO8 analyses: showing intermediate phases; chalcopyrite interpretation; a bornite reference within a cluster of observations, and at least two further observations.

Figure 63: PO9 mineral product, shown under (left), Scanning Electron Microscopy; and (right) Optical Microscopy

Figure 64: Interpretation of EBSD electron emission data from PO9 analyses: showing intermediate phases; chalcopyrite reference; a bornite reference, and two further observations.

Figure 65: PO10 mineral product grain 1, shown under (left), Scanning Electron Microscopy; and (right) Optical Microscopy

Figure 66: PO10 mineral product grain 2, shown under (left), Scanning Electron Microscopy; and (right) Optical Microscopy

Figure 67: PO10 mineral product grain 3, shown under (left), Scanning Electron Microscopy; and (right) Optical Microscopy

Figure 68: Interpretation of EBSD electron emission data from PO10 analyses: showing intermediate phases; chalcopyrite interpretations; bornite interpretations, and one further observation.

Figure 69: EBSD electron emission data from all pyrrhotite analyses: showing intermediate phases; chalcopyrite interpretations (orange dotted circle); bornite interpretations (purple dotted circle), and further observations.

Discussion:

Figure 70: Distribution of lithium concentration in hydrothermal fluids.

List of Tables

Literature Review

Meta-Analysis Section

Experimental Section

Discussion

INTRODUCTION

1.1.0 Defining This Work

This work considers ‘submarine hydrothermal vent products’ as the aqueous and/or particulate discharge from hydrothermal vents. In the eventuality that industry emerges to explore and exploit submarine hydrothermal deposits, can studying the vent products indicate the grade of the deposit? Or, even, could the vent products be worth exploiting in their own right?

To evaluate these questions, this research is divided into three sections.

First, a **literature review** will summarise the processes, which culminate in the mineralisation of ore material from hydrothermal solutions. Objectively, this section shall focus on how submarine hydrothermal deposits vary according to their host environment. These factors will include depth, temperature, tectonic setting, spreading rate, axial migration, *etc.*

A **meta-analysis** will then aim to produce and compare geochemical databases of *hydrothermal endmember fluids* and *submarine hydrothermal deposits,* with the latter as expanded from Hannington, *et al.,* (2004). The fluid and deposit geochemistry will be compared averaging over all high-temperature focused vent systems, where chemical data are identified. Analysis will seek trends in geochemistry with respect to host environment characteristics, as above.

Finally, an **experimental section** will evaluate the mineralisation of copper minerals: by reacting iron sulphide, with copper solutions at temperatures between 50 and 200°C. The aim of this section is to determine how copper ore minerals are produced in hydrothermal environments; and thus, to evaluate the mechanism of secondary copper enrichment. This will act as an analogy for ore enrichment and secondary processes, which will pose a challenge to resource estimation.

1.2.0 A 20th Century Discovery

The pivotal moment, which may have brought about an appreciation of submarine hydrothermal activity, was the unification of the theory of tectonic plates (Tanner, 1964). This drove a conquest to demonstrate a then-revolutionary theory. A 1977 expedition to the East Pacific Rise identified “tall, extremely irregular columnar edifices” with “open vents on top” (Fracheteau, et al., 1979; Corliss, et al., 1979). This, although far from the first instance of a hydrothermal vent discovery, was the first to be attributed to active plate tectonics (Corliss, et al., 1979).

While the coastal Panerea submarine vent system (Italy) was discovered as early as 1860 (Italiano & Nuccio, 1991), the revelation of submarine hydrothermal activity has largely occurred after the East Pacific Rise discovery. **Figure 1** shows the cumulative count of discoveries since 1950 (*since* Beaulieu, et al., 2013). A variable, sustained, increase in discovery frequency after Fracheteau, *et al.* (1979) is observed. A total of 707 systems have been identified at present by the InterRidge Vents Database (Version 3.4), although only 676 systems have discovery dates provided. (Beaulieu, et al., 2013)

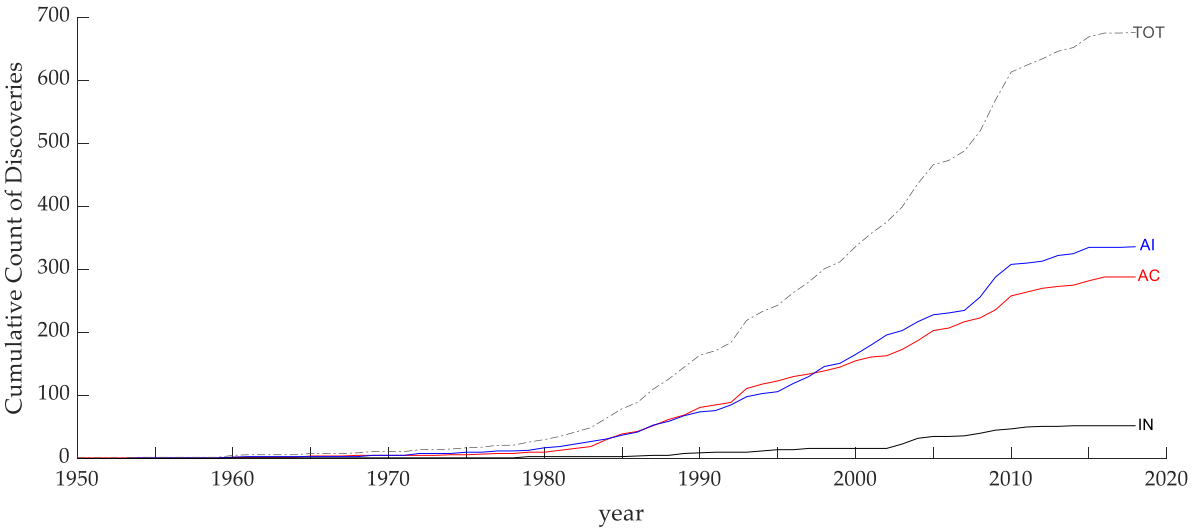

***Figure 3**: (blue) Active, inferred: (black) Inactive: (red) Active, Confirmed, (grey) Total. Graph of cumulative vent discoveries by year. (Beaulieu, et al., 2013)*

While it may be argued that recent advances in technology have enabled scientists to directly study these environments, their inaccessibility continues to breed an incomplete understanding, particularly in the case for inactive and/or off-axis deposits (Petersen, et al., 2016). Submarine hydrothermal systems are seen as a contemporary analouge to volcanogenic massive sulphides, where many camparisons have been drawn (Fallon, et al., 2017). However, pertainant insights and discoveries on how mineralisation occur continue to come to light (*eg.* Gartman, et al., 2018).

In the perspective of modern geology, submarine hydrothermal activity remains an exceptionally recent discovery.

1.3.0 A 21st Century Resource

Mining is an archaic practice: resources are physically and destructively removed from place, waste minerals are purged, and the desired resources are then enriched and liberated. Proposed methods for marine mining also follow this near-unchallenged trend: ore-rich mounds would be stripped, pulverised, pumped and processed (Frimanslund, 2016).

In the context of deep sea mining, this work reviews one of three prospective resources. Namely, submarine hydrothermal systems, as opposed to polymetallic nodules and ferromanganese crusts. Resource potential is highly reliant on the concentrations of target materials within these resources.

“Green Shift” is rapidly changing and pushing a range of target materials to become more economically important. In response, the European Union have identified ‘critical’ metals in five levels of supply chain risk for the current decade (Moss, et al., 2013).

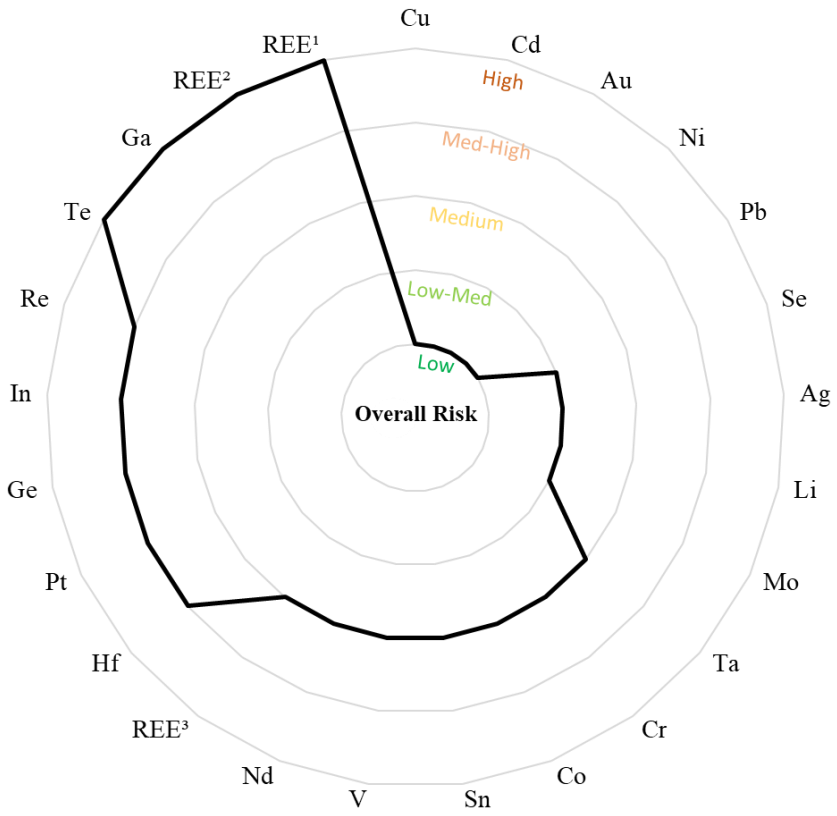

***Figure 4**: Criticality levels of metals proposed by the European Union. REE¹: Dy, Eu, Tb, Y. REE²: Pr. REE³: La, Ce, Sm, Gd (Moss, et al., 2013).*

The level of risk for each metal, see **Figure 2**, is assigned regarding four considerations: the geographic distribution of element concentration, where a high degree of inhomogeneity can cultivate a monopoly or an reliance on nations; the likelihood of constraints on supply; the political uncertainty of regions where said element is mined or processed; and the growth of demand for said element.

On a contemporary note, the COVID-19 pandemic, and the resultant impact on global supply chains highlights the vulnerabilities which are feared in global supply chain management.

As an example of how dynamic the threats are to these supply chains – consider the effect of the recent allied withdrawal from Afghanistan, where one of the world's largest Lithium deposits is now controlled by the Taliban (Horowitz, 2021); the Russian invasion of Ukraine (Josephs, 2022); or the developing diplomatic situation between China and the West regarding Taiwan (Brown, 2022).

Supply chain risks are mitigated by considering substitution options (reducing demand), moving towards a circular supply (reuse, recycling) and/or diversifying the primary supply of metals.

Notwithstanding these mitigations, supply chains will still require the primary production (mining) of a widening range of metals, if the global demand continues to grow (Hagelüken, et al., 2016).

To mine sustainably, globally, industry must strive toward ‘minimised responsible mining’. *i.e.,* where production is limited to fill the gap between demand and the supply satisfied by recycling. This involves mining selectively, exploring high grade, accessible deposits whilst minimising environmental and socio-political impacts (Jeswiet, 2017).

The submarine environment is increasing accessible, which unveils deep sea mineral deposits as potential contenders for new mines. Though, it must be strenuously noted: a good deposit does not necessarily prove to be a good mine (Grogan, 2019).

The geochemistry of the submarine hydrothermal systems will be compared with other prospective deep-sea resources in the discussion section of this work. This will pay particular attention to higher risk elements. However, even low risk materials - such as copper and gold - may become a concern in the coming decades.

Twenty million tonnes of copper were produced in 2017, for use across industry, construction, transport, electronics, and consumer products. Excluding submarine resources, 2100 million tonnes are within identified resources globally. Despite the rate of copper production growing by, on average, 3.2% per annum, it is highly improbable that copper will run out soon, as peak production is expected around 2040 (International Copper Study Group, 2018).

On the other hand, **Figure 3** shows average world copper grades have been falling since 2001, and as high-grade mines become exhausted, world averages will decrease further (Humphreys, 2013; Calvo, et al., 2016). A lower grade decreases the efficiency (per unit mass refined metal) of processing ore.

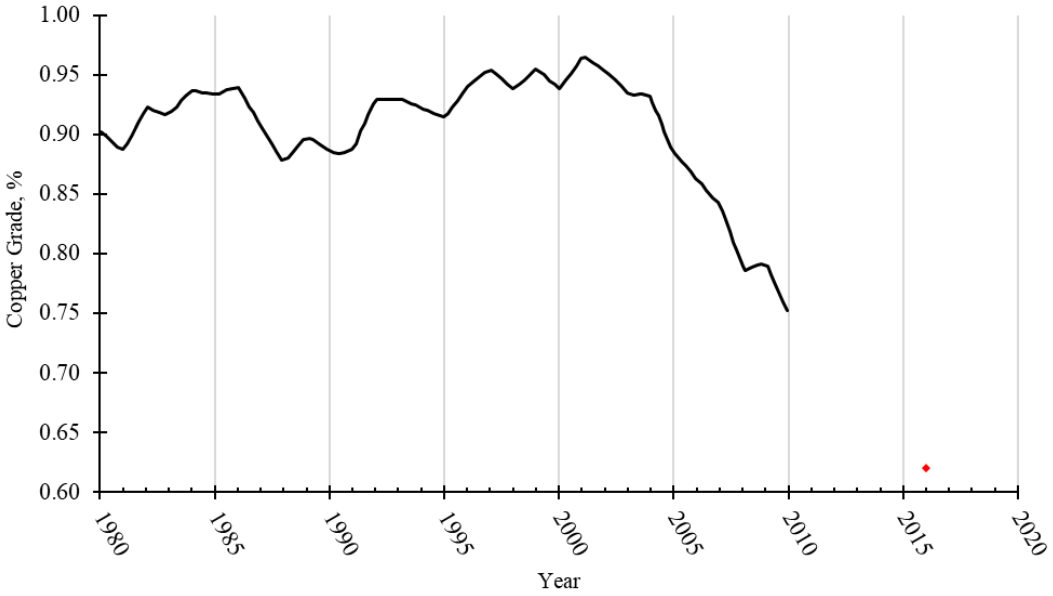

Figure 5: *Global average copper grade, %, between 1980 and 2010 (Humphreys, 2013) and 2016 datum given by red diamond (Calvo, et al., 2016)*

Where data are available, the average *active high temperature (>200°C)* submarine hydrothermal deposit copper grade is 5.52 ± 9.63% (n=26, *this work*). The most economic copper mines work kilometre-scaled supergene porphyry deposits, which only 'reach' up to 1-3% copper concentrations (Lee & Tang, 2020).

Hubbert modelling of gold production indicates that the global peak has occurred in the past decade. It is estimated that mining gold on land may not be feasible after 2030 (Sverdrup & Ragnarsdóttir, 2014).

Of the same hydrothermal deposits, the average gold grade is 3.96 ± 9.04 ppm (n=26, *this work*). If on land, this would be considered a very high grade (>2ppm) (Tetteh & Lartey, 2018). The global average mined ore grade on land was approximately four parts per million back in 2010 (Guirco, et al., 2010).

The median size of a submarine hydrothermal deposit is approximately 70,000 tonnes, as it stands, with about 1000 undiscovered systems predicted (Hannington, et al., 2011). This size is dwarfed by economic volcanogenic massive sulphides, which typically are 200,000 tonnes or larger (Galley, et al., 2007).

It is apparent from the standard deviations given for metal concentrations, that there is a high degree of geochemical variability between deposits. This work will show that there is also a high degree of geochemical variation within the whole system.

Understanding this is paramount in exploiting these environments sustainably. Selective mining could compliment growth in recycling, in the lead-up to a more sustainable, more circular economy.

It is reported that pilot operations have successfully taken place near Okinawa Prefecture, Japan (Ministry for Economy, Trade and Industry, 2017), in mining submarine hydrothermal deposits. This supports claims that current proposals are becoming possible.

Conversely, following the collapse of Nautilus Minerals (Nautilus Minerals, 2019), there have been government calls for a pacific-wide moratorium by Fiji and Papua New Guinea (Vari, 2019). This will inevitably be a sign of victory for the vehement opposition for deep sea mining.

In any case, every effort must be made to improve the collective understanding of the systems which produce these prospective resources, and influence metal abundances in adjacent deposits. This work focuses on submarine hydrothermal systems due to their dynamicity, and the inherent opportunities which that may present.

METHODOLGY

2.1.0 Literature Review Section

The term ‘submarine hydrothermal deposits/plumes/systems’ is used in this work: this is preferred to ‘seabed/seafloor massive sulphides/sulfides’, ‘polymetallic sulphides/sulphides, “black or white smokers”, *etc.* Each of these terms were used in research for this work, as it is recognised that results differ dependant on which nomenclature is used.

When introducing the fundamental science classical peer-reviewed papers or works are cited in the interest of accessibility. Approaching specific issues, recent focussed sources are used.

The foundation of the literature review is based on systems from the InterRidge Vents database 3.4 (Beaulieu, et al., 2013). This work takes an observational approach to illustrate how these systems work, and what factors influence the variability between hydrothermal systems.

2.2.0 Meta-Analysis Section

Data are sourced to evaluate how the geochemistry varies: within the hydrothermal system; how each stage is affected by the extrinsic conditions of the system (*i.e.,* depth, host geology, tectonic setting, *etc.*); and how each stage is affected by intrinsic conditions of the system (*i.e.,* temperature, phase change, *etc.*).

The InterRidge database contains 707 systems; 298 of which are confirmed active; 184 have a numerical reported temperature. This work is focussed on high temperature focussed venting. Therefore, a minimum threshold of 200°C for the ‘maximum or single reported temperature’ for the system venting temperature, was set. The number of systems which satisfy this criterion is 123.

Research then sought data for the fluid chemistry reported at these systems. After merging the entry for Logatchev I and II for ease of analysis, thirty-four were found to have even base metal fluid chemistry data. Deposit geochemistry data was then sought for these systems. Data was collated from an existing deposit geochemistry

database (Hannington, et al., 2004) and various other sources (see database). The number of systems with sufficient fluid and deposit chemistry is twenty-six.

This work recognises the paucity of data, having reduced known population of 707 systems to just 26. This low sample size will limit the works ability to infer characteristics for unanalysed systems

2.3.0 Experimental Section

The procedure of preparation and experiments are given in the proper place, within the experimental section. The procedures were designed to reconcile the results found by Rickard & Cowper (1994), whom used the McKibben & Barnes (1986) preperation methodology; and Pękala, *et al.,* (2011). Simplifications and substitutions of these methods are noted within the experimental section.

Intially, this work had intended to also run and compare experiments using Copper (I) solutions; to determine whether the same reaction mechanism was involved using Chalcopyrite and Bornite as reactants; and to analyse mineral products using elctron microprobe. All of these variables are disregarded due to the impact of the Coronavirus pandemic.

LITERATURE REVIEW

3.1.0 Hydrothermal Transport

Hydrothermal venting is an important mechanism in cooling the otherwise dynamic oceanic lithosphere. It is estimated that, in crust cooler than 600°C, hydrothermal activity transports heat eight times more efficiently than cooling by crustal conduction (Chen & Morgan, 1996). As a result, it is estimated that 30 to 60 billion tonnes of high temperature (modelled as 350°C) hydrothermal fluids are emitted each year around mid-ocean ridges alone (Elderfield & Schultz, 1996).

Analysis in this work finds that the variation in numerical vent temperature data, as it stands (Beaulieu, et al., 2013), is bimodal. This work conducted a t-test to demonstrate that two normal distributions exist. Where the distributions are taken as below and above 175°C, $t(177) \approx 1.654$, $p = 2.01 \times 10^{-71}$. This analysis demonstrates the temperature regimes are significantly different. The low temperature band (n=59) averages 67.5 ± 40.9°C; a high temperature band (n=120) average 312.3 ± 54.2°C.

The distribution of temperatures with depth is shown in **Figure 4**. This graph illustrates that incrementally higher temperature vents are limited to systems which are, themselves, incrementally deeper.

This graph is produced with ‘maximum or single reported temperature (°C)’ and ‘maximum or single reported depth (m)’ (Beaulieu, et al., 2013). Ambient Pressure is calculated using a simplified Stevin’s equation: $P = (\rho g h + P_{atm}) \times 10^{-6}$ (Macchia, 2016).

Where ‘*P’* is hydrostatic pressure [MPa]; ‘ρ’ is the density of seawater (~1025 kg m^{-3}); ‘*g*’ is acceleration due to gravity (9.81 m s^{-2}); ‘*h*’ is water depth (m) and ‘P_{atm}’ is atmospheric pressure [MPa]. For an estimation, pressure is found by multiplying depths (m) by 0.01 MPa m^{-1}.

Elevated ambient pressures prevent hydrothermal fluids from boiling, this increases the capacity and the efficiency of fluids to transport heat. The increase in the transport of solutes from the deep crust, depending on their properties, is the consequence of this (Monecke, et al., 2014).

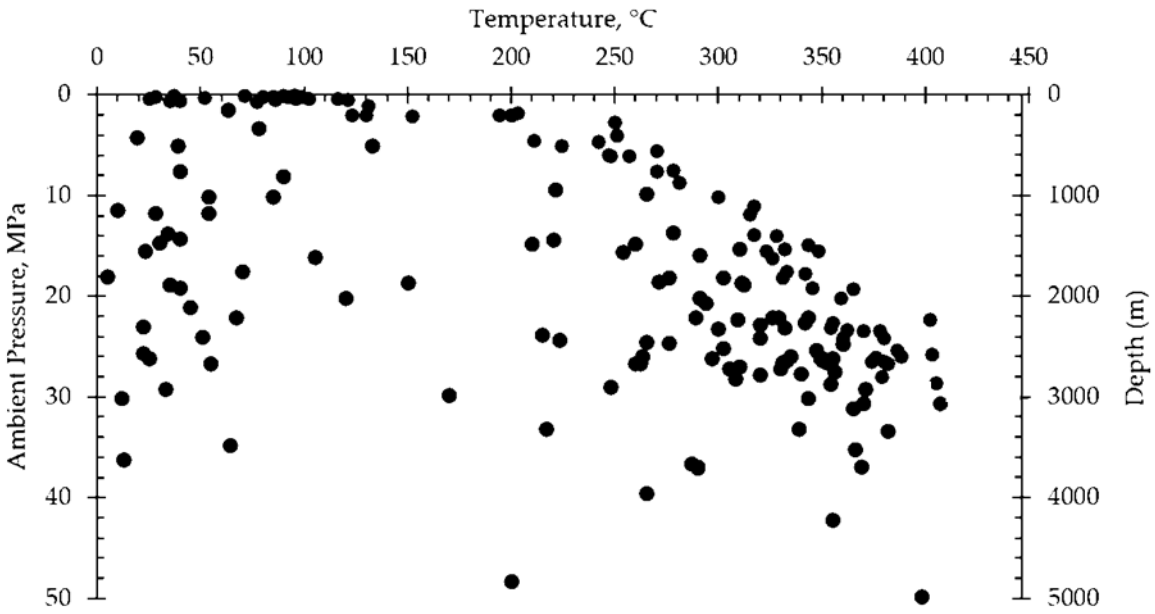

***Figure 4**: Temperature-Depth distribution of hydrothermal vents, illustrating higher temperature venting can only occur in deeper systems. Data extracted from Beaulieu, et. al. (2013)*

3.2.0 Tectonic Settings of Hydrothermal Systems

The depth distribution of submarine hydrothermal systems is multimodal. As apparent in **Figure 5**, where 'confirmed active', 'inferred active' and 'inactive' systems are presented (Beaulieu, et al., 2013). This is consistent with the data representing a range of tectonic settings. Although only 22% of Mid-Ocean Ridges (MOR), and 11% and Back-Arc Spreading Centres (BASC), have been surveyed (Beaulieu, et al., 2015).

The most notable outlier overall is the number of confirmed active systems in the shallowest hundred metres, where 59% of the vents are listed as associated with arc volcanism in coastal settings (Beaulieu, et al., 2013).

A t-test indicates hydrothermal systems associated to arc volcanism (Beaulieu, et al., 2013) exist at two statistically significantly different depth ranges. Where "deep arc hosted systems" are equal to or greater than 600 metres below sea level (mbsl.), and "shallow arc hosted systems" are less than 600 mbsl., $t(147) \approx 16.58$, $p = 5.94 \times 10^{-34}$.

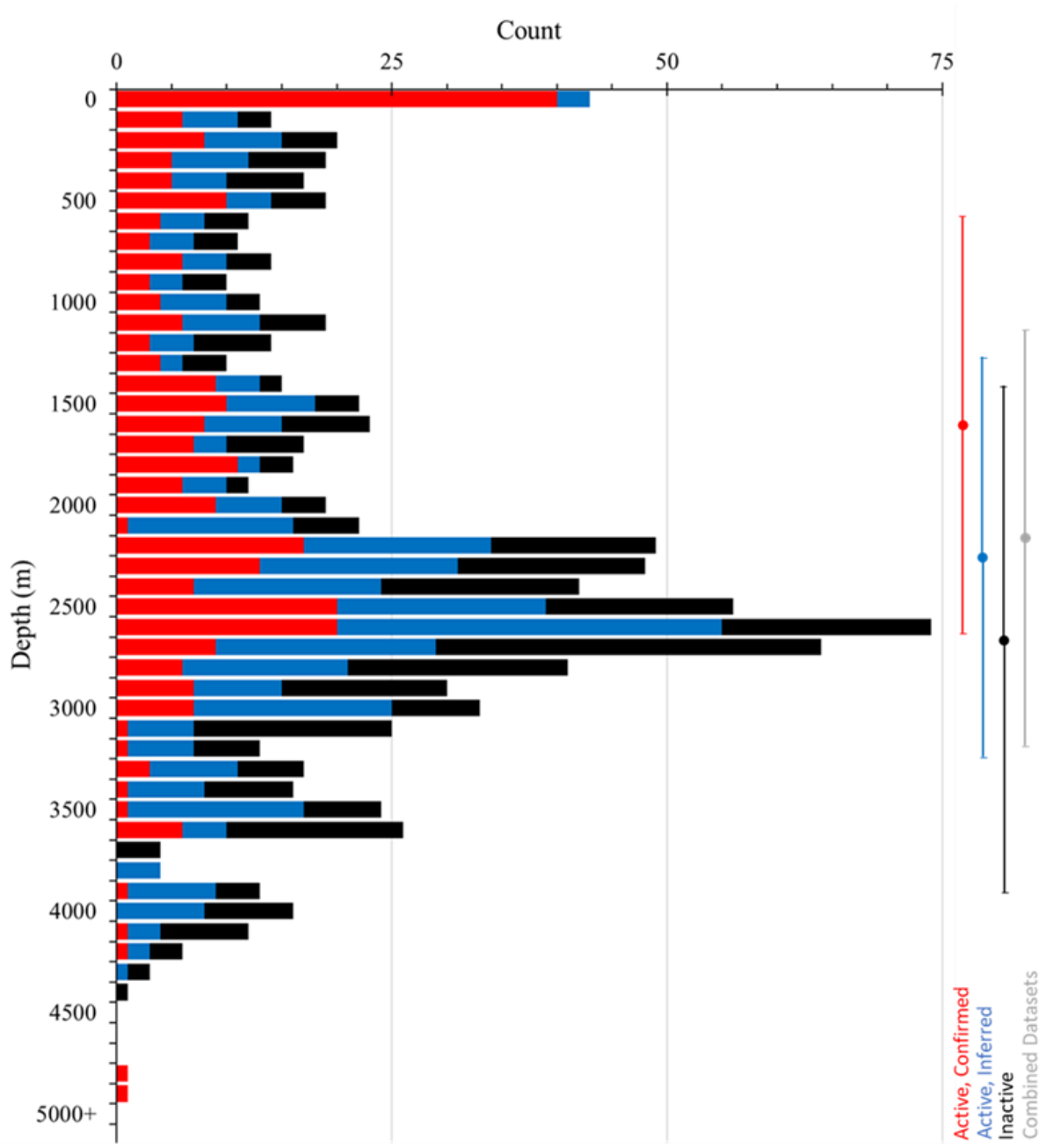

***Figure 5**: Depth frequency distribution of hydrothermal systems. Data extracted from Beaulieu, et. al. (2013)*

Table 1 collates data collectively, broken down into activity (Active Confirmed, AC; Active Inferred, AI; and Inactive, IN), and by tectonic settings (Mid-Ocean Ridge, MOR; Back-Arc Spreading Centre, BASC; Deep Arc Hosted, DAH; Shallow Arc Hosted, SAH; and Intra-Plate Volcanoes, IPV.) (Beaulieu, et al., 2013).

Table 4: *Depth analysis of hydrothermal systems, classified by their tectonic setting and activity. Data extracted from Beaulieu, et. al. (2013).*

Tectonic Setting	Activity	Count	Mean Depth (m)	Standard Deviation (m)	Skew
All	All	703	2100.15	1128.59	-0.193
All	AC	297	1676.25	1111.35	-0.008
All	AI	352	2359.33	989.54	-0.546
All	IN	54	2734.36	1275.91	+0.271
MOR	All	399	2662.39	805.48	-0.460
MOR	AC	132	2356.86	802.33	-0.736
MOR	AI	230	2801.03	707.41	-0.596
MOR	IN	37	2890.54	1062.31	+0.155
BASC	All	138	2055.36	880.96	+0.591
BASC	AC	66	1832.71	873.09	+0.048
BASC	AI	63	2137.46	665.08	-0.061
BASC	IN	9	3113.33	1395.56	+1.214
DAH	All	78	1294.50	540.43	+0.980
DAH	AC	46	1101.43	765.48	+0.474
DAH	AI	36	1277.86	503.50	+0.665
DAH	IN	6	1246.67	780.25	+1.544
SAH	All	71	214.44	187.86	+0.400
SAH	AC	48	178.85	194.68	+0.741
SAH	AI	22	292.73	153.27	-0.002
SAH	IN	1	200	nd	nd
IPV	All	8	1653.75	2056.92	+1.241
IPV	AC	6	1313.33	1790.19	+1.990
IPV	AI	1	350	nd	nd
IPV	IN	1	5000	nd	nd

Much of the interpretation of these data can be based on skew. If there were a bias due to shallower systems being easier to find, a positive skew would be expected, assuming the population fits a normal distribution. A positive skew is true for inactive deposits in every tectonic setting, and across the board for DAH and SAH systems. Thus, it can be suggested that the majority of undiscovered inactive, DAH and SAH systems are deeper than those already known.

Inferred Active MOR systems are negatively skewed. This may be symptomatic that it is more difficult to confirm the activity of deep systems. As naturally, when a systems is confirmed to be active, it changes category to ‘confirmed active’.

Though, confirmed Active MOR systems are negatively skewed to an even greater degree. The MOR depth averages are generally agreeable to the average depth of MOR crests at 2000-3000 mbsl. (Searle, 2013). Ultra-deep Mid-Ocean Ridges, such as the Mid-Cayman Rise do exist, and host systems such as Beebe (formerly known as Piccard) (Murton, et al., 2011). The negative skew may be a result of research being conducted more sparsely at the deeper ridges.

The various tectonic settings produce vent systems with different temperatures: MOR (n=82), 292.6 ± 106.4ºC; BASC (n=40), 261.0 ± 103.6ºC; DAH (n=23) 184.0 ± 125.1ºC; SAH (n=23) 135.8 ± 71.9ºC; IPV (n=5) 73.8 ± 74.9ºC (Beaulieu, et al., 2013). These data are not filtered into focused and diffuse flow.

This work discards IPV systems due to the paucity of identified systems, and notes that the temperature of fluids vented by these systems is below the 200°C threshold set in this work. This work also discards SAH systems due to low venting temperatures associated to these systems.

Only 13 Deep Arc Hosted systems remain after those which do not meet the 200ºC threshold are discarded. These will be briefly explored in *Geochemical Implications of Tectonic Setting*.

3.3.0 Systems at Spreading Centres

Back Arc Spreading Centres and Mid-Ocean Ridges are consequent of divergent tectonic processes. There is much variation in the spreading rate at divergent tectonic systems around the world. **Figure 6** shows how spreading rate affects the heat flux at Mid-Ocean Ridges (Chen & Morgan, 1996). This work assumes this trend also applies qualitatively to Back-Arc Spreading Centres.

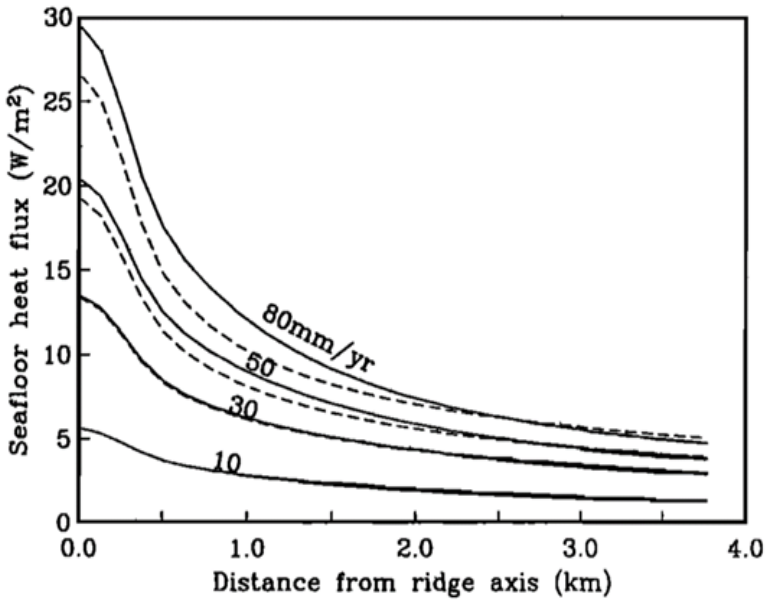

***Figure 6**: Seafloor heat flux models for spreading rates of 10-, 30-, 50- and 80-mm a^{-1}: showing a greater heat flux for more rapid spreading centres. Line style not relevant. (Chen & Morgan, 1996).*

Given that seafloor heat flux is proportional to spreading rate at the spreading axis, it can be expected that either: (a) the density of hydrothermal systems will be proportional to spreading rate, or (b) venting temperatures will be proportional to spreading rate.

(a) Globally, the spacing between hydrothermal deposits on Mid-Ocean Ridges is observed to be lower at *Fast-Intermediate spreading rates (Hannington, et al., 2011). This is corroborated on a regional scale, where observations suggest there is a higher density of venting occurring on the highest spreading rate section of the Mariana BASC (Baker, et al., 2017).

(b) The variation in the ratio of system **V**enting temperature to 'system **B**oiling temperature' (V:B Temperature Ratio), against the spreading rate is presented in **Figure 7**. Neither BASC or MOR V:B temperature ratios significantly correlate with spreading rate, having correlation coefficients of -0.078 and -0.002 respectively.

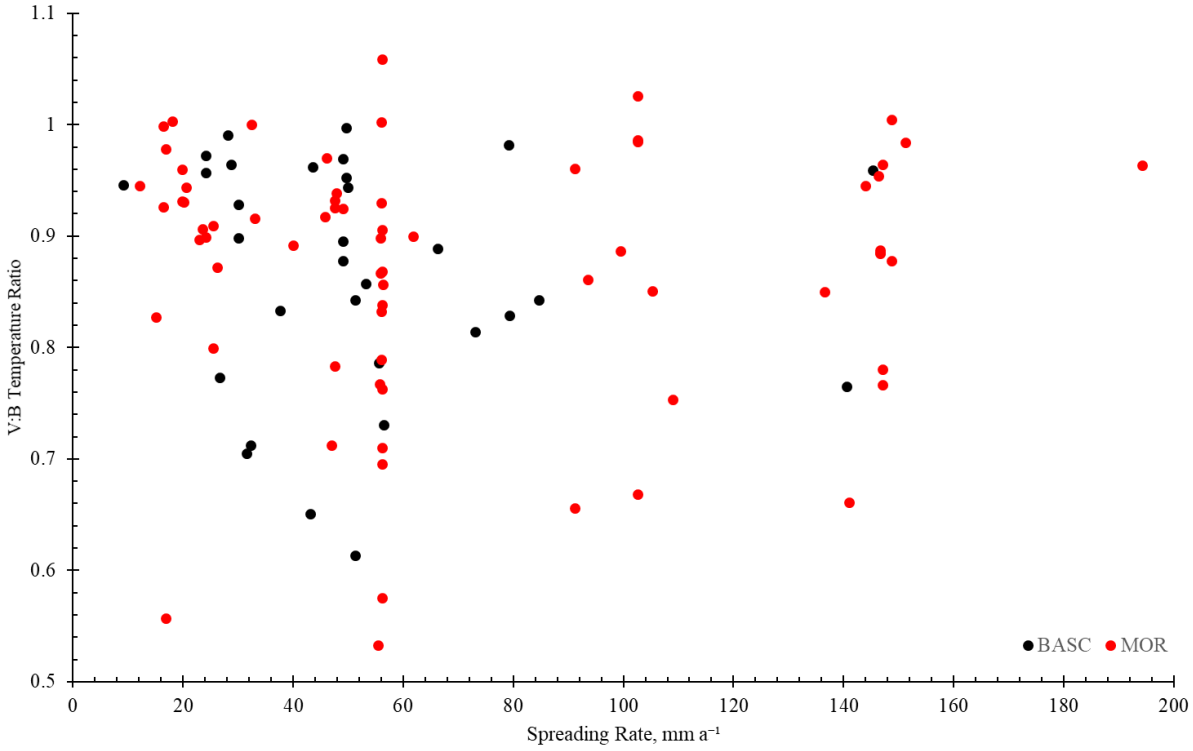

***Figure 7**: Distribution of V:B Temperature Ratio with respect to Spreading Rate, mm a^{-1}. No significant trends are observed. Data extracted from Beaulieu, et. al. (2013)*

The system boiling temperature, T_b, is the temperature hydrothermal fluids would boil, calculated from the depth of the system. This is achieved by estimating the ambient hydrostatic pressure (P, in *Hydrothermal Transport*), and applying hydrostatic pressure to the phase boundary curve equation (Engineering Toolbox, 2005): $T_{boil} = 178.59 \times P^{0.2432}$.

Where the V:B ratio is less than one, hydrothermal fluids will start boil on their ascent through the crust. Where the V:B ratio is greater than or equal to 1, fluids will boil in the water column, unless they are supercritical. The supercritical region is defined by the critical point, taken as 407ºC at 29.85 MPa for seawater (Bischoff & Rosenbauer, 1988). In other works, the critical point of pure water might be used, taken as 373.946ºC at 22.064MPa. (The International Association for the Properties of Water and Steam, 2007).

**Spreading Rate categories are given as: Ultra-slow, <20 mm a^{-1}; Slow, 20-50 mm a^{-1};*

Intermediate, 50-90 mm a^{-1}; Fast, 90-130 mm a^{-1}; Superfast, >130-150 mm a^{-1} (Searle, 2013).

The V:B temperature ratio is used to demonstrate that the temperature of venting is limited by the phase boundary, which is determined by the physical properties of the fluid. As the boiling point is approached, a greater quantity of energy is required to achieve each incremental unit of temperature, as energy is stored as ‘latent heat’. Latent heat is the quantity of heat communicated to a body without changing its temperature, contributing to the required energy to change the phase of the body (Maxwell, 1902). Therefore, temperature; “sensible heat” alone, is not a reliable measure of a systems energy.

The V:B temperature ratio distribution is almost indistinguishable between these tectonic systems: BASC, 0.870 ± 0.107 (-0.766); MOR, 0.872 ± 0.114 (-1.123). Both distributions are strongly negatively skewed, suggesting more vents at their maximum output have been discovered, than an average vent.

Referring back to **Figure 6**, this work would interpret the strong negative skew as, that most of the discovered systems are on the ridge axis. As systems migrate off-axis, heat flux is reduced, therefore the vent systems produce cooler vent fluids. Data with lower V:B temperature ratios may represent, variably off-axis systems.

It is perceivably inevitable that as vents drift away from the axis, they gradually cease to remain active: no more venting; no more growth. That they become to exist, only at the mercy of the ocean. Ancient Volcanogenic Massive Sulphides (VMS) are evidence that some must be preserved, but those processes remain obscure. Until recently, the sole means to find terminal or extinct systems was by visual observation: and this has often been entirely by chance (*e.g.* Cherkashev, et al., 2013).

Proximity to the ridge axis might be why there is a wider distribution of V:B datapoints (which only represent active systems) in slower spreading settings, because they were more likely to be identified when exploring the spreading axis. Also, as slower spreading rates although systems to spend a longer time on axis, they are likely to be larger than those at fast spreading centres (Hannington, et al., 2011).

3.4.0 Geochemical Implications of Tectonic Settings

This subsection compares three vent deposits created under similar conditions: at DAH, BASC and MOR settings. The following descriptions are extracted from Beaulieu, *et. al.* (2013). The major trace elements found in these deposits are collated in **Table 2** (Hannington, et al., 2004; Evans, et al., 2017).

Brothers Volcano (Kermadec Arc) represents DAH systems, at a depth of 1800 mbsl., venting temperatures are observed at 302ºC: a V:B ratio of 0.84. The host rock is described as Island-Arc Basalt (IAB), with minor Back-Arc Basin Basalt (BABB) and medium-potassium andesite.

Tu'i Malila (Lau Basin) represents BASC systems, in 1870 mbsl., venting temperatures are observed at 312ºC: a V:B ratio of 0.86. The spreading rate is 53.2 mm a^{-1}. The host rock is described as andesitic.

Magic Mountain (Explorer Ridge) represents MOR systems, in 1850 mbsl., venting temperatures are observed at 311ºC: a V:B ratio of 0.86. The spreading rate is 56.3 mm a^{-1}. The host rock is described as Normal- and Enhanced Mid-Ocean Ridge Basalt (N + EMORB).

***Table 5**: Comparison of Major trace elements found in a DAH, BASC and MOR hosted deposits. Data extracted from Hannington, et. al., (2004) and Evans, et. al., (2017). Z-Scores are calculated from the average element concentrations in Hannington, et. al. (2004) for BASC and MOR systems respectively.*

	Brothers Volcano (DAH)			Tu'i Malila (BASC)			Magic Mountain (MOR)		
	Mean	± St. Dev.	*Z Score	Mean	± St. Dev.	*Z Score	Mean	± St. Dev.	*Z Score
Cu (wt. %)	5.5	8.2	-	0.4	0.4	-0.43	5.4	7.0	+0.03
Fe (wt. %)	7.4	9.9	-	4.2	2.7	-0.80	30.4	11.3	+0.22
Zn (wt. %)	27.6	18.4	-	15.7	13.1	+0.06	1.5	1.5	-0.39
Pb (wt. %)	0.25	0.47	-	0.3	0.4	-0.25	0.12	0.24	-0.04
S (wt. %)	27.4	5.7	-	15.4	8.2	-0.61	26.2	12.4	-0.45
Reference	(Hannington, *et, al.,* 2004)			(Evans, *et. al* ., 2017)			(Hannington, *et, al.,* 2004)		
pH	4 - 7			4.51	0.52	+0.72	*Not Reported*		
Reference	(de Ronde, *et. al.,* 2005)			(Evans, *et. al* ., 2017)			-		

If the *Magic Mountain* hydrothermal vents emit fluids of similar pH to *Brothers Volcano* and *Tu'i Malila*: the hydrothermal transport of elements would not substantially differ. The variation in the deposit chemistry, therefore, would solely be influenced by the composition of deep host rock. Which is, indeed, the source of the elements which are hydrothermally transported. The host rock is known to vary in different tectonic settings, owed to the melting and differentiation of various magma types.

This work will later evaluate host geology as a factor in fluid chemistry, as would be a more direct relationship, in the meta-analysis section. This section continues only in identifying the tectonic setting as a factor of host petrology.

Divergent MORs are one extreme, *vis-à-vis* with convergent arc settings at the other. The former is a manifestation of upper mantle input, resulting in a young distinctly mafic (Fe, Mn rich; SiO_2 poor) seafloor. The latter, a result of subduction; remelting; mixing; and differentiation. Compared to *Magic Mountain, Brothers Volcano* is proportionally iron poor, as magma has been iteratively depleted in ferric elements. Back-Arc Spreading Centres are offset divergent boundaries driven by mass transport at these subduction zones. Therefore, BASCs can blur these distinct petrologies.

The nature of BASCs is indicated by the drop in sulphur concentration observed between *Tu'i Malila* and *Magic Mountain*. This drop is representative of data averaged across all deposit geochemistry data (Hannington, et al., 2004): MOR, 32.35 ± 13.68 wt.%; BASC, 23.64 ± 13.52 wt.%. Ultimately, the source of this difference may ultimately be due to natural fractionation in the mantle.

Whilst MORs are fed by the upper mantle, which was estimated contained 390 parts per million of sulphur in its primitive stage (Schmitt, et al., 1989): BASCs may be sourced by deeper portions of the mantle, with an estimated average of 300 parts per million (von Gehlen, 1993). Deeper portions of the mantle are suggested to be introduced by subduction-driven convection, illustrated in **Figure 8**.

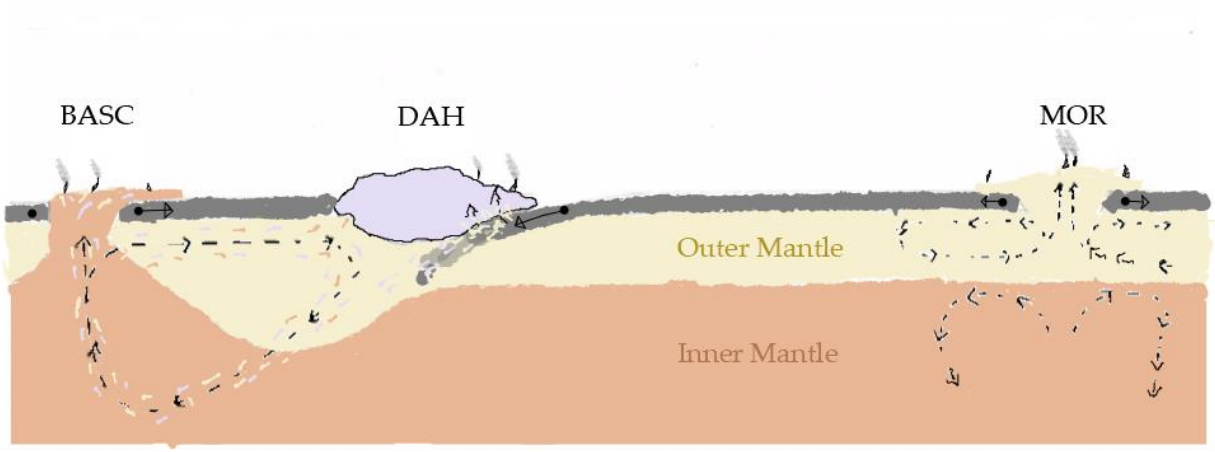

Figure 8**:** *Diagram comparing MOR, DAH and BASC tectonic settings, showing their magmatic input (illustrated by black arrows). The direction of tectonic plate movement is indicated by grey arrows with a ring at their tail. Asymmetric rifting at BASCs is indicated by having no arrow to the left of the rift. A similar schematic can be found in Ridley (2012). Not drawn to scale. (Ridley, 2012)*

Determining the composition and the inhomogeneity of the mantle cannot be done directly, estimates are drawn by studying “the right mix” of rocks. This involves a multitude of assumptions. As sulphur is a low-density element, it would be logical to assume that sulphur remains more concentrated in the uppermost regions.

The convection cell formed by subduction (Forsyth & Uyeda, 1975), as depicted in **Figure 8**, may circulate magma consisting of petrology from the MOR (outer mantle input), the plate superposing subduction, and an inner mantle input. Although, mantle mixing is not limited to BASCs.

Iceland is formed by a mantle plume beneath the Northern Mid-Atlantic Ridge. Geochemical analyses of the Reykjanes Ridge (Webber, et al., 2013), which extends southwest from Iceland, finds that chalcophilic elements (affinity to sulphur) are replaced by siderophilic elements (affinity to iron).

Gold, in the absence of sulphur, is very siderophilic (Goldschmidt, 1937): on Reykjanes Ridge, gold concentration increases exponentially with latitude, a result of mixing due to the mantle plume (Webber, et al., 2013). Average gold concentration is also much higher in BASC hosted systems, at 6702 ± 10891 ppb: compared to MOR hosted systems at 1306 ± 3859 ppb (Hannington, et al., 2011).

The extremely high standard deviation of gold concentration at BASCs is product of wide range of geology in these systems. *Tu'i Malila's* andesitic geology is most likely due to the melting and significant incorporation of a silicic rock from the Tonga plate.

There will be further analysis of tectonic setting and host geology in the Meta-Analysis section of this work. This is henceforth limited to BASC and MOR settings, due to the paucity of chemical data found for DAH systems.

3.5.0 Geochemical Implications of Fluid Properties

So far, this work has highlighted how hydrothermal deposit chemistry is limited by the availability of the minerals in the deep crust, but it has only *introduced* how elements are transported through the crust, to the deposit. Transport varies depending on the how ore minerals behave in hydrothermal fluids.

Take for example, that copper mineralisation is generally limited to systems at depths greater than a kilometre (Hannington, et al., 2011). This is a result of the temperature dependence of copper mineral solubility. **Figure 9** shows that copper minerals (highlighted) reach their peak solubility in the region above 300°C (Reed & Palandri, 2006). The calculation of boiling temperature (**in *Systems at Divergent Tectonic Settings***) a kilometre depth permits the boiling temperature to reach 312.65°C.

Solubility trends can be described by the solubility product constant, *K* (Rossotti & Rossotti, 1961). For the pure compound at saturation, $\Lambda_m\beta_n$, *K* is calculated as (Gresens, 1981): the concentration of the solvent is taken to equal one.

$K = [\Lambda]^m \cdot [\beta]^n$

The solubility of minerals gives rise to mineral zonation. Sketches of typical mineral zonation within a chimney and deposits are given in **Figure 10** and **Figure 11**, respectively.

The solubility product constant, *K,* expresses an equilibrium. When the concentration is less than the solubility constant, the saturation point, the net physical change is in the direction of dissolution. If the concentration is more than the saturation point, the net physical change is in the direction of precipitation. This net physical change brings the system back to the equilibrium point.

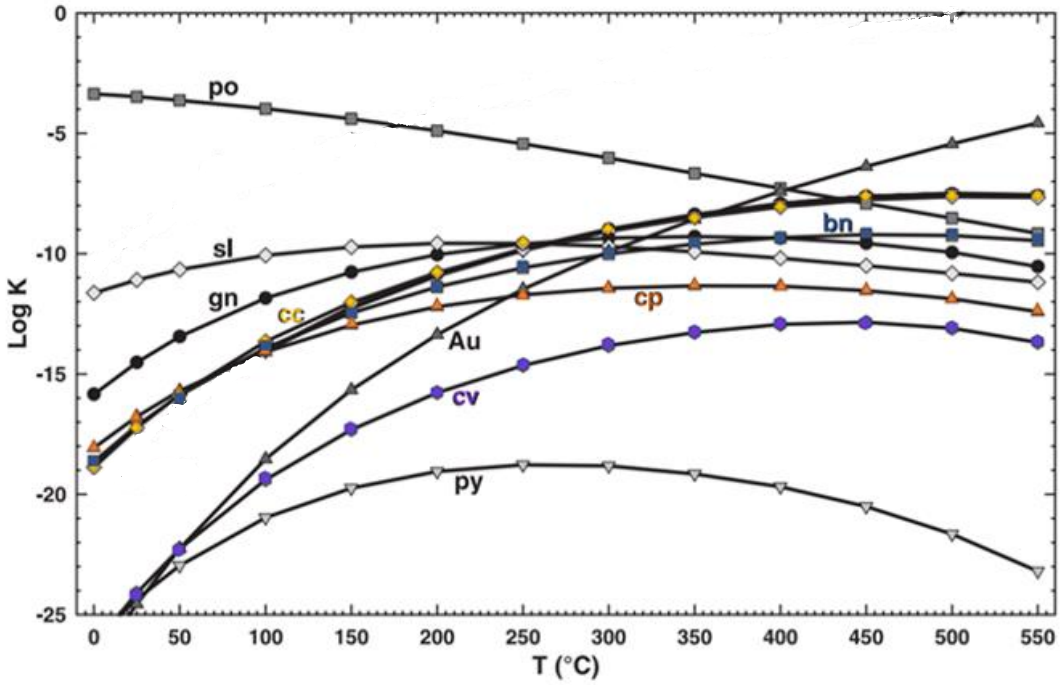

Figure 9*: Sulphide mineral dissolution log K vs. Temperature at 80 MPa. Log K's are normalized to a "per metal atom" basis by dividing log K by the number of metal atoms in the formula unit. Copper minerals (chalcocite (cc), chalcopyrite (cp), covellite (cv) and bornite (bn)) are highlighted. The remaining minerals are as follows: po, pyrrhotite; sl, sphalerite; gn, galena; Au, gold; py, pyrite.*
Adapted from Reed & Palandri, (2006)

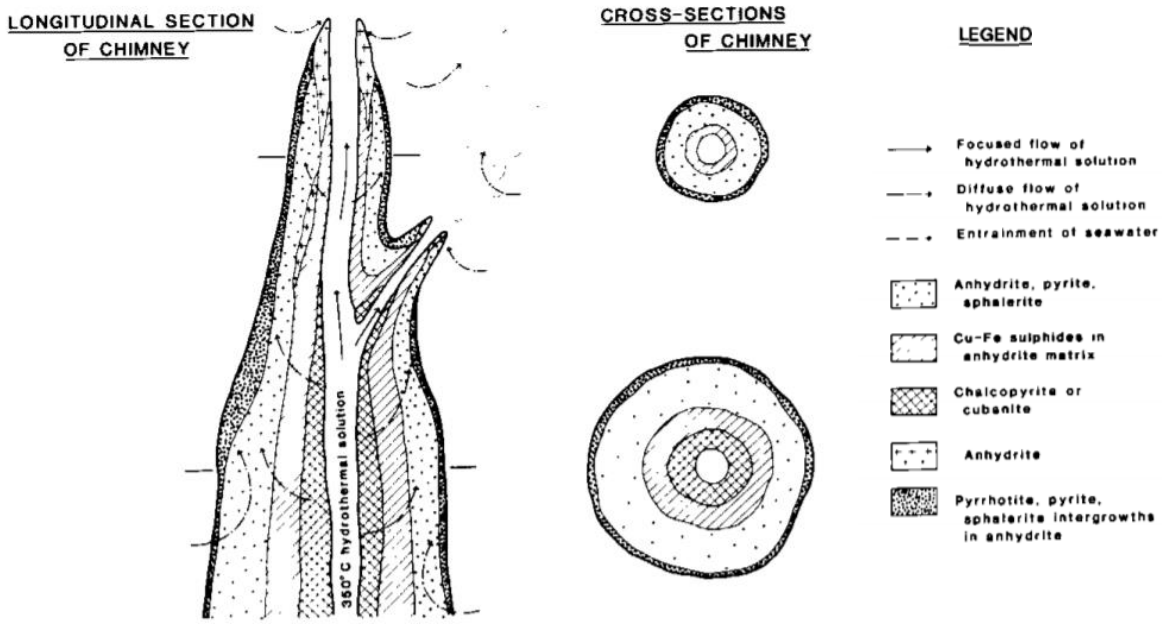

***Figure 10**: Typical mineral zonation pattern within hydrothermal vent chimneys. Adapted from Lyndon, (1988). Cited therein as after Haymon & Kastner, (1981); Haymon, (1983).*

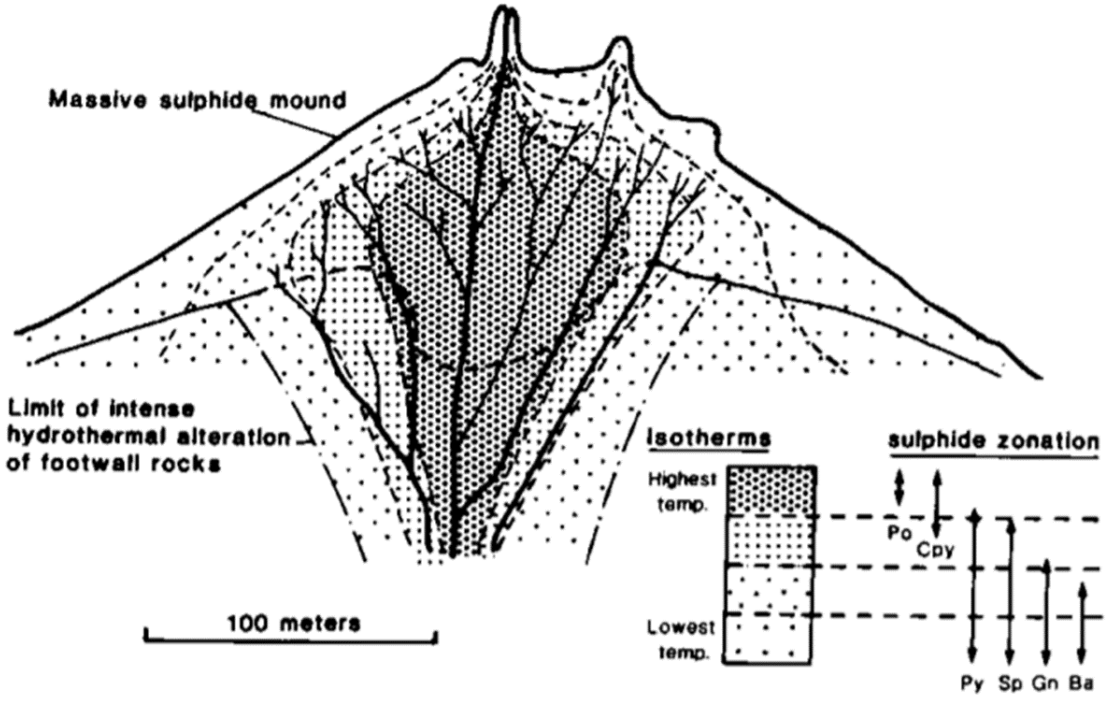

***Figure 11**: Idealised mineral zonation of a submarine hydrothermal deposit, showing a direct relationship between mineralisation and average maximum isotherms, assuming ore metals were dominantly present as chloride complexes. Po, pyrrhotite; Cpy, chalcopyrite; Py, pyrite; Sp, sphalerite; Gn, galena; Ba, baryte. (Lyndon, 1988)*

The distribution of minerals in **Figure 10** is understood to be formed by: the initial anhydrite structure forms, as it precipitates from seawater at the thermal interface (Haymon & Kastner, 1981; Haymon, 1983). This anhydrite forms a ‘collar’, which is indicated at the top of the longitudinal cross-section in **Figure 10** (Haymon, 1983).

This collar is partially porous, therefore a fraction (<1%) of the fluids seep through and rapidly precipitate in the pores of the structure. As the structure isolates the central conduit, the hydrothermal fluid remains at its high temperature, and continues to transport copper minerals: which precipitate on the inner margin of the conduit (Lyndon, 1988).

On a deposit scale, as in **Figure 11**, vents in the same system are shown to yield distinct mineralogies. The ‘ultra-deep’ Mid-Cayman Rise is host to a system venting supercritical 500°C fluids at *ca.* 5000 metres depth. Mineralisation is dominated by copper minerals at the centre of the sulphide mound, whilst peripheral chimneys are instead enriched in tin minerals (Murton, et al., 2011).

Although, the assumption given in **Figure 11** is a larger point of discussion.

There is a consensus that primary transport of metals in hydrothermal fluids occurs as chloride complexes (Xiao, et al., 1998; Fulton, et al., 2000; Liu, et al., 2001; Brugger, et al., 2007; Sherman, 2007; Schmidt, et al., 2018). However, in terms of deposits, secondary mineralisation may be more pertinent.

Drilling programs on the TAG submarine hydrothermal deposit find that upper few metres of the deposit have higher abundances of metals than the deeper stockwork (Humphris, et al., 1995). This follows the same, although upturned, processes that enrich supergene volcanogenic massive sulphides. In ancient land-based systems, surface water leaches minerals from the top of the deposit, and those fluids sink to the water table. In modern submarine hydrothermal deposits, seawater is entrained and circulated within the deposit: and minerals are deposited in the uppermost parts of the deposit. Minerals with very low solubilities are more resistant to remobilisation.

This means that the surface of the deposits cannot be representative of the entire vertical extent of deposit geochemistry. Nor, observing **Figure 11**, can the central vents represent the entire lateral extent of deposit geochemistry (Petersen, et al., 2018).

Enrichment processes will be discussed in greater depth during and after the **experimental section**.

It must be noted that the heterogeneity of concentrations within deposits is an enormous challenge in resource estimation; *and* in evaluating the relationship between deposit chemistry and fluid chemistry.

Indeed, the deposit geochemistry data (Hannington, et al., 2004) is vulnerable to the same biases, as they are analyses on samples consisting largely of chimney and grab samples.

3.6.0 Hydrothermal Venting

Breaching the surface, the hydrothermal discharge consists of the solution of metals yet to be precipitated and the passively mobile particles drawn up by fluids. The superheated fluid (>200°C) is thrown into thermodynamic and chemical disequilibria, as it interacts with the cold ambient seawater.

In the initial metre, hydrothermal fluids are cooled rapidly, causing the minerals in solution to precipitate. **Figure 12** shows the Clam Acres chimney at the 21°N EPR site, which emit fluids at temperatures of 346-355°C (Bemis, et al., 2002) and velocities of 1.03-2.14 metres per second (Converse, et al., 1984). Bemis *et. al.* (2002) observed the velocity of the vent to be one metre per second at the time of the photograph. The region above the vent orifice is clearly less attenuative close to the orifice.

***Figure 12**: Photograph of Clam Acres vent at 21°N EPR (20°49.8'N 109°06.2'W), showing precipitation of minerals above the orifice (Adapted from Bemis, et al., 2002).*

The North Tower vents at Grotto is like Clam Acres: vent temperatures are observed at 350-361°C, and focused velocities are observed at 1.0 to 1.5 metres per second (Rona, et al., 2015). Temperature profiles, in 2012 (blue) and 2014 (green), between six and eighteen metres above the vent both show a regular decay in temperature (Rona, et al., 2015): **Figure 13** extrapolates this decay to 350°C at the orifice with a fifth-degree polynomial. A similar model is used in Germanovich, *et. al.* (2015).

Following this trend: if ‘Mineral A’ is assumed to be negligibly soluble at 300°C, ‘Mineral A’ will have completely precipitated at *ca.* 36 centimetres above the orifice.

This, to some degree, is an oversimplification. Whilst a regular decrease in temperature may manifest in the centre of the plume, entrainment of seawater on the outer margins of the plume may cause more rapid cooling. The Gaussian coefficient of entrainment is defined by the ratio of the vertical upward velocity at the edge of the plume, to the vertical upward velocity of the centreline of the plume (Zhang, et al., 2019; Morton, et al., 1956; Turner, 1986).

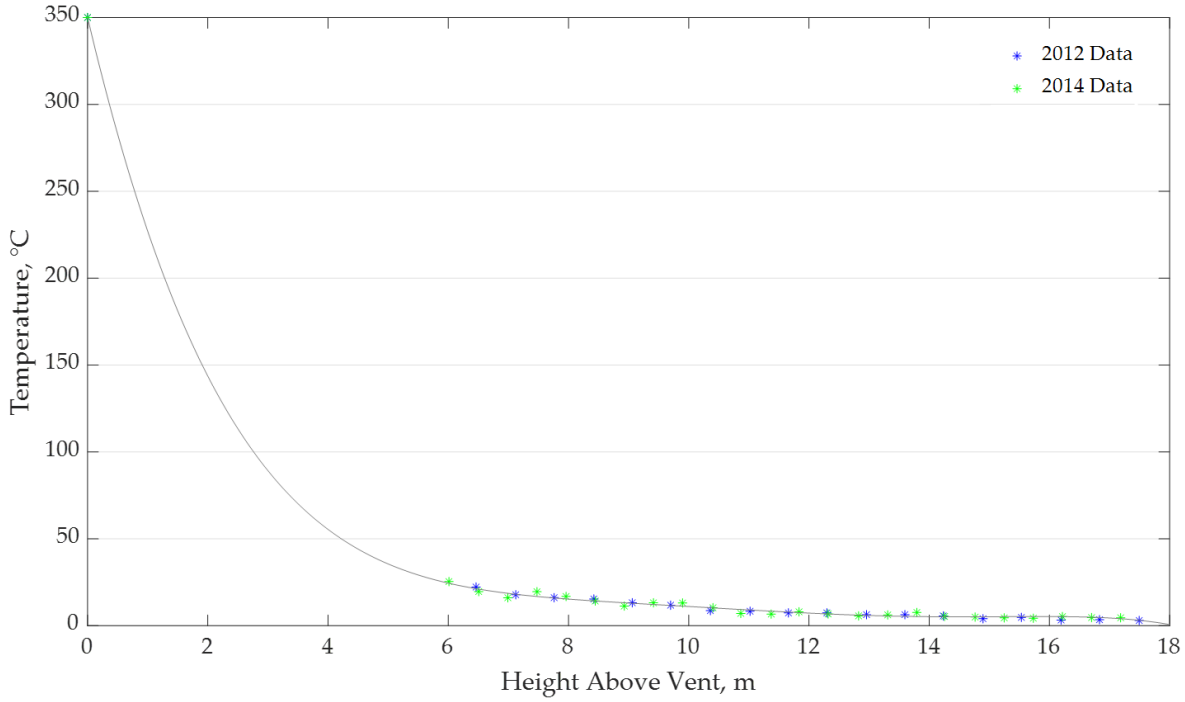

Figure 13: *Fifth degree polynomial model of temperature above the Grotto Vent. Fitting data of the orifice temperature and profile temperature from 2012 (blue) and 2014 (green) (Rona, et al., 2015).*

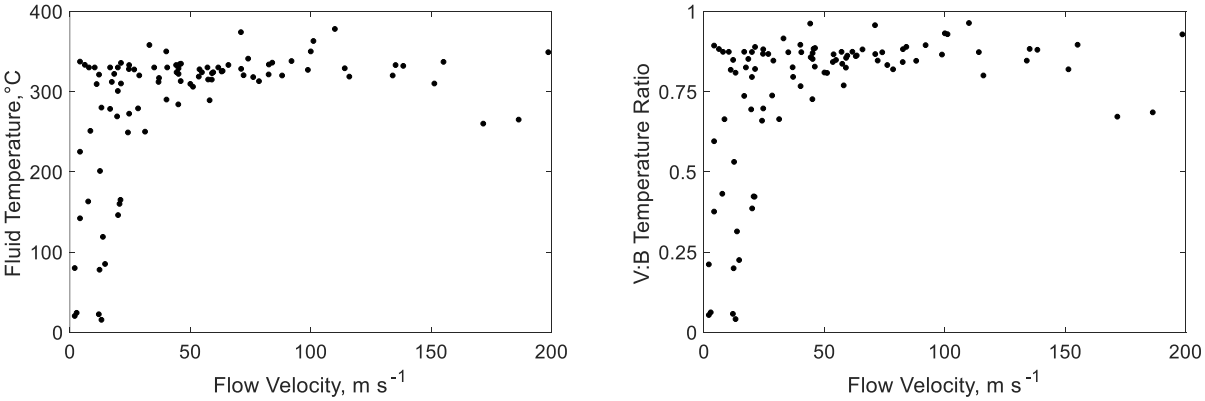

Figure 14*: (left) Scatter of temperatures and flow velocity measurements of focussed hydrothermal vents at Endeavour Field, Axial Seamount, Middle Valley, Lau Basin and East Pacific Rise. (right) Scatter of V:B ratios and flow velocity measurements of focussed hydrothermal vents at Endeavour Field, Axial Seamount, Middle Valley, Lau Basin and East Pacific Rise (Germanovich, et al., 2015).*

If it is assumed that focussed hydrothermal fluids initially behave like a jet (a source of momentum), it is easier to neglect the lesser influence of entrainment. Then, at a greater height, hydrothermal fluids would begin to behave like a plume (a source of buoyancy), which are affected more significantly by the entrainment of seawater (Turner, 1986).

Therefore, in predicting the height which minerals would initially precipitate, this work would only consider the endmember temperature of the vent fluids and the velocity of the vent fluids.

Figure 14 (left) is a scatter plot of temperatures and flow velocity measurements of focussed hydrothermal vents at the Endeavour Field, Axial Seamount, Middle Valley, Lau Basin and East Pacific Rise (Germanovich, et al., 2015).

The particles which form are typically sized between 0.500 – 100μm, as particles and agglomerates (Gartman, et al., 2019). The settling velocity for these particles are 7.72μm·s^{-1} and 0.14 m·s^{-1} for a 0.500μm cubic pyrite particle and a 100μm spherical pyrite agglomerate respectively (Saunders, *unpublished BSc dissertation, Bangor University*, 2018).

The positive buoyancy of hydrothermal plume lifts these particles into neutrally buoyant plumes. At the Rainbow Vent Field, considerable variation in particle concentration is observed. **Figure 15** plots how height relative to the vent relates to the percentage concentration anomaly, relative to each profile mean. Key: (dashed grey line) all metals listed; (purple solid line) REE, Rare Earth Elements; and (solid black line) SFM, major Sulphide Forming Metals (Cu, Fe and Zn). Data are extracted from Edmonds & German (2004).

Pronounced fluctuation around the mean is observed, in each group of metals selected. Consider dividing this vertical profile in three sections: as indicated by horizontal black dotted lines. The inferred distinction is determined by the adsorption of Rare Earth Elements.

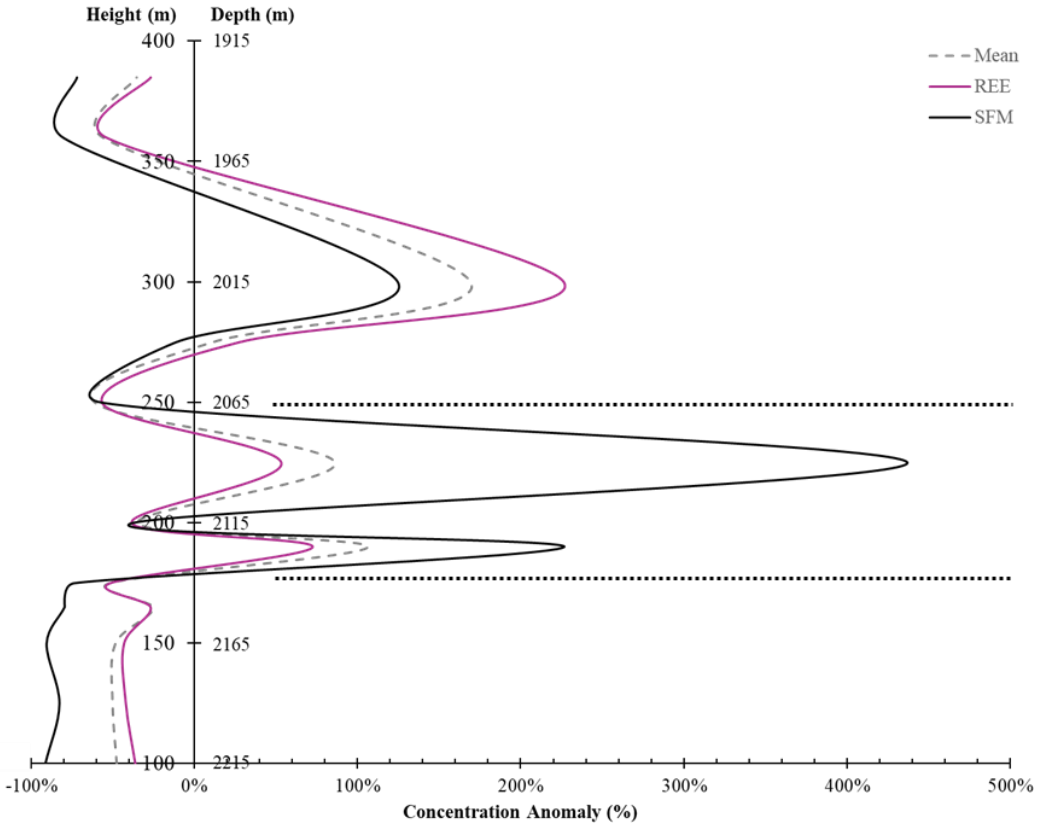

***Figure 15**: Concentration Anomaly of metals in hydrothermal vent precipitates, varying with height above Rainbow Vent, Mid-Atlantic Ridge (Edmonds & German, 2004).*

The section between 100 and 175 metres above the vent is interpreted as the positively buoyant section of the plume: turbulent mixing and interaction with seawater will favour oxidisation. Between 175 and 250 metres, the plume becomes neutrally buoyant: where a stable layer of high concentration SFM particles may be produced. Above 250 metres, tending to 350 metres above the vent, less-stable though neutrally buoyant fluids mix with oxidising seawater, promoting increased REE integration into precipitates.

At the 215 metres peak within the Rainbow plume, element concentrations are as follows: Fe, 9.3nmol·dm^{-3}; Co, 1.6pmol·dm^{-3}; Cu, 34.0pmol·dm^{-3}; Zn, 121pmol·dm^{-3}; Ag, 20fmol·dm^{-3}; REE (average), 410fmol·dm^{-3} (Edmonds & German, 2004). Therefore, roughly 463,000 Cubic metres of plume-water would have to be processed to produce just one gram of copper.

Out of intrigue, the thermal anomaly due to oxidation was calculated. The first stage of pyrite oxidisation is: $2FeS_2 + 7\ O_2 + 2\ H_2O = 2\ Fe^{2+} + 4\ H^+ + 4\ SO_4^{2-}$ (Rimstidt & Vaughan, 2003). The enthalpy change of this reaction is -147.70 $kJ \cdot mol^{-1}$ (Dos Santos, et al., 2016). Taking the concentration of iron as 9.3nM, the enthalpy change of the reaction is 1.37×10^{-6} kJ. Assuming the density and specific heat capacity of pure water, pyrite oxidation would increase the temperature of one cubic metre of water by only 3.26×10^{-7} °C.

This would assume, perhaps falsely, that the pyrite is completely chemically labile (Kleint, et al., 2016). A thermal anomaly like that of 0.08°C, in the Endeavour neutrally buoyant plume (Coogan, et al., 2017): is therefore far more likely to be attributed to remnant heat from the endmember fluid.

The ‘sink’ of hydrothermally derived particles is fallout. Less than two percent of the plume particles are deposited within the first 1.5 kilometres from the vent (Coogan, et al., 2017). However, it is apparent plume fallout occurs orderly, following the series “Cd > Ag > Cu > Co ~ Fe.” Coogan, *et. al.* (2017) suggests this is due to the metals’ relative reactivity to sulphides: citing similar sequences found in chimneys.

In summary, this literature review describes the nature of the three stages.

i. Vigorous hydrothermal transport draws dissolved minerals from the deep crust, where the least soluble minerals will precipitate and mineralise within the subsurface, forming deposits.
ii. A quantity of minerals will remain in solution and are vented into the ocean; rapid cooling causes precipitation into particles within the first metre.
iii. Particles are transported by buoyant fluids into the neutrally buoyant plume, a hundred-metre scaled nebula of dispersing particles.

The systemic geochemistry is controlled by the effectiveness of heat transport, and the chemical “budget” of the deep crust. The following section will describe the resulting proportions of geochemistry between these stages and extend on the variation observed between systems.

META-ANALYSIS SECTION

4.1.0 An Overview

This work has only identified twenty-six systems with both deposit and fluid chemistry data documented, these systems are listed in **Table 3.**

The sample systems have a temperature distribution of 348.0 ± 37.1°C (26) (Beaulieu, et al., 2013). This is analogous to the overall distribution of high temperature (>200°C) mid-ocean ridge and back-arc spreading centres: which is 325.6 ± 45.8°C (102) (Beaulieu, et al., 2013).

The depth distribution of sample systems is 2536.7 ± 870.1 metres (26) (Beaulieu, et al., 2013), which is also reasonably agreeable to the overall distribution (as above) of 2317.7 ± 811.8 metres (102) (Beaulieu, et al., 2013).

The V:B temperature ratio distribution of the sample systems is 0.901 ± 0.091 (26): which is also akin to the overall distribution, at 0.867 ± 0.114 (102) (Beaulieu, et al., 2013).

Therefore, in terms of hydrothermal transport, the sample systems are representative of hot systems overall: though, slightly skewed toward more energetic venting.

Table 6: *Systems with both fluid and deposit chemistry data identified, including the sources of data which are not included in the Hannington, et. al. (2004) deposit geochemistry database.*

Tectonic	Region	System Name	Fluid Chemistry Source(s)	[1]Deposit Chemistry Source(s)
MOR	Juan de Fuca Ridge	Main Endeavour Field	Seyfried Jr., et al., (2003)	-
		Axial Seamount	Butterfield, et al., (1990)	-
		North Cleft Segment	Butterfield & Massoth, (1994)	-
		Middle Valley	Butterfield, et al., (1994)	-
	Gulf of California	Guaymas Basin	Campbell, et al., (1988)	-
		Alarcon Rise, Meyibo	Paduan, et al., (2018)	Paduan, et al., (2018)
		Pescadero Basin, Auka	Paduan, et al., (2018)	Paduan, et al., (2018)
	East Pacific Rise	Rehu-Marka	Charlou, et al., (1996)	-
	Mid-Cayman Rise	Beebe ([2]*Piccard*)	McDermott, et al., (2018)	Webber, et al., (2015)
	Mid-Atlantic Ridge	Logatchev	Schmidt, et al., (2007); Schmidt, et al., (2011)	-
		TAG	Gamo, et al., (1996)	-
		Snake Pit	Edmond, et al., (1995)	-
		Broken Spur	James, et al., (1995)	-
		Rainbow	Seyfried, et al., (2011)	Marques, et al., (2007)
		Lucky Strike	Chavagnac, et al., (2018)	-
		Nibelungen	Schmidt, et al., (2011)	Petersen, (2012)
	South West Indian Ridge	Longqi	Ji, et al., (2017)	Tao, et al., (2014)
	Central Indian Ridge	Edmond Field	Gallant & Von Damm, (2006); Zeng, et al., (2015)	Cao, et al., (2016)
		Kairei	Gallant & Von Damm, (2006)	Wang, et al., (2014)
BASC	Okinawa Trough	Minami-Ensei Knoll	Kawagucci, (2014)	-
	East Scotia Ridge	E9	James, et al., (2014)	Fretzdorff, et al., (2002)
		E2	James, et al., (2014)	Fretzdorff, et al., (2002)
	Manus Basin	SuSu Knolls	Seewald, et al., (2019)	-
		Vienna Woods	Craddock, et al., (2010)	Ray, et al., (2018)
		PACMANUS	Bach, et. al., (2003)	-
	Lau Basin	Kulo Lasi	Konn, et. al., (2018)	Fouquet, et. al., (2018)

[1] Except sources cited in the Hannington, *et. al.*, (2004) database.

[2] The Beebe vent field was named Piccard by Connelly, *et. al.*, (2012) before visual confirmation.

4.2.0 Fluid Data

The following section summarises the concentrations of hydrothermal vent fluids, as **Table 4**.

Except for Rare Earth Elements, which are combined, this section will not analyse metals with less than fifteen datapoints. Elements are analysed in order with respect to the number of datapoints (n).

Inter-element concentration correlation tables are given in the appendices: see ***Table S1*** for correlations between elements excluding Rare Earth Elements; and ***Table S2*** for correlations involving Rare Earth Elements.

Table 4: *Statistical summary of hydrothermal fluid endmember concentrations by element in grams per cubic metre.*

	Au	Ag	As	B	Ba	Br	Ca	Cd	Ce
Count	0	13	0	60	55	73	106	26	15
Minimum		3.24E-01		2.20E-03	1.99E-02	9.99E+03	7.41E+04	2.25E-02	1.12E-02
Average		8.66E+00		6.21E+03	3.48E+03	6.89E+04	1.48E+06	1.05E+01	1.91E+02
Maximum		7.17E+01		4.11E+04	1.25E+04	1.28E+05	1.27E+07	3.11E+01	2.65E+03
St. Deviation		1.94E+01		5.77E+03	3.44E+03	2.31E+04	1.40E+06	9.51E+00	6.82E+02
St. Deviation		224%		93%	99%	34%	94%	90%	358%

		Cl	Co	Cs	Cu	Dy	Er	Eu	Fe
Count	*units*	81	22	51	86	15	15	15	105
Minimum	$g\ m^{-3}$	2.02E+01	1.06E-02	1.00E-05	2.35E+00	4.39E-03	2.61E-03	1.11E-03	2.51E+01
Average	$g\ m^{-3}$	1.78E+07	5.05E+01	5.65E+01	6.32E+03	5.67E+01	2.69E+01	1.32E+02	2.34E+05
Maximum	$g\ m^{-3}$	8.80E+07	8.25E+02	3.64E+02	6.50E+04	5.47E+02	2.52E+02	1.42E+03	1.23E+06
St. Deviation	$g\ m^{-3}$	1.08E+07	1.74E+02	7.99E+01	1.16E+04	1.56E+02	7.31E+01	3.84E+02	3.49E+05
St. Deviation	*percent*	61%	345%	142%	184%	275%	272%	291%	149%

		Gd	Hf	Hg	Ho	La	Li	Lu	Mn
Count	*units*	15	2	0	12	15	104	5	105
Minimum	$g\ m^{-3}$	3.66E-03			9.30E-04	3.48E-03	7.00E-03	8.57E-04	2.26E+02
Average	$g\ m^{-3}$	5.38E+01	1.89E-03		1.30E+01	5.11E+01	3.52E+03	9.20E+00	4.10E+04
Maximum	$g\ m^{-3}$	4.25E+02			1.03E+02	7.27E+02	3.89E+04	2.78E+01	2.33E+05
St. Deviation	$g\ m^{-3}$	1.41E+02			3.21E+01	1.87E+02	4.49E+03	1.31E+01	4.36E+04
St. Deviation	*percent*	263%			247%	366%	127%	142%	106%

		Mo	Nb	Nd	Ni	Pb	Pd	Pr	Rb
Count	*units*	9	2	15	10	25	4	12	67
Minimum	$g\ m^{-3}$	2.21E+00		9.06E-03	1.12E-01	3.12E+00	7.23E+00	1.69E-03	2.07E-03
Average	$g\ m^{-3}$	5.72E+00	2.59E-03	1.75E+02	2.16E+03	1.99E+02	1.02E+01	4.55E+01	2.04E+05
Maximum	$g\ m^{-3}$	9.79E+00		2.28E+03	2.13E+04	1.47E+03	1.29E+01	4.91E+02	5.06E+06
St. Deviation	$g\ m^{-3}$	2.84E+00		5.88E+02	6.72E+03	3.90E+02	2.35E+00	1.41E+02	9.38E+05
St. Deviation	*percent*	50%			311%	196%	23%	310%	460%

		Sm	Sr	Ta	Tb	V	Y	Yb	Zn
Count	*units*	15	95	2	12	2	4	13	81
Minimum	$g\ m^{-3}$	2.93E-03	4.03E+00		6.30E-04		2.39E-02	2.71E-03	9.42E+00
Average	$g\ m^{-3}$	4.96E+01	1.24E+04	1.60E-04	1.18E+01	2.68E-01	1.00E+03	2.45E+01	7.17E+03
Maximum	$g\ m^{-3}$	5.45E+02	5.12E+04		7.90E+01		2.61E+03	1.89E+02	7.09E+04
St. Deviation	$g\ m^{-3}$	1.46E+02	1.01E+04		2.76E+01		1.26E+03	6.06E+01	1.10E+04
St. Deviation	*percent*	294%	82%		234%		126%	247%	154%

4.2.1 The Effect of Host Geology

The ‘budget’ of elements in the deep crust is understood to be a factor in the abundance of elements in fluid. The following analyses are qualitative, as simplified from Beaulieu, *et. al.* (2013). **Figure 16** is a network diagram detailing how the descriptions were simplified. Mid-Ocean Ridge systems where the host geology is ‘not provided’ are discarded for this analysis.

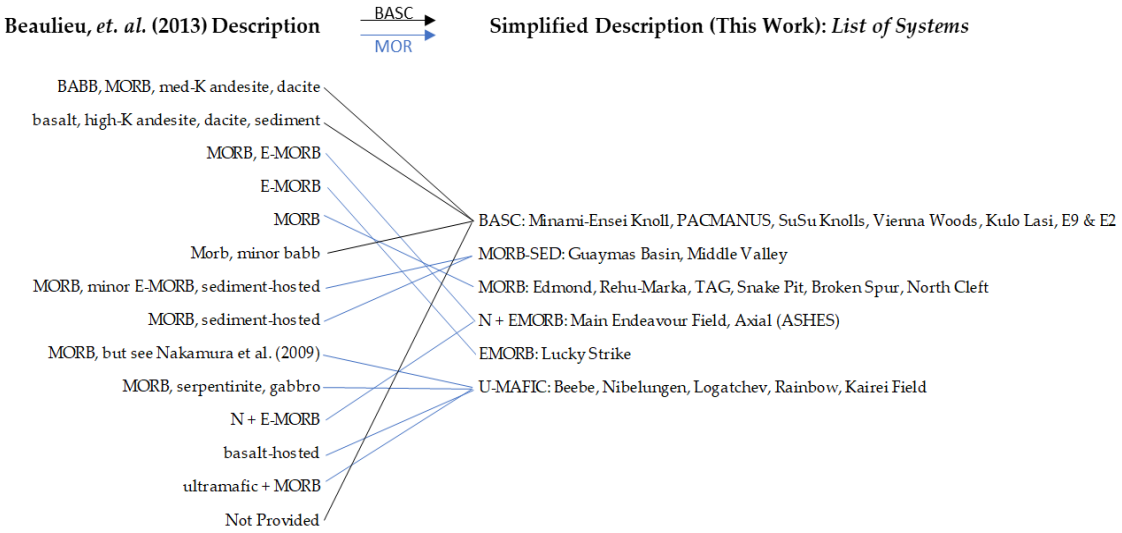

Figure 16: *Network Diagram comparing the original host rock descriptions from Beaulieu, et. al. (2013), to the simplified descriptions used by this work, with lists of systems by category.*

Back-Arc Spreading Centre petrologies vary greatly due to the mixing and recycling of magma, as described in ***“Geochemical Implications of Tectonic Settings”.*** While the seven systems represent a breadth of petrology, from ‘MORB, minor BABB’ to those with significant andesite and or sediment, the four of the seven have no provided host rock description (Beaulieu, et al., 2013). As a result, the BASC systems are compiled together: therefore, a high standard deviation relative to other categories is expected.

Those systems classified as ultramafic (UMAFIC) include those which are explicitly listed as ultramafic, *i.e.* Nibelungen (Melchert, et al., 2008) and Logatchev (Borowski, et al., 2007); Beebe, which is ‘likely to include’ some ultramafic host rock (Webber, et al., 2015) and those with reference to serpentisation, *i.e.* Kairei (Nakamura, et al., 2009), Rainbow (Dyment, et al., 2009). The process of serpentisation requires peridotite as a reactant, which is associated to ultramafic petrology (MacDonald & Fyfe, 1985).

The ‘minor EMORB’ (as defined in the following paragraph) component of the Middle Valley host geology is ignored, and the system is classified as MORB/SED.

The classification of Mid-Ocean Ridge Basalts is not without criticism: MORB refers to “Normal Mid-Ocean Ridge Basalts” (NMORB), away from mantle plumes. Enhanced, or Enriched, Mid-Ocean Ridge Basalt (EMORB) generally refers to basalts which have been influenced by a plume from the inner mantle. The notation N+EMORB refers to a mixed or transitional MORB partially influenced by a mantle plume. However, NMORB petrologies are found close to known mantle plumes: this indicates that this geographic rule of thumb is flawed (Gale, et al., 2013).

Rather, geochemical analyses of the basalt itself find that ratios of elements or isotopes can be used to determine how enriched the host rock may be (Gale, et al., 2013). This work recognises the limitation of using only categorical host rock data: but proceeds on this basis only.

Figure 17 shows the average (bar) and standard deviation (error bar) of fluid pH data for the collective dataset and divided into the host rock categories. The count of datapoints is given below the name of the category. The category MORB/SED (sediment) has a substantially greater pH than the remaining categories. **Table 5** is a matrix of ‘T test’ values between categories.

The MORB/SED category clearly has a significantly different pH to the remaining host rock categories, however, as demonstrated by **Table 5**, significant differences are found in systems which are less discrete. This may be reflected in the differences between elemental concentrations.

These analyses are repeated for temperature and V:B Ratio. **Figure 18** shows the average and standard deviation of fluid temperature data by host rock category. **Table 6** is a matrix of ‘T test’ values between categories. **Figure 19** shows the average and standard deviation of V:B temperature ratio data by host rock category. **Table 7** is a matrix of ‘T test’ values between categories.

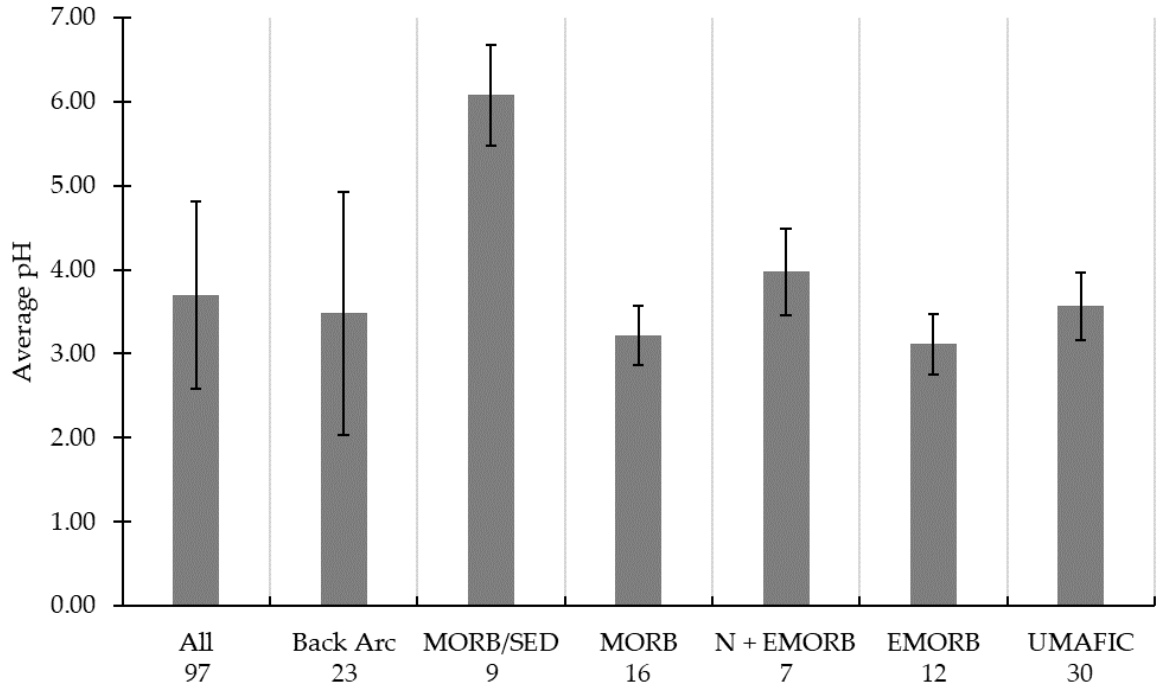

Figure 17: *Distribution of vent fluid pH data, collectively, and divided into host rock categories.*

Table 5: *Matrix of t-test values between host rock categories for pH, values of p < 0.05 are coloured red and presented in scientific notation. The values coloured red indicate the corresponding categories are significantly different. Values in black indicate the difference between host categories is not significant. There are no significantly similar host rock types.*

pH	All	Back Arc	MORB/SED	MORB	N + EMORB	EMORB	UMAFIC
All		0.44	6.96E-09	0.09	0.51	0.08	0.54
Back Arc			1.41E-05	0.48	0.39	0.40	0.76
MORB/SED				2.07E-13	3.27E-06	1.44E-11	5.80E-17
MORB					5.35E-04	0.46	5.70E-03
N + EMORB						4.80E-04	2.82E-02
EMORB							1.59E-03
UMAFIC							

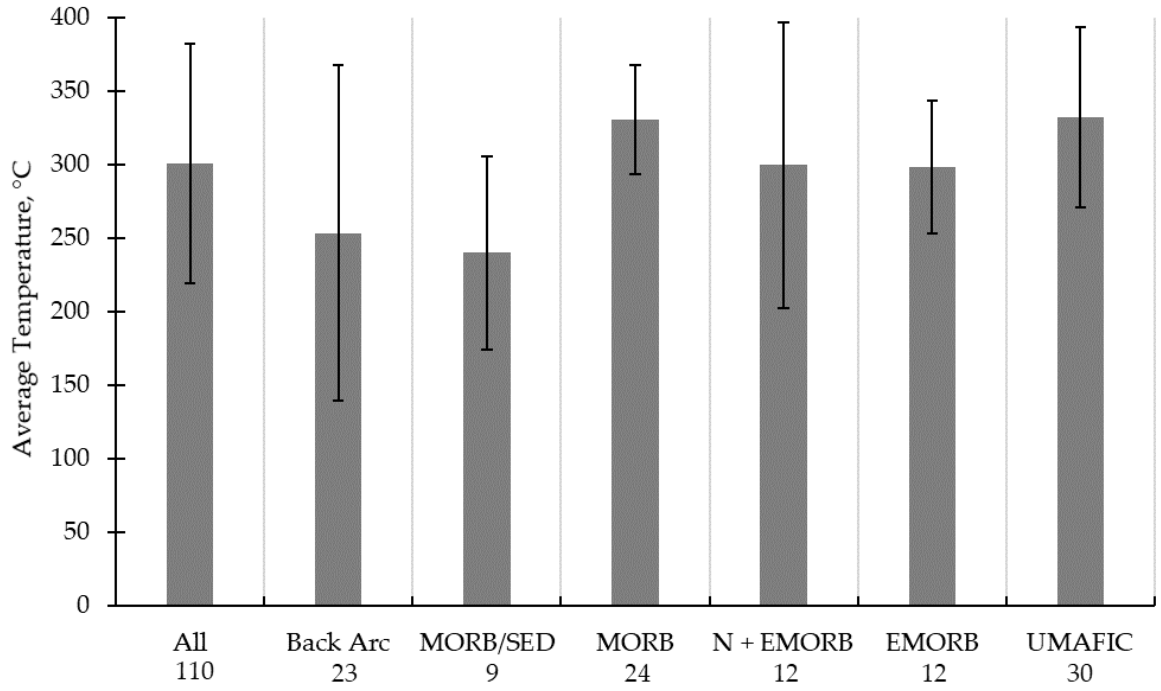

Figure 18: *Distribution of vent fluid temperature data by host rock category.*

Table 6*: Matrix of t-test values between host rock categories for temperature, the values coloured red indicate the corresponding categories are significantly different. Values in standard black indicate the difference between host categories is not significant. Significantly similar host rock types are indicated by bold black text.*

temp	All	Back Arc	MORB/SED	MORB	N + EMORB	EMORB	UMAFIC
All		2.04E-02	3.21E-02	0.08	**0.98**	0.93	0.05
Back Arc			0.75	2.94E-03	0.24	0.20	2.17E-03
MORB/SED				2.07E-05	0.13	2.54E-02	4.02E-04
MORB					0.18	2.90E-02	0.90
N + EMORB						**0.96**	0.20
EMORB							0.09
UMAFIC							

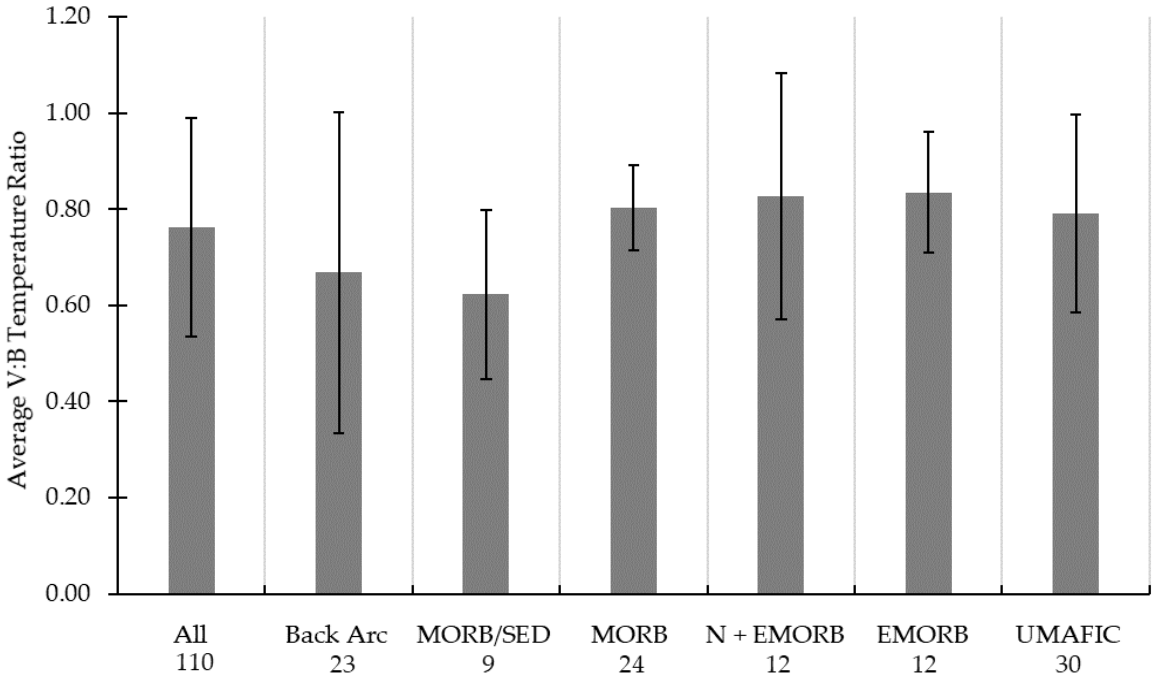

Figure 19: *Distribution of vent fluid V:B temperature ratio data by host rock category.*

Table 7: *Matrix of t-test values between host rock categories for V:B temperature ratio. The values coloured red indicate the corresponding categories are significantly different. Values in standard black indicate the difference between host categories is not significant. There are no significantly similar host rock types in terms of V:B ratio.*

V:B	All	Back Arc	MORB/SED	MORB	N + EMORB	EMORB	UMAFIC
All		0.18	0.05	0.46	0.39	0.31	0.61
Back Arc			0.50	0.12	0.22	0.15	0.19
MORB/SED				4.42E-04	0.05	4.35E-03	3.24E-02
MORB					0.68	0.38	0.80
N + EMORB						0.92	0.64
EMORB							0.50
UMAFIC							

Table 8 summarises the observations seen in element concentrations sorted by geologic setting. Where metals are observed at significantly greater fluid concentrations, *i.e.,* the T-Test indicates the mean is significantly different from the other tectonic settings; and the mean concentration is greater than the other geologic settings – the elements are shown above the grey. Conversely, elements which are observed at significantly lesser fluid concentrations, they are shown below the grey line.

Table 8: *Summary of observations of fluid concentrations with respect to host geologic setting, metals which exist in significantly greater fluid concentrations in host geologies are noted above the grey; metals which are significantly lesser concentrated in the fluid are shown below the grey.*

	Back Arc	MORB/SED	MORB	N + EMORB	EMORB	UMAFIC
Significantly Greater	Pb Rb	Cs	Fe Mn Cd			Fe Mn Cu Ba
Significantly Lesser	Ca	Fe Mn Cu Zn		Sr Br		B

Bar graphs and t-test matrices, like those seen in **Figure 17 – 19** and **Table 5 – 7** respectively, have also been produced to elements: these can be found as Supplementary **Figure S1 – S17** and Supplementary **Table S3 – S19** in the appendices.

4.2.2 Multi-Variable Analysis

This section aims to use observations to identify he predominant factors in the concentration of hydrothermal fluids. A 3D graph will coalesce the analysis of pH, temperature, V:B temperature ratio and host tock type for each element. It is first appropriate to review the variables, and what their effect on hydrothermal transport may be.

The variable, pH, is a measure of the molar concentration of hydrogen ions in solution: where pH is calculated as:

$$pH = -\log_{10}[H^+]$$

Therefore, an acid solution of pH 4 has a hydrogen cation concentration ten times greater than an acid solution at pH 5, and a thousand times greater than a neutral solution at pH 7 (Covington, et al., 1985). It is expected that some metals which are more mobilised in acidic conditions will have a strong negative relationship between fluid concentration and pH. Whereas some elements may not have any relationship between pH and fluid concentration. This is due to the inherent properties of the minerals.

Temperature has been shown to influence the solubility of minerals, the reasons for which are thermodynamic in nature, and therefore fall beyond the scope of this work. Temperature is discussed in the section ***"Geochemical Implications of Fluid Properties"*** as a factor in hydrothermal transport.

The distribution of observed pH and temperatures and hydrothermal fluids is shown in **Figure 20**.

The V:B temperature ratio was introduced in the **"Systems at Spreading Centres"** section of this work. In summary, it is the ratio of the venting temperature of a fluid, to the temperature at which it will boil. This is expressed as a product of the depth of the vent, *h (metres)*, which determines hydrostatic pressure, P (MPa): see ***"Hydrothermal Transport"***.

$$P \cong 0.01h$$

$$T_{boil} = 178.59 \times P^{0.2432}$$

The V:B temperature ratio can be thought of as an indicator to whether the hydrothermal transport is limited by the fluid limitations (boiling point, as V:B tends to one) or limited the amount of energy (as V:B tends to zero). If mineralisation occurs within the “plumbing” of the hydrothermal system, due to boiling, or due to the deficiency of energy, the concentration of elements in fluids at the orifice would be reduced.

Figure 20 clearly shows that the highest categories of V:B ratios are seen in higher temperature vents.

The following analyses are in descending order by the number of datapoints. Each figure comprises of a three-dimensional scatter plot, showing the distribution of the fluid elemental concentration (z-axis) with temperature (y-axis) and pH (x-axis, reversed). A scatter plot of the common logarithm of elemental concentration (y-axis) with temperature; and a scatter plot of the common logarithm of elemental concentration (y-axis) with pH, are included in the appendices.

Each figure has a corresponding table with the correlation coefficients between elemental concentration, temperature and pH. Details such as the slope and incept of strong trends will be noted below the tables.

The behaviour of the element will be addressed in text after each figure and table, drawing on the distribution with fluid characteristics and relationships with other critical metals (Moss, et al., 2013).

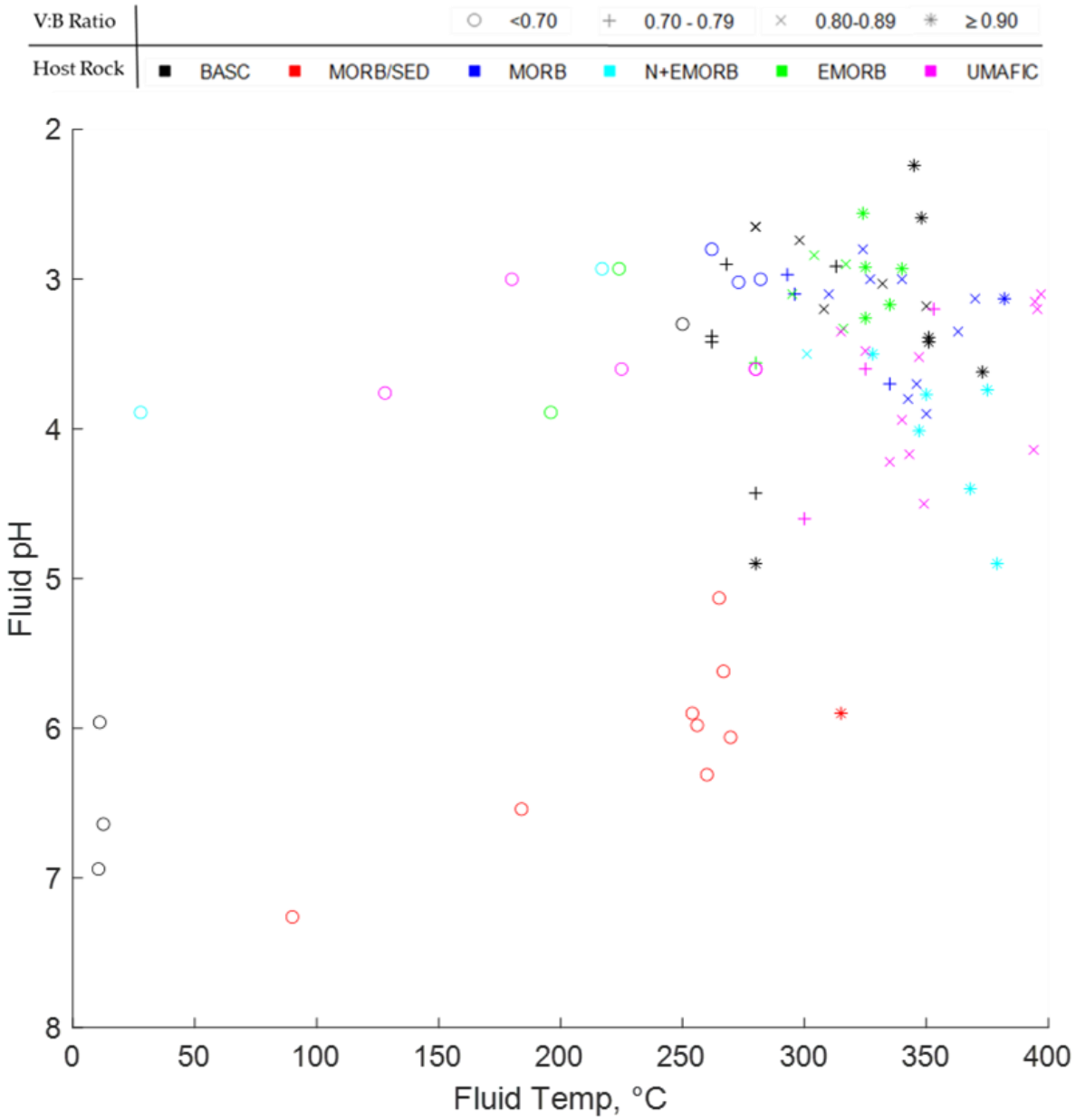

***Figure 20**: Distribution of pH and temperature observed in hydrothermal fluids analysed in this work key given to distinguish host rock settings and V:B ratio, given in intervals.*

Figure 21 to **Figure 43** will show the distribution of element concentrations with temperature and pH; with respect to host rock setting, and V:B ratio, given as intervals. Each element trend behaviour is described in is corresponding **Table 9** to **Table 31**.

Each element concentration distribution is also shown on a two-dimensional plot with respect to pH in Temperature, given in the appendix as **Figure S18** to **Figure S35**.

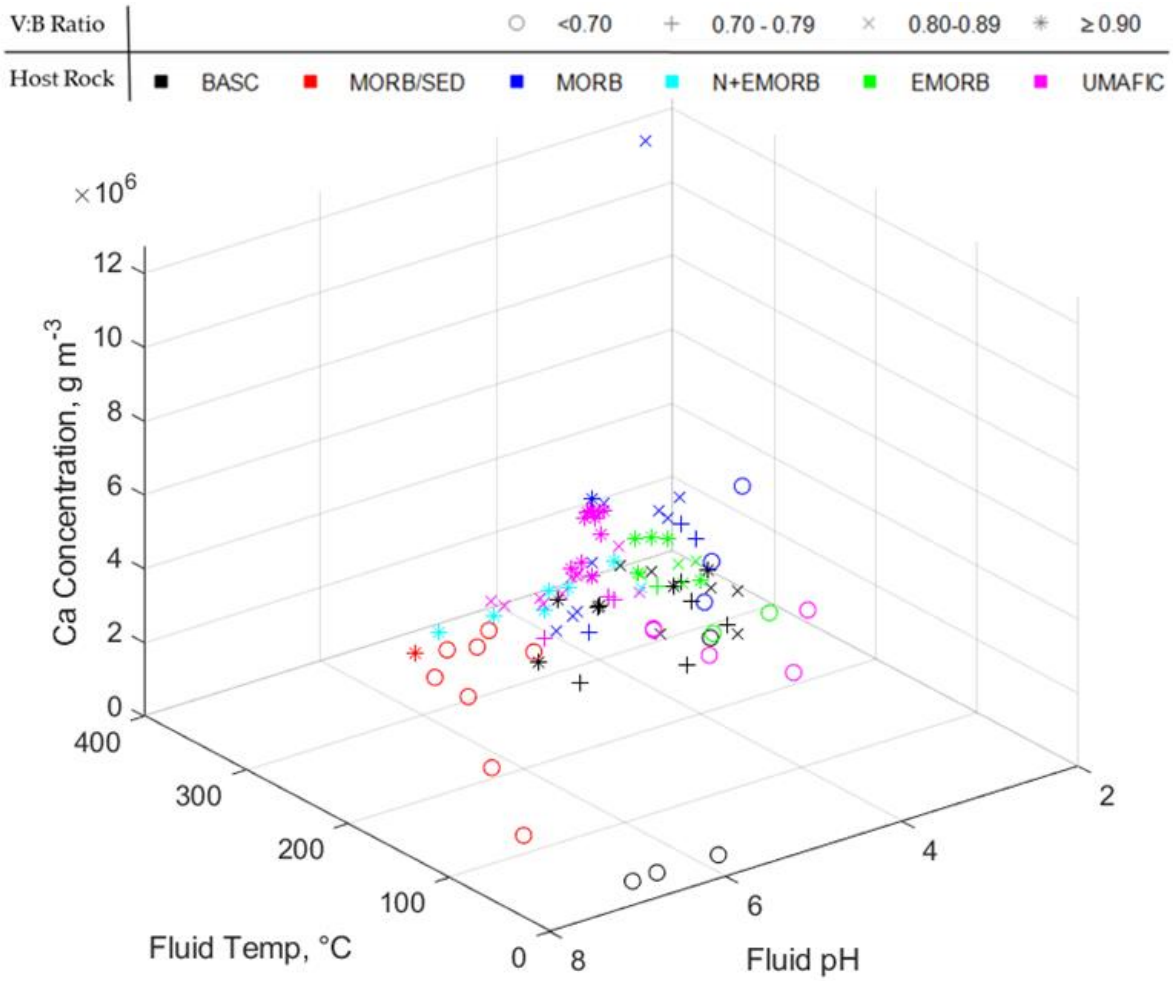

***Figure 21**: Distribution of calcium concentrations in hydrothermal fluids with temperature and pH: V:B ratio interval indicated by marker type; Host Rock type indicated by marker colour*

***Table 9:** Linear correlation coefficients between common logarithm of the calcium concentration of hydrothermal fluids and the pH, temperature, and V:B temperature ratios; by host rock category.*

Ca	All	Back-Arc	M/SED	MORB	N+EMORB	EMORB	UMAFIC
pH	-0.16	-0.25	-0.63	-0.81	-0.41	0.56	-0.02
Temp	-0.02	0.11	0.69	-0.29	-0.27	-0.21	-0.28
V:B Ratio	0.06	0.17	0.66	-0.06	-0.20	-0.21	0.09

Calcium is not a critical element. The element seems to be slightly depleted in deeper-mantle-input host rock types; however, this work will not investigate further.

Calcium concentrations are distributed seemingly independently from pH; temperature; and V:B temperature ratio, as seen in **Figure 21**. None of these parameters share a relationship with calcium concentration, as a common logarithm, having linear correlation coefficients (*r*) of -0.16, -0.02 and 0.06 respectively.

When the data are divided into host rock categories, the correlation analysis is repeated, and the results are found to be wildly inconsistent, as seen in **Table 9**. This supports that most of the variation in calcium concentration is likely a result of differences in host geology.

The outstanding datapoint is a single sample from the Nadir vent at Rehu Marka (Charlou, et al., 1996). The Rehu Marka lava flow is itself described to have a 'distinct', 'evolved' composition as the host lava is estimated to have formed 750 years ago (Rubin, et al., 2001). This raises the questions: are elements in the deep crust exhausted by hydrothermal transport? Do different elements replace those which may have become exhausted?

It is notable that fluid endmember concentrations of calcium and rare earth elements correlate reasonably well ($\bar{r} = 0.84$), see **Table S2**. Given that - like rare earth elements - calcium is a lithophile element, the correlation between them is reasonably expected (Goldschmidt, 1937).

See Supplementary **Figure S18** for Calcium temperature-concentration and pH-concentration plots.

As calcium concentration is already widely analysed in existing samples, could it be applied as a tool to predict the abundance of rare earth elements in submarine hydrothermal fluids?

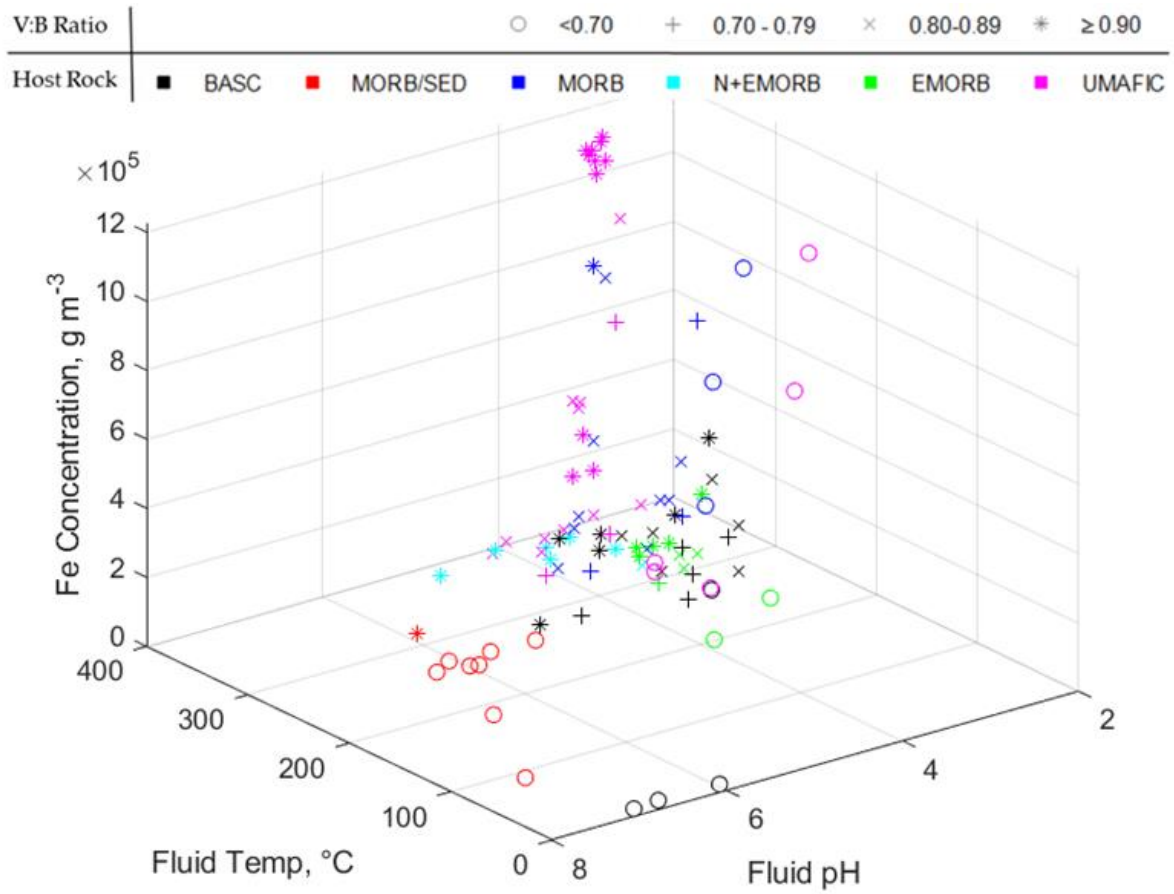

***Figure 22**: Distribution of iron concentrations in hydrothermal fluids with temperature and pH: V:B ratio interval indicated by marker type; Host Rock type indicated by marker colour*

***Table 10**: Linear correlation coefficients between common logarithm of the iron concentration of hydrothermal fluids and the pH, temperature, and V:B temperature ratios; by host rock category.*

Fe	All	Back-Arc	M/SED	MORB	N+EMORB	EMORB	UMAFIC
pH	-0.77	-0.97	0.01	-0.19	-0.53	-0.54	-0.60
Temp	0.57	0.88	0.05	-0.19	0.57	0.29	0.10
V:B Ratio	0.49	0.88	0.10	-0.24	0.56	0.29	0.23

Iron is not a critical metal (Moss, et al., 2013). The distribution of iron concentrations in hydrothermal fluids is unsurprisingly dominated by the effect of the host rock, as illustrated in **Figure 22** and indicated earlier in **Table 8**. Ultramafic and Mid-Ocean Ridge Basalt (MORB) are characteristically iron rich, this is reflected in that the two systems are not significantly different from each other but are significantly different from the other host rock categories.

Back-Arc, N+EMORB (Transitional) and EMORB (plume Enriched Mid-Ocean Ridge Basalt) hydrothermal fluid iron concentrations are not significantly different from one another. This is not surprising, given ***'Geochemical Implications of Tectonic Settings'***, highlights similarities between Back-Arc Spreading Centres and plume influenced Mid-Ocean Ridges, *i.e.,* Reykjanes Ridge (Webber, et al., 2013). Furthermore, **Figures 17 – 19** and corresponding **Tables 5 – 7**, indicate there is no significant difference in pH, temperature or V:B temperature ratio, and therefore, no significant difference in hydrothermal transport.

The fluid endmember concentration of iron is expected to have a negative relationship with pH and a positive relationship with temperature and V:B temperature ratio. The absolute value of the correlation coefficients determines the strength of the linear relationships. Relationships by host rock category are summarised by correlation coefficients in **Table 10**.

'Sedimented MORB' (MORB/SED or M/SED) is shown to have practically no correlation with the pH, temperature or V:B temperature ratio. The most surprising host rock category, however, is MORBs. At this stage, it would only be appropriate to review the relationship with a larger sample size, as more sampling and analysis is conducted. It is possible that this work, having omitted low temperature systems; and finding few low temperature vents in high temperature systems: is faced with a single cluster of Mid-Ocean Ridge Basalt data.

See Supplementary **Figure S19** for Iron temperature-concentration and pH-concentration plots.

Iron enjoys an affinity to cadmium (r = 0.73), cobalt (r = 0.79) and copper (r = 0.70), as seen in **Table S1**. The correlation coefficients between the concentration of iron and some rare earth elements in hydrothermal fluids is quite negative ($\bar{r} = -0.49$).

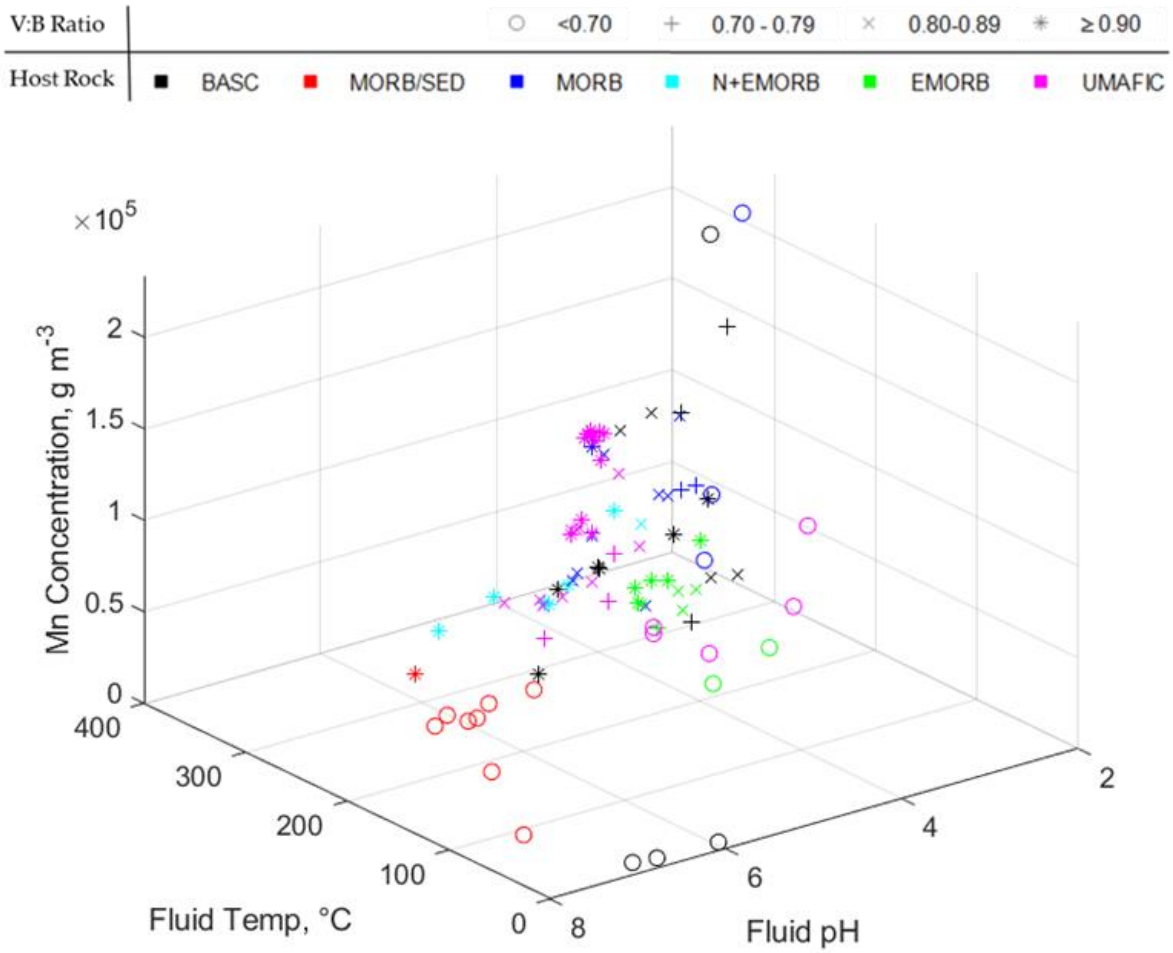

***Figure 23**: Distribution of manganese concentrations in hydrothermal fluids with temperature and pH: V:B ratio interval indicated by marker type; Host Rock type indicated by marker colour*

***Table 11:** Linear correlation coefficients between common logarithm of the manganese concentration of hydrothermal fluids and the pH, temperature, and V:B temperature ratios; by host rock category.*

Mn	All	Back-Arc	M/SED	MORB	N+EMORB	EMORB	UMAFIC
pH	-0.76	-0.83	-0.64	-0.24	-0.67	-0.64	-0.51
Temp	0.48	0.76	0.71	-0.39	-0.01	0.57	0.10
V:B Ratio	0.46	0.72	0.74	-0.35	0.09	0.57	0.30

The distribution of manganese concentration, in **Figure 23**, is less variable with host rock than is for iron, which it is closely associated to. The sedimented MORB host rock category is once again has significantly lower concentrations than the other datasets; and the ultramafic hock rock category has significantly higher concentrations than other host rock categories except the normal MORB systems.

The fluid endmember concentration of manganese is also expected to have a negative relationship with pH, and a positive relationship with temperature and V:B temperature ratio. These relationships are described by correlation coefficients in **Table 11**.

The relationships in sedimented MORB are substantially stronger in manganese than they are for iron, the remaining host rock categories have generally slightly weaker relationships, though the back arc categories remain the strongest of the relationships.

See Supplementary **Figure S20** for Manganese temperature-concentration and pH-concentration plots.

Manganese is correlated to the critical elements, lead (r = 0.92) and cadmium (r = 0.75) (Moss, et al., 2013), see **Table S1**. Unlike iron, manganese, is strongly correlated with rare earth elements ($\bar{r} = 0.88$): as seen in **Table S2**.

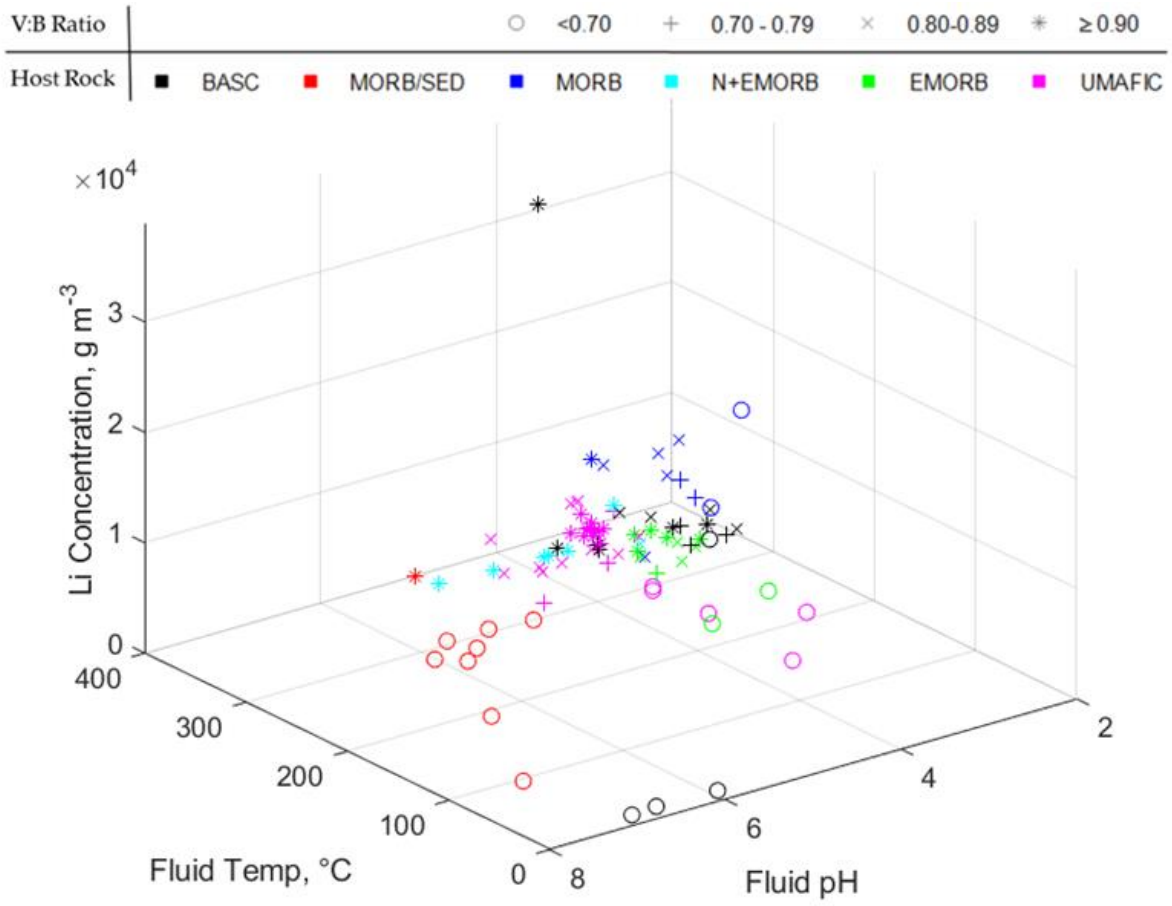

Figure 24: *Distribution of lithium concentrations in hydrothermal fluids with temperature and pH: V:B ratio interval indicated by marker type; Host Rock type indicated by marker colour*

Table 12*: Linear correlation coefficients between common logarithm of the lithium concentration of hydrothermal fluids and the pH, temperature, and V:B temperature ratios; by host rock category.*

Li	All	Back-Arc	M/SED	MORB	N+EMORB	EMORB	UMAFIC
pH	-0.37	-0.53	-0.72	-0.09	-0.65	0.49	-0.54
Temp	0.01	0.56	0.88	-0.48	-0.31	-0.14	0.34
V:B Ratio	0.07	0.66	0.90	-0.39	-0.22	-0.14	0.31

Regarding the fluid concentrations of lithium, no two host rock categories are significantly different.

The linear correlations between the common logarithm of lithium concentration and the venting characteristics are unusually the strongest in Sedimented MORB hosted systems. Overall, the relationships are weak relative to iron and manganese: but somewhat comparable to lithium's fellow lithophile element, calcium.

See Supplementary **Figure S21** for Lithium temperature-concentration and pH-concentration plots.

Lithium itself is a 'low-medium' critical element (Moss, et al., 2013), which shares a slight correlation with the rare earth elements ($\bar{r} = 0.31$). See **Table 6**.

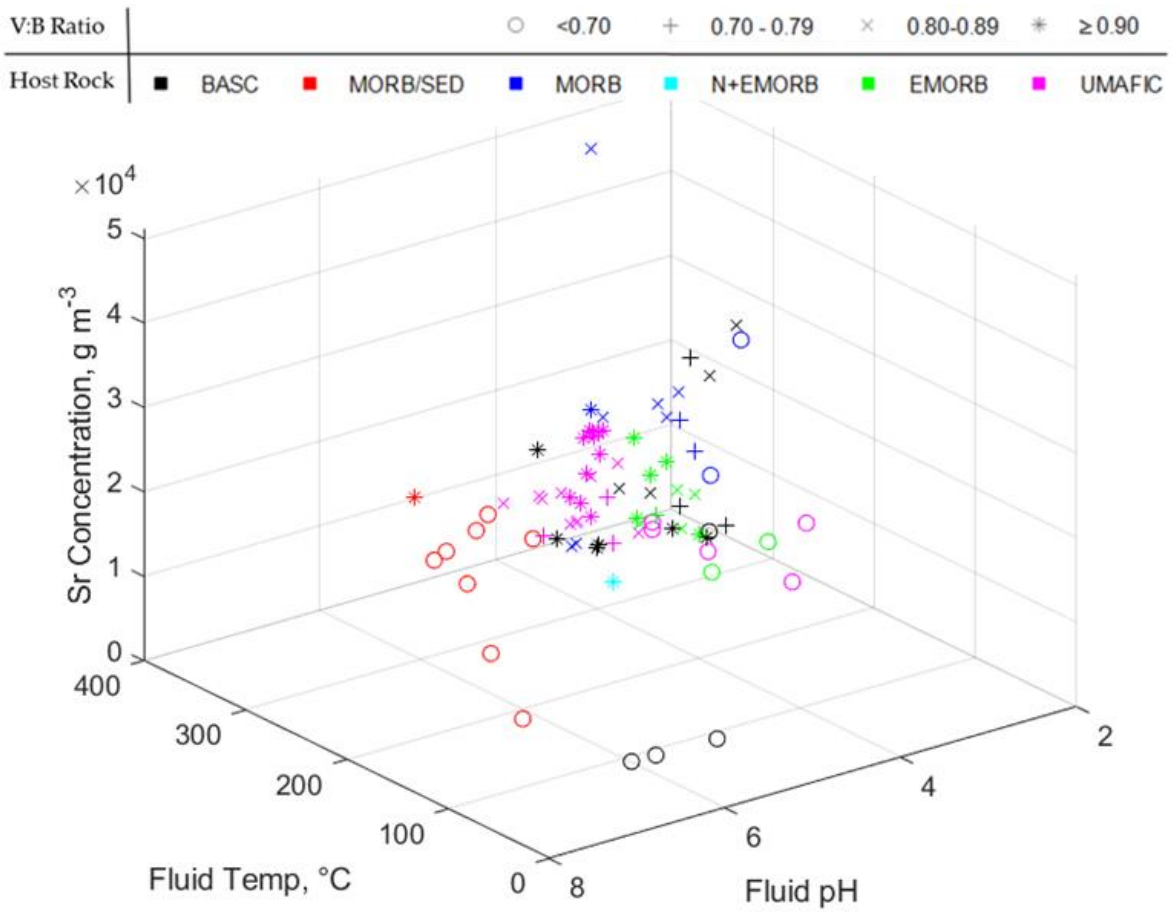

***Figure 25**: Distribution of strontium concentrations in hydrothermal fluids with temperature and pH: V:B ratio interval indicated by marker type; Host Rock type indicated by marker colour*

***Table 13:** Linear correlation coefficients between common logarithm of the strontium concentration of hydrothermal fluids and the pH, temperature, and V:B temperature ratios; by host rock category*

Sr	All	Back-Arc	M/SED	N+EMORB	EMORB	UMAFIC
pH	0.11	0.14	-0.66		0.36	0.31
Temp	-0.05	-0.23	0.82	0.46	-0.08	-0.34
V:B Ratio	-0.11	-0.16	0.82	0.46	-0.08	-0.03

Figure 25 shows how the concentrations of strontium fall dramatically in the region greater than 300°C and less than pH 4. On second viewing, the same fall is seen in **Figure S18** for Calcium concentrations.

Both elements are associated to the scaffolding formation as a chimney grows, as described in '***Geochemical Implications of Fluid Properties'*** (Lyndon, 1988). In the same way calcium ions in the hydrothermal fluid react with sulphate ions in seawater to produce anhydrite (Humphris & Bach, 2005): strontium ions in the hydrothermal fluid react with sulphate ions in seawater to produce celestine (Hanor, 2000).

It is known that the solubility of anhydrite ($CaSO_4$) behaves as retrograde as temperatures exceed 150°C (Humphris & Bach, 2005). Given that calcium and strontium are in the same periodic group, it is very possible that this is a shared characteristic.

The standout host rock category is N+EMORB, it is unclear whether the much lower concentrations are attributed to the quantity of high temperature fluid data in the category, or if it reflects lower concentration in the host rock.

See Supplementary **Figure S22** for Strontium temperature-concentration and pH-concentration plots.

Concentrations of strontium strongly correlate with rare earth elements ($\bar{r} = 0.88$), which is expected given strontium is also a lithophile element (Goldschmidt, 1937). See **Table S2**.

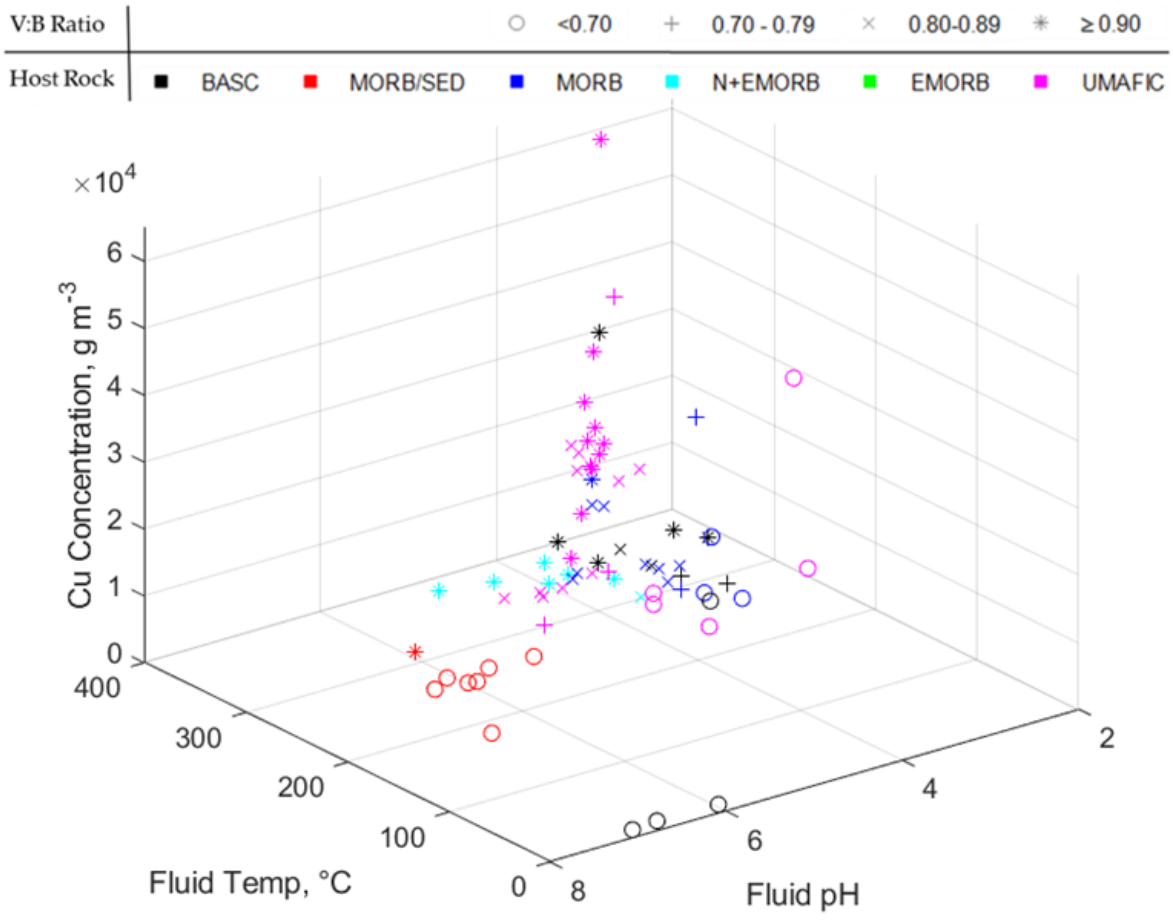

Figure 26: *Distribution of copper concentrations in hydrothermal fluids with temperature and pH: V:B ratio interval indicated by marker type; Host Rock type indicated by marker colour*

Table 14*: Linear correlation coefficients between common logarithm of the copper concentration of hydrothermal fluids and the pH, temperature, and V:B temperature ratios; by host rock category.*

Cu	All	Back-Arc	M/SED	MORB	N+EMORB	EMORB	UMAFIC
pH	-0.66	-0.77	-0.73	0.20	0.26		-0.74
Temp	0.50	0.84	0.70	0.49	0.78		0.01
V:B Ratio	0.44	0.85	0.64	0.32	0.80		0.07

The distribution of the common logarithm of copper concentration does not appear to have a linear relationship with pH, temperature or V:B temperature ratio. Instead, the common logarithm of concentration appears to grow exponentially as pH decreases: or as temperature and V:B ratio increase.

Considering this, the correlation coefficients in **Table 14** are not expected to be strong. Ultramafic hosted systems, which include the copper-rich Beebe system (Webber, et al., 2015), dominate the highest end of copper concentrations. **Figure S6** and **Table S8** show that the ultramafic category has significantly higher concentrations than all other categories, followed by MORB and Back Arc categories which are not significantly different from each other.

The fact that the average Back Arc and N+EMORB copper concentration are less than MORB copper concentrations is consistent with the decrease in chalcophile elements in deep mantle influenced melts, as discussed in ***'Geochemical Implications of Tectonic Settings'***.

See Supplementary **Figure S23** for Copper temperature-concentration and pH-concentration plots.

Copper itself is a 'low' level critical metal (Moss, et al., 2013), and a key target resource in submarine hydrothermal deposits. The only notable correlation it shares with another critical metal is cobalt ($r = 0.93$): although, given the small sample size of cobalt concentrations: this may be overstated. See **Table S1**.

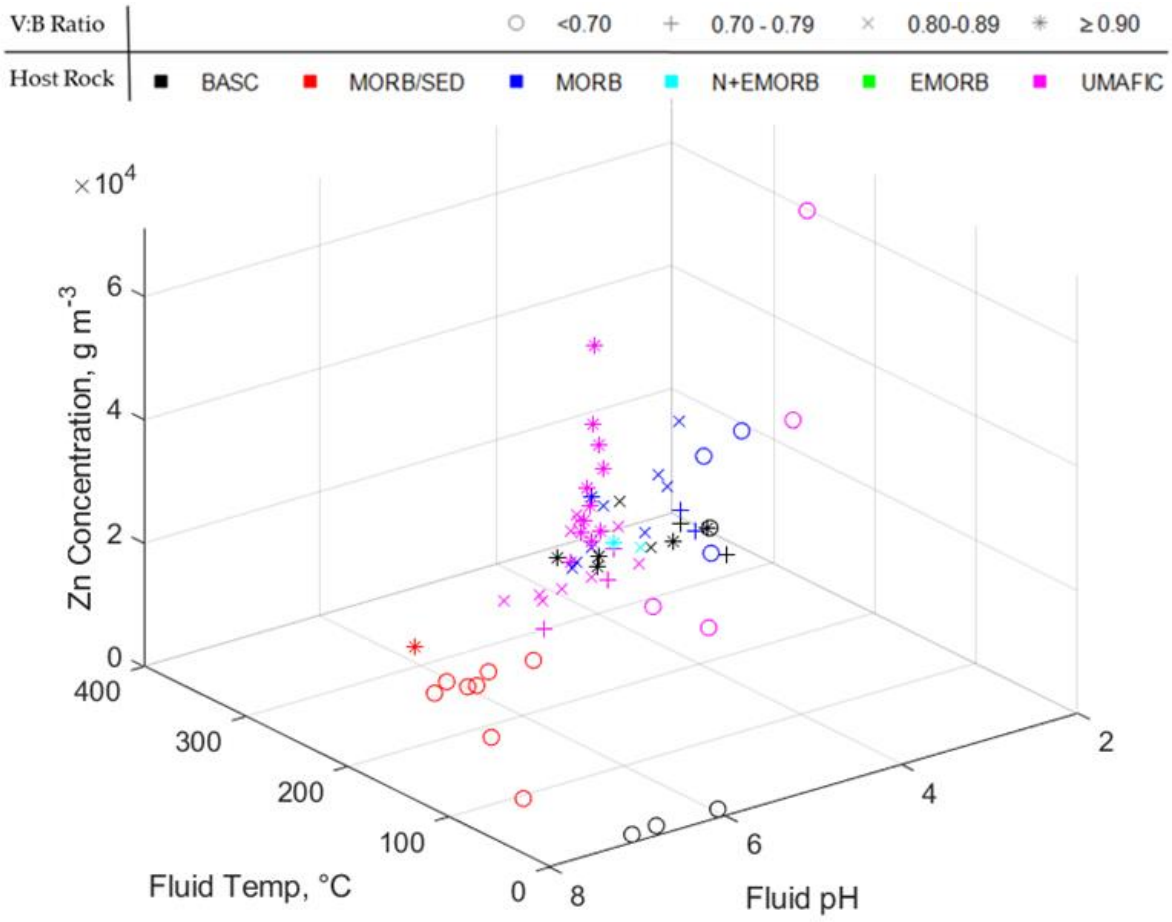

***Figure 27**: Distribution of zinc concentrations in hydrothermal fluids with temperature and pH: V:B ratio interval indicated by marker type; Host Rock type indicated by marker colour*

***Table 15:** Linear correlation coefficients between common logarithm of the zinc concentration of hydrothermal fluids and the pH, temperature, and V:B temperature ratios; by host rock category.*

Zn	All	Back-Arc	M/SED	MORB	N+EMORB	EMORB	UMAFIC
pH	-0.81	-0.90	0.22	-0.82			-0.69
Temp	0.43	0.85	-0.07	-0.03	0.62		-0.21
V:B Ratio	0.46	0.86	-0.02	0.19	0.62		-0.07

Similarly – but less so - to copper, the distribution of zinc appears to have an exponential-like trend instead of a linear trend.

Zinc concentrations have a stronger relationship with pH than it does with temperature or V:B temperature ratio: this is apparent in **Figure 27** and when comparing the correlation coefficients in **Table 15**.

Except for ‘Sedimented MORB’, no two host rock categories are significantly different from one another, as seen in **Figure S7** and **Table S9**.

See Supplementary **Figure S24** for Zinc temperature-concentration and pH-concentration plots.

Zinc, itself, is not a critical metal but does share correlation with cadmium ($r = 0.96$). Given the small sample size of cadmium, this may be overstated. See **Table S1**.

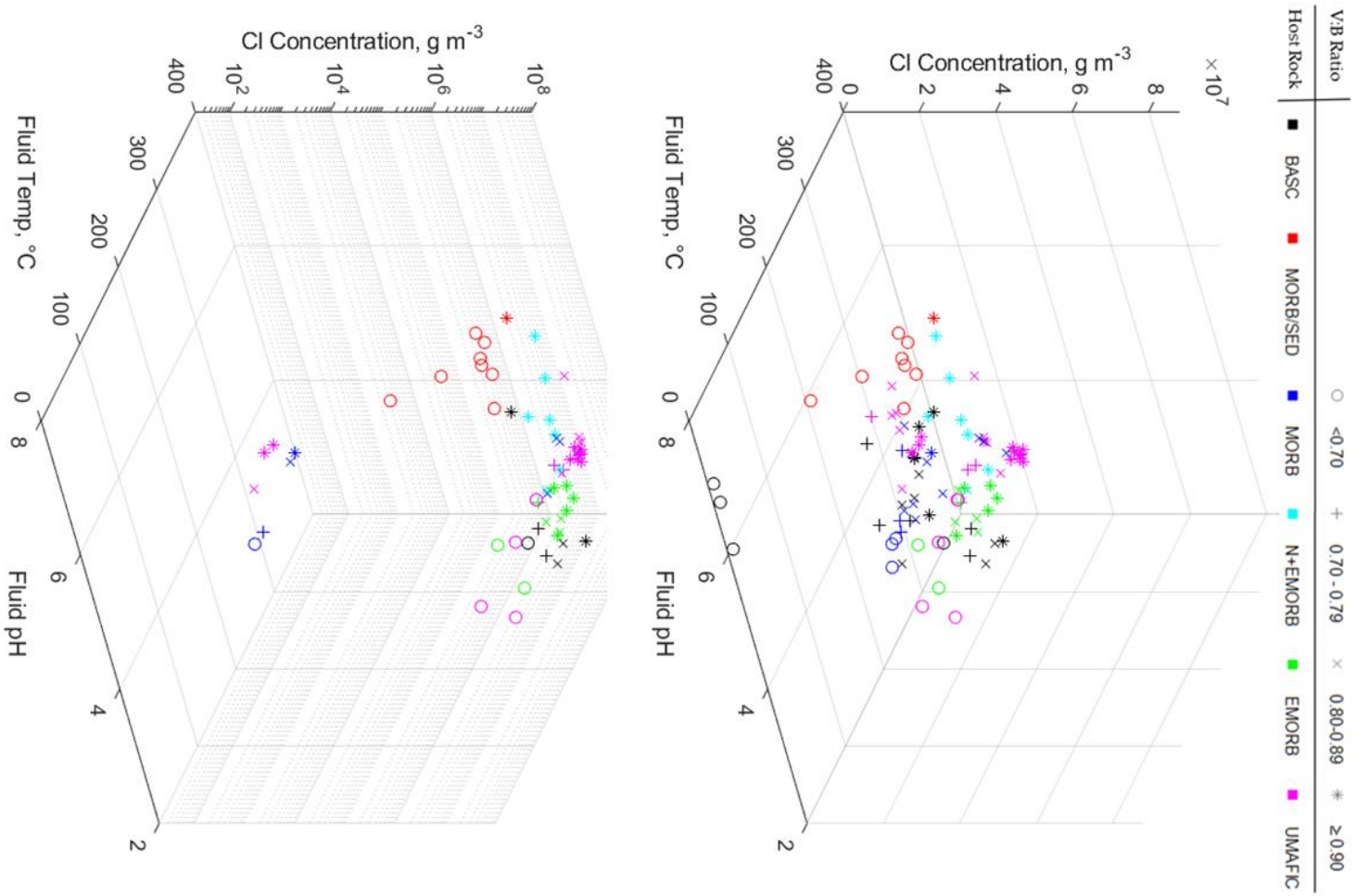

***Figure 28**: (top) Distribution of chlorine concentrations in hydrothermal fluids with temperature and pH: V:B ratio interval indicated by marker type; Host Rock type indicated by marker colour.*

(bottom) Distribution of chlorine concentrations in hydrothermal fluids with temperature and pH, given on a logarithmic axis: V:B ratio interval indicated by marker type; Host Rock type indicated by marker colour

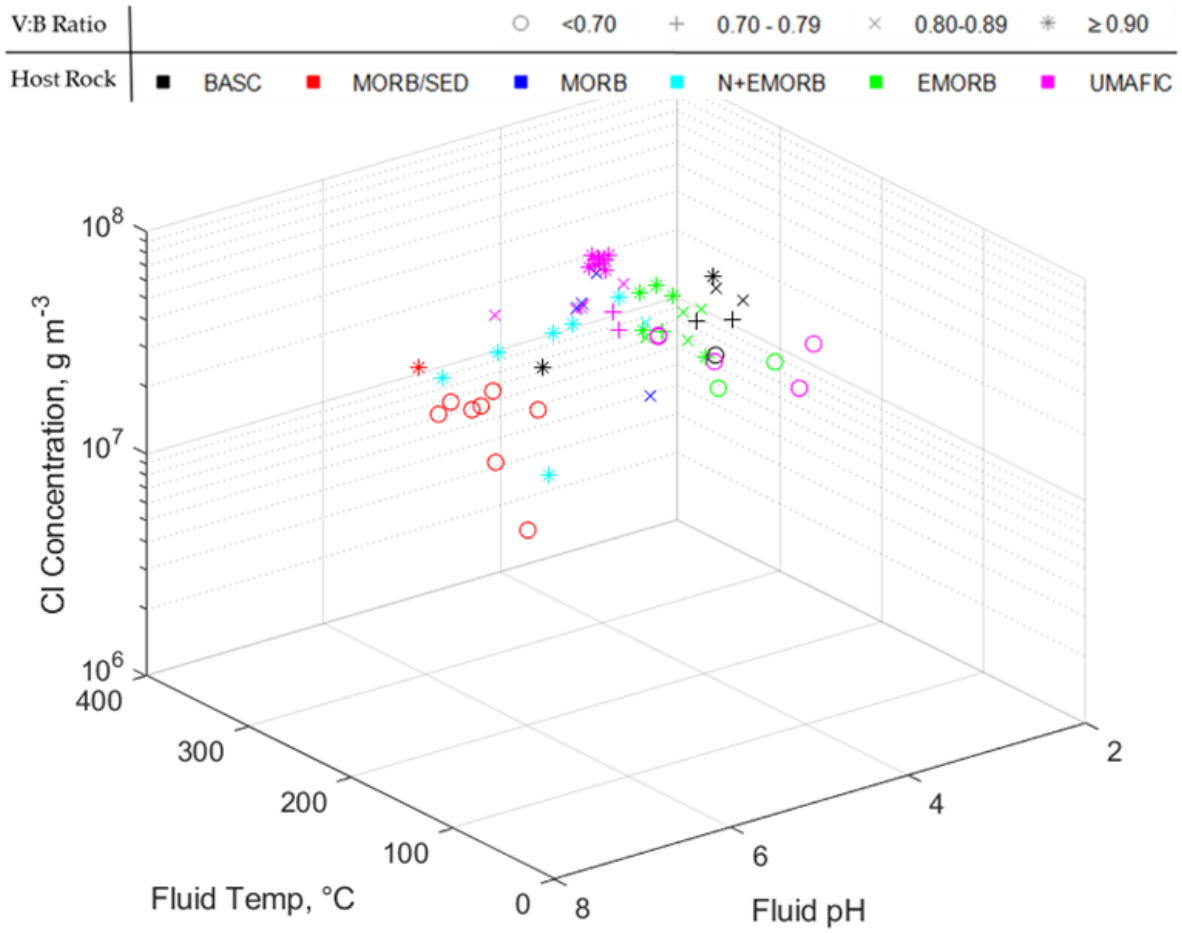

Figure 29: *Distribution chlorine concentrations in hydrothermal fluids with temperature and pH given on a logarithmic axis: V:B ratio interval indicated by marker type; Host Rock type indicated by marker colour*

Table 16: *Linear correlation coefficients between common logarithm of the chlorine concentration of hydrothermal fluids and the pH, temperature, and V:B temperature ratios; by host rock category. Greater concentration group only.*

Cl	All	Back-Arc	M/SED	MORB	N+EMORB	EMORB	UMAFIC
pH	0.05	0.04	0.37	0.79	-0.16	0.44	0.09
Temp	-0.03	-0.22	0.15	-0.30	0.11	-0.15	-0.36
V:B Ratio	0.01	-0.16	0.17	-0.52	0.18	-0.15	0.01

The distribution of the common logarithm of chlorine concentration in hydrothermal fluids is clearly bimodal. The lower selection are fluids from the Edmond Field and Kairei Field and has an average chlorine concentration of 32.9 ± 1.1 and 21.1 ± 0.87 grams of chlorine per cubic metre, respectively. The upper selection has an average concentration of $1.79 \times 10^7 \pm 9.74 \times 10^6$ grams.

For context, the concentration of chlorine in seawater at a salinity of 35 grams per litre is approximately 19370 grams per cubic metre (Huber, et al., 2000).

As fluids percolate to the reaction zone in the deep crust, where the elements are dissolved into the fluids, they can undergo phase separation. As the fluids ascend, they can either be vapour-like at low salinity and/or high temperature; or liquid-like at high salinity and/or low temperature (Coumou, et al., 2009). In **Figure S25**, it is shown that these low salinity fluids only occur at temperatures above 250°C. Conversely, most fluids in this study conform to the liquid-like at high salinity description.

There are very few significant differences between host rock categories in terms of chlorine concentration.

Table 16 contains the correlation coefficients for the higher band of chlorine concentrations only, overall, there is no correlation.

There is a negative correlation between the concentrations of chlorine and cadmium ($r = -0.76$), which may suggest that cadmium is found in greater concentrations in vapor-like fluid vents. However, given the paucity of cadmium data, this may too be overstated.

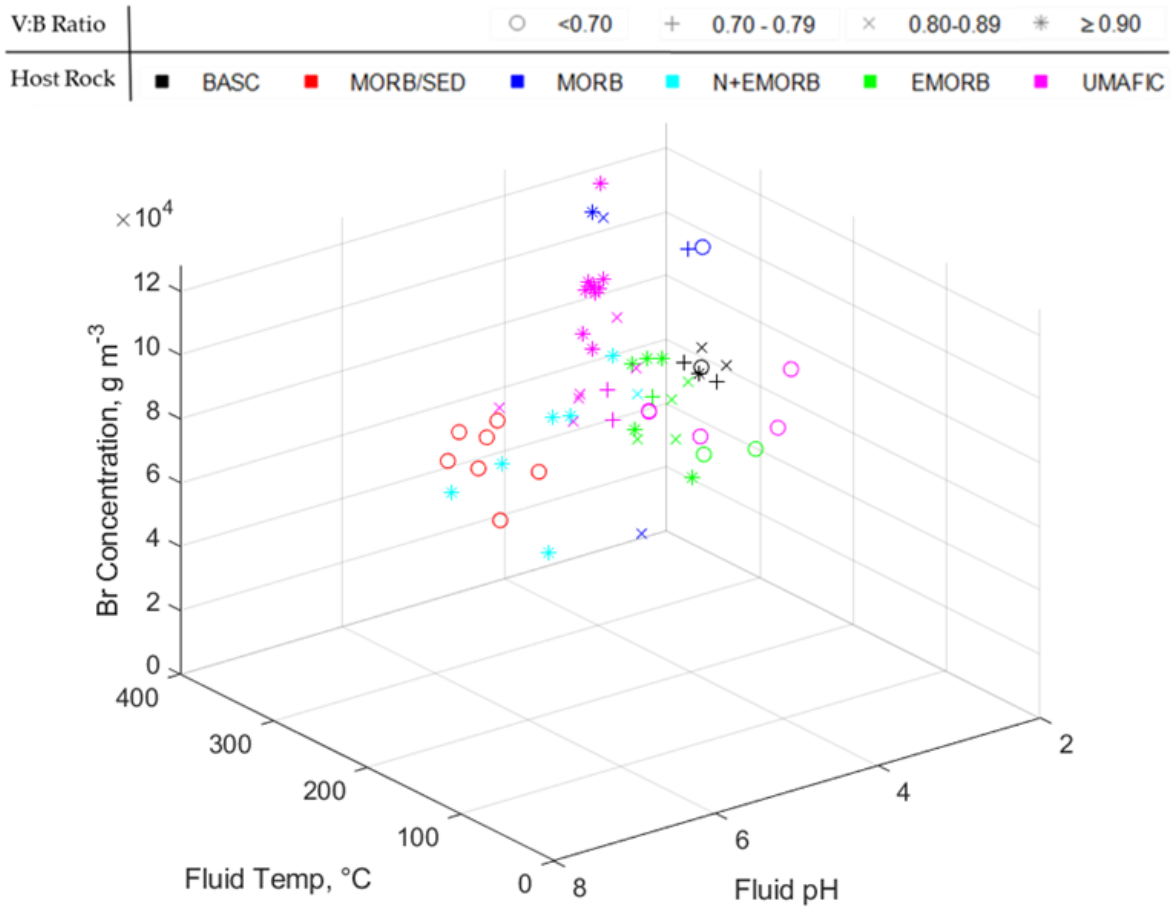

Figure 30: *Distribution of bromine concentrations in hydrothermal fluids with temperature and pH: V:B ratio interval indicated by marker type; Host Rock type indicated by marker colour*

Table 17*: Linear correlation coefficients between common logarithm of the bromine concentration of hydrothermal fluids and the pH, temperature, and V:B temperature ratios; by host rock category.*

Br	All	Back-Arc	M/SED	MORB	N+EMORB	EMORB	UMAFIC
pH	0.01	0.90	0.30	0.37	-0.16	0.43	0.01
Temp	-0.06	-0.89	0.29	-0.20	-0.07	-0.16	-0.22
V:B Ratio	-0.10	-0.86	0.29	-0.33	-0.02	-0.16	0.13

Bromine (**Figure 30**) has a symmetrical distribution above and below the average concentration, with no overall trends apparent between concentrations and pH, temperature nor V:B temperature ratio. It is also clear from the standard deviations, shown by host rock category in **Figure S9** and quantified as just 34% of the overall mean in **Table 4**, that there is a small range of bromine concentrations.

Experiments find that bromine partitions into the brine phase only after barium, strontium, calcium, potassium, sodium-chlorine and lithium, in the stated order (Berndt & Seyfried, 1990).

See Supplementary **Figure S27** for Bromine temperature-concentration and pH-concentration plots.

Bromine has a strong correlation with rare earth element concentrations ($\bar{r} = 0.88$), see **Table S2**.

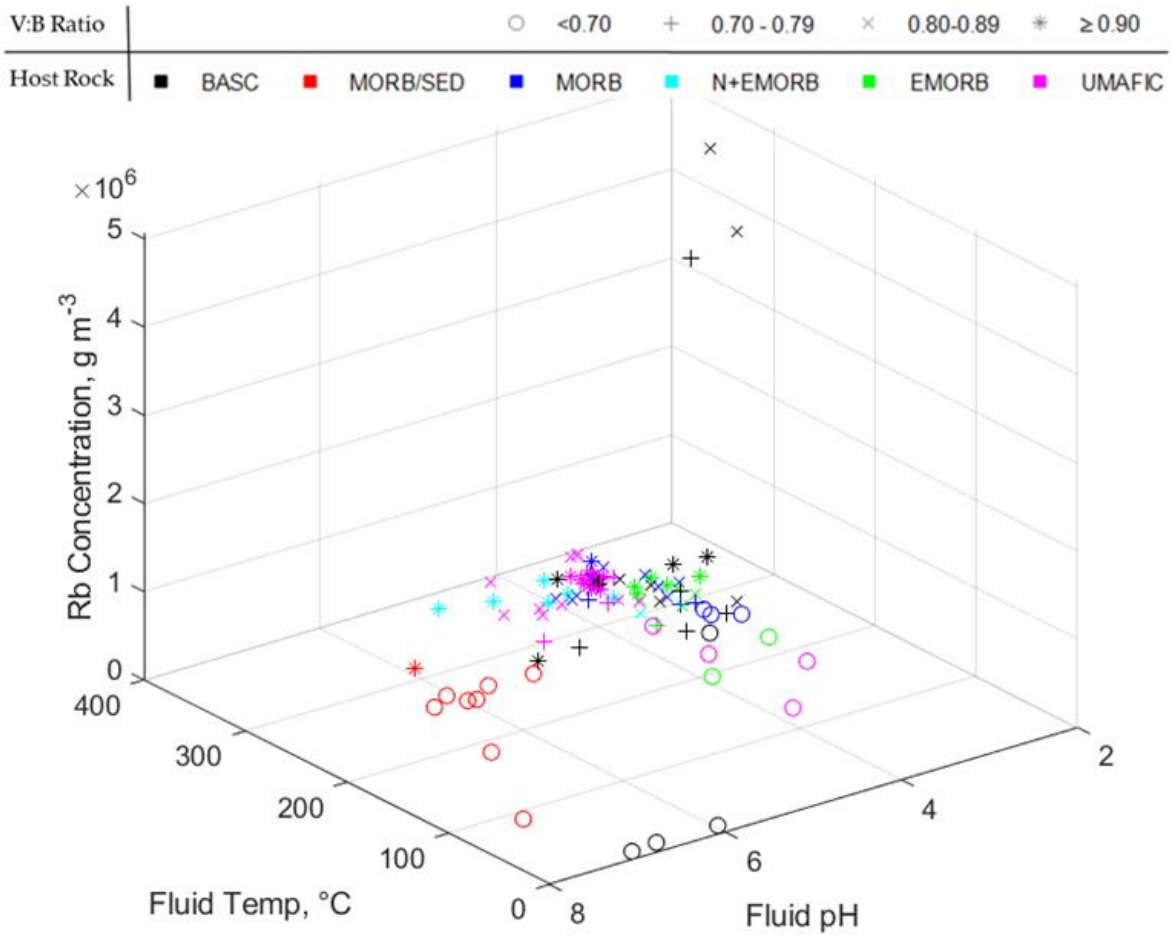

Figure 31: *Distribution of rubidium concentrations in hydrothermal fluids with temperature and pH: V:B ratio interval indicated by marker type; Host Rock type indicated by marker colour*

Table 18: *Linear correlation coefficients between common logarithm of the rubidium concentration of hydrothermal fluids and the pH, temperature, and V:B temperature ratios; by host rock category. Disregarding SuSu Knolls vents.*

Rb	All	Back-Arc	M/SED	MORB	N+EMORB	EMORB	UMAFIC
pH	-0.36	0.97	-0.71	-0.50	-0.37	0.39	0.34
Temp	-0.22	-1.00	0.87	-0.59	-0.96	-0.09	-0.27
V:B Ratio	-0.09	-1.00	0.89	-0.51	-0.96	-0.09	0.08

The distribution of rubidium, shown in **Figure 31**, has three outliers which are all associated to the SuSu Knoll vent fluids. These data have been discarded for the analysis in **Table 18**. See Supplementary **Figure S28** for rubidium temperature-concentration and pH-concentration plots. Rubidium is again a lithophile element with strong correlation to Rare Earth Elements ($\bar{r} = 0.87$), see **Table S2**.

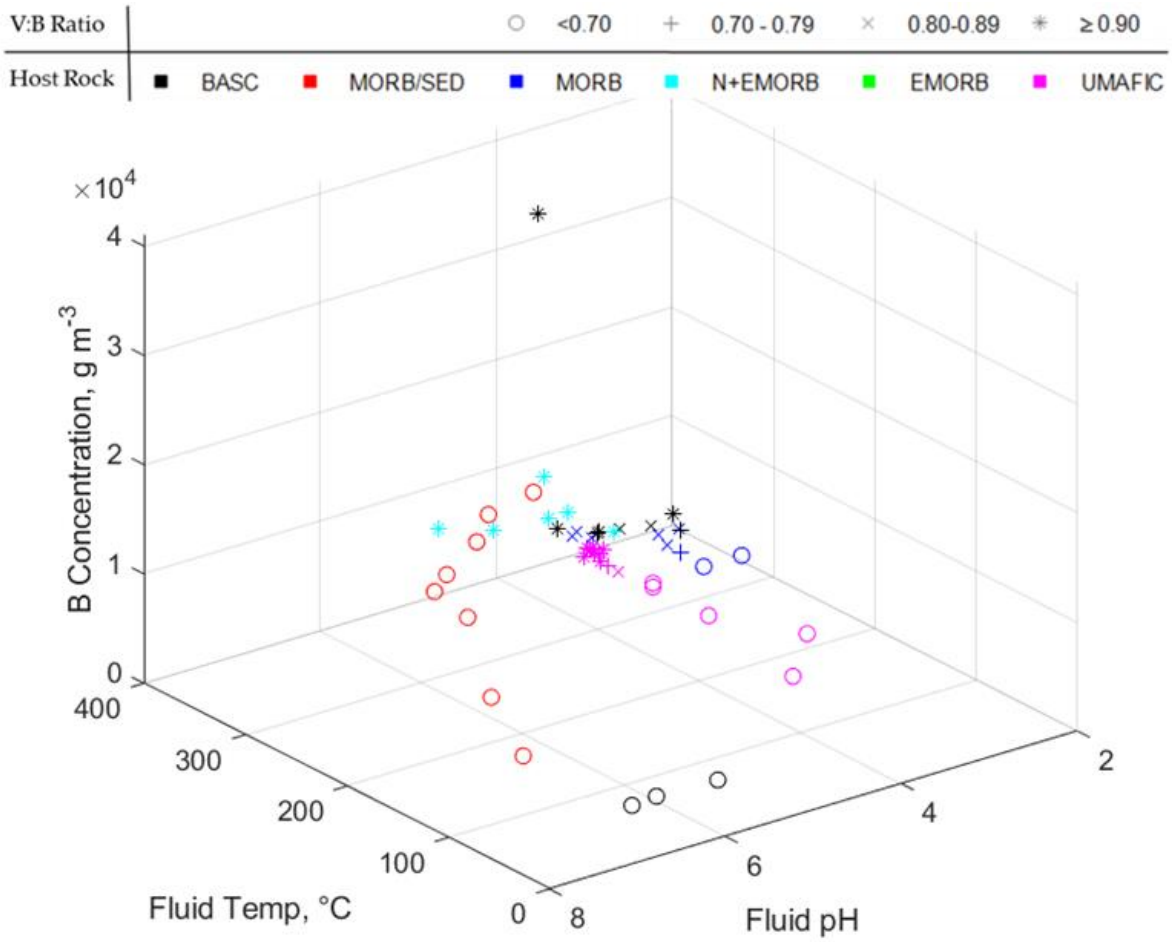

***Figure 32**: Distribution of boron concentrations in hydrothermal fluids with temperature and pH: V:B ratio interval indicated by marker type; Host Rock type indicated by marker colour*

***Table 19:** Linear correlation coefficients between common logarithm of the boron concentration of hydrothermal fluids and the pH, temperature, and V:B temperature ratios; by host rock category*

B	All	Back-Arc	M/SED	MORB	N+EMORB	EMORB	UMAFIC
pH	0.46	0.05	-0.83	0.32	-0.05		0.66
Temp	-0.19	0.14	0.74	-0.52	0.83		-0.49
V:B Ratio	-0.12	0.32	0.74	-0.45	0.69		-0.58

Boron is another lithophile element (Goldschmidt, 1937), and is subsequently slower to partition into brines, coming after bromine (Berndt & Seyfried, 1990). Like bromine, the concentrations of boron a prograde with increasing temperature and decreasing pH in the lower temperature-higher pH ‘Sedimented MORB’ category, then appear to fall at temperatures and pH seen in other categories.

See Supplementary **Figure S29** for boron temperature-concentration and pH-concentration plots.

Boron concentrations share a strong correlation with rare earth element concentrations in hydrothermal fluids ($\bar{r} = 0.89$).

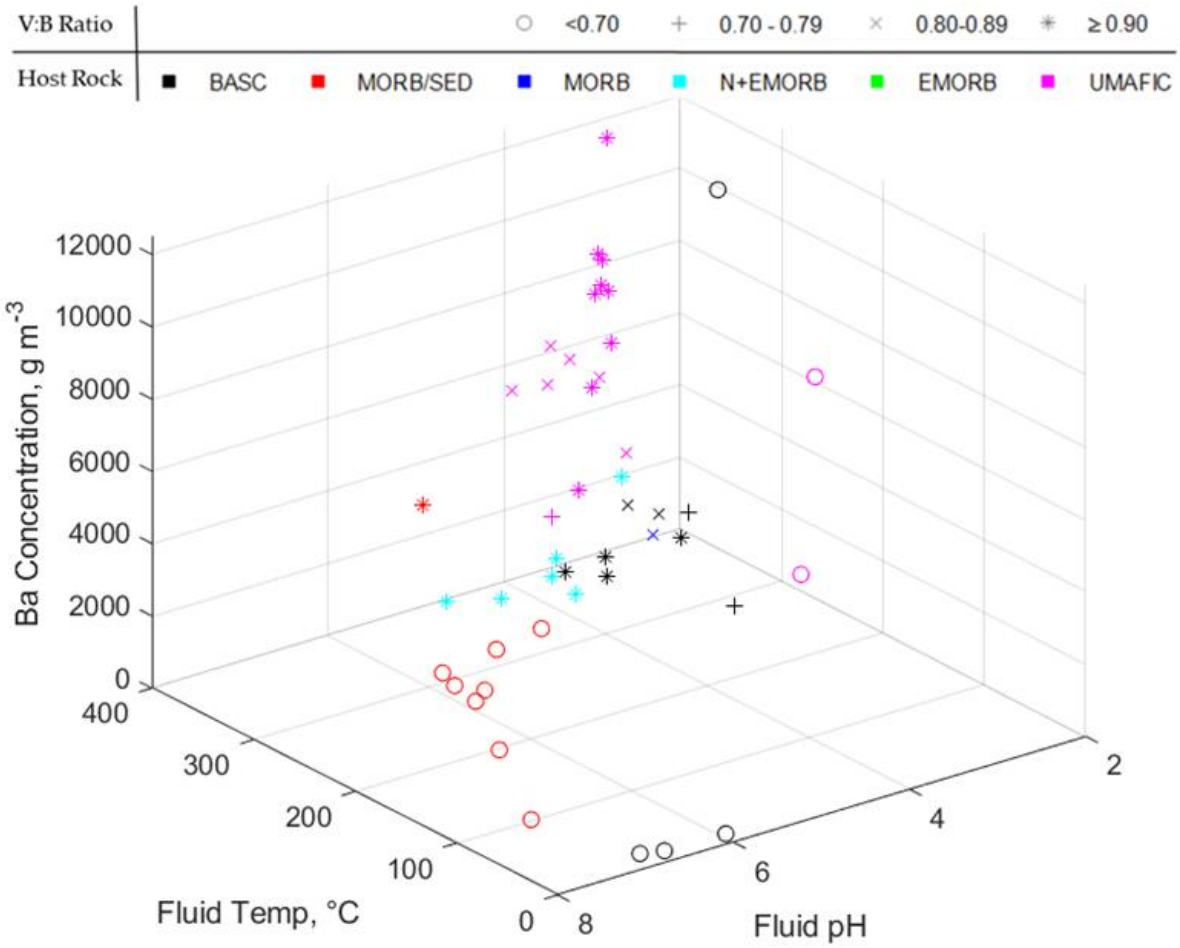

***Figure 33**: Distribution of barium concentrations in hydrothermal fluids with temperature and pH: V:B ratio interval indicated by marker type; Host Rock type indicated by marker colour*

***Table 20:** Linear correlation coefficients between common logarithm of the barium concentration of hydrothermal fluids and the pH, temperature, and V:B temperature ratios; by host rock category*

Ba	All	Back-Arc	M/SED	MORB	N+EMORB	EMORB	UMAFIC
pH	-0.58	-0.74	-0.54		-0.38		-0.33
Temp	0.14	0.68	0.67	-0.84	-0.56		0.24
V:B Ratio	0.18	0.69	0.70	-0.93	-0.32		0.30

Barium is shown experimentally to partition into brines more easily than Sr, Ca, K, Na-Cl, Li, Br and B in sequence (Berndt & Seyfried, 1990): it will be interesting to evaluate whether there are trends in the strengths of relationships (**Table 20**), given this series, in the ***Discussion*** section of this work. See Supplementary **Figure S30** for barium temperature-concentration and pH-concentration plots. Barium has a negative correlation with cadmium (r = -0.48) and a positive correlation with rare earth elements ($\bar{r} = 0.62$) in hydrothermal fluids.

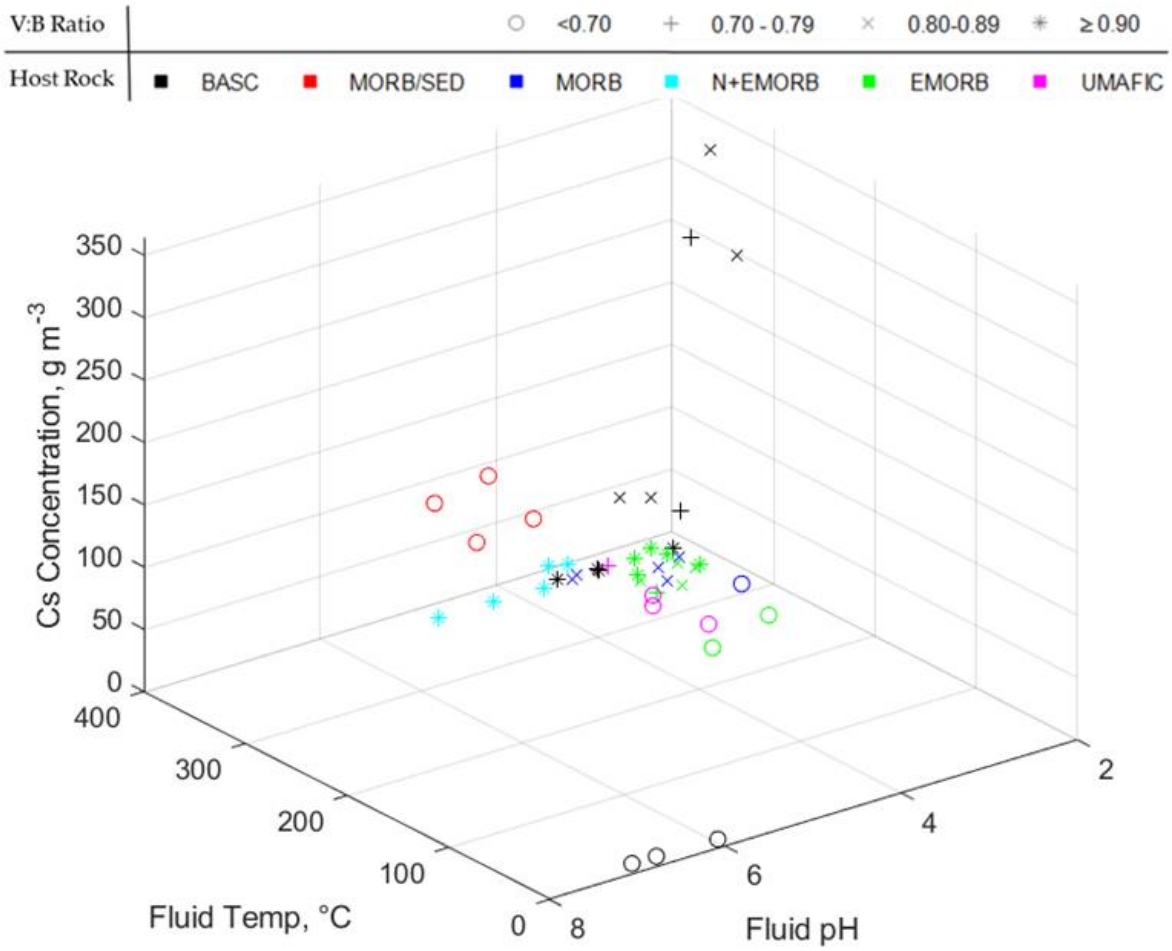

***Figure 34**: Distribution of barium concentrations in hydrothermal fluids with temperature and pH: V:B ratio interval indicated by marker type; Host Rock type indicated by marker colour.*

***Table 21:** Linear correlation coefficients between common logarithm of the caesium concentration of hydrothermal fluids and the pH, temperature, and V:B temperature ratios; by host rock category*

Cs	All	Back-Arc	M/SED	MORB	N+EMORB	EMORB	UMAFIC
pH	-0.38	-0.86	0.51	-0.58	-0.42	0.44	
Temp	-0.01	0.73	0.39	-0.59	-0.97	-0.19	0.29
V:B Ratio	0.07	0.78	0.39	-0.55	-0.97	-0.19	0.29

Caesium, a group 1 element, seems to have a similar retrograde trend as strontium beyond 350°C, compare **Figure 34** to **Figure 25**. It is also notable that the lowest average temperature host rock category, ‘Sedimented MORB’ has significantly higher concentrations than transitional, enriched and ultramafic categories.

See Supplementary **Figure S31** for caesium temperature-concentration and pH-concentration plots.

In **Table S1**, caesium is shown to have a negative correlation with lead (r = -0.55); in **Table S2**, it is shown to have a positive correlation with rare earth elements ($\bar{r} = 0.93$).

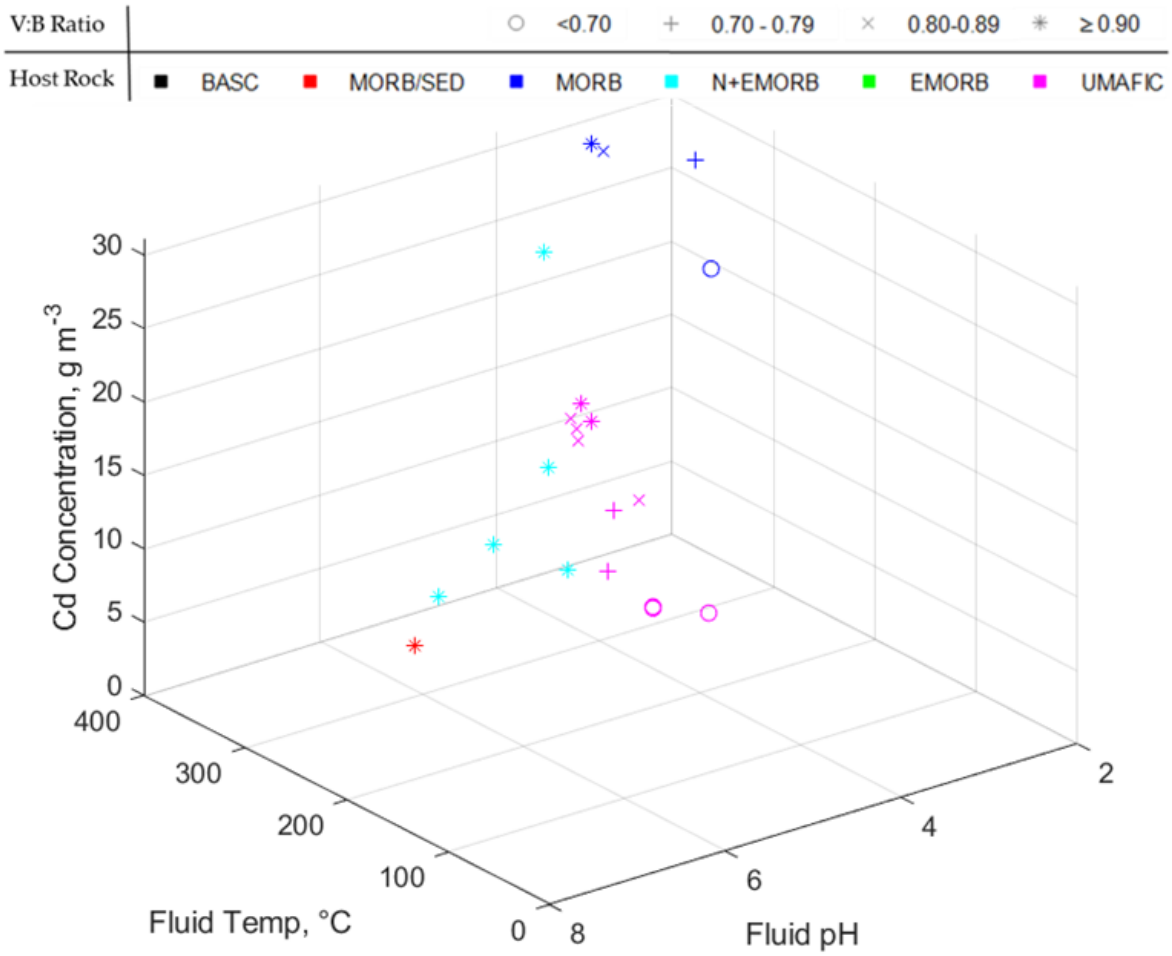

***Figure 35**: Distribution of cadmium concentrations in hydrothermal fluids with temperature and pH: V:B ratio interval indicated by marker type; Host Rock type indicated by marker colour*

***Table 22:** Linear correlation coefficients between common logarithm of the cadmium concentration of hydrothermal fluids and the pH, temperature, and V:B temperature ratios; by host rock category*

Cd	All	Back-Arc	M/SED	MORB	N+EMORB	EMORB	UMAFIC
pH	-0.58			0.08	-0.62		-0.62
Temp	0.27			-0.29	-0.01		0.74
V:B Ratio	0.14			-0.35	-0.01		0.80

Cadmium (**Figure 35**) is a critical element (Moss, et al., 2013). Although a moderately strong correlation is seen in ultramafic hosted settings, this is not the case for other host rock settings. See Supplementary **Figure S32** for cadmium temperature-concentration and pH-concentration plots. Cadmium has a strong affinity to zinc (r = 0.96), and a good affinity to the rare earth elements ($\bar{r} = 0.68$).

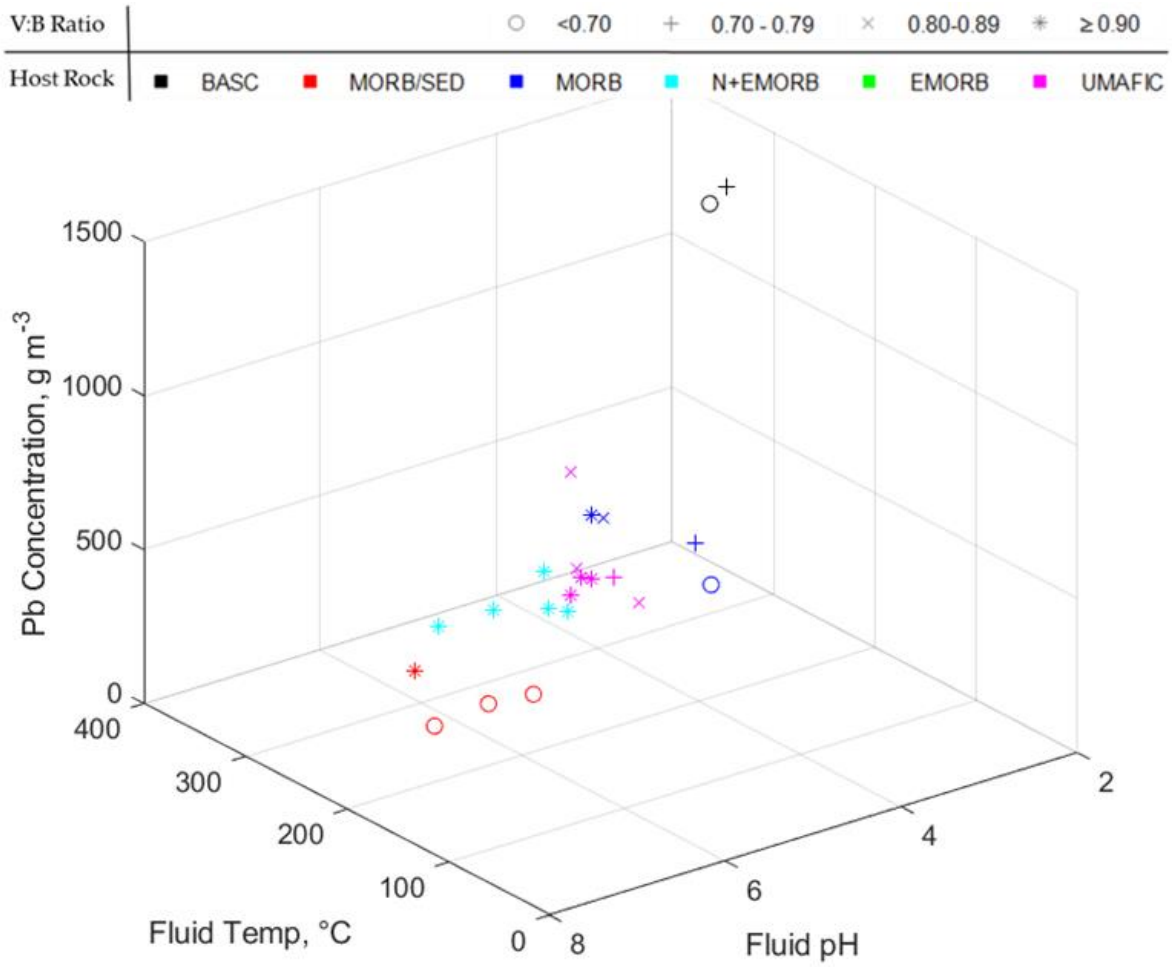

***Figure 36**: Distribution of lead concentrations in hydrothermal fluids with temperature and pH: V:B ratio interval indicated by marker type; Host Rock type indicated by marker colour*

***Table 23:** Linear correlation coefficients between common logarithm of the lead concentration of hydrothermal fluids and the pH, temperature, and V:B temperature ratios; by host rock category*

Pb	All	Back-Arc	M/SED	MORB	N+EMORB	EMORB	UMAFIC
pH	-0.51		0.50	-0.09	-0.48		-0.29
Temp	-0.22		0.91	-0.32	0.10		-0.07
V:B Ratio	-0.24		0.92	-0.38	0.10		-0.29

Lead (**Figure 36**) does not seem to have any strong reliable relationships between fluid concentration and any of the fluid characteristics analysed. See Supplementary **Figure S33** for Lead temperature-concentration and pH-concentration plots.

Lead is a critical element (Moss, et al., 2013), which does not share significant correlations with any other critical element: as seen in **Table S2**.

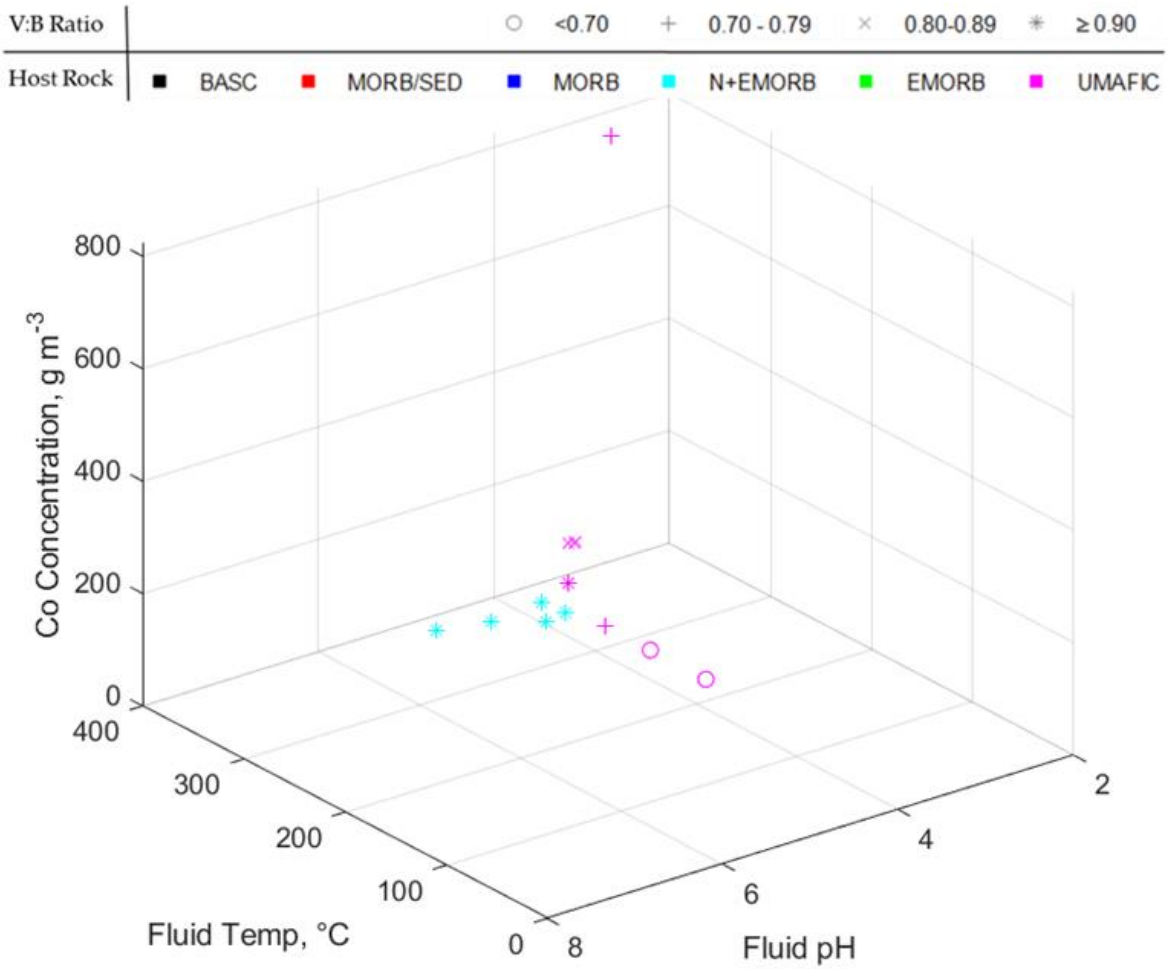

***Figure 37**: Distribution of cobalt concentrations in hydrothermal fluids with temperature and pH: V:B ratio interval indicated by marker type; Host Rock type indicated by marker colour*

***Table 24:** Linear correlation coefficients between common logarithm of the cobalt concentration of hydrothermal fluids and the pH, temperature, and V:B temperature ratios; by host rock category.*

Co	All	Back-Arc	M/SED	MORB	N+EMORB	EMORB	UMAFIC
pH	-0.23				-0.06		-0.90
Temp	0.62			-0.93	-0.80		0.84
V:B Ratio	0.42			-0.89	-0.80		0.70

Cobalt is shown to have elevated fluid concentrations only at temperatures above 340°C, seen in **Figure 37** and **Figure S34**. Cobalt is medium-level critical element (Moss, et al., 2013), which shares positive correlations to copper (r = 0.93); molybdenum (r = 0.83); neodymium (r = 0.91); and rare earth elements ($\bar{r} = 0.73$).

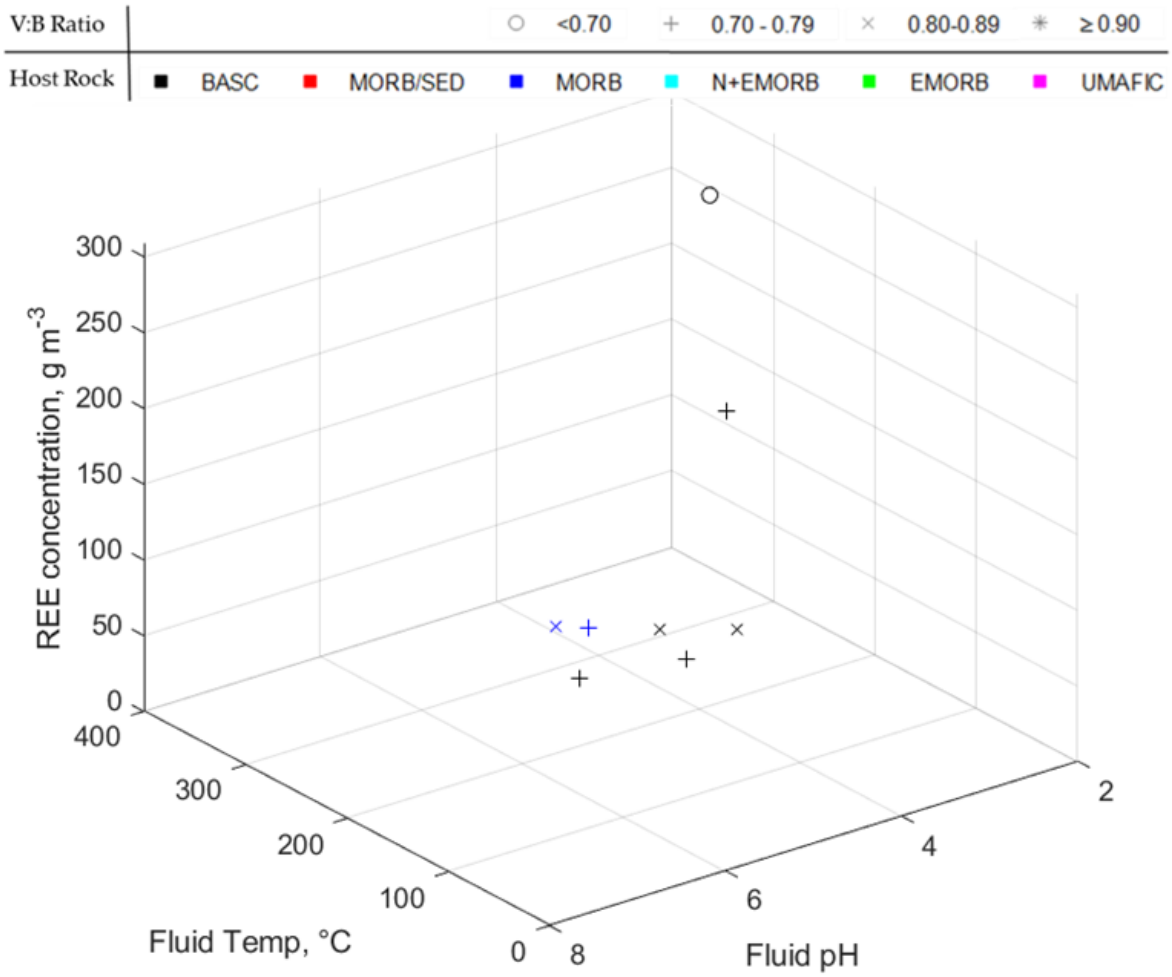

***Figure 38**: Distribution of cobalt concentrations in hydrothermal fluids with temperature and pH: V:B ratio interval indicated by marker type; Host Rock type indicated by marker colour*

***Table 24:** Linear correlation coefficients between common logarithm of the REE concentration of hydrothermal fluids and the pH, temperature, and V:B temperature ratios; by host rock category*

REE	All	Back-Arc	M/SED	MORB	N+EMORB	EMORB	UMAFIC
pH		-0.23					
Temp	-0.57	-0.23		-0.88			
V:B Ratio	-0.50	-0.23		-0.79			

The paucity of data on rare earth element abundances in hydrothermal fluid is the reason the elements are analysed as a group in this work.

Given these very small datasets, there is no apparent relationships between abundance and the fluid characteristics analysed.

4.3.0 Deposit Data

The following section summarises the raw concentrations of hydrothermal deposits, as **Table 25**, and strength of correlations found between elements, in **Table S3** and **Table S4**. Correlation tables are again divided into relationships excluding rare earth elements, and exclusively including rare earth elements, respectively.

Table 25: *Statistical summary of hydrothermal deposit concentrations by element in kilograms per cubic metre.*

	Au	Ag	As	B	Ba	Br	Ca	Cd	Ce
Count	940	1050	932	52	878	271	913	744	275
Minimum	1.00E-05	2.50E-01	5.00E-02	1.00E+00	8.60E-02	2.50E-01	2.00E-02	3.00E-01	5.00E-02
Average	3.72E+00	1.15E+02	1.19E+03	2.28E+01	1.61E+04	8.41E+00	2.80E+04	1.88E+03	4.09E+00
Maximum	9.36E+01	1.40E+04	2.94E+05	1.10E+02	4.76E+05	1.00E+02	4.72E+05	1.88E+05	2.00E+02
St. Deviation	9.04E+00	4.88E+02	1.01E+04	2.48E+01	5.52E+04	1.24E+01	6.29E+04	1.39E+04	1.28E+01
St. Deviation	243%	424%	842%	109%	342%	148%	225%	740%	314%

		Cl	Co	Cs	Cu	Dy	Er	Eu	Fe
Count	*units*	54	1055	308	1034	131	131	284	1085
Minimum	$kg\ m^{-3}$	5.00E-02	5.00E-01	8.00E-03	2.98E+00	1.00E-02	2.00E-02	4.00E-03	3.60E+02
Average	$kg\ m^{-3}$	1.99E+03	2.11E+03	9.05E-01	5.14E+04	5.51E-01	3.19E-01	3.65E-01	2.74E+05
Maximum	$kg\ m^{-3}$	8.90E+03	4.80E+05	1.31E+02	6.83E+05	6.13E+00	3.69E+00	6.70E+00	1.09E+06
St. Deviation	$kg\ m^{-3}$	2.19E+03	2.68E+04	7.46E+00	9.64E+04	1.42E+00	8.57E-01	6.39E-01	1.47E+05
St. Deviation	*percent*	110%	1274%	825%	187%	258%	269%	175%	53%

		Gd	Hf	Hg	Ho	La	Li	Lu	Mn
Count	*units*	131	268	370	131	368	38	241	793
Minimum	$kg\ m^{-3}$	2.00E-02	1.00E-02	3.00E-02	2.00E-02	1.00E-01	1.50E-02	2.00E-02	1.00E-02
Average	$kg\ m^{-3}$	5.26E-01	7.10E-01	9.99E+00	1.22E-01	2.13E+02	4.89E-01	5.44E-02	3.31E+07
Maximum	$kg\ m^{-3}$	5.58E+00	3.95E+00	2.70E+02	1.30E+00	7.40E+03	4.03E+00	5.31E-01	5.92E+09
St. Deviation	$kg\ m^{-3}$	1.25E+00	7.24E-01	1.99E+01	2.99E-01	7.51E+02	8.73E-01	8.51E-02	3.94E+08
St. Deviation	*percent*	237%	102%	199%	245%	352%	179%	156%	1189%

		Mo	Nb	Nd	Ni	Pb	Pd	Pr	Rb
Count	*units*	891	203	241	810	981	1	132	381
Minimum	$kg\ m^{-3}$	5.00E-01	7.00E-03	1.00E-01	1.53E-01	3.00E-02	2.10E+00	2.00E-02	2.30E-02
Average	$kg\ m^{-3}$	8.33E+01	1.93E+00	4.21E+00	8.53E+02	1.65E+04	2.10E+00	1.55E+00	1.57E+01
Maximum	$kg\ m^{-3}$	2.35E+03	3.50E+01	2.00E+02	1.57E+05	1.76E+06	2.10E+00	1.55E+02	1.58E+02
St. Deviation	$kg\ m^{-3}$	1.42E+02	5.62E+00	1.31E+01	8.48E+03	8.62E+04	#DIV/0!	1.35E+01	2.12E+01
St. Deviation	*percent*	171%	291%	310%	994%	522%	#DIV/0!	868%	135%

		Sm	Sr	Ta	Tb	V	Y	Yb	Zn
Count	*units*	278	783	247	273	471	331	340	1143
Minimum	$kg\ m^{-3}$	2.00E-02	1.00E+00	5.00E-02	2.00E-02	1.71E-01	7.00E-03	5.00E-02	2.00E+00
Average	$kg\ m^{-3}$	4.82E-01	4.72E+02	9.87E-01	3.80E+00	3.38E+01	3.96E+00	4.59E-01	7.14E+04
Maximum	$kg\ m^{-3}$	4.63E+00	9.40E+03	7.55E+01	9.60E+02	4.00E+02	5.00E+01	3.55E+00	5.80E+05
St. Deviation	$kg\ m^{-3}$	8.58E-01	1.02E+03	4.78E+00	5.81E+01	5.77E+01	6.15E+00	6.91E-01	1.35E+05
St. Deviation	*percent*	178%	216%	484%	1530%	170%	156%	150%	189%

4.3.1 Processing Deposit Data

Standard deviation as a percent of the average element concentration - is an interesting point of comparison between hydrothermal fluid (**Table 4**) and deposit geochemistry (**Table 25**). This is compared in **Figure 39**: where deposit standard deviation (as a percent of the elemental mean concentration) is shown is the positive x-axis; and fluid standard deviation (as a percent of the elemental mean concentration) is shown is the negative x-axis. The order of elements in the y-axis will sort elements which have more variation in deposits than in fluids at the top, to *Vice versa* at the bottom.

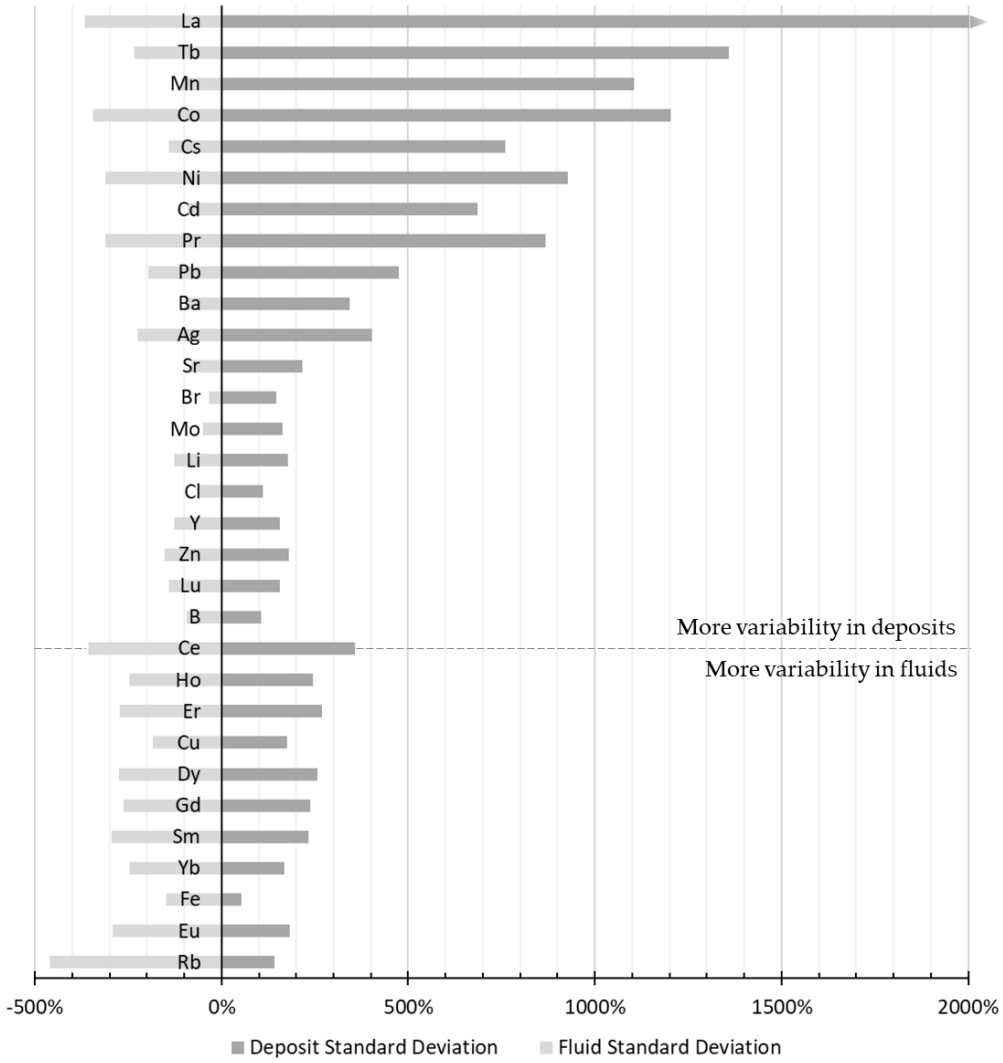

Figure 39: *Standard deviation as a percent of the average element concentration. Deposit standard deviation is shown is the positive x-axis; and fluid standard deviation is shown is the negative x-axis.*

This work has presented that variability in fluid chemistry is determined by the “budget” of the host rock, and the efficacy of hydrothermal transport. If deposit chemistry were determined only by fluid chemistry, no elements would be expected to be present with more variability in the deposit than in the fluid. The distribution of elements with a greater variability in the deposits, than in fluids, might be influenced more by secondary enrichment processes than by primary hydrothermal transport.

In the scope of this work, commenting on the role of enrichment is a challenge.

On one hand, it might be possible to consider an idealised model of a deposit, and qualitatively interpret whether a sample is enriched depending on where from the deposit it was collected. For example, a surface grab or chimney sample is likely more enriched than a deeper core sample.

On the other: notwithstanding a paucity in compositional data, yet alone isotope data, perhaps a rudimentary elemental ratio might indicate a degree of enrichment. The Scheuermann series observes the order in which metals are enriched in volcanogenic massive sulphides: stated as palladium, (mercury,) silver, copper, bismuth, cadmium, lead, zinc, nickel, cobalt, iron, thallium, and manganese (Emmons, 1917). Iron-Manganese ratios are used when discussing ferromanganese crusts and polymetallic nodules: in these examples, a Fe/Mn ratio of greater than five indicates nodules are primarily diagenetically enriched, rather than hydrogenetically enriched (Kuhn, et al., 2018).

Figure 40 is annotated version of the idealised model of a deposit, see **Figure 11** (p.15) (Lyndon, 1988). To demonstrate the difference in enrichment observed in materials collected by different methods (chimney/core/surface/other), this work has averaged the Fe/Mn ratio of samples collected by category for each of the 26 systems. **Table 26** shows the mean Fe/Mn average ± standard deviation and count (in brackets) for each category of sample in each system. In blue, a ‘normalised’ mean Fe/Mn ratio is calculated by dividing the mean categorised deposit Fe/Mn ratio by the average Fe/Mn ratio of the systems hydrothermal fluid. By considering the degree of enrichment relative to the fluid composition, enrichment can be compared between systems.

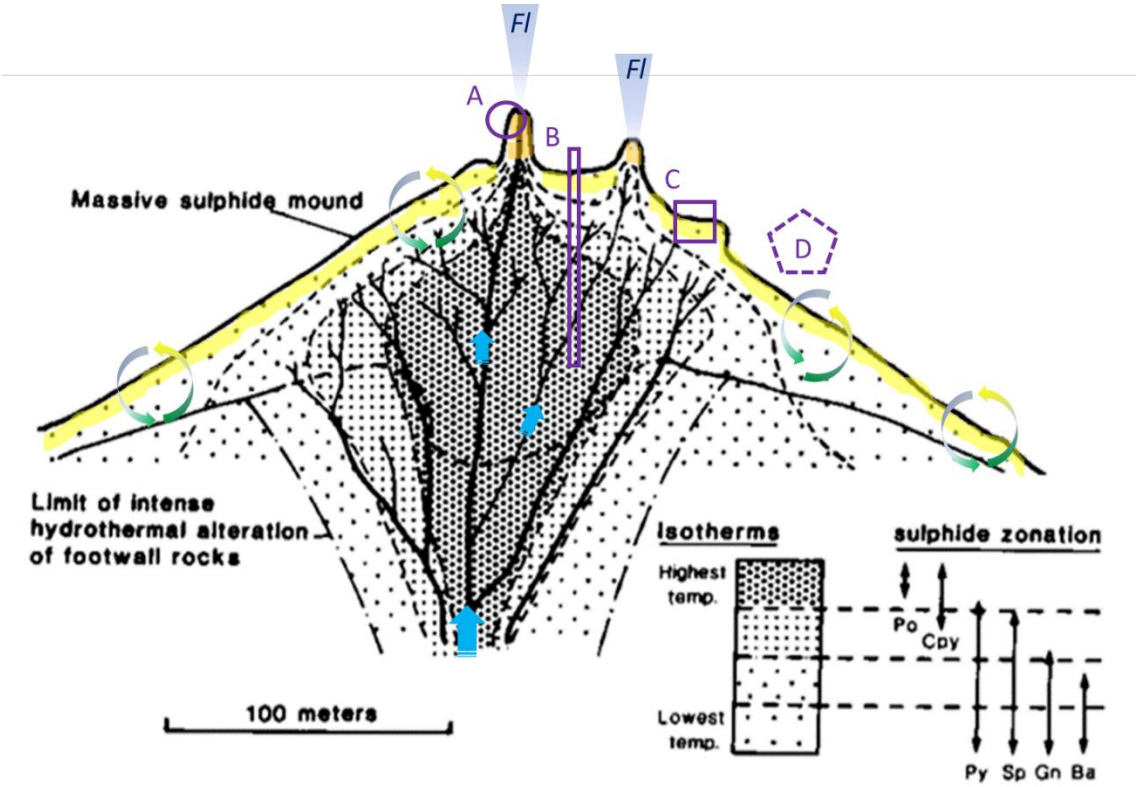

***Figure 40**: Idealised mineral zonation of a submarine hydrothermal deposit, showing a direct relationship between mineralisation and average maximum isotherms, assuming ore metals were dominantly present as chloride complexes. Po, pyrrhotite; Cpy, chalcopyrite; Py, pyrite; Sp, sphalerite; Gn, galena; Ba, baryte. (Lyndon, 1988). Annotated to include entrainment of seawater into deposit, and enrichment processes, indicated by cycled arrows; enriched surface and chimney mineralogy, indicated by highlighted margins; and how sampling techniques may recover a range of depleted to highly enriched samples. Fl, fluid; A, chimney samples; B, core samples; C, surface/grab/dredge samples; and D, other/miscellaneous/overall average samples.*

Table 26: *Mean ± Standard Deviation (Count) of Fe/Mn ratios, given to compare the degree of enrichment between hydrothermal deposit sampled from the chimneys, cores, surface, and 'other' types. "Normalised" Fe/Mn ratios refer to the Fe/Mn ratio relative to the Fe/Mn ratio of the systems' hydrothermal fluid.*

Fe/Mn Ratio	Chimney	Core	Surface	All (Inc. Other)
Endeavour	3.28E+03 ± 6.91E+03 (35) *7.91E+02 (Normalised)*	4.19E+02 ± 1.01E+02 (2) *1.01E+02 (Normalised)*	2.83E+03 ± 3.32E+03 (42) *6.83E+02 (Normalised)*	2.93E+03 ± 5.16E+03 (79) *7.08E+02 (Normalised)*
Beebe	1.79E+04 ± 1.48E+04 (13) *1.21E+03 (Normalised)*	1.19E+03 ± 1.48E+03 (10) *8.06E+01 (Normalised)*	6.76E+03 ± 1.43E+04 (16) *4.56E+02 (Normalised)*	9.31E+03 ± 1.40E+04 (39) *6.29E+02 (Normalised)*
Logatchev	3.03E+03 ± 2.40E+03 (7) *4.57E+02 (Normalised)*	-	2.95E+03 ± 3.48E+03 (52) *4.45E+02 (Normailsed)*	3.19E+03 ± 3.29E+03 (*59+3*) *4.81E+02 (Normalised)*
TAG	2.00E-01 ± 2.52E-01 (37) *3.83E-02 (Normalised)*	4.11E-01 ± 1.29E-01 (160) *7.85E-02 (Normalised)*	2.64E-01 ± 2.71E-01 (122) *5.04E-02 (Normalised)*	3.38E-01 ± 2.24E-01 (*319+1*) *6.47E-02 (Normalised)*
Snake Pit	4.35E+03 ± 3.69E+03 (18) *8.51E+02 (Normalised)*	2.64E+03 ± 6.09E+03 (13) *5.16E+02 (Normailised)*	4.67E+03 ± 3.43E+03 (75) *9.14E+02 (Normalised)*	4.48E+03 ± 3.94E+03 (106) *8.77E+02 (Normalised)*
Broken Spur	3.09E+03 ± 3.77E+03 (10) *3.93E+02 (Normalised)*	-	6.33E+06 ± 2.28E+06 (8) *8.04E+05 (Normalised)*	5.52E+03 ± 9.37E+03 (*18+4*) *7.01E+02 (Normalised)*
Guaymas Basin	3.61E+00 ± 6.71E+00 (6) *7.03E+00 (Normalised)*	-	7.48E+02 ± 7.33E+01 (7) *1.46E+03 (Normalised)*	1.74E+01 ± 1.53E+03 (*13+1*) *3.39E+01 (Normalised)*
ASHES	5.63E+02 ± 7.77E+02 (47) *1.44E+00 (Normalised)*	-	-	5.43E+02 ± 7.67E+02 (*47+2*) *1.39E+00 (Normalised)*
North Cleft	7.90E+02 ± 5.47E+02 (20) *2.83E+02 (Normalised)*	-	-	-
Pacmanus	2.67E+03 ± 2.75E+03 (2) *5.67E+03 (Normalised)*	-	-	-
Middle Valley	5.58E+02 ± 1.35E+03 (8) *1.11E+03 (Normalised)*	4.99E+03 ± 7.39E+03 (42) *9.89E+03 (Normalised)*	4.71E+02 ± 6.74E+02 (3) *9.34E+02 (Normalised)*	2.93E+03 ± 6.78E+03 (*53+1*) *5.81E +03 (Normalised)*

As there is an absence of either iron or manganese abundance data to produce a deposit Fe/Mn ratio, the following systems are not included in **Table 26**: Edmond; ESR E9; Longqi; Rehu Marka; Nibelungen; Rainbow; Kairei; Alarcon Rise; ESR E2; Kulo Lasi; Lucky Strike; Auka; and Minami-Ensi.

The Vienna Woods system is not included in **Table 26**, as an absence in fluid iron or manganese data prevents a normalised ratio from being given.

Secondary processes clearly redistribute minerals in submarine hydrothermal deposits. The normalised Fe/Mn ratios indicate that these deposits are, generally, significantly enriched within the chimneys and the surface samples. As these types of samples are the most accessible, but not necessarily representative of the complete deposit, referring to them alone may produce inflated metal abundances for resource estimation.

The ethos of this work is to evaluate whether the impact of exploiting submarine hydrothermal systems, for critical minerals, can be minimised. In categorising parts of deposits and comparing their metal abundance to that of fluid concentrations: the links may be more direct. There is also the opportunity that, if these analyses identify that a metal is usually found in the surface of a deposit, rather than the chimney: the focus of exploration and exploitation may adapt.

4.4.0 Relationships Between Deposit Sample Types

This section will determine whether there may be relationships between the abundance of elements in chimney deposits, surface deposits and those observed in cores. **Table 27** provides a summary the strengths and trends of relationships between abundances in chimney, surface and core type samples, after anomalies are removed.

Graphs are provided for Chimney-Core and Surface-Core concentration distributions in Supplementary **Figure S36** – **S49**.

Table 27: *Strengths of relationships between observed concentrations from different sample types across the twenty-six systems.*

	Chimney-Core	Chimney-Surface	Surface-Core
Au	y = 0.3058x	y = 0.3096x	y = 1.5246x
Ag	y = 0.3338x	y = 0.2044x	y = 1.5076x
As	y = 1.3705x	y = 0.3157x	y = 1.4618x
Ba	y = 0.1283x	y = 0.4903	y = 0.0273x
Br		y = 0.8601x,	
Ca			y = 0.715x
Cd	y = 0.7003x		y = 0.5794x
Ce		y = 0.7011x	
Co		y = 0.0236x	y = 1.5803x
Cs		y = 1.1341x	
Cu	y = 0.5877x	y = 0.695x	y = 1.1307x
Eu		y = 1.0672x	
Fe	y = 0.1896x + 301.59	y = 0.7655x + 114.62	y = 0.2294x + 272.57
Hg		y = 0.8429x	
La		y = 0.4961x	
Mo	y = 1.2307x	y = 2.9652x	
Nb		y = 1.1179x	
Ni		y = 1.3986x	
Pb	y = 0.2633x	y = 0.8422x	y = 1.9465x
Rb		y = 0.9277x	
Sm		y = 0.7179x	
Sr	y = 0.1848x	y = 0.5806x	
V		y = 1.041x	
Y		y = 1.0641x	
Yb		y = 0.9979x	
Zn		y = 0.4896x	y = 1.1472x

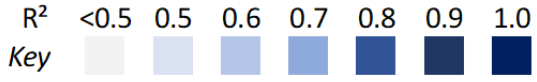

4.5.0 Relationships Between Fluid and Deposit Geochemistry

This project set out to determine whether the geochemistry of submarine hydrothermal deposits could be inferred by the geochemistry of hydrothermal fluids. A meritable 707 global systems (Beaulieu, et al., 2013), were reduced to a mere twenty-six.

The short answer: there is not enough data. Ergo, the long answer is found in asking the question: how much can this work maximise the value of the data already analysed?

Table 28 provides a count of datapoints between fluid geochemistry and each deposit sample type geochemistry. This work will set an unusually low bar for number of data points and recognises that these are presented with less-than-ideal confidence. Distributions with less than four datapoints are hereby discarded.

Table 28: *Number of datapoints observed for submarine hydrothermal systems with corresponding fluid and deposit category data, for each element. Elements with less than four datapoints are discarded in the following analyses.*

No. of datapoints:	Chimneys	Cores	Surface
16	Ca; Fe		
15			
14	Cu		Cu
13			
12			Fe
11	Mn		Ca; Mn; Zn
10	Zn		
9	Ba		Sr
8	Sr		Ba
7			Pb
6	Cd; Pb	Ca; Cu; Fe; Mn	Cd; Rb
5			Co
4	Br; Co; Rb		Br; Cs
3		Ba; Pb; Rb; Sr; Zn	B
2	B; Cl; Cs	Cd; Co	Cl; La; Mo; Ni
1	Ce; Eu; La; Li; Lu; Mo; Nd; Ni; Sm; Y; Yb	Br; Ce; Cs; Li; Mo; Ni	Ce; Eu; Li; Lu; Nb; Nd; Sm; V; Yb
0	Nb; V	B; Cl; Eu; La; Lu; Nb; Nd; Sm; V; Y; Yb	Y
nil: Au; Ag; As; Dy; Er; Gd; Hf; Hg; Ho; Pd; Pr; Ta; Tb			

No trends are observed in the fluid-deposit barium distribution: barium is rejected.

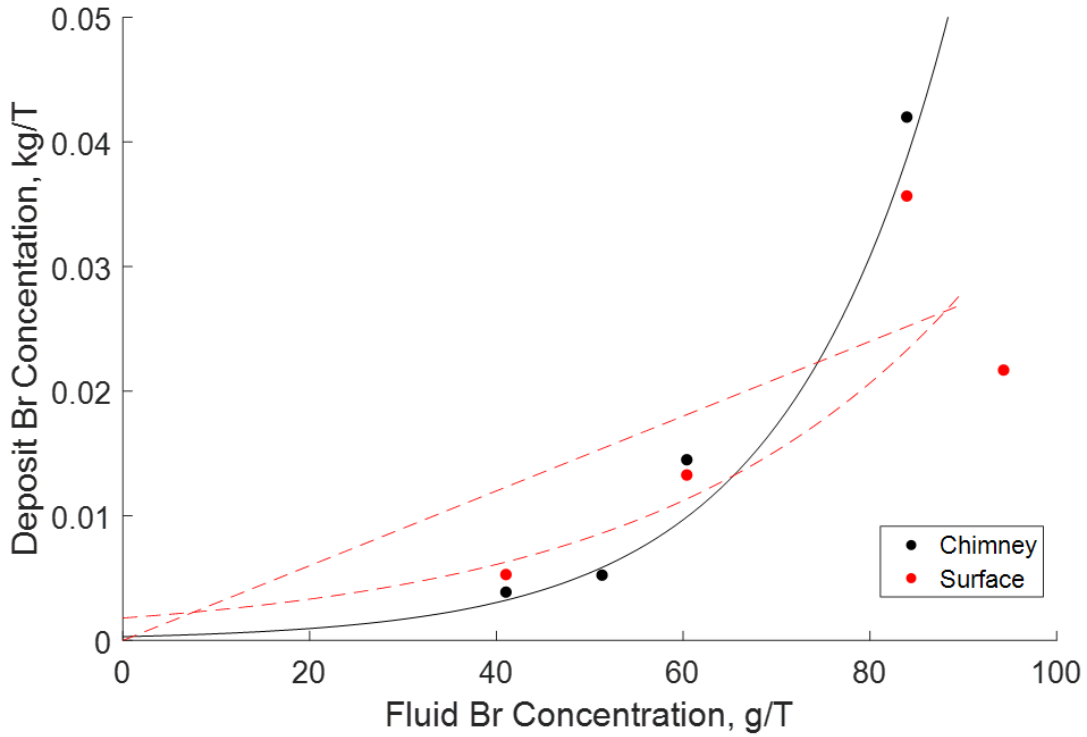

Figure 41: *Distribution of bromine average Chimney and Surface deposit abundance with fluid barium concentration. Chimney data (black) seem to follow the exponential curve (black line), $y = 0.0003e^{(0.0579x)}$, with an R^2 value of 0.9861.*

The distribution of surface data (red) is less obvious. Following an exponential trend, $y = 0.0018e^{0.0305x}$, the R^2 value is 0.5151; however, a linear fit following $y = 0.0003x$, has a R^2 of 0.8864. Both lines of best fit are dashed red.

Bromine follows a fairly strong, albeit low confidence, relationship between fluid and deposit geochemistry data, see **Figure 41**. Bromine itself is not a critical element, but it does have reasonably high R^2 values for fluids: cadmium (0.59); caesium (0.56); and rare earth elements.

In terms of deposits, a much larger dataset, bromine has a relatively high R^2 with cerium (0.54); europium (0.55); lanthanum (0.50); neodymium (0.52) and samarium (0.53).

Bromine is classified as a lithophile element (Goldschmidt, 1937).

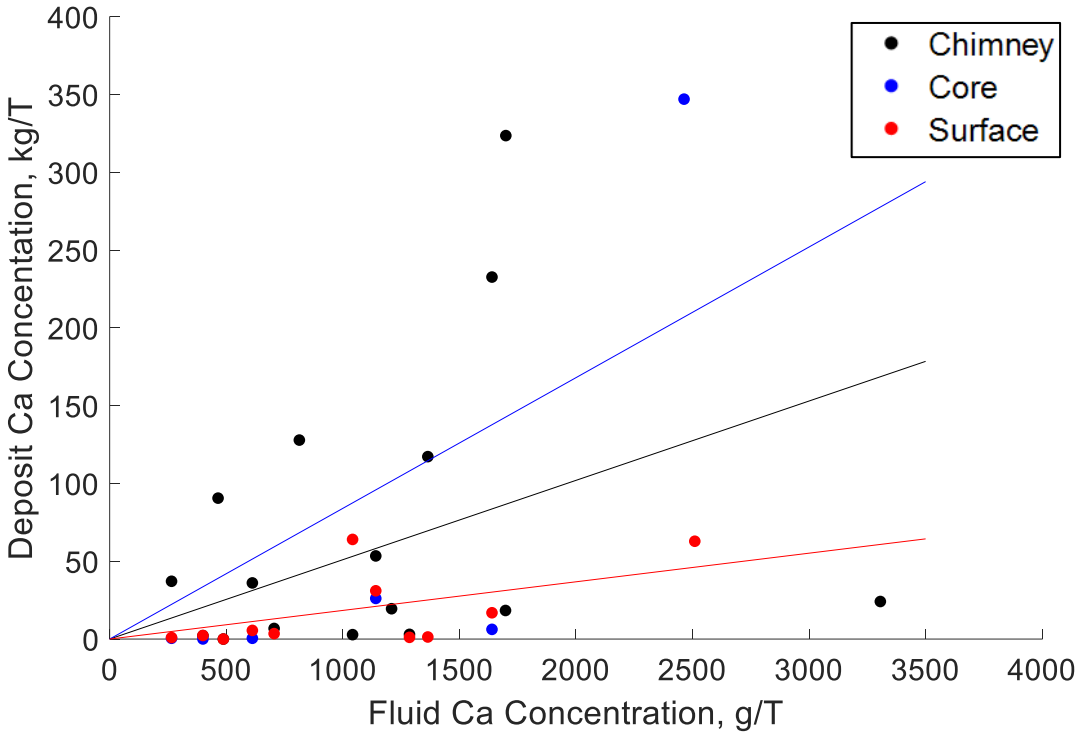

Figure 42: *Distribution of calcium average Chimney, Core and Surface deposit abundance with fluid calcium concentration. Chimney data (black) is fit to the line y = 0.051x, with an R^2 value of 0.3693. Core data (blue) is fit to the line y = 0.084x, with an R^2 value of 0.6205. Surface data (red) is fit to the line y = 0.0184x, with an R^2 value of 0.5845.*

Calcium has a positive trend between fluid and deposit abundance, see **Figure 42**. The variation is likely a factor of temperature: as anhydrite, calcium sulphate, has retrograde solubility over 150°C (Humphris & Bach, 2005). Those data with high fluid/low deposit concentrations are likely cooler venting systems.

No trends are observed in Cobalt or Caesium, these are both rejected.

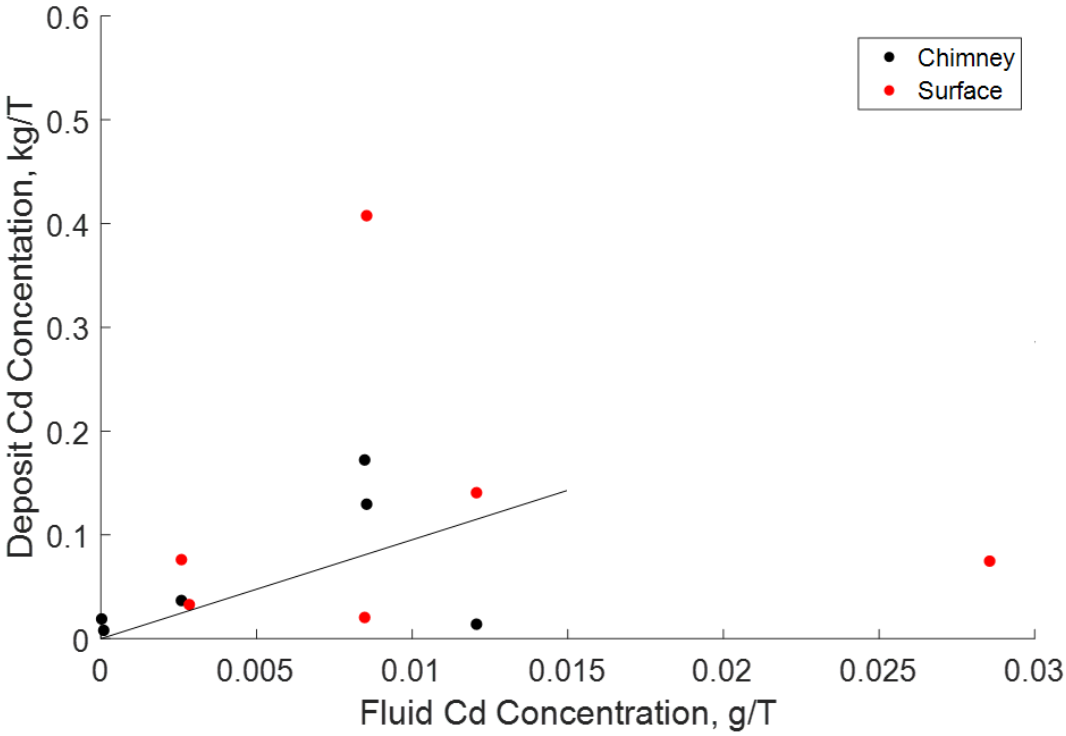

Figure 43: *Distribution of cadmium average Chimney and Surface deposit abundance with fluid cadmium concentration. Chimney data (black) is fit to the line y = 9.5313x, with an R^2 value of 0.557. No surface trend is observed.*

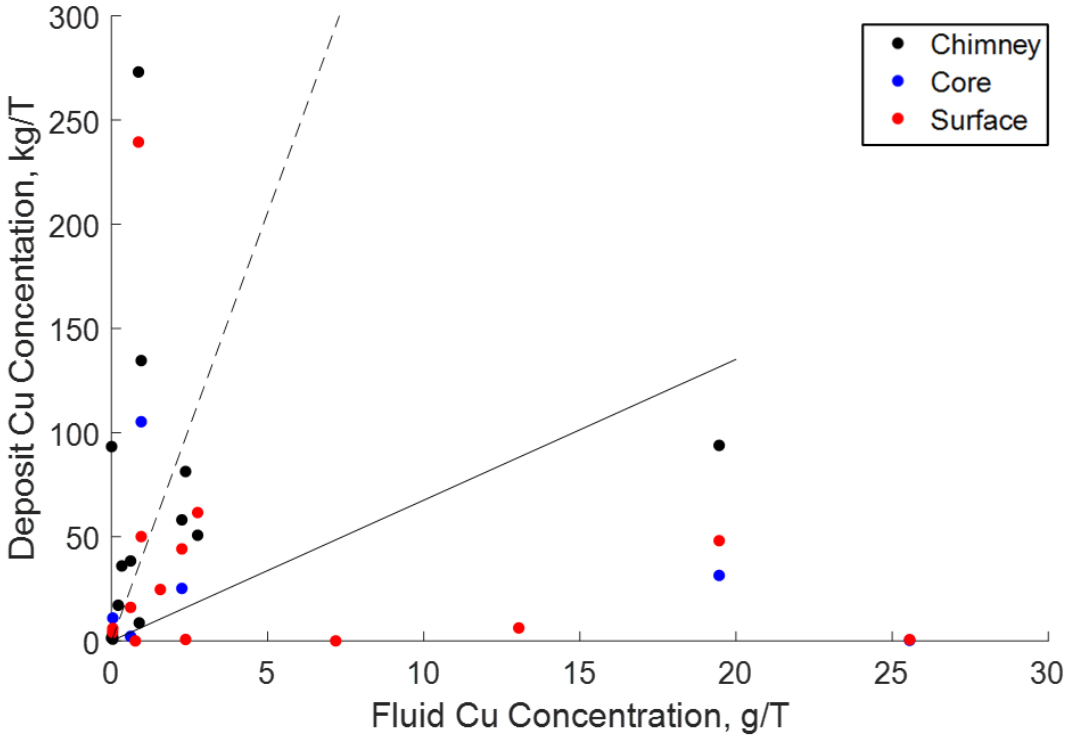

Figure 44: *Distribution of copper average Chimney, Core and Surface deposit abundance with fluid copper concentration. Chimney data (black) is fit to the line y = 6.7573x, with an R^2 value of 0.1451. Identifying Beebe, the supercritical venting system, as a high fluid concentration anomaly – the trend indicated by the dashed line is increased to y = 41.108x, with an R^2 value of 0.3077.*

No trends in Core or Surface data.

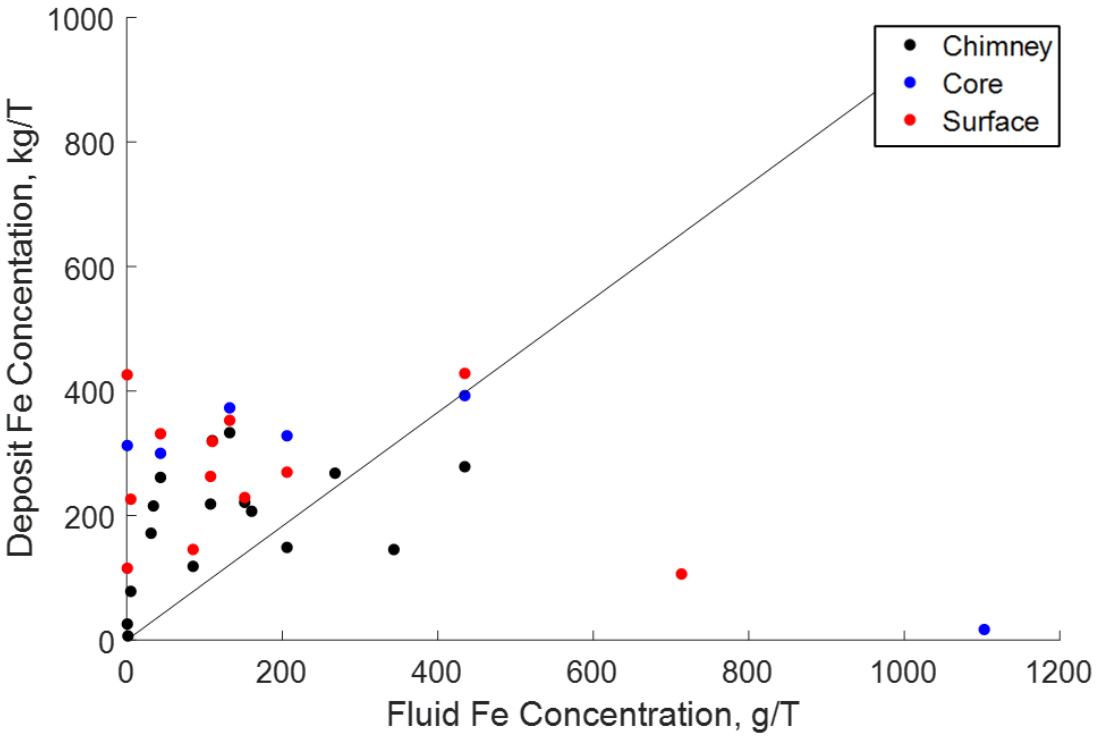

Figure 48: *Distribution of iron average Chimney, Core and Surface deposit abundance with fluid iron concentration. Chimney data (black) is fit to the line y = 0.9146x, with an R^2 value of 0.6145.*

No trends in Core or Surface data.

Manganese; Lead; Strontium; and Rubidium have no notable relationships between fluid and deposit data, they are all rejected.

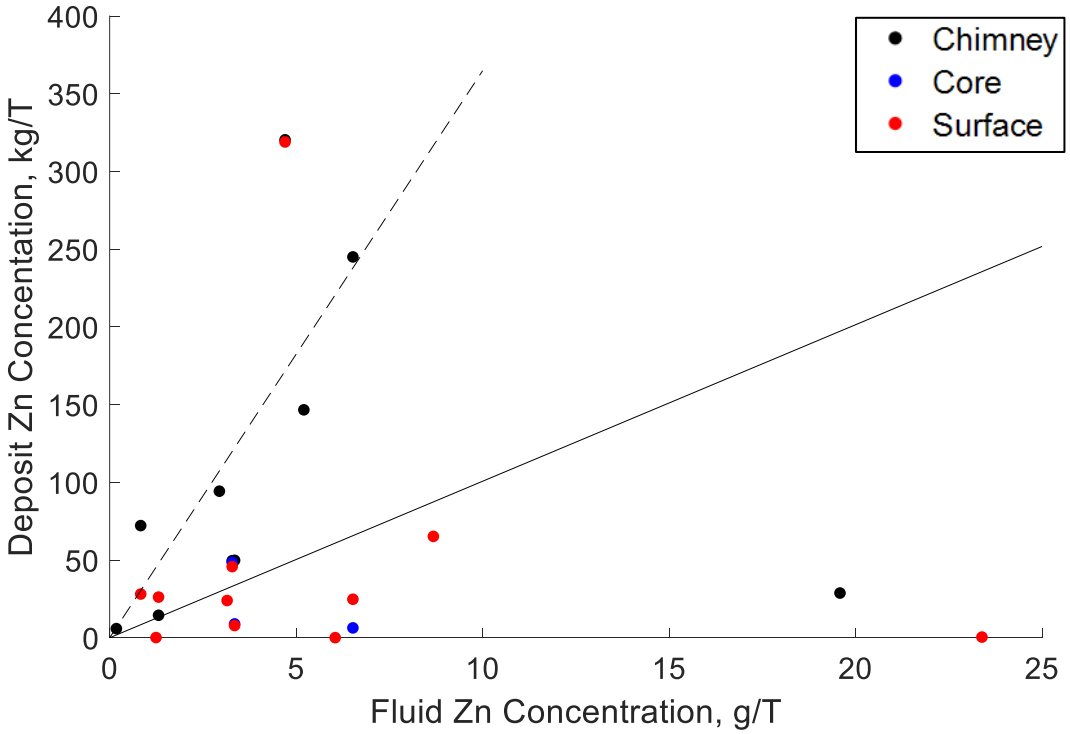

Figure 49: *Distribution of Zinc average Chimney, Core and Surface deposit abundance with fluid iron concentration. Chimney data (black) is fit to the line y = 10.071x, with an R^2 value of 0.2524. Identifying Lucky Strike as an anomaly, the dashed line represents a reviewed relationship as y = 36.483x, with an R^2 value of 0.8168.*

The trends between fluid and deposit chemistry are strongest between fluid and chimney-type sample chemistry. These analyses represent positive trends between fluid and deposit chemistry for lithophile, siderophile and chalcophile elements.

There are clearly anomalies in these relationships for example, Lucky Strike for zinc, and Beebe for copper. Ideally, if both variables have a normal distribution of data, a line of best fit for a trend would have 50% of data above the line, and 50% below.

As the data on both fluid and deposit chemistry increases, it may be possible in the future to provide 50th percentile figures to estimate chimney concentrations from fluid concentrations. Then to use estimations based on inter-element concentration trends, and trends between concentrations at different parts of the deposit. However, at the levels of confidence this work can achieve, due to the paucity of data, the relationships are worth little more than a fermi approximation.

EXPERIMENTAL SECTION

5.1.0 Purpose of Experiments

This section addresses the enrichment of copper minerals in hydrothermal environments. The purpose of these experiments is to identify the reaction mechanisms in copper mineralisation. This work used temperature, copper concentration and mineral reactants as independent variables.

Copper is transported as Cu^{1+} cations in primary hydrothermal fluids (Xiao, et al., 1998; Fulton, et al., 2000; Liu, et al., 2001; Brugger, et al., 2007; Sherman, 2007; Schmidt, et al., 2018): however Cu^{2+} is more stable at low temperatures, thus is more pertinent in reactions involved in secondary sulphide enrichment (Reich & Vasconcelos, 2015; Cowper & Rickard, 1989). Therefore, this study uses copper sulphate ($CuSO_4$) solutions. Reactions are run at 50, 100 and 200°C, and at 0.005, 0.010 and 0.050M.

The mechanism of copper mineralisation – which manifests as a sequence of phases - has been queried for over a century:

Zies, *et. al.* (1916) (p. 500) found that pyrrhotite alters to chalcopyrite in 5% $CuSO_4$ solution at 40, 100 and 200°C, then with an excess of copper in solution, subsequently to bornite; covellite; chalcocite; native copper; and copper oxides. The same work also found that pyrite alters to covellite and subsequently chalcocite.

Shouten (1934) found that pyrrhotite was altered to chalcopyrite, bornite and chalcocite. Covelitte was only produced in experiments in “concentrated” copper sulphate solutions.

Cowper & Rickard (1989) found that pyrrhotite altered to chalcopyrite via two metastable intermediary phases and a cubanite-type phase; and observed no reaction between pyrite and aqueous copper sulphate. The Cowper & Richard (1989) experiments were conducted at <100°C in solutions of 0.003 to 0.080M copper sulphate solution.

Rickard & Cowper (1994) found pyrite alters to chalcopyrite; then in solutions with excess copper; chalcopyrite is replaced by bornite and subsequently digenite. The Rickard & Cowper (1989) experiments were conducted in 0.003 to 0.030M copper

sulphate solutions at temperatures up to 127°C. That work comments that the absence of chalcopyrite as a product of pyrite experiments in the Zies, *et. al.* (1916) experiments, is due to the high concentrations which had been used.

Pękala, *et al.* (2011) found that ‘Fe sulphides’ alter sequentially to form minerals which *include* chalcopyrite, bornite, covellite and digenite. The Pękala, *et al.* (2011) experiments used concentrations of 0.008 and 0.050M copper solutions at temperatures of 40, 100 and 200°C.

This section is distinct from Pękala, *et al.* (2011), as the latter focuses on isotope fractionation: although both share in the benefit of the contemporary technology and development of analytical capabilities.

5.2.0 Reactants

This study uses pyrrhotite from an unspecified location in Brazil (Pękala, et al., (2011) library sample); pyrite from Navajún, La Rioja, Spain; chalcopyrite from Concepción del Oro, Zacatecas, Mexico; and bornite from Tsumeb Mine, Tsumeb, Namibia. The pyrite, bornite and chalcopyrite were obtained through a mineral supplier, see acknowledgements. This section details the preparation of these minerals for the experimental work.

5.2.1 Crushing and Sieving

The required particle size for the experimental section was decided as 180 - 250μm. This range was the largest size range used in Rickard & Cowper (1994); and closest to the lower range in Pękala, et al., (2011), of 250 - 1000μm. To achieve this size, the mineral material was broken using a Retsch mechanical jaw crusher. A jaw crusher was chosen to prevent material becoming too fine, too rapidly. The tungsten carbide jaws were thoroughly wiped with acetone before and between each mineral being crushed.

Initially, the material was crushed to a nominal grade three. The dry materials were sorted using a Retsch AS200 vibratory sieve stack, into the fractions: <180μm, 180 – 250μm, 250 – 1000μm and >1000μm. As a result of a poor yield of pyrite at the required size: each mineral was crushed thrice more, by processing the larger materials in the jaw crusher on the lowest possible grade. Recrushed minerals were sieved again.

The <180μm size fractions for each mineral were rejected, although retained as library samples. The 250 - 1000μm and >1000μm were combined and bagged, to be recrushed had more mineral reactant been required. The yield of each mineral of the required size was: 1.74 grams of pyrite; 13.74 grams of chalcopyrite; and, 7.07 grams of bornite. The minerals were kept in plastic sample bottles overnight.

A subsample of each of these materials was taken to check for impurities and fine material. It was found that chalcopyrite contained a substantial amount of quartz, and all samples would require the removal of extremely fine material.

The 150 - 250μm library pyrrhotite sample was added to the crushed library sample, and sieved together to the required 180 - 250μm fraction. The mass of pyrrhotite was not recorded at this stage, but was not enough to conduct all of the planned experiments.

The pyrrhotite sample fraction of >250μm was too fine for the jaw crusher to break, therefore, this was ground manually with an agate pestle and mortar. Starting with the finer material, the sample was lightly pestled, and sieved into the fractions: <180μm, 180 – 250μm, >250μm. The fraction >250μm was iteratively ground and sieved until an adequate mass of 180 – 250μm pyrrhotite (6.73 grams) had accumulated.

5.2.2 Cleaning and Purifying

To remove any residual grease, the materials were transferred to 25ml glass beakers and immersed in acetone for 180 seconds. Every thirty seconds the beaker was agitated to ensure all of the material surface was cleaned. After the 180 seconds had elapsed, the material was transferred to a vacuum filter (5 to 13μm pore) for five minutes, residue in the beaker was washed out over the filter with deionised water.

The sample was rinsed with the deionised water for thirty seconds during filtration. The samples were carefully removed on the filter papers, and placed in a drying oven to be left for approximatley eighteen hours. Pękala, et al., (2011) simalarly immersed the material in a 1:1 acetone-petroleum ether mixture to remove grease. This step was skipped for pyrrhotite, as acetone was used for ultrasonic cleaning.

The dry samples were immersed in acetone in clean 25ml glass beakers, and ultrasonically cleaned for 180 seconds. In previous works ultrasonic cleaning was conducted by with ethanol (McKibben & Barnes, 1986) (Rickard & Cowper, 1994). The purpose of ultrasonic cleaning is to lift and suspend the extremely fine mineral flour from the surfaces of particles. The ethanol, or acetone, can be decanted away to remove the fine material. This samples in this work were returned to the drying oven, in the glass beakers, and left for approximately 90 minutes.

To ensure any remaining fine material was removed, this work adopted and adapted a method used in previous work (Rigonat, 2017). Each sample was emptied into a petridish, and an upturned 180μm mesh sieve was rested onto the brim of the petridish. A standard household vacuum cleaner was then used to draw the material to the mesh, and move it around the sieve. After this stage, the minerals were returned into their respective pre-vacuumed plastic sample bottles.

The minerals were once again weighed, to account for losses of the removal of grease and fines, as well as any unintended losses. The new mass of pyrite was 1.42 grams, after a loss of 0.31 grams (17.8%); chalcopyrite had a new mass of 11.36 grams after a loss off 2.38 grams (17.3%); and bornite had a new mass of 6.67 grams after a loss of 0.402 grams (5.68%). For the pestled pyrrhotite, the new mass was 6.46 grams, after a loss of 0.27 grams (4.01%).

Density seperation was required to remove quartz from the chalcopyrite. Given the density of quartz is *ca.* 2600 $kg \cdot m^{-3}$, and chalcopyrite is 4300 $kg \cdot m^{-3}$ (Korbel & Novák, 1999), seperation required a liquid between these two densities. Sodium metatungstate ($Na_6[H_2W_{12}O_{40}]$) was selected due to its non-toxicity and reusablity (Gregory & Johnston, 1987). A solution of approximatley 2900 $kg \cdot m^{-3}$ was produced by gradually adding 50.0 grams of crystalline sodium metastungstate hydrate to 9.87 grams of deionised water, in a plastic beaker.

It is noted that aqueous sodium metatungstate should not be contained in glassware, due to the aggressive removal of calcium ions from glass (Sometu, 2010). During preparation, the salt had a tendency to clump together on the suface of the solution, therefore a PTFE rod was used to submerge and disaggregate the salt to hasten dissolution. The viscous solution produced was not suitable for membrane filteration, therefore the method would require gravity filteration.

The chalcopyrite was dropped onto the sodium metatungstate solution, and stirred in with the PTFE rod. The beaker was agitated by sporadic stirring, swirling and ultrasonication before being left to rest.
As per their density, the particles either were: *i*) less dense than the solution, so floated on the surface; *ii*) of near equal density to the solution, and were suspended in the fluid; or, *iii*) more dense than the solution, and settled to the bottom of the container. This is illustrated in **Figure 50a**.

The suspended and floating material was removed by pippette and deposited into a filtered funnel, and washed with deionised water. The diluted soloution was collected in a Erlenmeyer flask. The denser chalcopyrite was deposited into a second filtered funnel in a second flask, and also washed with deioninised water. Both filters were left to empty of liquid, before the filterates were submerged in deionised water, and covered over with petridishes to filter overnight. It was observed that the less dense material seemed finer than that of the chalcopyrite. The filterates can be compared in **Figure 50b** and **Figure 50c** respectively.

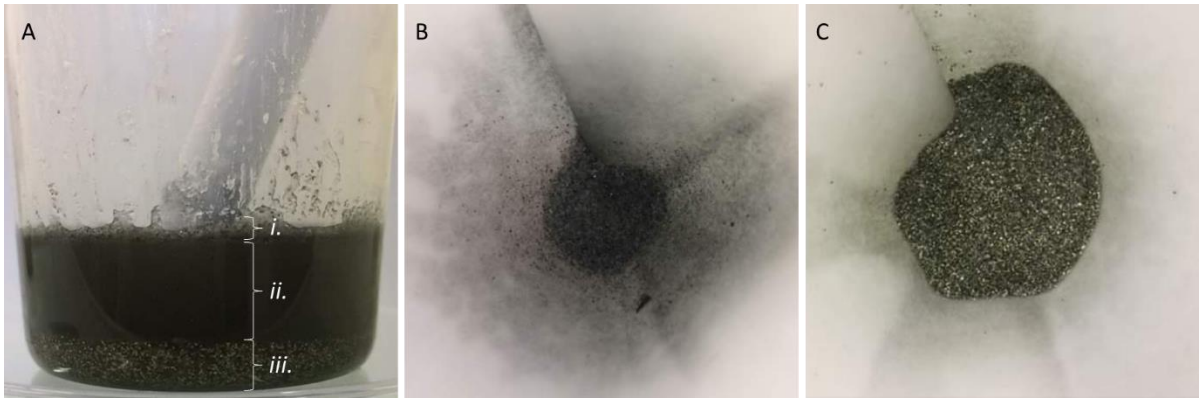

Figure 50: (*A) Density Separation of Chalcopyrite, where regions **i** and **ii** have less than, and equal density to the sodium meta-tungstate respectively (B), and region **iii** is the chalcopyrite concentrate (C).*

The less dense quartz rich material was discarded. The chalcopyrite concentrate was washed into a beaker with an excess of deionised water, and ultrasonically cleaned for 180 seconds, for any remaining sodium metatungstate to be decanted away in solution. Ultrasonic cleaning was repeated with deionisd water for 180 seconds, before the concentrate was vacuum filtered. The concentrate was transferred to the drying oven and left for two hours. This process removed 1.84 grams of material, leaving 9.52 grams of chalcopyrite concentrate.

5.2.3 Acid Washing

The purpose of acid washing was to remove the monatomic oxide layer from the surface of the mineral reactants. This layer would otherwise impede any reaction in these experiments.

Pyrrhotite was submerged in a beaker with 10% hydrocloric acid for one hour. The mineral and acid were deposited in a gravity filter and washed through with deoxygenated deionised water. The wet mineral was doused in acetone, which would increase the rate of drying under a stream of nitrogen.

Pyrite was acid washed in a beaker with 10% hydrocloric acid overnight. Then, simalarly, the mineral and acid were deposited in a gravity filter; washed in deoxygenated deionised water; washed with acetone; and then dried in a stream of nitrogen.

Bornite and chalcopyrite are also washed overnight; deposited in a gravity filter; washed in deionised water (not deoxygenated); washed with acetone; and then dried in air.

Pyrrhotite and pyrite oxidise far quicker than chalcopyrite (Steger & Desjardens, 1978), therefore, the use of deoxygenated deionised water and drying in acetone was not deemed as necessary for chalcopyrite and, by extension, bornite.

A benefit in using acetone in the drying process is that when the aroma of acetone dissapates, the sample is known to be dry.

The dry minerals are then distributed into their respective experimental vessels, by adding approximatley 0.2500 grams to each vessel on tared mass scales. The true masses are given in the results section. When a satisfactory mass of dry mineral was added to vessel, the vessel was briefly closed with a rubber seal.

5.2.4 Aqueous Reactants

This section details the procedure of producing the copper solutions used in the experiments: Each solution was prepared in a volumetric flask, transferred to a plastic bottle, and deoxygenated by purging solutions with nitrogen for approximately ten minutes.

Copper sulphate was used for Cu^{2+} reactions and prepared by dissolving analytical grade copper sulphate pentahydrate ($CuSO_4 \cdot 5H_2O$) in deionised water. Each solution was made up to 250ml in a volumetric flask. The target masses of copper sulphate pentahydrate (249.685 grams per mole) dissolved to produce each solution is as follows (Haynes, 2011): 0.005M, 0.3121 grams; 0.010M, 0.6242 milligrams; and 0.050M, 3.1210 grams. The true masses are given in the results section.

5.3.0 Reaction Conditions

This section describes the procedure of setting up, heating and ending the experiments. The procedure of experiments was different for runs at low temperature (50 & 100°C) and high temperature (200°C). These procedures are discussed in their respective subsection.

5.3.1 Low Temperature Experiments

Low temperature experiments were conducted in borosilicate glass serum bottles. The rubber stopper was removed and a quantity* of copper solution ($CuSO_4$ or CuCl, as applicable) was added with an automatic pipettor. The solution was purged with nitrogen, to remove any remnant oxygen. As the bottles were individually purged, the rim of the bottle was lightly smeared in silicon adhesive. The rubber stopper was replaced to seal the vessel, and this was secured in place with a crimped aluminium cap.

The 50°C experiments were heated in a thermostat controlled SciQuip-55S oven. The 100°C experiments were heated in a Genlab MINO/40/F, using a RS PRO 206-3722 Type-K thermocouple to observe the oven temperature, readings were typically 98±3°C. The durations of experiments (in days) are given in the results section.

Due the risk of thermal shock, when removing the 100°C experiments from the oven, the bottles were first permitted to cool in room temperature for about ten minutes, before they were stored in a refrigerator.

The volume of copper solution was planned to be 40ml. For the low temperature copper sulphate runs, there was a consistent pipetting error. The plunger on the mechanical pipette was mistakenly pressed to the second stop on drawing the solution, instead of to the first stop. This error was repeated ten times with deionised water to determine the difference in volume dispensed between the second stop and the first. It was found that, on average, the second stop draws 2.62 ± 0.06 millilitres more than the first stop. Therefore, the low temperature copper sulphate runs will likely contain 50.48 ± 0.023 millilitres.

5.3.2 High Temperature Experiments

High temperature experiments were conducted in PTFE jars, with viton rubber sealing disks (pierced) inserted into the cap. As increased pressure is required to prevent boiling, approximately 1.65 MPa for 200°C, the PTFE jars were sealed in autoclaves. Two autoclaves were produced to match the autoclave used by a previous work (Holloway, 2018). **Figure 51** is an annotated cross sectional diagram of the autoclaves used.

All high temperature experiments were put in the oven at 17:00 on day 0, to heat overnight; the oven temperature was monitored during day1 and turned off at 17:00 on day 1, the door opened to cool the samples overnight.

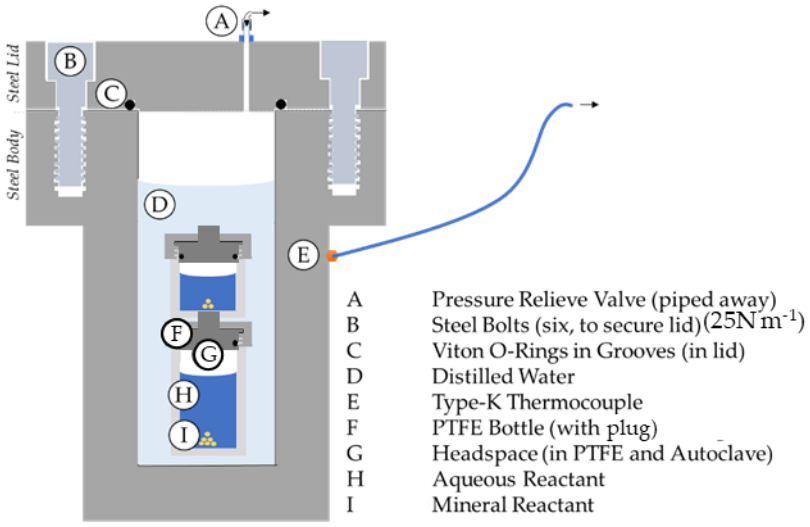

Figure 51: *Cross section diagram of the autoclaves used for high temperature experiments.*

5.4.0 Preparation for Analysis

This section describes the procedure of preparing the aqueous and mineral products for analysis.

5.4.1 Separation of Products

The products were separated using a Nalgene vacuum membrane filter. As not to excessively dilute the aqueous products, the minerals and filter paper were washed through with deionised water using a transfer pipette. Upon releasing the vacuum and disassembling the filter apparatus, the filter membrane was rolled up and inserted into a three-millilitre sample vial. The vial was labelled accordingly and stored.

The slightly diluted aqueous product was decanted, through a nozzle, into a 100ml volumetric flask. A few drops of deionised water were added around the neck of the flask to wash any aqueous product down. The aqueous product was acidified by adding one millilitre of 37% analytical reagent grade hydrochloric acid. Deionised water was then added to produce 100ml of acidified solution. This was decanted into a plastic sample bottle, sealed and labelled.

5.4.2 Mounting Mineral Products

The mineral products were rinsed off the membrane filters with deionised water into a vacuum assisted gravity filter, then washed through and submerged in their vials with acetone, the products were left to dry in a fume cupboard with an extractor fan (1.00 $m \cdot s^{-1}$) for approximately 36 hours.

The dry mineral products were then mounted. This involved transferring an amount of sample from each vial onto templated double-sided adhesive tape. This tape was mounted on a rubber pad, itself on a small pane of glass: this ensures the flatness of the mounting face. Various methods were employed to transfer the minerals to the tape, with various success. The preferred method was to use a laboratory sampling spoon to lift, transfer, and flatten the grains of mineral in a gentle circular motion, this may require a steady hand.

A plastic mould was aligned with the template and pressed onto the double-sided adhesive tape, a quantity of two-part EPO-TEK 301 1LB epoxy resin was gently poured around the inside edge of the mould, as to minimise the risk of samples escaping.

The resin was set at room temperature in pressure vessel at 0.2 MPa (approximately twice standard room pressure) for 24 hours, this has the benefit of decreasing the size of any bubbles which may be present on the face to be polished. Once set, the resin was cured on a hotplate at 80°C for four hours.

The face was ground flat using 2500-grit silicon carbide sandpaper and water. This face was polished with 0.3μm aluminium oxide powder with a Kemet PSU-M cloth on a 200mm polishing machine. The desired finish was achieved after six to twelve minutes of polishing using 500 grams of force, with the machine running at 200 rotations per minute.

5.5.0 Analysis Methods

This section describes the methods of analysing the experiment products, the reason why these methods were selected and a brief overview of how the equipment works.

5.5.1 Inductively Coupled Plasma Optical Emission Spectroscopy (ICP-OES)

The Varian Vista Pro ICP-OES was selected to measure the concentrations of copper and iron in the aqueous products, to determine how much copper had been reacted. The facility is designed to measure concentrations between the orders of magnitude from parts per billion (ppb) to parts per million (ppm). Given that the experiment products may have concentrations in the parts per thousand (ppt), the aqueous products were further diluted by a factor of forty.

Plasma is formed when electrons are completely dissociated from the nuclei of gaseous atoms. A plasma “torch” is established by electromagnetically exciting argon gas, which emits electromagnetic radiation (Lajunen & Perämäki, 2004).

When an atomised sample is introduced to the torch, it too will emit electromagnetic radiation as it ionises. Each metal in the sample will emit a ‘fingerprint’ of electromagnetic radiation consisting of several frequencies. The intensity of this radiation is proportional to the concentration of the metal.

Optical Emission Spectroscopy resolves the intensity of different frequencies by manipulating the emitted radiation using mirrors and a diffraction grating. Ultimately, the intensities of selected wavelengths are quantified by a sensor.

Using standard solutions where the concentrations of the queried metal are known, it is possible to plot a calibration curve, which relates the observed intensities to benchmark concentrations. Therefore, each measurement of intensity, which a sample gives off, can be calculated into metal concentrations.

Each sample is spiked with yttrium - an element chosen as it is naturally absent in the sample - to determine and correct for the ‘matrix effect’. This effect is observed where elements, which are not the analyte nor the solvent, supress the intensity of the radiation which the analyte emits. The wavelengths with the strongest correlations were: 324.754 nm for copper; and 259.940 nm for iron.

5.5.2 Optical Microscopy

This work has analysed mineral products in reflected light using a Zeiss Ultraphot II, which has been modified to capture images remotely using a mounted Canon DS126291 DSLR camera. The products are illuminated vertically using 4, 8 and 16x Epiplan objectives, giving a final magnification at the camera of 40, 80 and 160x.

Optical microscopy is used for preliminary investigation, and to identify particles with reaction rims for more focussed analysis.

5.5.3 Scanning Electron Microscopy

As a contrast to Optical Microscopy, this work has also analysed mineral products using Oxford AZtec ED Electron Backscatter Diffraction (EBSD) analysis, on a Carl Zeiss SIGMA HD VP Field Emission Scanning Electron Microscope.

EBSD imaging was complimented using energy-dispersive X-ray spectroscopy or “spot analysis”: both methods used a 20 KeV electron beam.

ESBD is a qualitative analytical method which can be used to effectively observe the distribution of minerals within the sample, especially where adjacent phases are similar in colour under optical microscopy. Spot analysis measures the intensity of characteristic X-rays, which are emitted by elements in proportion to their concentration. In conjunction with analyses of the mineral reactants, it is possible to estimate relative abundances of elements as a method of indicating what a mineral may be.

5.5.4 Electron Microprobe Analysis

This project originally anticipated to use EMPA for semi-quantitative analyses. These analyses were curtailed as a result of disruption caused by the Coronavirus pandemic.

5.6.0 Findings

This work revisits reactions between copper solutions and pyrrhotite, previously studied by Zies, *et al*. (1916); Cowper & Rickard (1989) and Pękala, *et al.* (2011). The pyrrhotite use was a library sample from an unspecified location in Brazil (Pękala, et al., 2011).

5.6.1 Low Temperature Experiments (50°C)

Table 29 summarises the reactants in low temperature reactions conducted at 50°C, and experimental charges of 50 millilitres: and the aqueous products after 56 days of reaction. Final copper and iron concentrations were determined by Inductively Coupled Plasma Optical Emission Spectroscopy.

***Table 29**: Reactants and Aqueous Products in low temperature reactions between pyrrhotite and copper sulphate solutions. Reactions were conducted with 50ml of solution at 50°C, for a duration of 56 days.*

Exp. ID	Po Mass (grams)	$CuSO_4$ Mass (grams in 250ml DI water)	$CuSO_4$ Conc. (mM)	Final Cu Conc. (mM)	Final Fe Conc. (mM)	Cu Utilisation (%)
PO1	0.2502	0.3121	5.002	3.358	0.035	33
PO2	0.2508	0.6242	10.000	9.258	0.032	7
PO3	0.2507	3.1209	49.998	45.042	0.072	10

The optical microscopy on PO1 did not visually identify any reaction rims. However, EBSD spot analyses identified the apparent uptake of copper. These points also indicate the presence of Aluminium, which is likely residue of the aluminium oxide powder used in polishing.

Figure 52 shows a grain of PO1 reaction product under Backscatter Scanning Electron Microscope (SEM, left) and Optical Microscopy (OM, right). The EBSD records approximately 47.4 cps/eV of electron emission at 0.915 KeV, a value characteristic of copper.

Within a second PO1 grain, a supplementary EBSD analysis produces an electron emission of approximately 8.24 cps/eV. This spot analyses may be from a grain where the surface has been polished to just above unaltered pyrrhotite. It may be a second, lesser intermediary phase of copper uptake in pyrrhotite.

Therefore, PO1 could present two intermediate phases of copper uptake into pyrrhotite, given the copper utilisation. Approximate EBSD findings are provided in **Table 30.**

Table 30: *EBSD electron emission rates associated with copper, iron and sulphur from PO1 experiment mineral products.*

Exp. ID	EBSD Spectrum	Electron emission rate (cps/eV)			Interpretation
		Cu (≈ 0.9 KeV)	Fe (≈ 6.4 KeV)	S (≈ 2.4 KeV)	
PO1	1, 2, 5, 6	nil	153.46	442.77	unaltered pyrhottite
	7	8.24	151.00	446.39	intermediate phase
	4	47.50	146.88	438.750	intermediate phase

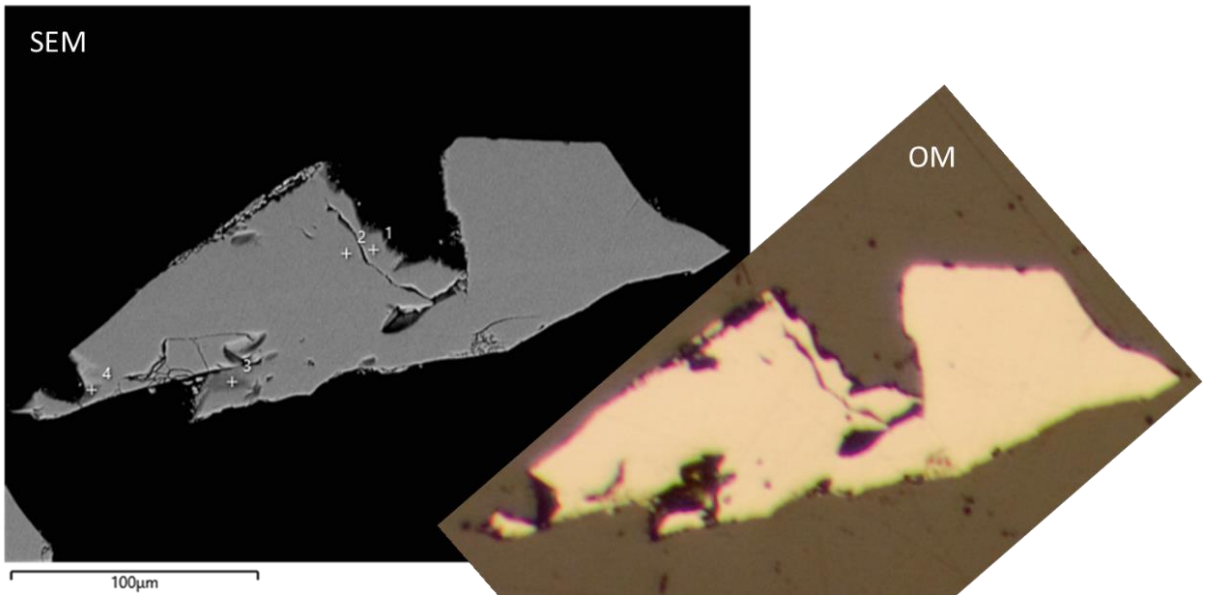

Figure 52*: (Left) Scanning Electron Microscopy image of reacted grain, showing spot (EBSD) analysis locations where potential copper uptake is observed. (Right) grain under optical microscopy (OM)*

This uptake of copper is not seen on any EBSD trace in PO2 or PO3.

5.6.2 Low Temperature Experiments (100°C)

Reactions at 100°C were conducted in 50ml experiment charges, for a duration of seven days. These reactions were clearly more developed than the earlier 50°C experiments. **Table 31** summarises the reactants and aqueous products in these experiments.

***Table 31**: Reactants and Aqueous Products in low temperature reactions between pyrrhotite and copper sulphate solutions. Reactions were conducted with 50ml of solution at 100°C, for a duration of 7 days. *PO6 and PO7 are a duplicated*

Exp. ID	Po Mass (grams)	$CuSO_4$ Mass (grams in 250ml DI water)	$CuSO_4$ Conc. (mM)	Final Cu Conc. (mM)	Final Fe Conc. (mM)	Cu Utilisation (%)
PO4	0.2507	0.3121	5.000	0.095	4.919	98
PO5	0.2505	0.6242	10.000	7.992	0.090	20
PO6*	0.2506	3.1209	49.998	0.014	0.060	13
PO7*	0.2505	3.1209	49.998	43.592	3.840	100

Experiment PO4 is a near complete reaction between the pyrrhotite and the copper solution. **Figure 53** shows a highly reacted grain, under both (left) Backscatter SEM and (right) optical microscopy (OM). Under optical microscopy, pyrrhotite is surrounded in reaction rims of colours characteristic of known copper-iron sulphides. A layer of yellow is interpreted as chalcopyrite; the muted grey-purple layer is interpreted as bornite; which is followed by a grey-blue reaction rim.

Under SEM, backscatter images show an apparent uptake of copper within the pyrrhotite: indicated by paler grey areas within the pyrrhotite.

Table 32 summarises the EBSD analyses of spots queried in the PO4 experiment products. Reference EBSD data is given for unreacted chalcopyrite and bornite.

EBSD analyses are not quantitative, therefore interpretation from EBSD data is difficult. This work calculates the electron emission rate of copper, divided by the electron emission rate of sulphur; and the electron emission rate of copper, divided by the electron emission rate of iron.

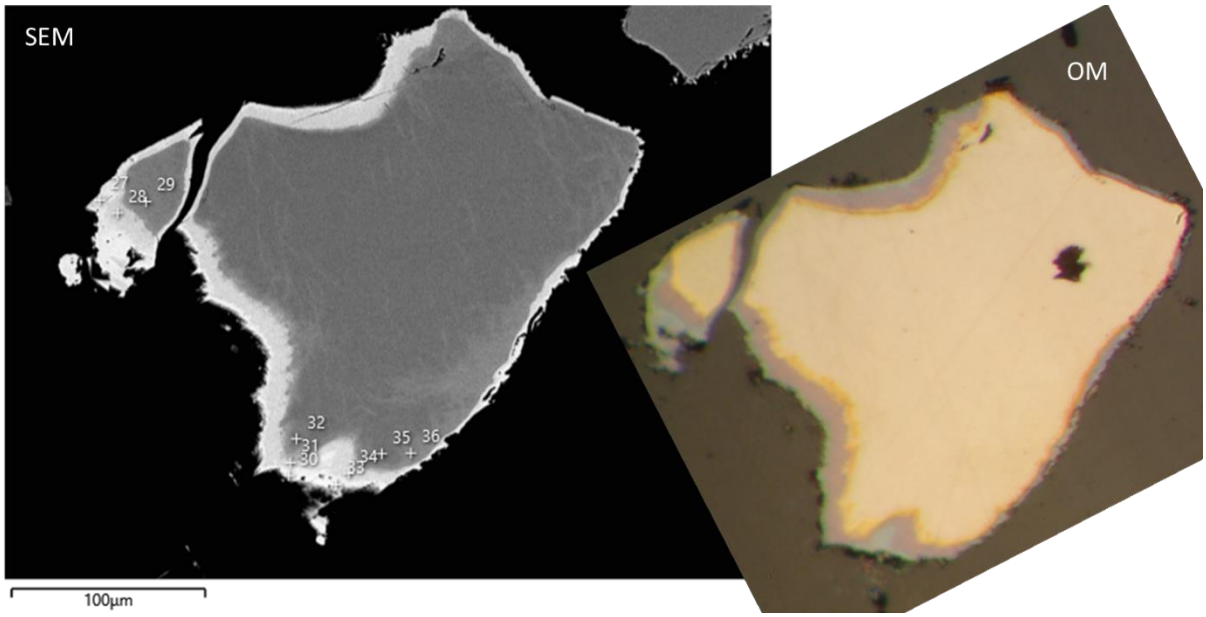

Figure 53: *Highly reacted pyrrhotite grain in PO4 experiment, showing multiple successive reaction rims.*

Table 32: *EBSD electron emission rates associated with copper, iron and sulphur from PO4 experiment mineral products.*

Exp. ID	EBSD Spectrum	Electron emission rate			Interpretation
		Cu (≈ 0.9 KeV)	Fe (≈ 6.4 KeV)	S (≈ 2.4 KeV)	
CCP ref	-	108.22	74.46	322.08	
BOR ref	-	264.39	30.89	224.08	
PO4	17	0	153.91	439.56	unaltered pyrhottite
	16	6.06	149.49	436.95	intermediate
	22	3.41	151.74	441.16	intermediate
	20, 21	324.77	36.94	260.36	Bornite
	19	458.82	18.30	228.76	
	29	31.74	137.57	394.71	intermediate
	28	309.96	45.23	265.15	Bornite
	32	23.03	144.41	419.06	intermediate
	31	315.21	47.60	266.42	Bornite
	36	23.70	145.95	392.82	intermediate
	35	14.26	145.18	427.36	intermediate
	34	318.86	45.43	258.86	Bornite
	33	513.18	15.62	209.14	

.

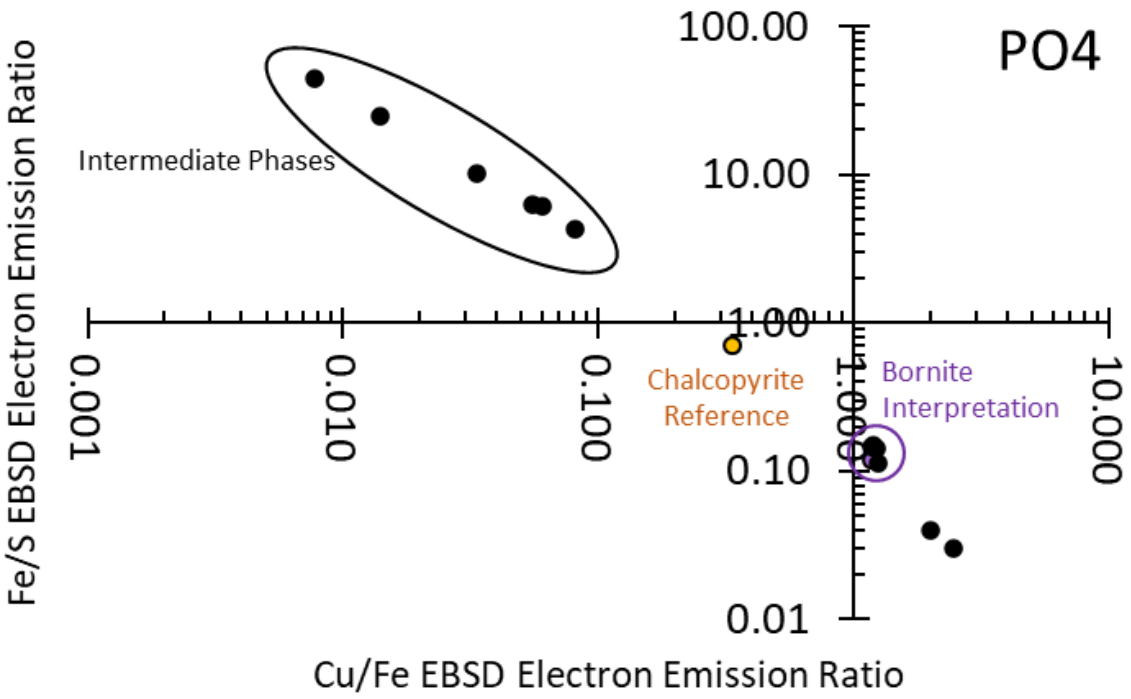

***Figure 54**: Interpretation of EBSD electron emission data from PO4 analysis: showing unaltered pyrrhotite; intermediate phases; chalcopyrite reference, without observed chalcopyrite; bornite reference with a cluster of observations; and two distinct minerals with higher copper concentrations.*

Presented in a log-log scatter plot, with reference points for unaltered chalcopyrite and bornite, different minerals should be observed as round clusters. This is seen around the bornite reference point in **Figure 54.**

In overlaying OM images and the positions of EBSD, it is possible that spot analyses missed the chalcopyrite reaction rim.

Experiment PO5 has a very limited reaction. On the mineral product, reaction rims were only identified on one crescent shaped grain, within a ‘strait’ between the two terminuses. The magnification under microscopy was insufficient to get a good image, therefore, **Figure 55** is composed of two SEM images.

Table 33 provides an overview of the EBSD analyses of the PO5 grain.

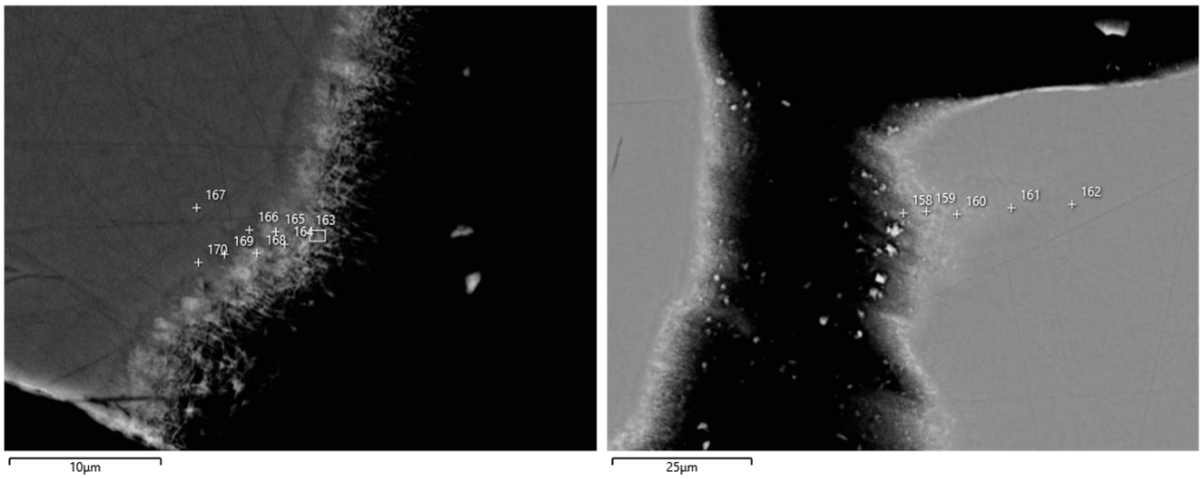

***Figure 55**: SEM analyses on PO5 mineral product. Very fine mineralisation seen in strait of crescent of grain*

***Table 33**: EBSD analyses of PO5 grain, showing the intermediate phases: EBSD indicates oxygen in outer reaction rim.*

Exp. ID	EBSD Spectrum	Electron emission rate			Interpretation
		Cu (≈ 0.9 KeV)	Fe (≈ 6.4 KeV)	S (≈ 2.4 KeV)	
PO5	162	nil	137.88	381.27	unaltered pyrrhotite
	161	36.74	124.86	369.07	intermediate phase
	167, 170				unaltered pyrrhotite
	169	17.80	136.42	376.79	intermediate phase
	166	27.44	132.86	372.89	intermediate phase

Oxidisation of produced copper minerals is observed in EBSD analyses and in the irregular mineralisation pattern. Therefore, this work can only identify intermediate mineralisation.

PO6 and PO7 are duplicate reactions, as such they are considered together.

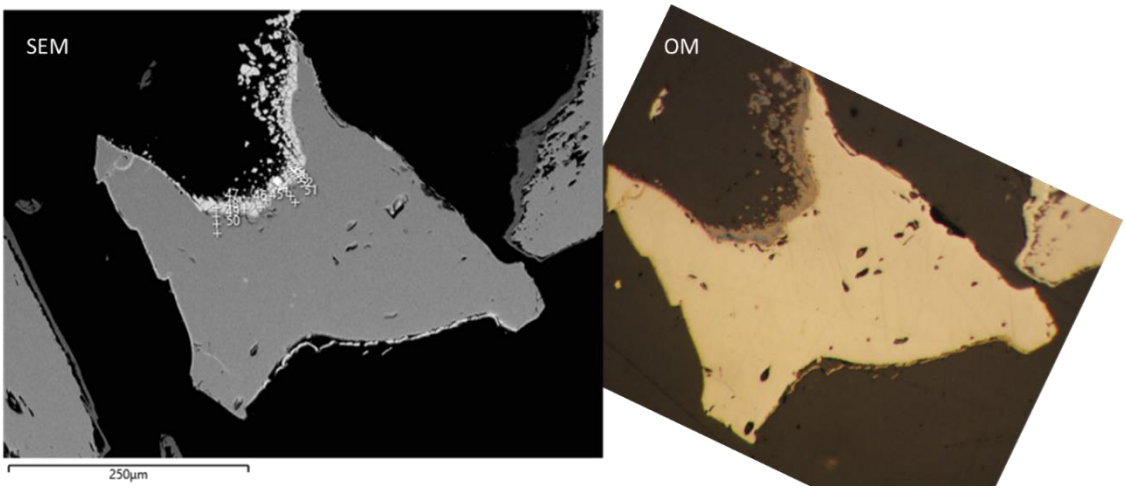

***Figure 56**: PO6 (grain 1) mineral product shown under (left), Scanning Electron Microscope; and (right), Optical Microscopy*

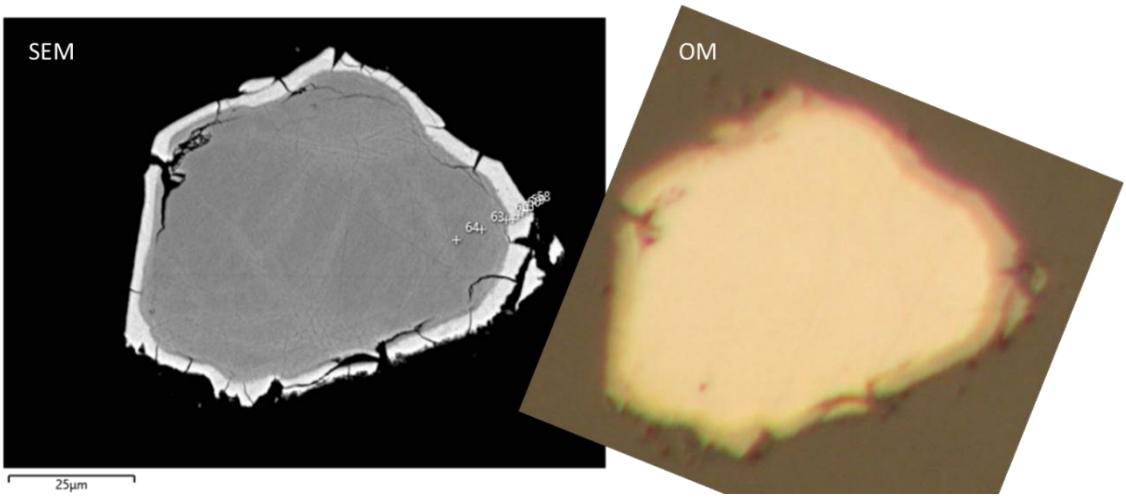

***Figure 57**: PO6 (grain 2) mineral product shown under (left), Scanning Electron Microscopy; and (right), Optical Microscopy*

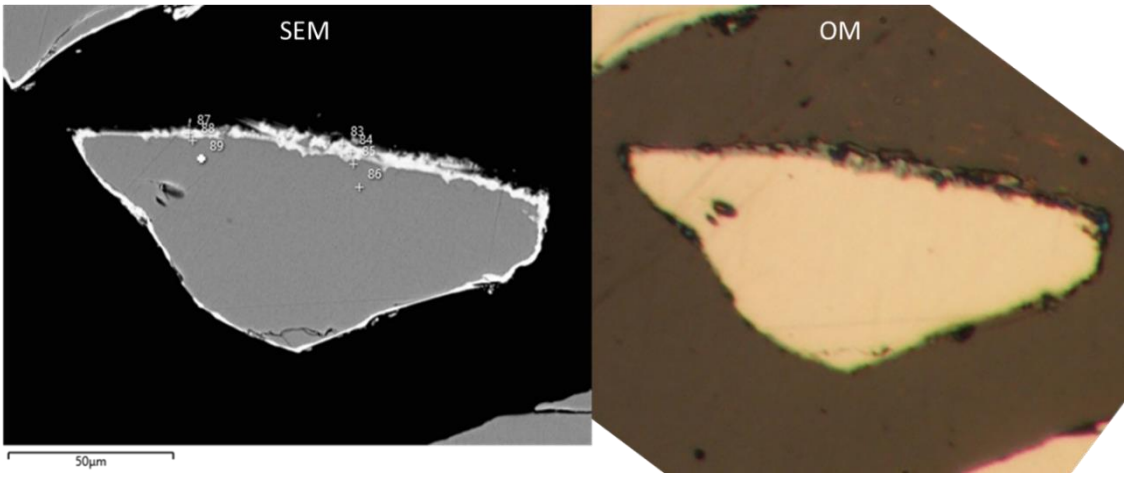

***Figure 58**: PO7 mineral product shown under (left), Scanning Electron Microscopy; and (right) Optical Microscopy*

Table 34: *EBSD analyses of PO6 and PO7 grains, showing the intermediate phases: EBSD indicates oxygen in outer reaction rims.*

Exp. ID	EBSD Spectrum	Electron emission rate			Interpretation
		Cu (≈ 0.9 KeV)	Fe (≈ 6.4 KeV)	S (≈ 2.4 KeV)	
CCP ref	-	108.22	74.46	322.08	
BOR ref	-	264.39	30.89	224.08	
PO6 (1)	50	nil	140.13	395.92	unaltered pyrrhotite
	49	nil	141.10	408.49	unaltered pyrrhotite
	48	nil	138.66	404.71	unaltered pyrrhotite
	47	406.11	18.33	252.73	
	46	354.03	24.15	264.82	
	45	280.12	62.78	276.03	
	44	328.13	35.16	268.75	
	51	nil	138.06	405.95	unaltered pyrrhotite
	52	nil	140.16	403.2	unaltered pyrrhotite
	53	nil	140.45	402.23	unaltered pyrrhotite
	54	295.44	56.84	277.89	
	55	344.36	27.60	255.13	
	56	300.09	31.90	258.04	
	57	277.23	34.98	264.03	
PO6 (2)	64	4.30	137.58	401.27	intermediate phase
	63	7.27	136.92	387.46	intermediate phase
	62	125.10	78.88	321.18	chalcopyrite
	61	259.05	42.98	264.62	
	60	279.19	31.40	249.92	
	59	297.87	28.37	242.55	
PO7	89	nil	141.27	399.75	unaltered pyrrhotite
	88	27.97	134.44	379.85	intermediate phase
	86	nil	141.67	404.56	unaltered pyrrhotite
	85	9.43	140.57	396.23	intermediate phase
	84	428.50	31.55	221.88	

Oxidisation is observed in each PO6 grain this work has analysed and observed in the PO7 analysed. As such, this work will only identify the unoxidized reaction rims.

Table 34 provides the EBSD analysis of PO6 and PO7 experiments, **Figure 59** plots the ratio of these characteristic copper to sulphur electron emission under EBSD analysis is plotted against the characteristic copper to iron electron emission ratio under EBSD analysis. The cluster around bornite are not all interpreted as Bornite.

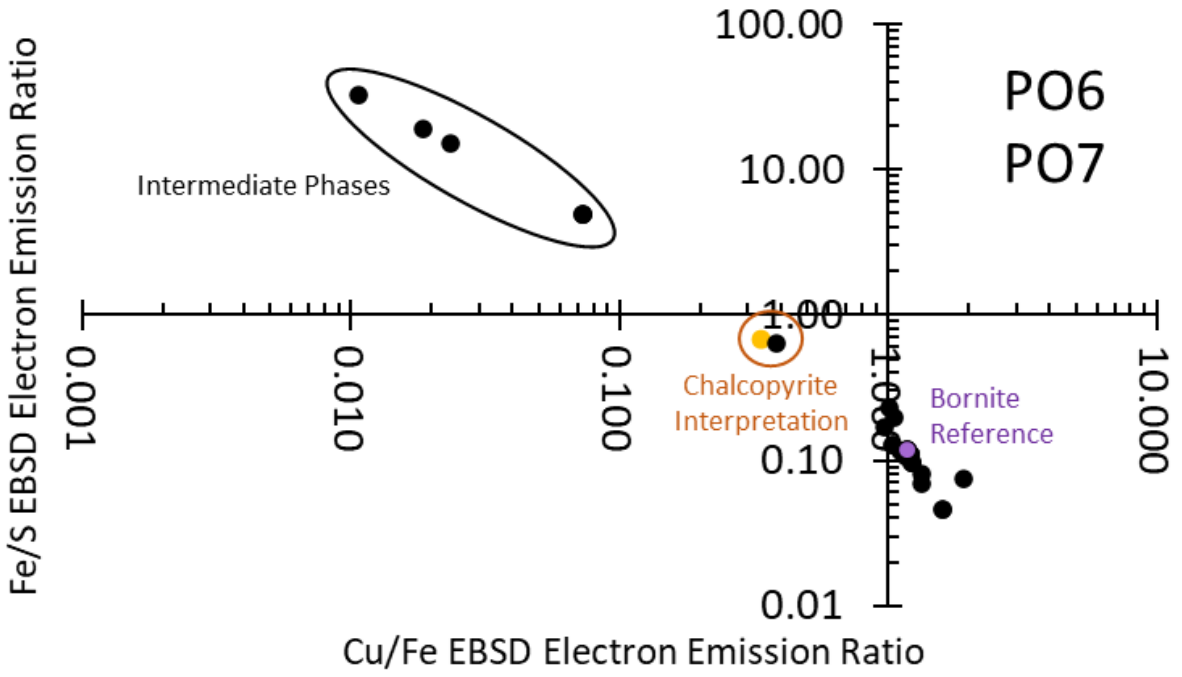

***Figure 59**: Interpretation of EBSD electron emission data from PO6 and PO7 analyses: showing intermediate phases; chalcopyrite reference, without observed chalcopyrite; bornite reference within a cluster of observations.*

5.6.3 High Temperature Experiments (200°C)

Reactions at 200°C were conducted in 15ml experiment charges, for a duration of two days. **Table 35** summarises the reactants and aqueous products in these experiments.

***Table 35**: Reactants and Aqueous Products in high temperature reactions between pyrrhotite and copper sulphate solutions. Reactions were conducted with 15ml of solution at 200°C, for a duration of 2 days.*

Exp. ID	Po Mass (grams)	$CuSO_4$ Mass (grams in 250ml DI water)	$CuSO_4$ Conc. (mM)	Final Cu Conc. (mM)	Final Fe Conc. (mM)	Cu Utilisation (%)
PO8	0.0756	0.3122	5.002	1.861	0.609	63
PO9	0.0757	0.6241	9.998	8.937	0.242	11
PO10	0.0756	3.1213	50.005	46.254	0.430	7

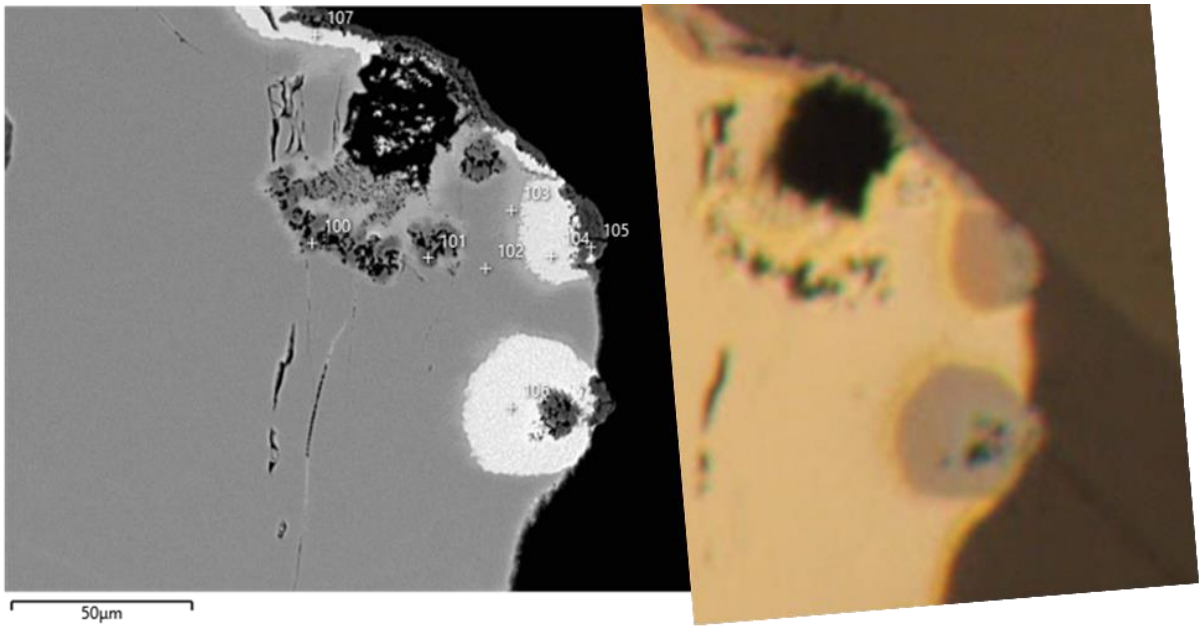

***Figure 60**: PO8 mineral product grain 1, shown under (left), Scanning Electron Microscopy; and (right) Optical Microscopy*

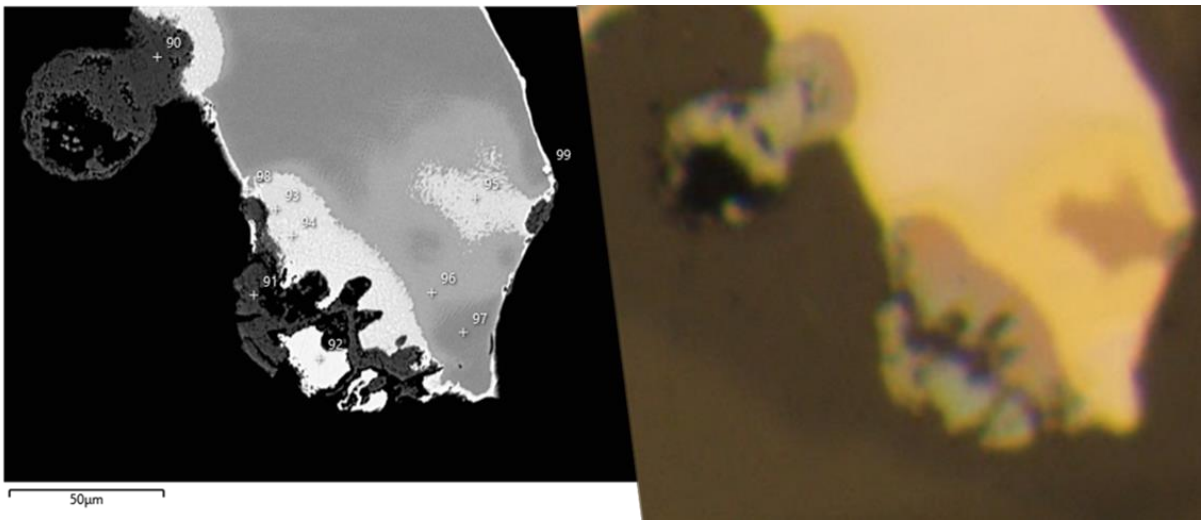

***Figure 61**: PO8 mineral product grain 2, shown under (left), Scanning Electron Microscopy; and (right) Optical Microscopy*

***Table 36**: EBSD analyses of PO8 grains.*

Exp. ID	EBSD Spectrum	Electron emission rate			Interpretation
		Cu (≈ 0.9 KeV)	Fe (≈ 6.4 KeV)	S (≈ 2.4 KeV)	
CCP ref	-	108.22	74.46	322.08	
BOR ref	-	264.39	30.89	224.08	
PO8	97	4.79	139.95	395.76	Intermediate phase chalcopyrite
	96	104.49	85.61	338.07	
	95	284.57	43.04	243.050	
	99	351.07	48.50	234.45	
	94, 98	380.18	18.06	206.85	
	93	288.50	34.69	221.85	
	92	452.13	8.09	195.90	
	102	5.28	138.91	393.49	intermediate phase chalcopyrite
	103	102.87	87.46	337.16	
	104	292.11	35.03	228.14	
	106	334.03	26.42	215.37	
	107	278.46	40.13	225.70	

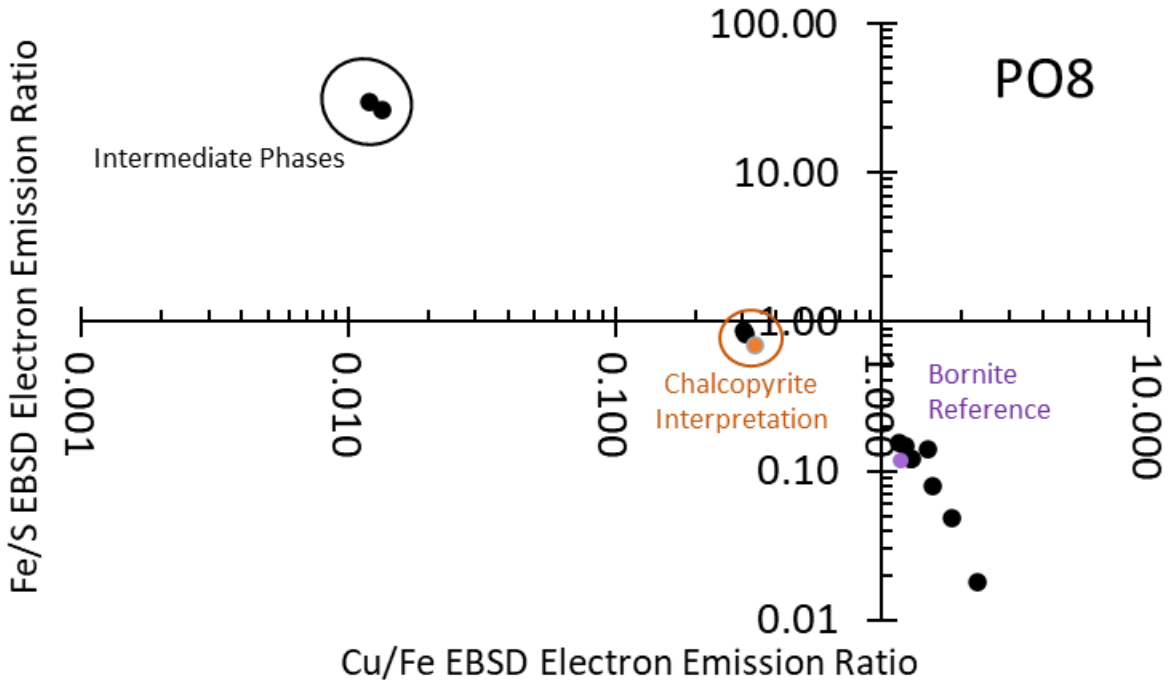

***Figure 62**: Interpretation of EBSD electron emission data from PO8 analyses: showing intermediate phases; chalcopyrite interpretation; a bornite reference within a cluster of observations, and at least two further observations.*

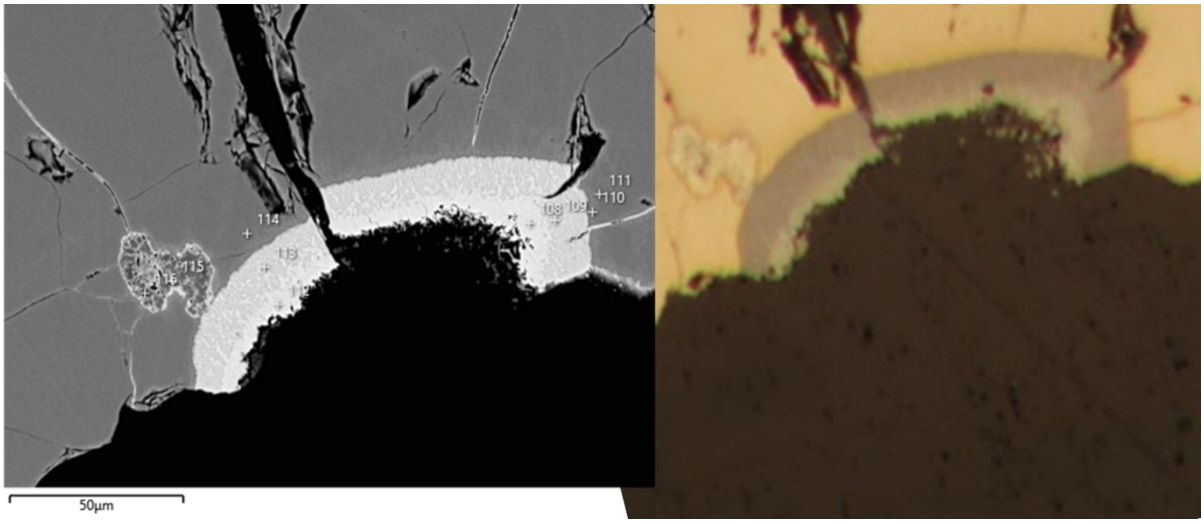

***Figure 63**: PO9 mineral product, shown under (left), Scanning Electron Microscopy; and (right) Optical Microscopy*

***Table 37**: EBSD analyses of PO9 grain.*

Exp. ID	EBSD Spectrum	Electron emission rate			Interpretation
		Cu (≈ 0.9 KeV)	Fe (≈ 6.4 KeV)	S (≈ 2.4 KeV)	
CCP ref	-	108.22	74.46	322.08	
BOR ref	-	264.39	30.89	224.08	
PO9	111, 114	8.39	135.42	385.49	intermediate phase
	110	31.74	125.81	357.49	intermediate phase
	109, 113	373.36	20.36	201.610	
	108, 112	500.92	7.64	173.17	

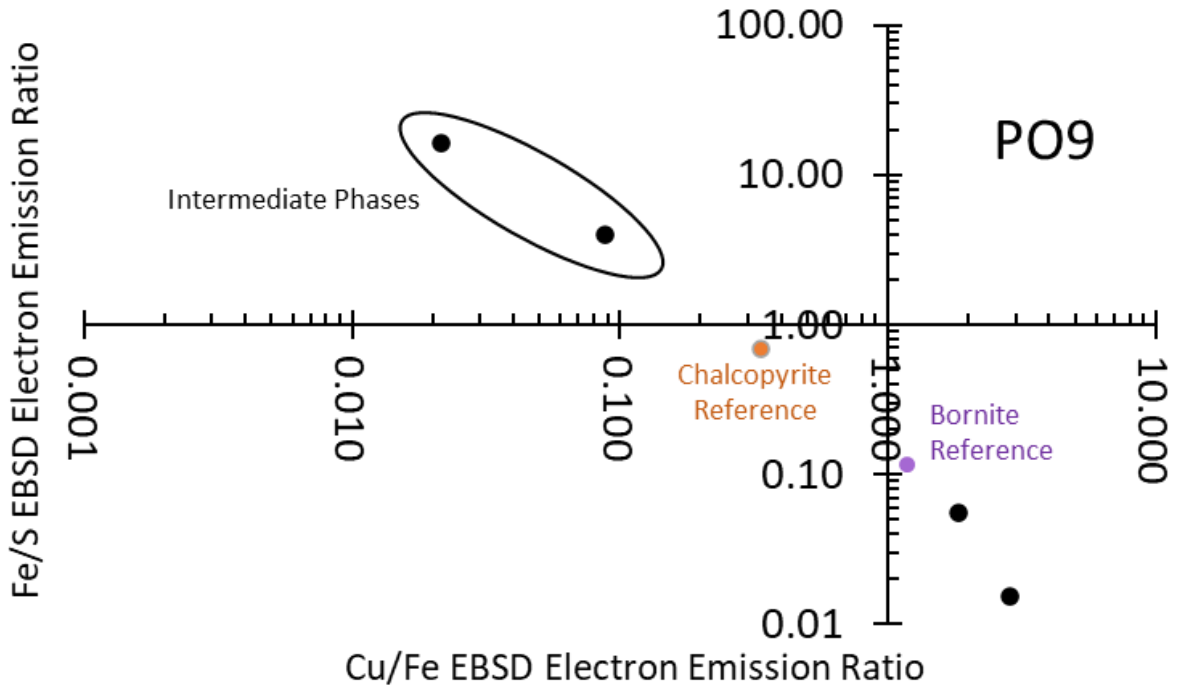

Figure 64: *Interpretation of EBSD electron emission data from PO9 analyses: showing intermediate phases; chalcopyrite reference; a bornite reference, and two further observations.*

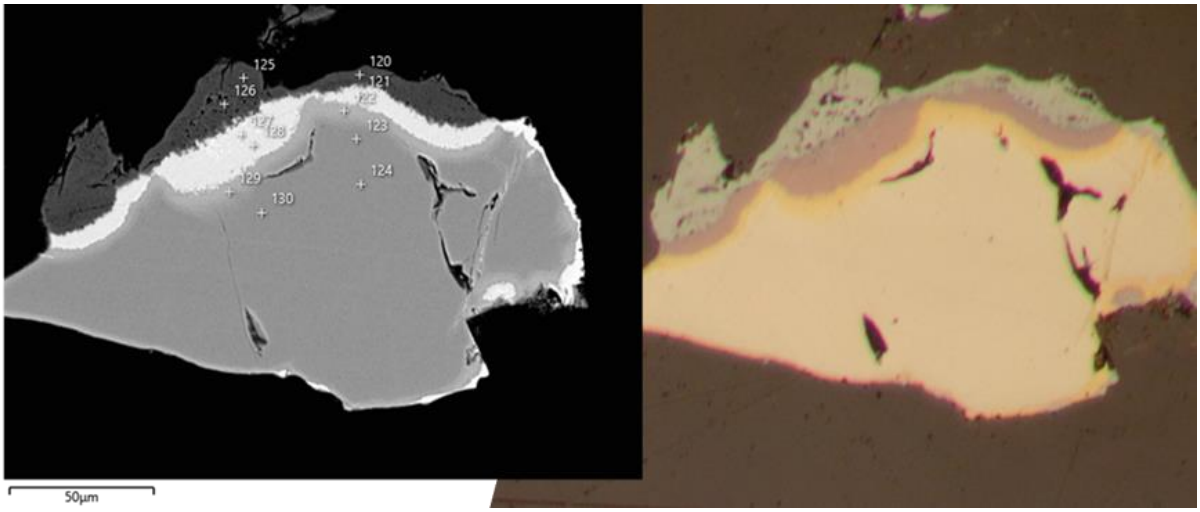

Figure 65*: PO10 mineral product grain 1, shown under (left), Scanning Electron Microscopy; and (right) Optical Microscopy*

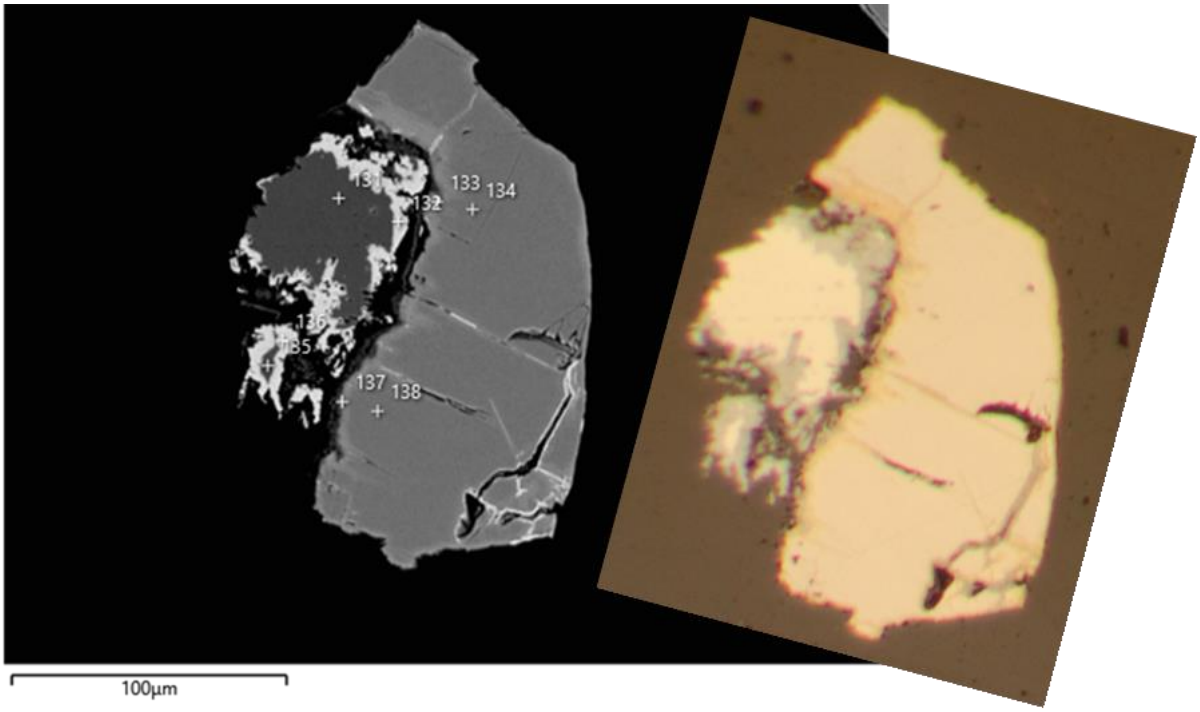

***Figure 66**: PO10 mineral product grain 2, shown under (left), Scanning Electron Microscopy; and (right) Optical Microscopy*

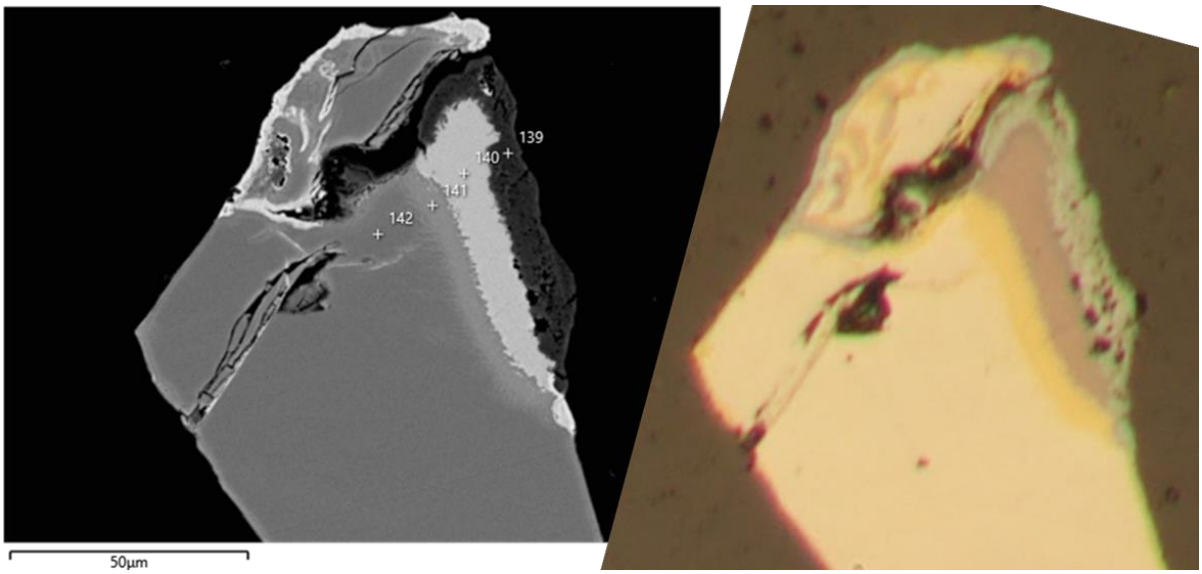

***Figure 67**: PO10 mineral product grain 3, shown under (left), Scanning Electron Microscopy; and (right) Optical Microscopy*

Table 38: *EBSD analyses of PO10 grains.*

Exp. ID	EBSD Spectrum	Electron emission rate			Interpretation
		Cu (≈ 0.9 KeV)	Fe (≈ 6.4 KeV)	S (≈ 2.4 KeV)	
CCP ref	-	108.22	74.46	322.08	
BOR ref	-	264.39	30.89	224.08	
PO10	123, 130	6.26	134.41	387.49	intermediate phase
	122, 129	109.13	77.30	326.31	chalcopyrite
	121, 128	286.63	36.14	225.74	bornite
	127	348.36	26.35	205.99	
	134	nil	-	-	unaltered pyrrhotite
	138	6.08	137.84	391.22	intermediate phase
	133	97.33	78.67	321.01	chalcopyrite
	142	5.29	139.07	382.78	intermediate phase
	141	106.35	79.43	328.16	chalcopyrite
	140	284.41	34.23	228.25	bornite

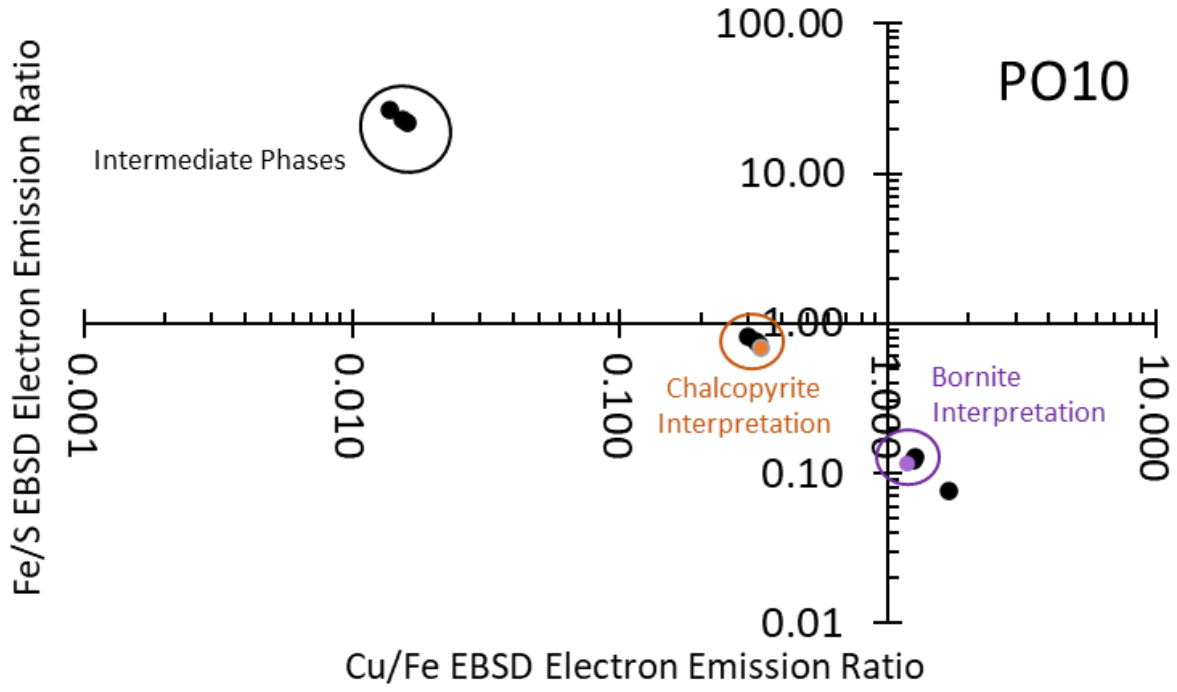

Figure 68: *Interpretation of EBSD electron emission data from PO10 analyses: showing intermediate phases; chalcopyrite interpretations; bornite interpretations, and one further observation.*

5.7.0 Comparisons with Previous Works

This work will evaluate the enrichment of copper into pyrrhotite stage by stage. An overall 'cluster' plot of observations, with the reference points for chalcopyrite and bornite is given in **Figure 69**.

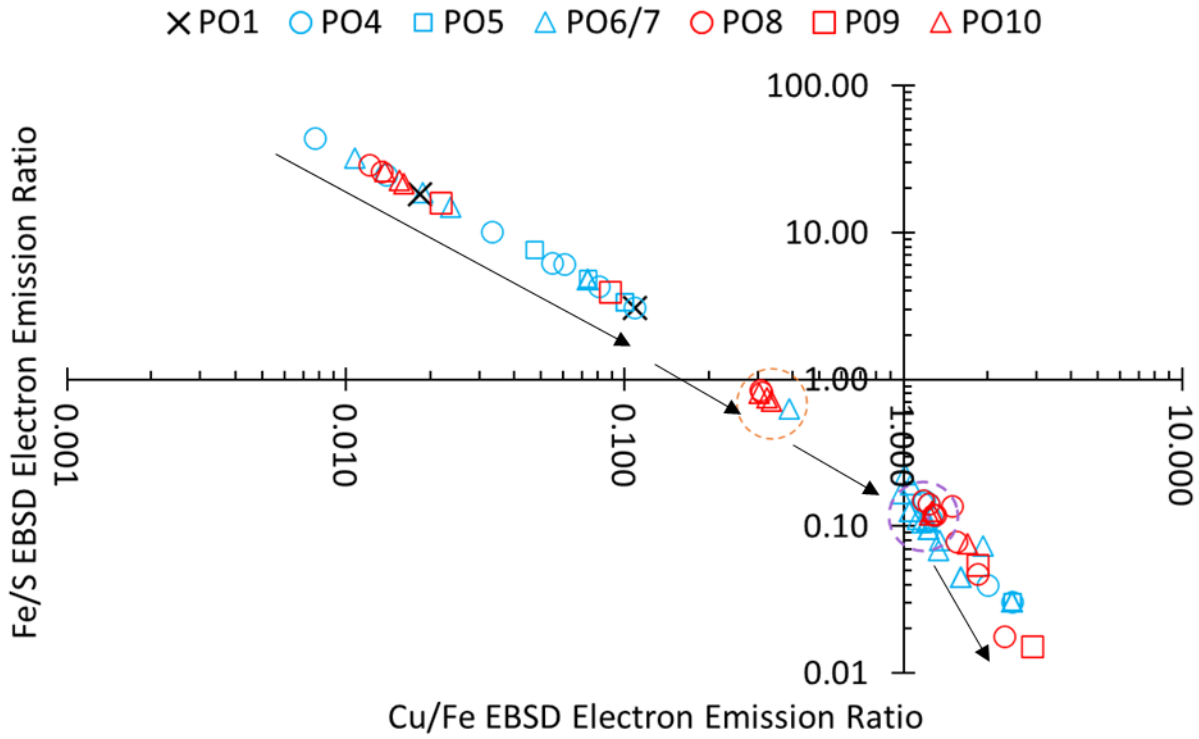

Figure 69: *EBSD electron emission data from all pyrrhotite analyses: showing intermediate phases; chalcopyrite interpretations (orange dotted circle); bornite interpretations (purple dotted circle), and further observations.*

5.7.1 Intermediate Phases

Two intermediate phases have been identified in previous work (Cowper & Rickard, 1989). This work interprets a continuous uptake of copper due to the linearity of data, rather than the presence of clusters in this initial stage. The presence of an intermediary phase is observed in every reacted experiment product.

While products which reacted at 50 and 100°C seem to have an extended intermediary phase, all but one observation of the intermediate phase in the 200°C experiments are in a lesser band of copper concentration.

5.7.2 Chalcopyrite

Previous works have commented that Cubanite ($CuFe_2S_3$) has a yellow colouration under optical microscopy, like Chalcopyrite ($CuFeS_2$) (Cowper & Rickard, 1989). Therefore, this work will make note of chalcopyrite identified only by colour.

Chalcopyrite was not observed in any 50°C experiment.

A yellow mineral is observed in PO4; and in PO9, but neither are analysed with EBSD. Oxidisation prevents analysis beyond the intermediate phase in PO5.

Therefore, the interpretation, is that the activation energy for the transition from intermediate phase to Chalcopyrite, is greater than that achieved at 50°C.

5.7.3 Bornite

Bornite is interpreted from its characteristic grey-lilac colour under optical microscopy, in all 100 and 200°C experiments except PO5 (oxidised). Bornite is not confirmed by a spot analysis (ESBD) in PO9.

5.7.4 Beyond Bornite

Beyond Bornite, colour is the most useful indicator.

PO4 has light blue grey reaction rim, this is interpreted as digenite (Pracejus, 2016). The same light grey blue is seen in PO6, PO8, and PO10.

A vivid blue is seen in PO6 and PO8, interpreted as chalcocite (Hjeltström, 2015).

PO9 has an outer reaction rim which is very pale in colour, and EBSD analyses return a very low proportion of iron. Although not conclusive, the description reasonably matches Anilite (Pracejus, 2016). Due to limitations in this work, the mineral will not be identified.

5.7.5 Summary

The loss of the opportunity to use electron microprobe analysis has significantly hindered the possibility of determining the sequence of minerals, using colour alone is very relative and subjective. EBSD, as mentions is qualitative, as seen in **Figure 69**, these analyses do not fit perfectly into discrete clusters.

In the intermediate phase, low temperature (<100°C) experiments are observed to use both Phase A and B as transitional phases. Only one EBSD observation is made with electron emission counts which indicate Phase B.

Chalcopyrite and Bornite likely form at each concentration experimented, at temperatures 100°C or above.

Inferred Digenite and Chalcocite are limited to temperatures above 100°C, but do not seem to be controlled by copper concentration.

As seen in the images of the reacted grains, this work does not observe a uniform reaction rim. Instead, the reactions are largely limited to certain areas: for example, within the strait in PO5; or within crescents in PO6, PO8 and PO9.

Table 39 provides the methods of how each mineral product was identified.

Table 39: *Overview of mineral products from Pyrrhotite experiments and method of identification. OM: Optical Microscopy, by colour; EBSD: Electron BackScatter Diffraction, to distinguish minerals*

Temperature (°C)	50	100				200		
$CuSO_4$ Concentration (mM)	05 (PO1)	05 (PO4)	10 (PO5)	50 (PO6)	50 (PO7)	05 (PO8)	10 (PO9)	50 (PO10)
Intermediate "A"	EBSD	EBSD	EBSD	EBSD		EBSD	EBSD	EBSD
Intermediate "B"	EBSD	EBSD	EBSD		EBSD	-	EBSD	-
Chalcopyrite ($CuFeS_2$)	-	OM Only	-	OM/EBSD		OM/EBSD	OM	OM/EBSD
Bornite (Cu_5FeS_4)	-	OM/EBSD	-	OM		OM/EBSD	OM	OM/EBSD
Digenite (Cu_9S_5)	-	OM/EBSD	-	EBSD		OM/EBSD		OM/EBSD
Chalcocite (Cu_2S)	-	-	-	OM/EBSD	EBSD	OM/EBSD		-
Unidentified Mineral	-	-	-	-		-	OM/EBSD	-

A note on Pyrite: No reaction was observed with pyrite at 50 or 100°C. Pyrite at 200°C reacted and oxidised: therefore, the reaction was rejected.

DISCUSSION

6.1.0 Lessons from the 2022 UN Oceans Conference, Lisbon

This sub-section is written in the first person, in a more human tone.

For me, attending the One Sustainable Ocean conference, alongside the UN Oceans Conference in Lisbon: was a reset, a return to form. It was an opportunity to reevaluate and gain valuable perspectives.

This project has straddled the global coronavirus pandemic. This was a period of immense disruption; a loss of research funding; and a huge reduction in the scope of what this project can achieve. The wider impact of the pandemic has since been compounded by ongoing war in Ukraine, and a developing situation over Taiwan and the South China Sea. These global challenges were acknowledged at the conference.

The One Sustainable Ocean conference was a side event to the UN Oceans conference: attended by NGOs, sustainable businesses; and government delegates from the main events.

It was quickly clear that the debate around deep sea mining is dogmatic, even the mention deep sea mining at a few stalls returned a wincing reaction. I found it particularly striking that the opposition to the industry - for example the Pacific Blue Line (Pacific Parlimentarians Alliance on Deep Sea Mining, 2022) - outrightly reject the narrative that minerals produced by deep-sea mining would benefit the transition to green energy, or to a circular economy. This may be indicative that literature tends to emphasize the base economic metals and treat critical metals as a ‘silver lining’.

In conversation with young Ocean Leaders from the Sustainable Ocean Alliance, and the Pacific Blue Line, there is a sense of distrust about scientific research into submarine deposits, as it could be used as a back door into exploitation. Furthermore, for the Pacific Islands “marine scientific research is conducted by international teams” which causes concern regarding the “sharing of benefits and results of the research with the host country.” (Office of the Pacific Ocean Commissioner, 2021).

If this feeling is true for other developing communities: in my own opinion, this should be seen broadly, as a failure by the marine scientific community. More effort should be made to include host countries as stakeholders in our research.

The debate is further intensified by quite emotive provocative voices, an example was Mariama Williams, who equated the investment into deep sea mining to modern day colonialism. Who suggested it would be criminal for investors in the developed world to seek to profit from the exploitation of nations they would never visit, nor share the direct impacts of exploitation with.

Surprisingly, I encountered no overt deep sea mining companies in Lisbon. However, I was interrupted whilst in conversation with a representative from the Pacific Network of Globalisation, by a gentleman who reminded the representative about a closed-door strategy meeting and making an underhand remark about granting exploration licenses in contradiction to the regional position.

This may be because the opposition to deep sea mining has momentum. In April 2022, Tuvalu became the first nation in the world to unilaterally withdraw from a state-sponsored submarine mineral exploration project. Foreign Minister, Simon Kofe, cited that the agreement with Circular Metals Tuvalu was signed with the previous government – in contradiction with the views of the current administration (Srinivasan, 2022). With this emboldened sense, nations are holding a very conservative negotiating position.

There is widespread criticism of the International Seabed Authority (ISA) regarding their transparency and standards. Topically, the ISA are currently in negotiations with the Metals Company, who may begin exploiting polymetallic nodules within a year on only interim approval (Scales, 2022).

Notwithstanding the legitimate concerns, it seems like it would be foolish to neglect scientific research into submarine hydrothermal deposits, even during a proposed international moratorium on deep-sea mining. If, in the fullness of time, this moratorium is a pause instead of a stop: a greater understanding of the distribution of critical metals in, and within, submarine mineral resources would allow society to make more informed decisions on where to produce these resources per demand.

6.2.0 Deep Sea Mining and Mining Economics

The cost of primary metal production is driven by the volume of ore to be processed: therefore, it is natural for industry to pursue projects which contain higher metal concentration. Lower volume, higher value.

Across the mining industry, the debate between prioritising either value or volume, is surprisingly recent. During the last commodity cycle, between 2003 and 2013 (Hutton, 2022), mining companies prioritised volume with the aim to drive down production costs using “greater economies of scale” logic. As this approach was not economically sustainable, having heavily relied on high demand premium, the benefits were only very briefly envisaged (Hutton, 2022).

Regarding deep sea mining concepts, it is apparent that ore processing would be conducted onshore. Following this, could regional cooperation to build centralised processing capacity be both economically and environmentally favorable?

A criticism of submarine hydrothermal systems (seafloor massive sulfides) as metal deposits is their scale (Hannington, et al., 2011). However, lessons from the early 21st century highlight those smaller projects have both less commercial and less technical risk than larger projects. Therefore, in a new paradigm for the mining industry, they may become more attractive to investors.

I recall in 2015, attending the Underwater Mining Conference in Tampa, Florida: when conference was told that the potential for seafloor massive sulphide to contribute to global metal reserves was not significant (Petersen, 2015).

Over the course of the past few years, it has become clearer that if, or when, deep sea mining goes ahead – it would be the exception, not the rule. Therefore, to reduce the impact that deep sea mining would have, we need to identify these exceptional deposits.

Are those deposits going to be submarine hydrothermal systems?

6.3.0 Critical Metals in Other Deposits

At the start of this project, in 2018, the first deep sea mine was due to be Nautilus Mineral's Solwara 1 project in Papua New Guinea: a seafloor massive sulphide deposit. Today, the first project is due to be a polymetallic nodule mine in the Clarion Clipperton Zone agreed between Nauru and The Metals Company (The Metals Company, 2022).

To use an analogy, could submarine massive sulphides have been used as a 'gateway' proof of concept? Take wireless charging phones for instance, as a 'gateway' proof of concept for, something currently bombastic like a wireless electric car charger in your driveway – or a charging lane for electric cars on the motorway. Develop a commercial project, drive down costs by improving technology and processes, then upscale the concept.

Ferromanganese crusts and polymetallic nodules exist deeper in our oceans and have a greater potential for critical metals. Polymetallic nodules have long been proposed as a submarine mineral resource (Mero, 1965), where the primary target metals are copper, cobalt and nickel (Keber, et al., 2020; Randhawa, et al., 2016).

Nodules form as a result of hydrogenetic or diagenetic precipitation (Kuhn, et al., 2018), which are noted as being among the slowest known geological phenomena (Kobayashi, et al., 2000). Either type of precipitation enriches a selection of elements:

- Hydrogenetic precipitations form around a core sourcing those minerals from seawater, this type of precipitation is characterised by a Mn/Fe ratio of less than or equal to five, and enriches titanium, rare earth elements, yttrium, zirconium, niobium, tantalum, and hafnium. Cobalt, cerium, and tellurium can also be incorporated into oxidised layers (Kuhn, et al., 2018).
- Diagenetic precipitations form as a result of manganese remobilisation. In these precipitates the Mn/Fe ratio is characterised as greater than five, and the commonly enriched metals include nickel, copper, barium, molybdenum, lithium, and gallium (Kuhn, et al., 2018).

The elements found in hydrogenetic nodules are more critical than those in diagenetic nodules. The same hydrogenetic process forms ferromanganese crusts.

Table 40: *A comparison of critical element abundances in Ferromanganese Crusts (Hein, et al., 2013); Polymetallic Nodules (Hein, et al., 2013); Hydrothermal Fluids (this work); and Hydrothermal Deposits (expanded from (Hannington, et al., 2004). Highest grade is noted, HD: Hydro. Deposit; HF: Hydro. Fluid; C: Crust; N: Nodules.*

		Crusts					*Nodules*			*Hydrothermal Systems*	
		Atlantic Ocean	Indian Ocean	N. Pacific Prime	Non-Prime N. Pacific	S. Pacific	CA margin	CCZ	Peru Basin nodules	I. Ocean nodules	Fluid	Chimney
Element		**Mean**	**Mean**	**Mean**	**Mean**	**Mean**	**Mean**	**Mean**	**Mean**	**Mean**	**Mean**	**Median**
"Low" Level Critical Elements												
Cu	HD	861.00	1105.00	982.00	1074.00	1082.00	438.00	10714.00	5988.00	10406.00	6320.00	11500.00
Cd	HD	4.10	3.50	16.00	17.00	4.10	15.00	16.00	19.00	18.00	10.50	350.00
Au (ppb)	C	6.00	21.00	55.00	25.00	33.00	6.60	4.50	-	-	-	1.26
Ni	N	2581.00	2563.00	4216.00	3495.00	4643.00	2299.00	13002.00	13.01	11.01	2160.00	11.00
Pb	C	1238.00	1371.00	1636.00	1470.00	1057.00	1541.00	338.00	121.00	731.00	199.00	845.00
"Low-Medium" Level Critical Elements												
Se	C	0.44	1.70	2.80	13.00	5.10	1.00	0.72	0.50 -		8.66	106.00
Ag	HD	0.20	0.37	0.10	1.50	0.97	1.20	0.17	0.05 -		3520.00	0.19
Li	HF	33.00	83.00	33.00	73.00	3.50	15.00	131.00	311.00	110.00		
Mo	N	409.00	392.00	463.00	516.00	418.00	354.00	590.00	547.00	500.00	5.72	34.00
"Medium" Level Critical Elements												
Ta	C	1.30	0.91	1.20	3.10	12.00	0.75	0.33	0.23	1.80	0.00	0.50
Cr	C	47.00	22.00	28.00	30.00	35.00	52.00	17.00	16.00	18.00		
Co	C	3608.00	3291.00	6655.00	3733.00	6167.00	2977.00	2098.00	475.00	1111.00	50.50	7.00
Sn	C	83.00	9.70	13.00	9.00	11.00	3.30	5.30	0.90 -			
V	C	849.00	634.00	642.00	679.00	660.00	613.00	445.00	431.00	497.00	0.27	14.50
Nd	C	243.00	259.00	255.00	275.00	184.00	253.00	140.00	63.00	146.00	175.00	5.00
La	C	272.00	290.00	338.00	320.00	204.00	269.00	114.00	68.00	129.00	51.00	3.00
Ce	C	1392.00	1469.00	1311.00	1360.00	818.00	1351.00	284.00	110.00	486.00	191.00	3.00
Sm	N	55.50	60.80	51.30	56.80	38.10	53.50	340.00	14.00	32.40	49.60	0.10
Gd	C	57.90	67.20	55.80	66.30	43.90	55.40	31.80	15.60	32.00	53.80	0.03
"Medium-High" Level Critical Elements												
Hf	C	8.70	9.80	9.20	6.90	9.10	63.00	4.70	4.70	14.00	0.00	1.00
Pt	C	567.00	211.00	66.00	24.00	15.00	23.00	12.00				
Ge	C	0.66	0.64		15.00	2.40	0.96		0.60 -			
In	C	0.18	0.26	0.60	0.79	0.87	0.14	0.27	0.08 -			
"High" Level Critical Elements												
Te	C	43.00	31.00	60.00	30.00	38.00	11.00	16.00	17.00	40.00		
Ga	C	15.00	16.00	18.00	18.00	29.00	11.00	36.00	32.00 -			
Pr	C	63.80	66.20	61.00	61.20	40.80	60.40	33.40	14.10	33.00	45.50	0.03
Dy	C	47.10	55.60	59.20	56.00	40.70	48.70	28.50	15.80	26.50	56.70	0.03
Eu	C	11.50	123.00	12.40	137.00	17.50	114.00	8.03	3.87	7.83	132.00	0.02
Tb	C	9.17	9.99	8.73	955.00	598.00	8.83	4.98	2.52	5.00	11.80	0.50
Y	HF	181.00	178.00	222.00	190.00	177.00	169.00	96.00	69.00	108.00	1000.00	4.50

Most critical elements are shown in **Table 40** to be found in greater concentrations in either polymetallic nodules or ferromanganese crusts. Therefore, a shift in focus towards these deposits is expected.

In 2015, the UK government explicitly suggested Deep Sea Mining as a method to reduce dependency on China for the supply of Rare Earth Elements (Carver, et al., 2020). In a question-and-answer session at the 2019 Trondheim Ocean Week conference, I heard a Norwegian minister asking how soon the mining of nodules could contribute to their windfarm projects.

It seems that since the collapse of Nautilus (Nautilus Minerals, 2019), the tide has changed on Deep Sea Mining: and submarine hydrothermal systems are no longer the focus.

6.4.0 The Use of Hydrothermal Fluids

If this work has achieved one thing, it has been to demonstrate the paucity of data on hydrothermal fluids. Of 298 confirmed active hydrothermal systems, only 62% (184) have a reported venting temperature.

Of 123 high temperature venting systems, only 28% (34) have any geochemistry data. Of those 34, only our twenty-six also had deposit data.

Although in low confidence, this work has demonstrated positive trends between hydrothermal fluids and chimneys abundances for bromine, calcium, cadmium, copper, iron and zinc. These metals represent each of the lithophile, chalcophile and siderophile Goldschmidt classifications.

These empirical observations, if improved upon, may be coupled with first principles and relationships between elements to approximate abundances in deposits.

However, this work also set out to determine whether hydrothermal fluids could themselves be considered as a resource. **Table 40** lists Lithium and Yttrium to be found in greater concentrations in hydrothermal fluids than other submarine mineral deposits.

In terms of lithium, operational hard rock mines typically offer grades between 0.9-1.6% Li_2O; in brines, from evaporative lakes in South America, the highest concentrations vary between 680-1570ppm (European Lithium, 2020). **Figure 70** shows the distribution of lithium concentration in hydrothermal fluids, as greater than the highest concentrations in lakes.

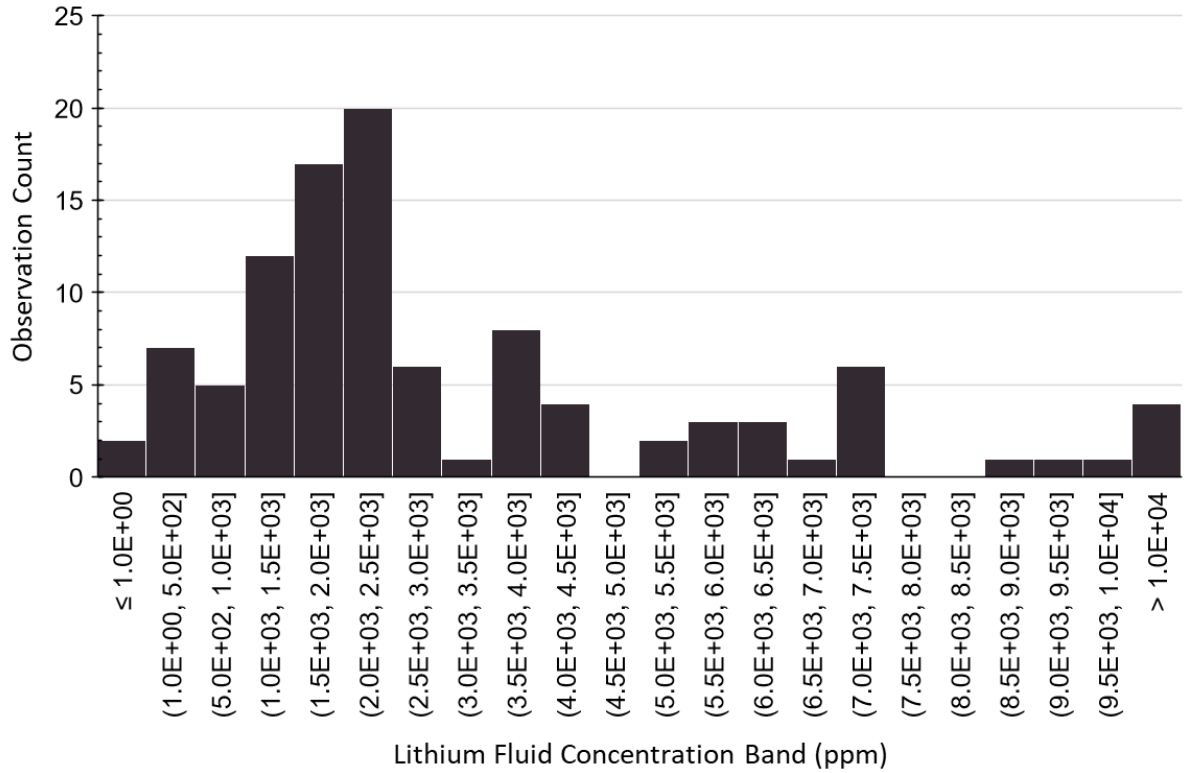

***Figure 70**: Distribution of lithium concentration in hydrothermal fluids.*

Consider an exceptional hydrothermal system, Minami-Ensei at 610-740 mbsl in the Okinawa Trough, Japanese EEZ. The system vents at 280°C, at a near boiling V:B ratio of 0.96. Vent fluids have a pH of 4.9, and the concentration of lithium is 38,900 ppm, 5.6mM (Kawagucci, 2014).

No flow rate of hydrothermal fluid is known for this system but compared to the 1.0 metres per second at Clam Acres (p. 26) which is hotter but has a V:B ratio of 0.90 (355°C at 2600mbsl), this work will assume a conservative one metre per second exit velocity. For a round number, assume the vent orifice of 0.1 metre cubed area: approximately 12.6 cm diameter.

A calculation gives 0.1 metre cubed per second: therefore, at 5.6mM Lithium, 3.9mg of lithium is emitted each second. In a day (86,400 seconds), 336 grams of lithium are emitted. Lithium is currently on a rally, in March 2022 the value of battery grade lithium carbonate was averaging $76,700 per tonne, up from $13,400 per tone in March 2021. Therefore, even at these inflated prices, the potential revenue per day for Lithium is just $25.75. That assumes 100% of the lithium is collected.

The same thought experiment could be repeated for Yttrium, but there is insufficient data.

6.5.0 The Use of Submarine Hydrothermal Deposits

Do we need to mine submarine hydrothermal systems?

It seems like the industry has moved away from submarine hydrothermal systems. This work has demonstrated that even when critical minerals are concentrated more in hydrothermal fluids, than any submarine mineral deposit, the potential revenue is insignificant.

Hydrothermal deposits have concentrations of Copper, Cadmium and Silver greater than those observed in polymetallic nodules, or ferromanganese crusts. However, the are all low, low-medium level critical elements: and, more importantly, are all present as a potential by-product in nodules and crusts.

This work has shown both the complexity of these systems, and paucity of data we have on them. There are tectonic settings such as intraplate volcanoes, where there is no representation in the data at all.

This work has focussed on deeper, base metal rich hydrothermal systems. It is possible that this study fell for the same pitfalls that an exploiter might. The appendices of this work show that rare earth elements have stronger relationships with the lithophile type elements (Goldschmidt, 1937). Mentioned previously, Calcium (a lithophile element) has retrograde solubility with temperature. Perhaps future research in hydrothermal activity should focus on ‘white smokers’, in line with a renewed focus on critical metals.

CONCLUSIONS

7.1.0 Meta-Analysis Section

This work has compiled a dataset of hydrothermal fluid endmember geochemistry across 26 submarine hydrothermal systems. Interelement analysis has shown that elements behave according to their core geochemical classification (Goldschmidt, 1937): and that low confidence trends have been identified between hydrothermal fluids and chimney type deposits.

Relationships are observed between abundances of metals between chimney-, surface-, and core-type samples. With a larger dataset in future work, there is a basis to work upon in estimating the abundance of metals via less invasive sampling.

Hydrothermal fluids present with greater concentrations of Lithium and Yttrium than other proposed submarine resources, but the rate of emission is too little to consider exploiting.

Submarine hydrothermal systems are shown to be complex environments, and there is a worrying paucity of data on these environments.

Compared to polymetallic nodules and ferromanganese crusts, submarine hydrothermal systems present little potential for a source of critical metals.

7.2.0 Experimental Section

This work evaluates the mechanism of copper enrichment into pyrrhotite, after previous works (Zies, et al., 1916) (Shouten, 1934) (Cowper & Rickard, 1989) (Rickard & Cowper, 1994) (Pękala, et al., 2011).

This work identifies a continuous intermediate phase between Pyrrhotite and Chalcopyrite. A second stage of this phase is only observed in one high temperature (200°C) experiment.

Chalcopyrite and Bornite replace sequentially at temperatures above 100°C. Beyond Bornite, this work identifies minerals by colour as Digenite and Chalcocite. An unidentified mineral is observed at 200°C. The loss of the opportunity to analyse products under EMPA has drastically impacted the findings of this work.

7.3.0 Final Remarks

Whilst researching and writing for this degree, the world has changed. In 2018, supply chain woes were ironic: like KFC running out of chicken throughout the UK.

Events over the past few years have highlighted the seriousness of supply chain vulnerabilities: In response to Coronavirus, more than half of humanity were asked to confine themselves at the same time (Sandford, 2020), the ramifications of this pandemic continue.

In 2021, the global supply chain figuratively had a heart attack. On March 23rd, the *Ever Given* grounded and obstructed passage through the Suez Canal – an artery of global trade (Nabil, 2021).

Later in 2021, the hasty withdrawal of US and Allied troops from Afghanistan left the worlds most significant Lithium deposits in the hands of the Taliban (Horowitz, 2021).

In 2022, Russia invaded Ukraine, the breadbasket of Europe: and is now positioning itself in closer ties with China (Brant, 2022)

A developing diplomatic dispute between China and Taiwan is widening the gap between China and the west. As I write this, two US warships are passing through the Taiwan strait in an act of defiance against China, who are on High Alert (BBC News, 2022).

The developed world is in competition to reduce their environmental impact: and concurrent the collapse of globalisation, and of international cooperation – is exacerbating the demand for ‘critical minerals’ as nations are forced to diversify their supply chains.

The pacific island states report a slow uptake of renewable energy, due to negative perceptions about the technology and cost (Office of the Pacific Ocean Commissioner, 2021). This region will likely be most effected by the impacts of deep-sea mining, as the developed worlds source of ‘critical metals’ for these technologies. Are these perceptions going to improve? How are these perceptions effected if exploration and exploitation is done without consideration of the impact?

Mining submarine deposits needs to be selective, the exception – not the rule. The focus seems to be rightfully shifting towards the most critical of critical elements.

REFERENCES

Baker, E. T. et al., 2017. The Effect of Arc Proximity on Hydrothermal Activity AlongSpreading Centers: New Evidence From the Mariana Back Arc (12.78N–18.38N). *Geochemistry, Geophysics, Geosystems,* Volume 18, pp. 4211-4228.

BBC News, 2022. *Taiwan: Two US warships sail through strait.* [Online] Available at: https://www.bbc.co.uk/news/world-asia-62704449 [Accessed 28 August 2022].

Beaulieu, S. E., Baker, E. T. & German, C. R., 2015. Where are the Undiscovered Hydrothermal Vents on Oceanic Spreading Ridges?. *Deep Sea Research Part II: Topical Studies in Oceanography,* Volume 121, pp. 202-212.

Beaulieu, S. E., Baker, E. T., German, C. R. & Maffei, A., 2013. An authoritative global database for active submarine hydrothermal vent fields. *Geochemistry, Geophysics, Geosystems,* 14(11), pp. 4892-4905.

Bemis, K. G. et al., 2002. A Comparison of Black Smoker Hydrothermal Plume Behavior at Monolith Vent and Clam Acres Vent Field: Dependence on Source Configuration. *Marine Geophysical Researches,* Volume 23, pp. 81-96.

Berndt, M. E. & Seyfried, W. E., 1990. Boron, bromine, and Other Trace Elements as Clues to the Fate of Chlorine in Mid-Ocean Ridge Vent Fluids. *Geochimica et Cosmochimica Acta,* Volume 54, pp. 2235-2245.

Bischoff, J. L. & Rosenbauer, R. J., 1988. Liquid-vapour relations in the critical region of the system NaCl-H2O from 380°C to 415°C - a refined determination of the critical point and two phase boundary of seawater. *Geochimica et Cosmochimica Acta,* 52(8), pp. 2121-2126.

Borowski, C. et al., 2007. New Coordinates for the Hydrothermal Structures in the Logatchev Vent Field At 14°45'N on Mid-Atlantic Ridge. *International Research: InterRidge News,* Volume 16, pp. 13-14.

Brant, R., 2022. *China joins Russia in opposing Nato expansion.* [Online] Available at: https://www.bbc.co.uk/news/world-asia-60257080 [Accessed 29 August 2022].

Brown, D., 2022. *China and Taiwan: A really simple guide.* [Online] Available at: https://www.bbc.co.uk/news/world-asia-china-59900139 [Accessed 29 August 2022].

Brugger, J. et al., 2007. An XAS Study of the Structure and Thermodynamics of Cu(I) Chloride Complexes in Brines up to High Temperature (400 °C, 600 bar). *Geochimica et Cosmochimica Acta,* Volume 71, pp. 4920-4941.

Calvo, G., Mudd, G., Valero, A. & Valero, A., 2016. Decreasing Ore Grades in Global Metallic Mining: A Theoretical Issue of a Global Reality?. *Resources,* 5(4), pp. 1-14.

Carver, R. et al., 2020. A critical social perspective on deep sea mining: Lessons from the emergent industry in Japan. *Ocean and Coastal Management,* 193(105242), pp. 1-10.

Charlou, J. L. et al., 1996. Mineral and gas chemistry of hydrothermal fluids on an ultrafast spreading ridge: East Pacific Rise, 17° to 19°S (Naudur cruise, 1993) phase seperation processescontrolled by volcanic and tectonic activity. *Journal of Geophysical Research,* 101(B7), pp. 15899-15919.

Chen, Y. J. & Morgan, J. P., 1996. The effects of spreading rate, the magma budget, and the geometry of magma emplacement on the axial heat flux at mid-ocean ridges. *Papers on Geomagnetism and Paleomagnetism Marine Geology and Geophysics,* 101(B5), pp. 11475-11482.

Converse, D. R., Holland, H. D. & Edmond, J. M., 1984. Flow Rates in the Axial Hot Springs of the East Pacific Rise (21°N): Implications for the Heat Budget and the Formation of Massive Sulphide Deposits. *Earth and Planetary Science Letters,* 69(1), pp. 159-175.

Coogan, L. A. et al., 2017. Near-Vent Chemical Processes in a Hydrothermal Plume: Insights From an Integrated Study of the Endeavour Segment. *Geochemistry, Geophysics, Geosystems,* Volume 18, pp. 1641-1660.

Corliss, J. B. et al., 1979. Submarine Thermal Springs on the Galapagos Rift. *Science,* 203(4385), pp. 1073-1083.

Coumou, D., Driesner, T., Weis, P. & Heinrich, C. A., 2009. Phase separation, brine formation, and salinity variation at Black Smoker hydrothermal systems. *Journal of Geophysical Research,* 114(B03212), pp. 1-16.

Covington, A. K., Bates, R. G. & Durst, R. A., 1985. Definition of pH Scales, Standard Reference Values, Measurement of pH and Related Terminology. *Pure and Applied Chemistry,* 57(3), pp. 531-542.

Cowper, M. & Rickard, D., 1989. Mechanism of Chalcopyrite Formation from Iron Monosulphides in Aqueous Solutions (<100°C, pH 2-4.5). *Chemical Geology,* 78(3-4), pp. 325-341.

Dos Santos, E. G., de Mendonça Silva, J. C. & Duarte, H. A., 2016. Pyrite Oxidation Mechanism by Oxygen in Aqueous Medium. *The Journal of Physical Chemistry,* Volume 120, pp. 2760-2768.

Dyment, J. et al., 2009. Detailed investigation of hydrothermal site Rainbow, Mid-Atlantic Ridge,. *International Research,* Volume 18, pp. 22-24.

Edmonds, H. E. & German, C. R., 2004. Particle Geochemistry in the Rainbow Hydrothermal Plume, Mid-Ocean Ridge. *Geochimica et Cosmochimica Acta,* 68(4), pp. 759-772.

Elderfield, H. & Schultz, A., 1996. Mid-Ocean Ridge Hydrothermal Fluxes and the Chemical Composition of the Ocean. *Annual Review of Earth and Planetary Sciences,* Volume 24, pp. 191-224.

Emmons, W. H., 1917. *The Enrichment of Ore Deposits,* Washington: Department of the Interior; United States Geological Survey.

Engineering Toolbox, 2005. *Boiling Points at High Pressure.* [Online]
Available at: https://www.engineeringtoolbox.com/boiling-point-water-d_926.html
[Accessed 28 June 2019].

European Lithium, 2020. *Lithium.* [Online]
Available at:
https://europeanlithium.com/lithium/#:~:text=Lithium%20Sources,lithium%20carbonate%20or%20lithium%20hydroxide.
[Accessed 28 August 2022].

Evans, G. N., Tivey, M. K., Seewals, J. S. & Wheat, C. G., 2017. Influences of the Tonga Subduction Zone on seafloor massive sulfide deposits along the Eastern Lau Spreading Center and Valu Fa Ridge. *Geochimica et Cosmochimica Acta,* Volume 215, pp. 214-246.

Fallon, E. K., Petersen, S., Brooker, P. A. & Scott, T. B., 2017. Oxidative Dissolution of Hydrothermal Mised-Sulphide Ore: An Assement in Current Knowledge in Relation to Seafloor Massive Sulphide Mining. *Ore Geology Reviews,* Volume 86, pp. 309-377.

Forsyth, D. & Uyeda, S., 1975. On the Relative Importance of the Driving Forces of Plate Motion. *Geophysical Journal of the Royal Astronomical Society,* 43(1), pp. 163-200.

Fracheteau, J. et al., 1979. Massive deep-sea sulphide ore deposits discovered on the East Pacific Rise. *Nature,* 277(5697), pp. 523-528.

Frimanslund, E. K. T., 2016. *Feasibility of Deep-Sea Mining Within Norweigan Jurisdiction,* Trondheim: Norweigan University of Science and Technology (NTNU).

Fulton, J. L., Hoffman, M. M. & Darab, J. G., 2000. An X-ray Absorption Fne Structure Study of Copper(I) Chloride Coordination Structure in Water up to 325°C. *Chemical Physics Letters,* 330(3-4), pp. 300-308.

Gale, A. et al., 2013. The Mean Composition of Ocean Ridge Basalts. *Geochemistry, Geophysics, Geosystems,* 14(3), pp. 489-518.

Galley, A., Hannington, M. & Jonasson, I., 2007. Volcanogenic Massive Sulphide Deposits. In: *Mineral Deposits of Canada: A Synthesis of Major Deposit Types.* St. Johns: Geological Association of Canada, pp. 141-162.

Gartman, A. et al., 2019. The Role of Nanoparticles in Mediating Element Deposition and Transport at Hydrothermal Vents. *Geochimica et Cosmochimica Acta,* 261(In Press), pp. 113-131.

Germanovich, L. N. et al., 2015. Measuring Fluid Flow and Heat Output in Seafloor Hydrothermal Environments. *Journal of Geophysical Research: Solid Earth,* Volume 120, pp. 8031-8055.

Goldschmidt, V. M., 1937. The Principles of Distribution of Chemical Elements in Minerals and Rocks. The seventh Hugo Müller Lecture, delivered before the Chemical Society.. *Journal of the Chemical Society,* pp. 655-673.

Gregory, M. R. & Johnston, K. A., 1987. A Nontoxic Substitute for Hazardous Heavy Liquids - Aqueous Sodium Polytungstate ($3Na_2WO_4.9WO_3.H_2O$) solution (Note). *New Zealand Journal of Geology and Geophysics,* 30(3), pp. 317-320.

Gresens, R. L., 1981. The Aqueous Solubility Product of Solid Solutions 1. Stoichiometric Saturation; Partial and Total Solubility Product. *Chemical Geology,* Volume 32, pp. 59-72.

Grogan, R., 2019. *Sustainable deep sea mining. A contradiction in terms?.* Trondheim: NTNU.

Guirco, D. et al., 2010. *Peak Minerals in Australia: A Review of Impacts and Benefits,* Sydney: University of Technology Sydney.

Hagelüken, C., Lee-Shin, J. U., Carpentier, A. & Heron, C., 2016. The EU Circular Economy and its Relevance to Metal Recycling. *Recycling,* Volume 1, pp. 242-253.

Hannington, M. D., Petersen, S., Herzig, P. M. & Jonasson, I. R., 2004. *A global database of seafloor hydrothermal systems, including a digital database of geochemical analyses of seafloor polymetallic sulfides,* Vancouver: Geological Society of Canada.

Hannington, M. et al., 2011. The Abundance of Seafloor Massive Sulfide Deposits. *Geology,* 39(12), pp. 1155-1158.

Hanor, J. S., 2000. Barite-Celestine Geochemistry and Environments of Formation. *Reviews in Mineralogy and Geochemistry,* 40(1), pp. 193-275.

Haymon, R. M., 1983. Growth History of Hydrothermal Black Smoker Chimneys. *Nature,* Volume 301, pp. 695-698.

Haymon, R. M. & Kastner, M., 1981. Hot Spring Deposits on th East Pacific Rise at 21°N: Preliminary Description of Mineralogy and Genesis. *Earth and Planetary Science Letters ,* Volume 53, pp. 363-381.

Haynes, W. M., 2011. *CRC Handbook of Chemistry and Physics.* 92nd ed. London: Taylor & Francis.

Hein, J. R., Mizell, K., Koschinsky, A. & Conrad, T. A., 2013. Deep-ocean mineral deposits as a source of critical metals for high- and green-technology applications: Comparison with land-based resources. *Ore Geology Reviews,* Volume 51, pp. 1-14.

Hjeltström, A., 2015. *Copper minerals under the microscope,* Uppsala: Uppsala Universitet.

Holloway, M., 2018. *(Doctoral Thesis) Experimental study of REE carbonate and fluorocarbonate synthesis as a basis for understanding hydrothermal REE mineralisation,* Edinburgh: University of Edinburgh.

Horowitz, J., 2021. *The Taliban are sitting on $1 trillion worth of minerals the world desperately needs.* [Online]
Available at: https://edition.cnn.com/2021/08/18/business/afghanistan-lithium-rare-earths-mining/index.html
[Accessed 29 August 2022].

Huber, C. et al., 2000. Optical sensor for seawater salinity. *Fresenius' Journal of Analytical Chemistry,* Volume 368, pp. 196-202.

Humphreys, D., 2013. The Mining Industry and the Supply of Critical Minerals. In: G. Gunn, ed. *Critical Metals Handbook.* Chichester: John Wiley & Sons Ltd.; American Geophysical Union; British Geological Survey, pp. 20-39.

Humphris, S. E. & Bach, W., 2005. On the Sr Isotope and REE Compositions of Anhydrites from the TAG Seafloor Hydrothermal System. *Geochimica et Cosmochimica Acta,* 69(6), pp. 1511-1525.

Humphris, S. E. et al., 1995. The Internal Structure of an Active Sea-Floor Massive Sulphide Deposit. *Nature,* Volume 377, pp. 713-716.

Hutton, C., 2022. *Mining Economics Explained: A Guide for Boards, Executives, Managers and Investors.* Wandsbeck: Reach Publications.

International Copper Study Group, 2018. *The World Copper Factbook 2018,* Lisbon: International Copper Study Group.

Italiano, F. & Nuccio, P. M., 1991. Geochemical investigations of submarine volcanic exhalations to the east of Panarea, Aeolian Islands, Italy. *Journal of Volcanology and Geothermal Research,* Volume 46, pp. 125-141.

Jeswiet, J., 2017. Including Towards Sustainable Mining in evaluating mining impacts. *Procedia CIRP,* 62(Open Access), pp. 494-499.

Josephs, J., 2022. *Ukraine war to halve global trade growth, warns WTO.* [Online]
Available at: https://www.bbc.co.uk/news/business-60949053
[Accessed 29 August 2022].

Kawagucci, S., 2014. Fluid Geochemistry of High-Temperature Hydrothermal Fields in the Okinawa Trough . In: J. Ishibashi, K. Okino & M. Sunamura, eds. *Subseafloor Biosphere Linked to Hydrothermal Systems.* Tokyo: Springer Toyo, pp. 387-403.

Keber, S., Brückner, L., Elwert, T. & Kuhn, T., 2020. Concept for a Hydrometallurgical Processing of a Copper-Cobalt-Nickel Alloy Made from Manganese Nodules. *Chemie Ingenieur Technik,* 92(4), pp. 379-386.

Kleint, C., Hawkes, J. A., Sander, S. G. & Koschinsky, A., 2016. Voltammetric Investigation of Hydrothermal Iron Speciation. *Frontiers in Marine Science,* 3(75).

Kobayashi, T., Nagai, H. & Kobayashi, K., 2000. Concentration profiles of 10Be in large manganese crusts. *Nuclear Instruments and Methods in Physics Research Section B: Beam Interactions with Materials and Atoms,* 172(1-4), pp. 579-582.

Korbel, P. & Novák, M., 1999. *The Complete Encyclopedia of Minerals.* s.l.:Rebo International.

Kuhn, T., W. A., Rühlemann, C. & Vink, A., 2018. Composition, Formation, and Occurrence of Polymetallic Nodules. In: R. Sharma, ed. *Deep Sea Mining: Resource Potential, Teechnical and Environmental Considerations.* s.l.:Springer, pp. 23-64.

Lajunen, L. H. J. & Perämäki, P., 2004. *Spectrochemical Analysis by Atomic Absorption and Emission.* 2nd ed. Cambridge: The Royal Society of Chemistry.

Lee, C. A. & Tang, M., 2020. How to Make Porphyry Copper Deposits. *Earth and Planetary Science Letters,* 529(1), pp. 1-11.

Liu, W., McPhail, D. C. & Brugger, J., 2001. An Experimental Study of Copper(I)-Chloride and Copper(I)-Acetate Complexing in Hydrothermal Solutions Between 50 °C and 250 °C and Vapor-Saturated Pressure. *Geochimica et Cosmochimica Acta,* Volume 65, pp. 2937-2948.

Lyndon, J. W., 1988. Ore Deposit Models #14. Volcanogenic Massive Sulphide Deposits Part 2: Genetic Models. *Geoscience Canada,* 15(1), pp. 43-65.

Macchia, S., 2016. Analysing Stevin's Law with the smartphone barometer. *The Physics Teacher,* 54(1), p. 373.

MacDonald, A. H. & Fyfe, W. S., 1985. Rate of serpentinization in seafloor environments. *Tectonophysics,* 116(1-2), pp. 123-135.

Maxwell, J. C., 1902. *Theory of Heat.* London: Longmans Green and Co.

McKibben, M. A. & Barnes, H. L., 1986. Oxidation of Pyrite in Low Temperature Acidic Solutions: Rate Laws and Surface Textures. *Geochimica et Cosmochimica Acta,* Volume 50, pp. 1509-1520.

Melchert, B. et al., 2008. First evidence for high-temperature off-axis venting of deep crustal/mantle heat:The Nibelungen hydrothermalfield, southern Mid-Atlantic Ridge. *Earth and Planetary Science Letters,* Volume 275, pp. 61-69.

Mero, J. L., 1965. *The Mineral Resources of the Sea.* New York: Elsevier Oceanography Series.

Ministry for Economy, Trade and Industry, 2017. *World's First Success in Continuous Ore Lifting test for Seafloor Polymetallic Sulphides: Pilot test of excavating and ore lifting conducted for seafloor polymetallic sulphides under the sea area near Okinawa Prefecture.* [Online]
Available at: https://www.meti.go.jp/english/press/2017/0926_004.html
[Accessed 22 June 2019].

Monecke, T., Petersen, S. & Hannington, M. D., 2014. Constraints on Water Depth of Massive Sulfide Formation: Evidence from Modern Seafloor Hydrothermal Systems in Arc-Related Systems. *Economic Geology,* Volume 109, pp. 2079-2101.

Morton, B., Taylor, G. & Turner, J., 1956. Turbulent Gravitational Convection from Maintained and Instantaneous Sources. *Proceedings of the Royal Society A,* Volume 234, pp. 1-23.

Moss, R. L. et al., 2013. *Critical Metals in the Path towards the Decarbonisation of the EU Energy Sector: Assessing Rare Metals as Supply-Chain Bottlenecks in Low-Carbon Energy Technologies ,* Luxembourg City: European Commission .

Murton, B., Copley, J. & Connely, D., 2011. *Hydrothermal Vents at 5000m on the Mid-Cayman Rise: where basement lithology and depth of venting controls sulphide deposit composition.* Waikoloa, HI, USA, Institute of Electrical and Electronics Engineers.

Nabil, S., 2021. *Suez Canal: Owner of cargo ship blocking waterway apologises.* [Online]
Available at: https://www.bbc.co.uk/news/world-middle-east-56522178
[Accessed 29 August 2022].

Nakamura, K. et al., 2009. Serpentinized troctolites exposed near the Kairei Hydrothermal Field, Central Indian Ridge: Insights into the origin of the Kairei hydrothermal fluid supporting a unique microbial ecosystem. *Earth and Planetary Science Letters,* Volume 280, pp. 128-136.

Nautilus Minerals, 2019. *TSX Announcements.* [Online]
Available at:
http://www.nautilusminerals.com/irm/PDF/2096_0/Nautilusobtainscourtapprovalofplanofcompromiseandarrangement
[Accessed 22 October 2019].

Office of the Pacific Ocean Commissioner, 2021. *Blue Pacific Ocean Report 2021,* Suva: Office of the Pacific Ocean Commissioner.

Pacific Parlimentarians Alliance on Deep Sea Mining, 2022. *Currents of Political Change: Reviewing Our Common Heritage and Common Responsibility in light of the Climate Crisis and Dangers of Deep Sea Mining.* Lisbon, One Sustainable Ocean.

Pękala, M. et al., 2011. Experimental Study of Cu Isotope Fractionation During the Reaction of Aqueous Cu(II) with Fe(II) Sulphides at Temperatures Between 40 and 200°C. *Chemical Geology,* Volume 289, pp. 31-38.

Petersen, S., 2015. *The Metal Endowment of Seafloor Massive Sulfides: A Global Perspective.* Tampa, Underwater Mining Conference.

Petersen, S. et al., 2016. News from the seabed–Geological characteristics and resourcepotential of deep-sea mineral resources. *Marine Policy,* 70(1), pp. 175-187.

Petersen, S., Lehrmann, B. & Murton, B. J., 2018. Modern Seafloor Hydrothermal Systems: New Perspectives on Ancient Ore-Forming Processes. *Elements,* Volume 14, pp. 307-312.

Pracejus, B., 2016. II/B - Sulfides with Metal : Sulfur, Selenium, and Tellurium > 1 : 1. In: *The Ore Minerals Under the Microscope: An Optical Guide.* Muscat: Elsevier Science, pp. 190-253.

Randhawa, N. S., Hait, J. & Jana, R. K., 2016. A Brief Overview on Manganese Nodules Processing Signifying the Detail in the Indian Context Highlighting the International Scenario. *Hydrometallurgy,* 165(1), pp. 166-181.

Reed, M. H. & Palandri, J., 2006. Sulfide Mineral Precipitation from Hydrothermal Fluids. *Reviews in Mineralogy & Geochemistry,* Volume 61, pp. 609-631.

Reich, M. & Vasconcelos, P. M., 2015. Geological and Economics of Supergene Metal Deposits. *Elements,* 1 October, 11(5), pp. 305-310.

Rickard, D. & Cowper, M., 1994. Kinetics and Mechanism of Chalcopyrite Formation from Fe(II) Disulphide in Aqueous Solution (<200°C). *Geochimica et Cosmochimica Acta,* 58(18), pp. 3795-3802.

Ridley, W. I., 2012. *Petrology of Associated Igneous Rocks in Volcanic Massive Sulfide Occurence Model,* Reston: US Geological Survey.

Rigonat, N., 2017. *Development of a novel magnetic monitoring system for Engineered Barriers of Geological Disposal Facilities,* Edinburgh: Edinburgh Research Archives.

Rimstidt, J. D. & Vaughan, D. J., 2003. Pyrite Oxidation: A state-of-the-art Assessment of the Reaction Mechanism. *Geochimica et Cosmochimica Acta,* 67(5), pp. 873-880.

Rona, P. A., Bemis, K. G., Xu, G. & Mitsuzawa, K., 2015. Estimations of Heat Transfer from Grotto's North Tower: A NEPTUNE Observatory Case Study. *Deep-Sea Research II,* Volume 121, pp. 95-111.

Rossotti, F. J. C. & Rossotti, H., 1961. Solubility. In: D. N. Hume, et al. eds. *The Determination of Stability Constants.* London: McGraw-Hill, pp. 189-202.

Rubin, K. H. et al., 2001. *Eruption Recurrence Rates and Compositional Variability of Discrete Lava Flows on the S-EPR from 238U-230Th-226Ra- 210Pb-232Th.* s.l., American Geophysical Union.

Sandford, A., 2020. *Coronavirus: Half of humanity now on lockdown as 90 countries call for confinement.* [Online]
Available at: https://www.euronews.com/2020/04/02/coronavirus-in-europe-spain-s-death-toll-hits-10-000-after-record-950-new-deaths-in-24-hou
[Accessed 28 August 2022].

Scales, H., 2022. *Deep-sea mining talks end with no agreement on environmental rules,* s.l.: The Guardian.

Schmidt, C. et al., 2018. Copper Complexation and Solubility in High-Temperature Hydrothermal Fuids: A Combined Study by Raman, X-ray Fluorescence, and X-ray Absorption Spectroscopies and ab initio Molecular Dynamics Simulations. *Chemical Geology,* Volume 494, pp. 69-79.

Schmitt, W., Palme, H. & Wänke, H., 1989. Experimental determination of metal/silicate partition coefficients for P, Co, Ni, Cu, Ga, Ge, Mo, and W and some implications for the early evolution of the Earth. *Geochimica et Cosmochimica Acta,* 53(1), pp. 173-185.

Searle, R., 2013. *Mid-Ocean Ridges.* 1 ed. Cambridge: Cambridge.

Sherman, D. M., 2007. Complexation of Cu+ in Hydrothermal NaCl Brines: ab initio Molecular Dynamics and Energetics. *Geochimica et Cosmochimica Acta,* Volume 71, pp. 714-722.

Shouten, C., 1934. Structure and Textures of Synthetic Replacements in "Open Space". *Economic Geology,* Volume 29, pp. 611-658.

Sometu, 2010. *How to Use Sodium Polytungstate.* [Online]
Available at: http://www.sometu.de/howtouse.html
[Accessed 18 November 2019].

Srinivasan, P., 2022. *Tuvalu Reverses Controversal Decision to Sponsor Seabed Mining,* s.l.: Deep Sea Conservation Coalition.

Steger, H. F. & Desjardens, L. E., 1978. Oxidation of Sulfide Minerals, 4. Pyrite, Chalcopyrite and Pyrrhotite. *Chemical Geology,* Volume 23, pp. 225-237.

Sverdrup, H. & Ragnarsdóttir, K. V., 2014. Natural Resources in a Planetary Perspective. *Geochemical Perspectives,* 3(2), pp. 129-341.

Tanner, W. F., 1964. Unified Basis for Tectonic Theory. *Tectnophysics,* 1(2), pp. 135-158.

Tetteh, G. M. & Lartey, E. O., 2018. Texture And Gold Grade As Guides To Blending Of Conglomerate Ore. *International Journal of Scientific and Technology Research,* 7(9), pp. 61-66.

The International Association for the Properties of Water and Steam, 2007. *Revised Release on the IAPWS Industrial Formulation 1997 for the Thermodynamic Properties of Water and Steam.* Lucerne, IAPWS.

The Metals Company, 2022. *NORI-D Project - Nauru Ocean Resources Inc..* [Online]
Available at: https://metals.co/nori/
[Accessed 27 August 2022].

Turner, J. S., 1986. Turbulent Entrainment: The Development of the Entrainment Assumption, and its Application to Geophysical Flows. *Journal of Fluid Mechanics,* Volume 173, pp. 431-471.

Vari, M., 2019. *Marape Leaning Toward Moratorium On Deep Sea Mining,* Port Moresby: Papua New Guinea Post-Courier.

von Gehlen, K., 1993. Sulfur in the Earth's Mantle - A Review. In: M. Schidlowski, et al. eds. *Early Organic Evolution.* Berlin: Springer, pp. 359-366.

Webber, A. P., Roberts, S., Murton, B. J. & Hodgkinson, M. R. S., 2015. Geology, sulfide geochemistry and supercritical venting at the Beebe Hydrothermal Vent Field, Cayman Trough. *Geochemistry, Geophysics, Geosystems,* Volume 16, pp. 2661-2678.

Webber, A. P., Roberts, S., Taylor, R. N. & Pitcairn, I. K., 2013. Golden Plumes: Substantial Gold Enrichment of Oceanic Crust during Ridge-Plume Interaction. *Geology,* 41(1), pp. 87-90.

Xiao, Z., Gammons, C. H. & Williams-Jones, A. E., 1998. Experimental Study of Copper(I) Chloride Complexing in Hydrothermal Solutions at 40 to 300°C and Saturated Water Vapor Pressure. *Geochimica et Cosmochimica Acta,* Volume 62, pp. 2949-2964.

Xu, G., Jackson, D. R., Bemis, K. G. & Rona, P. A., 2014. Time-series measurement of hydrothermal heat flux at the Grotto mound, Endeavour Segment, Juan de Fuca Ridge. *Earth and Planetary Science Letters,* Volume 404, pp. 220-231.

Zhang, X., Lin, J. & Jiang, H., 2019. Time-Dependent Variations in Vertical Fluxes of Hydrothermal Plumes at Mid-Ocean Ridges. *Marine Geophysical Research,* Volume 40, pp. 245-260.

Zies, E. G., Allen, E. T. & Merwin, H. E., 1916. Some Reactions Involved in Secondary Sulphide Enrichment. *Economic Geology,* Volume 11, pp. 407-503.

APPENDIX

Table S7: *Inter-elemental correlation matrix of hydrothermal fluid endmember concentrations excluding Rare Earth Elements. Red cells indicate a strong negative correlation; blue cells indicate a strong positive correlation.*

	Au	Ag	As	B	Ba	Br	Ca	Cd	Ce	Cl	Co	Cs	Cu	Dy	Er	Eu	Fe	Gd	Hf	Hg
Au																				
Ag																				
As																				
B		-0.50																		
Ba		0.62		-0.30																
Br		-0.14		-0.33	0.64															
Ca		-0.36		-0.06	0.18	0.14														
Cd		0.21		0.06	-0.48	0.59	0.58													
Ce																				
Cl		-0.15		-0.23	0.62	0.17	0.00	-0.76												
Co		0.06		0.07	-0.02	-0.06	-0.30	-0.02		-0.18										
Cs		0.47		0.66	0.46	0.56	0.16	-0.45		0.52	0.00									
Cu		0.33		-0.37	0.38	0.47	0.08	0.31		0.04	0.93	-0.16								
Dy																				
Er																				
Eu																				
Fe		0.44		-0.37	0.65	0.61	0.27	0.73		0.10	0.79	0.07	0.70							
Gd																				
Hf																				
Hg																				

***Table S1**: (Continued)*

	Ho	La	Li	Lu	Mn	Mo	Nb	Nd	Ni	Pb	Pd	Pr	Rb	Sm	Sr	Ta	Tb	V	Y	Yb	Zn
Au																					
Ag			0.434		0.527	-0.604			-0.188	0.954	0.346		-0.287		-0.537						0.105
As																					
B			0.699		-0.336	0.582			0.725	-0.478	-0.378		0.133		0.138						-0.330
Ba			0.308		0.573	0.484			0.642	0.560			0.043		0.453						0.459
Br			0.469		0.554	-0.171			0.821	0.201	0.250		0.124		0.506						0.327
Ca			0.096		0.220	0.077			0.691	-0.086	0.796		-0.050		0.393						0.295
Cd			0.341		0.752	0.056			-0.320	0.677	0.580		-0.423		0.204						0.956
Ce																					
Cl			-0.014		0.128	-0.229			0.696	0.189	0.013		0.177		0.127						0.181
Co			0.064		0.211	0.834			-0.409	0.039	0.143		-0.148		-0.319						0.096
Cs			0.192		-0.004	-0.135			-0.157	-0.546	0.405		0.861		0.668						-0.222
Cu			-0.084		0.236	-0.686			-0.454	-0.045	-0.087		-0.069		-0.026						0.334
Dy																					
Er																					
Eu																					
Fe			0.039		0.544	-0.402			-0.350	-0.017	0.428		-0.069		0.150						0.584
Gd																					
Hf																					
Hg																					
Ho																					
La																					
Li					0.255	0.204			0.820	0.286	0.287		0.122		0.276						0.276
Lu																					
Mn						0.281			-0.295	0.917	0.382		-0.076		0.161						0.529
Mo									0.483	-0.398	-0.457		-0.111		-0.777						-0.867
Nb																					
Nd																					
Ni										-0.709			0.938		1.000						
Pb													0.786		0.008						0.643
Pd													0.182		0.260						0.658
Pr																					
Rb															0.523						0.022
Sm																					
Sr																					0.167
Ta																					
Tb																					
V																					
Y																					
Yb																					
Zn																					

Table S8: *Inter-elemental correlation matrix of hydrothermal fluid endmember concentrations exclusively including Rare Earth Elements. Red cells indicate a strong negative correlation; blue cells indicate a strong positive correlation.*

	Au	Ag	As	B	Ba	Br	Ca	Cd	Ce	Cl	Co	Cs	Cu	Dy	Er	Eu	Fe	Gd	Hf	Hg
Au																				
Ag																				
As																				
B																				
Ba																				
Br																				
Ca																				
Cd																				
Ce				0.89	0.96	0.88	0.95	0.99												
Cl									-0.02											
Co									0.95											
Cs									0.90											
Cu									-0.08											
Dy				0.97	0.27	0.75	0.62	0.79	0.49	0.93	0.80	0.97	-0.22							
Er				0.97	0.31	0.78	0.65	0.53	0.52	0.91	0.75	0.98	-0.22	1.00						
Eu				0.96	0.86	0.99	0.99	0.53	0.95	0.31	0.90	0.96	-0.14	0.74	0.76					
Fe									-0.91					-0.01	-0.05	-0.75				
Gd				0.93	0.62	0.96	0.89	0.92	0.77	0.68	0.85	0.94	-0.20	0.93	0.94	0.93	-0.42			
Hf																				
Hg																				
Ho																				
In																				
La																				
Li																				
Lu																				
Mn																				
Mo																				
Nb																				
Nd																				
Ni																				
Pb																				
Pd																				
Pr																				
Rb																				
Sm																				
Sr																				
Ta																				
Tb																				
V																				
Y																				
Yb																				
Zn																				

Table S2: *(Continued)*

	Ho	La	Li	Lu	Mn	Mo	Nb	Nd	Ni	Pb	Pd	Pr	Rb	Sm	Sr	Ta	Tb	V	Y	Yb	Zn
Au																					
Ag																					
As																					
B		0.99		0.33				0.92						0.94						0.98	
Ba	0.20	0.96		0.23				0.95				1.00		0.88			0.46		0.24	0.37	
Br		0.87		0.81				0.92						0.98						0.82	
Ca		0.94		0.69				0.97						0.99						0.70	
Cd		0.29		0.31				1.00						0.94						0.52	
Ce	0.44	1.00	0.22	0.45	0.80			1.00		0.67		1.00	0.78	0.96	0.79		0.63		0.28	0.57	0.94
Cl		-0.04		0.89				0.06						0.27						0.88	
Co		0.74		-0.22				0.91						0.86						0.75	
Cs		0.99		0.69				0.93						0.95						0.99	
Cu		-0.08		-0.22				-0.10						-0.14						-0.22	
Dy	1.00	0.47	0.16	1.00	0.84			0.56		0.93		0.51	0.88	0.71	0.86		0.98		1.00	1.00	0.52
Er	1.00	0.50	0.17	1.00	0.86			0.59		0.95		0.54	0.90	0.74	0.88		0.99		1.00	1.00	0.55
Eu	0.70	0.94	0.23	0.71	0.95			0.97		0.87		0.96	0.93	1.00	0.94		0.84		0.57	0.79	0.96
Fe		-0.91		-0.11				-0.88						-0.77						-0.12	
Gd	0.91	0.76	0.21	0.94	0.99			0.82		1.00		0.79	0.99	0.92	0.99		0.98		0.88	0.96	0.82
Hf																					
Hg																					
Ho		0.42	0.83					0.51				0.47	0.83	0.67			0.98		1.00	0.99	
La			0.22	0.42	0.79			0.99		0.65		1.00	0.76	0.95	0.77		0.61		0.25	0.54	0.94
Li				-0.97				0.23				0.77		0.23			0.95		0.85	0.18	
Lu					0.89			0.52		0.96			0.91	0.69	0.90					1.00	0.60
Mn								0.85						0.94						0.90	
Mo																					
Nb																					
Nd										0.72		1.00	0.82	0.98	0.83		0.69		0.35	0.63	0.96
Ni																					
Pb														0.86						0.97	
Pd																					
Pr													0.76	0.97			0.65		0.31	0.58	
Rb														0.92			0.95		0.85	0.92	
Sm															0.93		0.82		0.54	0.77	0.96
Sr																				0.91	
Ta																					
Tb																			0.97	1.00	
V																					
Y																				0.99	
Yb																					0.61
Zn																					

THIS PAGE IS INTENTIONALLY BLANK

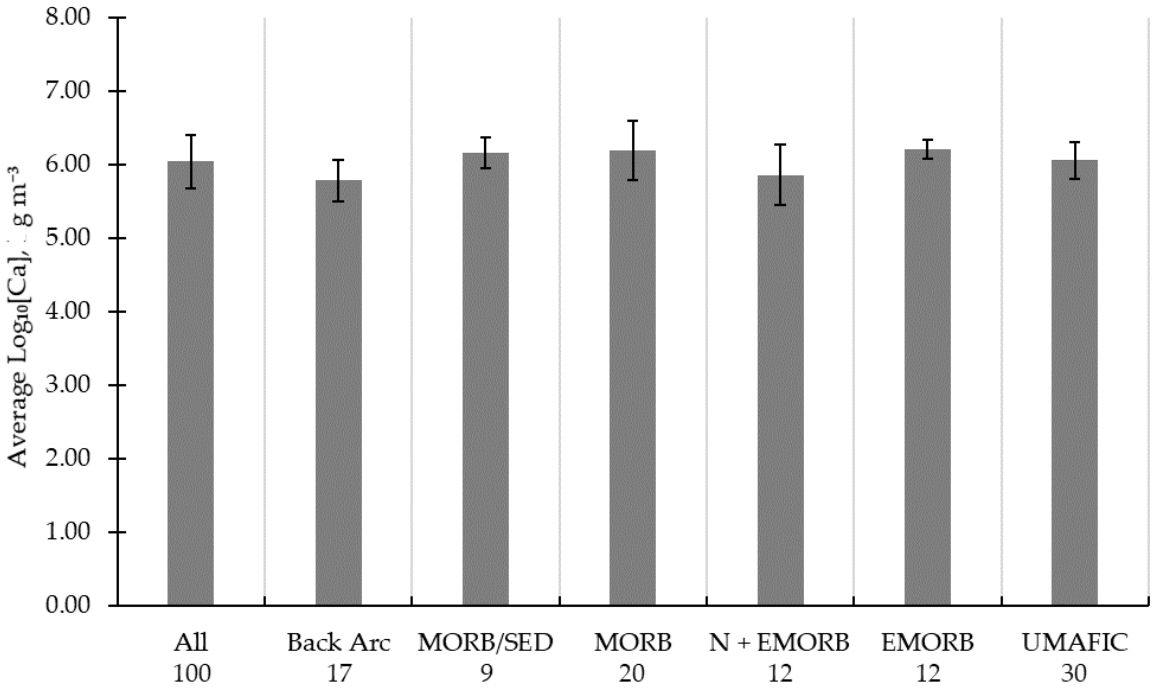

Figure S1: *Means and standard deviations of fluid endmember calcium concentrations, as common logarithms of the concentration in grams per cubic metre, by host rock category.*

Table S3*: Matrix of t-test values between host rock categories for the common logarithm of calcium concentration in fluid endmembers. The values coloured red indicate the corresponding categories are significantly different. Values in standard black indicate the difference between host categories is not significant. There are no significantly similar host rock types in terms of calcium concentration.*

Ca	All	Back Arc	MORB/SED	MORB	N + EMORB	EMORB	UMAFIC
All		5.16E-03	0.32	0.10	0.10	0.10	0.82
Back Arc			1.72E-03	1.31E-03	0.56	3.85E-05	6.64E-03
MORB/SED				0.85	0.06	0.51	0.39
MORB					3.27E-02	0.85	0.22
N + EMORB						8.89E-03	0.11
EMORB							0.13
UMAFIC							

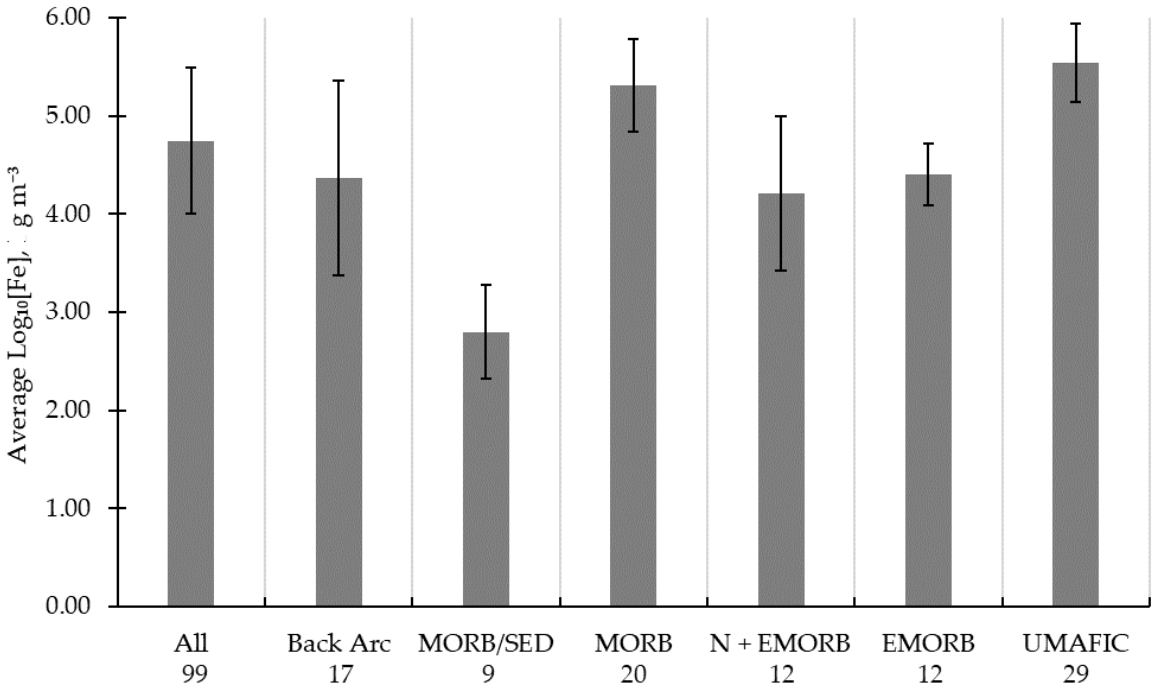

Figure S2: *Means and standard deviations of fluid endmember iron concentrations, as common logarithms of the concentration in grams per cubic metre, by host rock category.*

Table S4: *Matrix of t-test values between host rock categories for the common logarithm of iron concentration in fluid endmembers. The values coloured red indicate the corresponding categories are significantly different. Values in standard black indicate the difference between host categories is not significant. There are no significantly similar host rock types in terms of iron concentration.*

Fe	All	Back Arc	MORB/SED	MORB	N + EMORB	EMORB	UMAFIC
All		0.16	1.31E-07	1.70E-02	0.08	0.25	7.34E-05
Back Arc			1.61E-04	5.76E-04	0.64	0.91	1.70E-06
MORB/SED				2.82E-13	1.42E-04	1.63E-08	1.19E-17
MORB					2.52E-05	1.83E-06	0.09
N + EMORB						0.44	3.35E-08
EMORB							1.11E-09
UMAFIC							

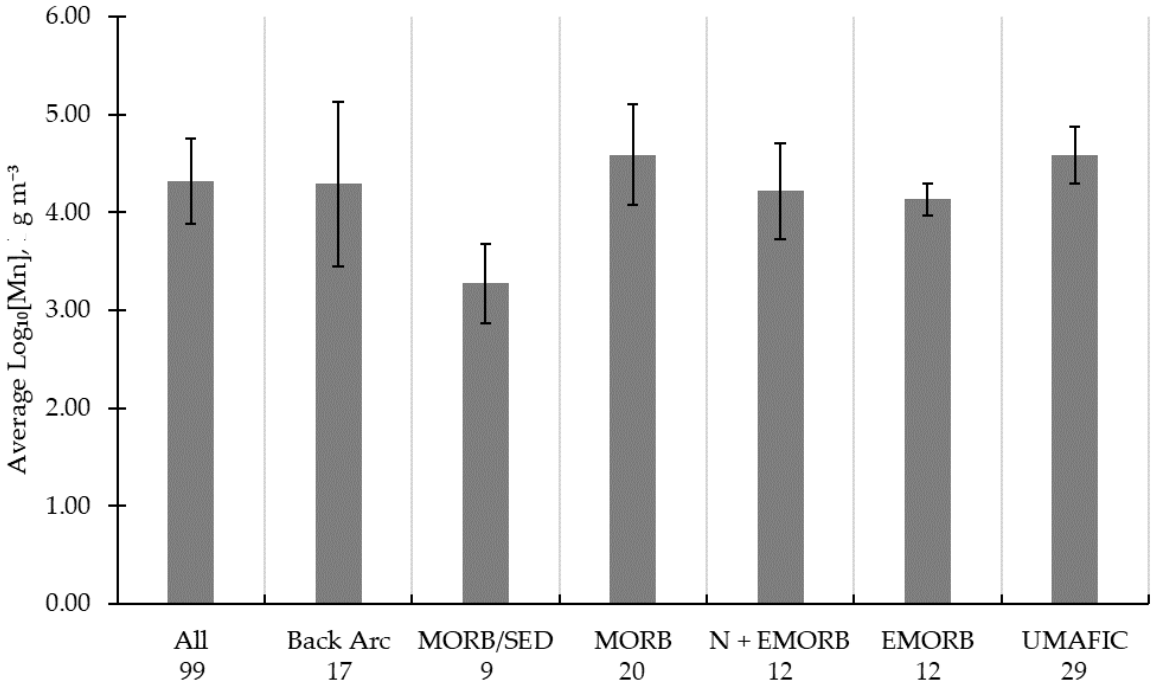

***Figure S3**: Means and standard deviations of fluid endmember manganese concentrations, as common logarithms of the concentration in grams per cubic metre, by host rock category.*

***Table S5:** Matrix of t-test values between host rock categories for the common logarithm of manganese concentration in fluid endmembers. The values coloured red indicate the corresponding categories are significantly different. Values in standard black indicate the difference between host categories is not significant. Significantly similar host rock types are indicated by bold black text.*

Mn	All	Back Arc	MORB/SED	MORB	N + EMORB	EMORB	UMAFIC
All		0.87	3.03E-06	0.07	0.60	0.31	2.72E-02
Back Arc			2.48E-03	0.19	0.80	0.53	0.10
MORB/SED				3.20E-07	1.62E-04	2.33E-06	9.64E-12
MORB					0.05	6.04E-03	**0.97**
N + EMORB						0.57	8.07E-03
EMORB							6.22E-05
UMAFIC							

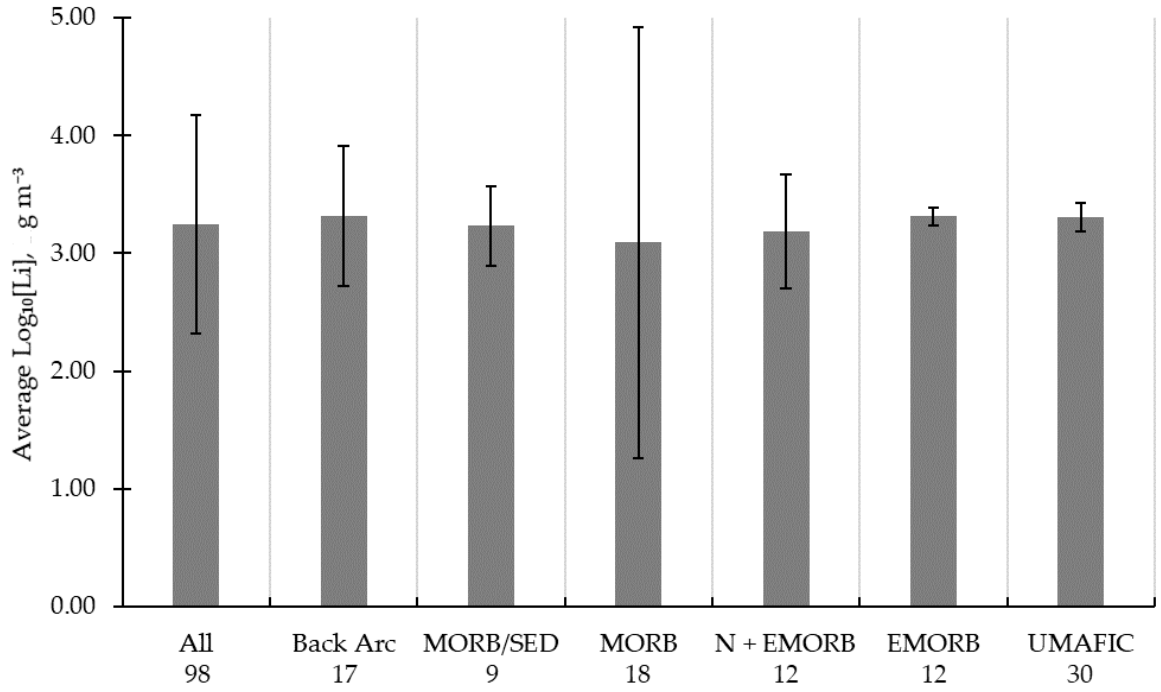

Figure S4: *Means and standard deviations of fluid endmember lithium concentrations, as common logarithms of the concentration in grams per cubic metre, by host rock category.*

Table S6: *Matrix of t-test values between host rock categories for the common logarithm of lithium concentration in fluid endmembers. There are no significantly different host rock types in terms of lithium concentration. Values in standard black indicate the difference between host categories is not significant. Significantly similar host rock types are indicated by bold black text.*

Li	All	Back Arc	MORB/SED	MORB	N + EMORB	EMORB	UMAFIC
All		0.74	**0.96**	0.56	0.80	0.79	0.71
Back Arc			0.70	0.63	0.53	**0.98**	0.92
MORB/SED				0.82	0.80	0.43	0.36
MORB					0.86	0.68	0.52
N + EMORB						0.38	0.22
EMORB							0.88
UMAFIC							

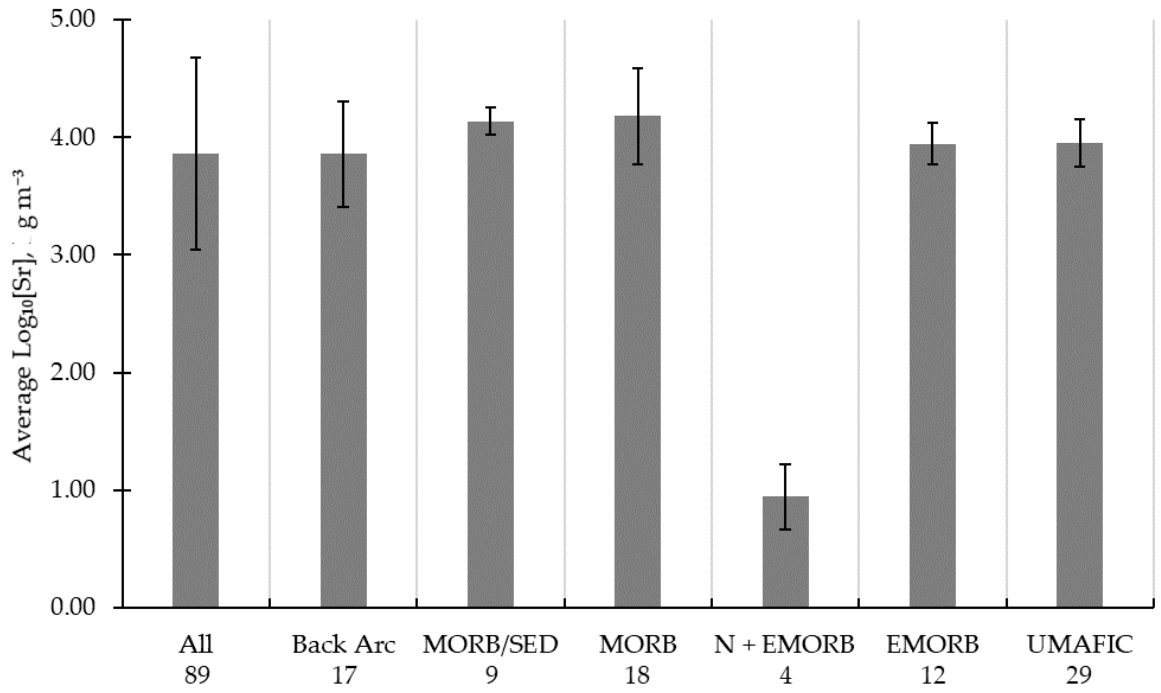

Figure S5: *Means and standard deviations of fluid endmember strontium concentrations, as common logarithms of the concentration in grams per cubic metre, by host rock category.*

Table S7: *Matrix of t-test values between host rock categories for the common logarithm of strontium concentration in fluid endmembers. The values coloured red indicate the corresponding categories are significantly different. Values in standard black indicate the difference between host categories is not significant. Significantly similar host rock types are indicated by bold black text.*

Sr	All	Back Arc	MORB/SED	MORB	N + EMORB	EMORB	UMAFIC
All		**0.97**	0.26	0.07	3.30E-12	0.69	0.52
Back Arc			0.08	3.23E-02	1.75E-10	0.52	0.38
MORB/SED				0.76	6.30E-12	1.17E-02	0.06
MORB					2.41E-12	0.07	2.71E-02
N + EMORB						3.31E-13	1.87E-19
EMORB							**0.95**
UMAFIC							

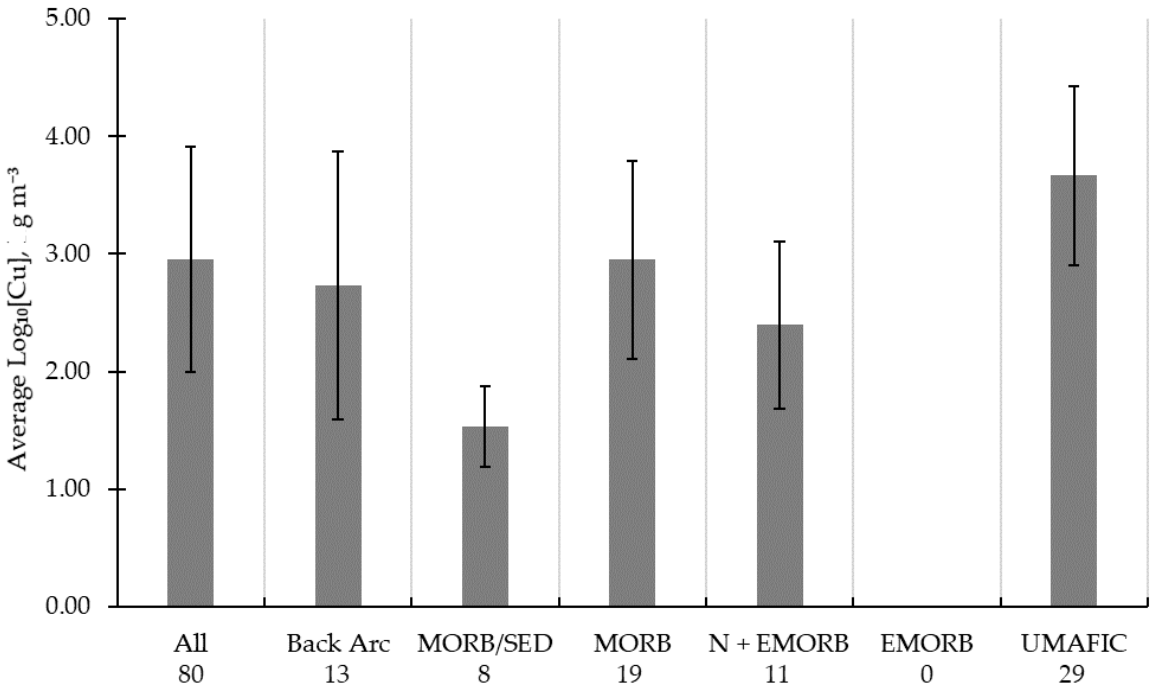

***Figure S6**: Means and standard deviations of fluid endmember copper concentrations, as common logarithms of the concentration in grams per cubic metre, by host rock category.*

***Table S8:** Matrix of t-test values between host rock categories for the common logarithm of copper concentration in fluid endmembers. The values coloured red indicate the corresponding categories are significantly different. Values in standard black indicate the difference between host categories is not significant. Significantly similar host rock types are indicated by bold black text.*

Cu	All	Back Arc	MORB/SED	MORB	N + EMORB	EMORB	UMAFIC
All		0.49	3.33E-04	**0.98**	0.10		1.76E-03
Back Arc			9.54E-03	0.54	0.40		5.88E-03
MORB/SED				1.07E-04	5.55E-03		8.00E-08
MORB					0.08		6.80E-03
N + EMORB							1.08E-04
EMORB							
UMAFIC							

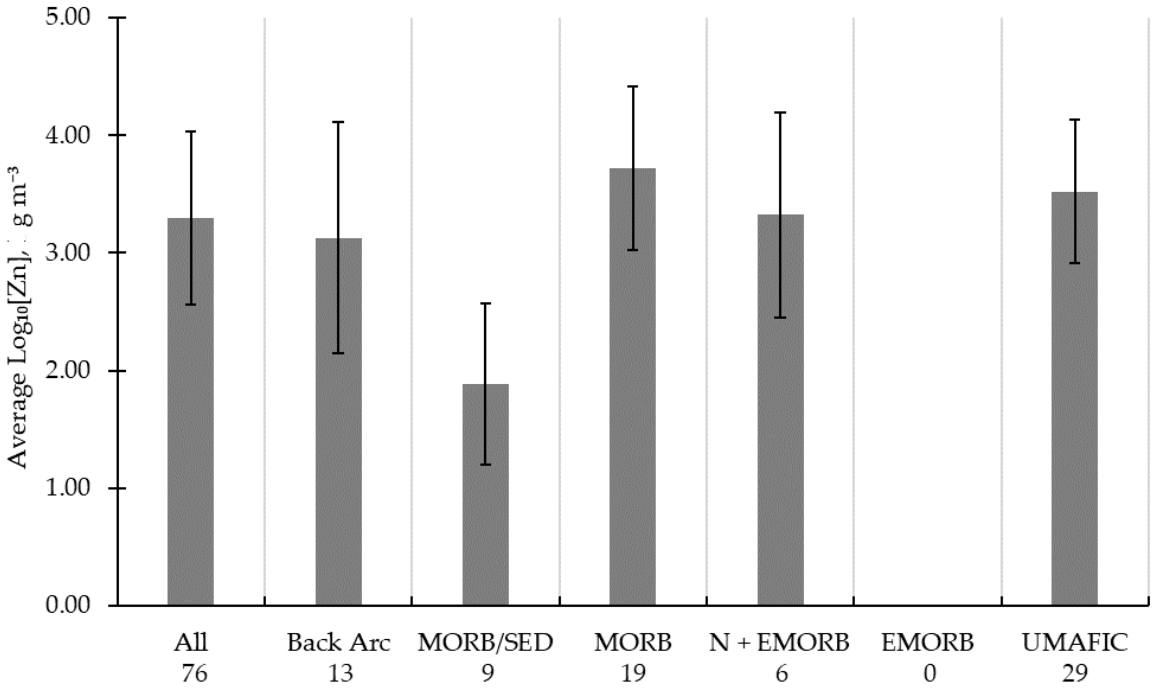

***Figure S7**: Means and standard deviations of fluid endmember zinc concentrations, as common logarithms of the concentration in grams per cubic metre, by host rock category.*

***Table S9:** Matrix of t-test values between host rock categories for the common logarithm of zinc concentration in fluid endmembers. The values coloured red indicate the corresponding categories are significantly different. Values in standard black indicate the difference between host categories is not significant. There are no significantly similar host rock types in terms of zinc concentration.*

Zn	All	Back Arc	MORB/SED	MORB	N + EMORB	EMORB	UMAFIC
All		0.56	3.85E-05	0.07	0.94		0.25
Back Arc			3.70E-03	0.05	0.68		0.16
MORB/SED				5.94E-07	3.43E-03		1.05E-06
MORB					0.26		0.36
N + EMORB							0.57
EMORB							
UMAFIC							

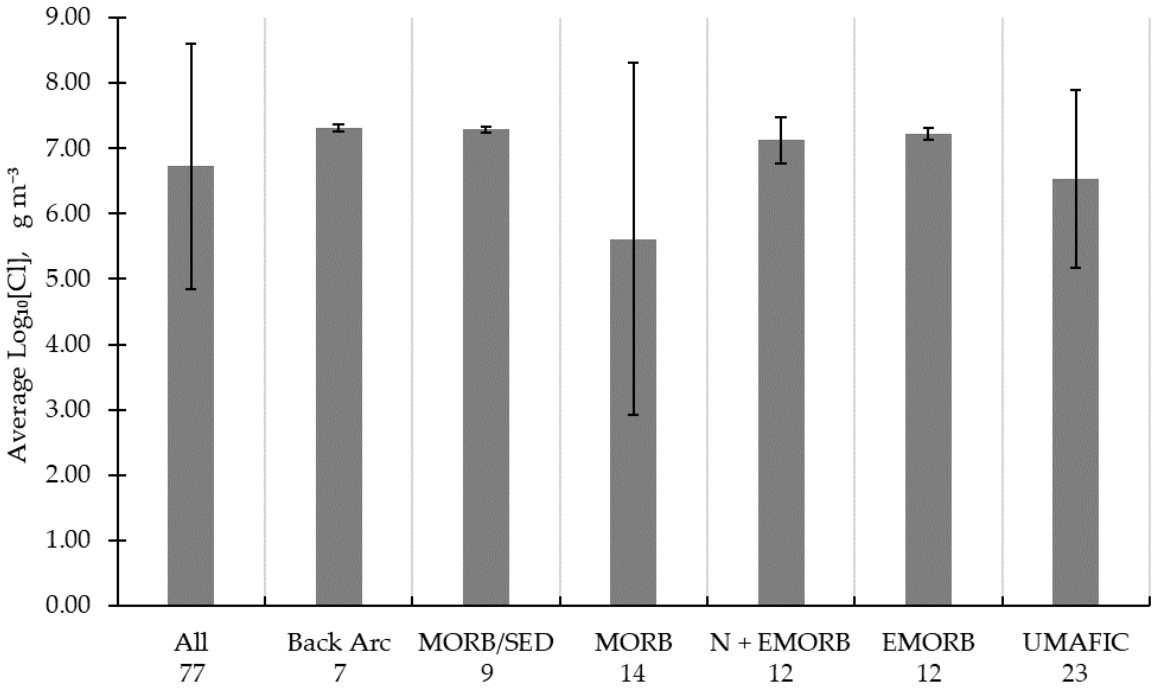

Figure S8: *Means and standard deviations of fluid endmember chlorine concentrations, as common logarithms of the concentration in grams per cubic metre, by host rock category.*

Table S10: *Matrix of t-test values between host rock categories for the common logarithm of chlorine concentration in fluid endmembers. The values coloured red indicate the corresponding categories are significantly different. Values in standard black indicate the difference between host categories is not significant. There are no significantly similar host rock types in terms of chlorine concentration.*

Cl	All	Back Arc	MORB/SED	MORB	N + EMORB	EMORB	UMAFIC
All		0.37	0.33	4.44E-02	0.42	0.31	0.65
Back Arc			0.37	0.12	0.20	4.75E-02	0.34
MORB/SED				0.08	0.20	0.09	0.29
MORB					0.07	0.05	0.25
N + EMORB						0.37	0.34
EMORB							0.26
UMAFIC							

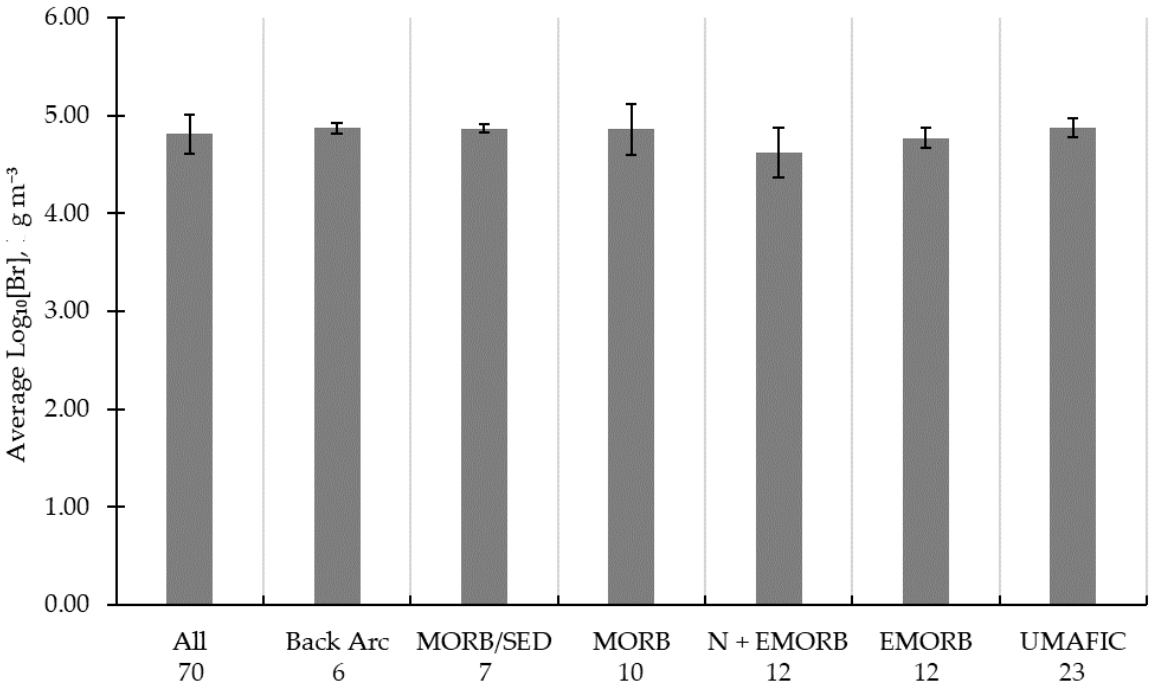

***Figure S9**: Means and standard deviations of fluid endmember bromine concentrations, as common logarithms of the concentration in grams per cubic metre, by host rock category.*

***Table S11:** Matrix of t-test values between host rock categories for the common logarithm of bromine concentration in fluid endmembers. The values coloured red indicate the corresponding categories are significantly different. Values in standard black indicate the difference between host categories is not significant. There are no significantly similar host rock types in terms of bromine concentration.*

Br	All	Back Arc	MORB/SED	MORB	N + EMORB	EMORB	UMAFIC
All		0.42	0.43	0.48	2.64E-03	0.48	0.11
Back Arc			0.84	0.89	3.02E-02	3.73E-02	0.94
MORB/SED				0.93	2.17E-02	3.07E-02	0.83
MORB					4.42E-02	0.31	0.77
N + EMORB						0.07	2.19E-04
EMORB							1.13E-02
UMAFIC							

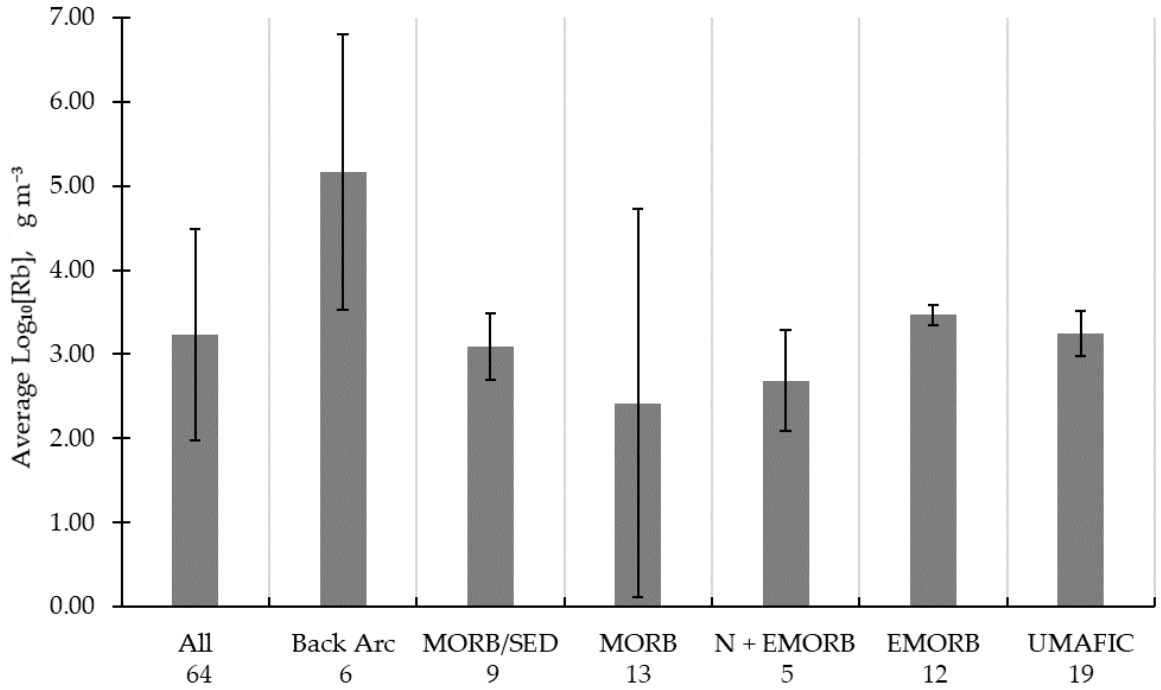

Figure S10: *Means and standard deviations of fluid endmember rubidium concentrations, as common logarithms of the concentration in grams per cubic metre, by host rock category.*

Table S12: *Matrix of t-test values between host rock categories for the common logarithm of rubidium concentration in fluid endmembers. The values coloured red indicate the corresponding categories are significantly different. Values in standard black indicate the difference between host categories is not significant. Significantly similar host rock types are indicated by bold black text.*

Rb	All	Back Arc	MORB/SED	MORB	N + EMORB	EMORB	UMAFIC
All		1.58E-03	0.77	0.09	0.38	0.56	**0.97**
Back Arc			2.64E-03	1.80E-02	1.09E-02	1.92E-03	4.25E-05
MORB/SED				0.39	0.15	5.97E-03	0.31
MORB					0.80	0.13	0.13
N + EMORB						4.06E-04	9.70E-03
EMORB							3.24E-02
UMAFIC							

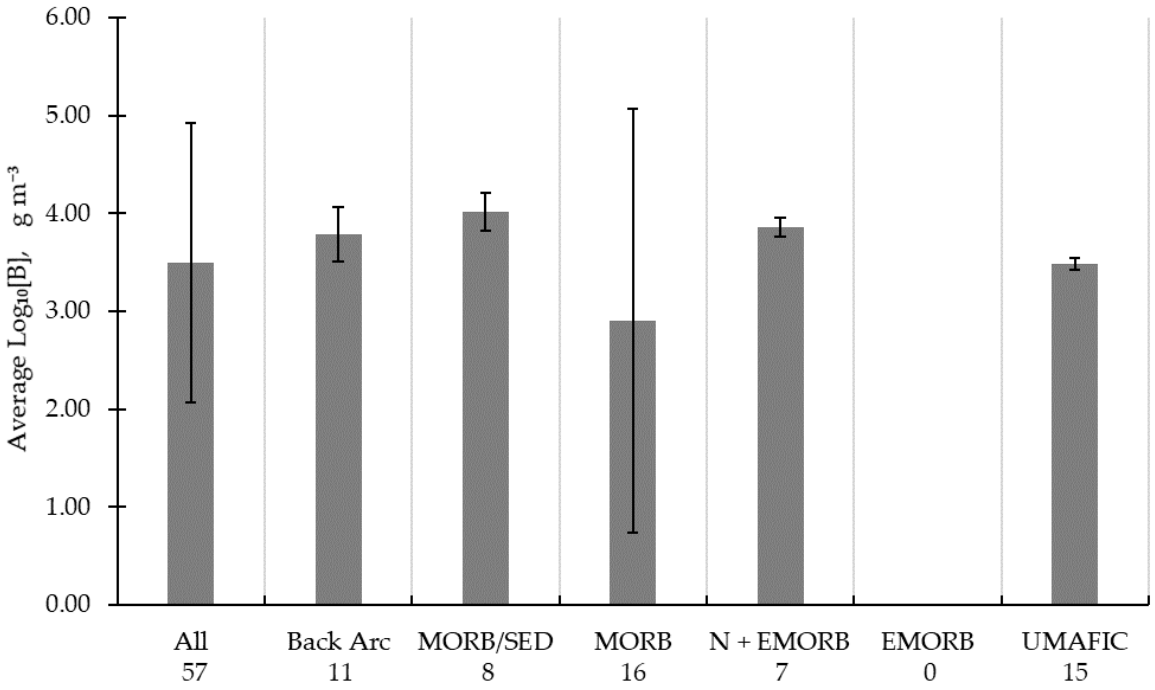

Figure S11: *Means and standard deviations of fluid endmember boron concentrations, as common logarithms of the concentration in grams per cubic metre, by host rock category.*

Table S13: *Matrix of t-test values between host rock categories for the common logarithm of boron concentration in fluid endmembers. The values coloured red indicate the corresponding categories are significantly different. Values in standard black indicate the difference between host categories is not significant. Significantly similar host rock types are indicated by bold black text.*

B	All	Back Arc	MORB/SED	MORB	N + EMORB	EMORB	UMAFIC
All		0.44	0.23	0.16	0.44		**0.96**
Back Arc			0.06	0.20	0.50		5.02E-04
MORB/SED				0.17	0.07		2.81E-09
MORB					0.26		0.31
N + EMORB							1.94E-09
EMORB							
UMAFIC							

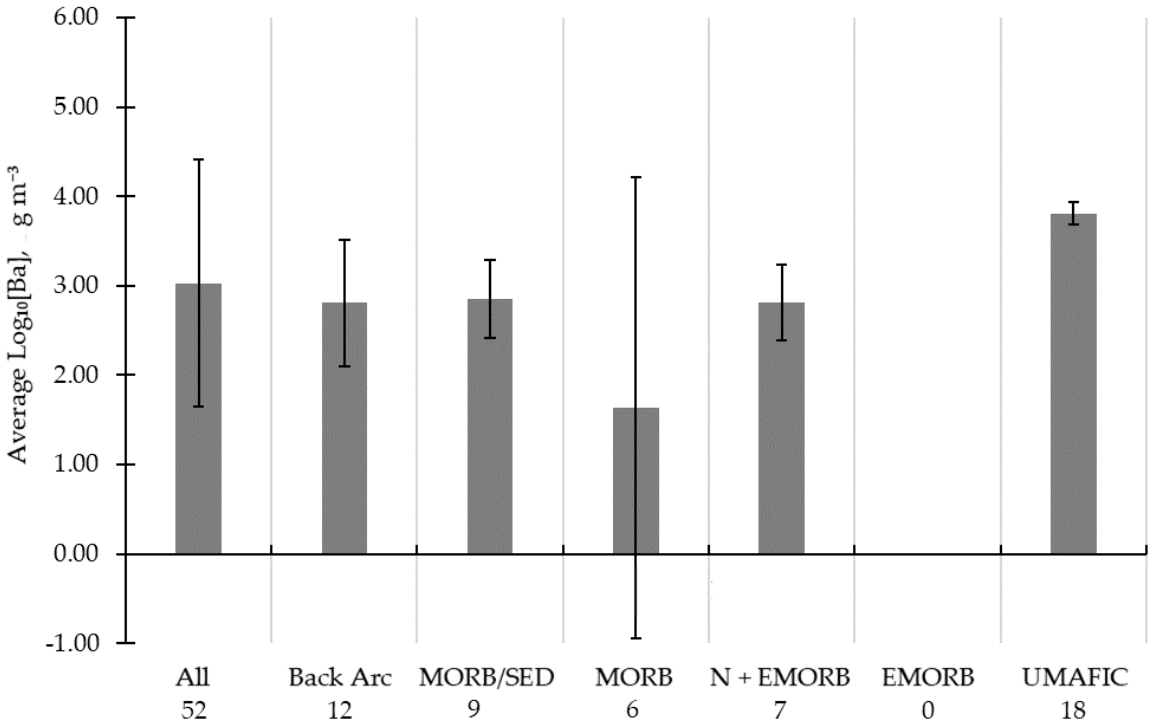

Figure S12: *Means and standard deviations of fluid endmember barium concentrations, as common logarithms of the concentration in grams per cubic metre, by host rock category.*

Table S14: *Matrix of t-test values between host rock categories for the common logarithm of barium concentration in fluid endmembers. The values coloured red indicate the corresponding categories are significantly different. Values in standard black indicate the difference between host categories is not significant. Significantly similar host rock types are indicated by bold black text.*

Ba	All	Back Arc	MORB/SED	MORB	N + EMORB	EMORB	UMAFIC
All		0.52	0.65	1.83E-02	0.62		5.02E-03
Back Arc			0.87	0.15	**0.99**		3.04E-06
MORB/SED				0.18	0.85		1.13E-08
MORB					0.26		1.17E-03
N + EMORB							1.16E-08
EMORB							
UMAFIC							

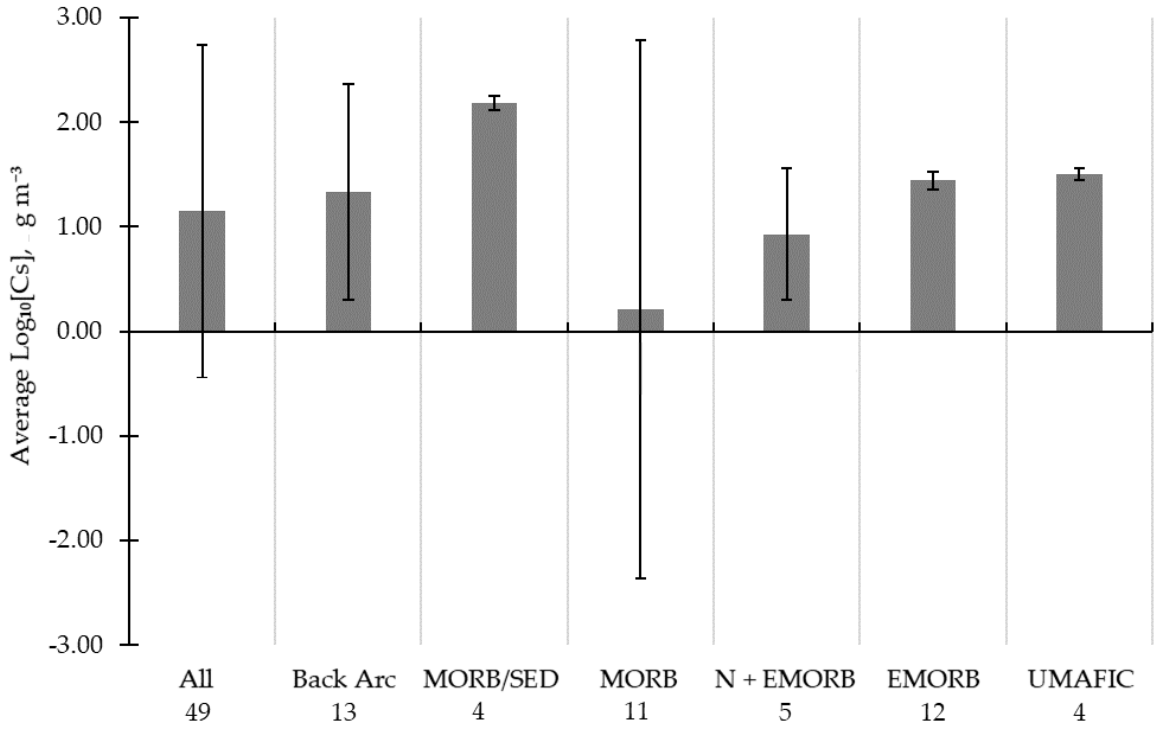

Figure S13: *Means and standard deviations of fluid endmember caesium concentrations, as common logarithms of the concentration in grams per cubic metre, by host rock category.*

Table S15: *Matrix of t-test values between host rock categories for the common logarithm of caesium concentration in fluid endmembers. The values coloured red indicate the corresponding categories are significantly different. Values in standard black indicate the difference between host categories is not significant. There are no significantly similar host rock types in terms of caesium concentration.*

Cs	All	Back Arc	MORB/SED	MORB	N + EMORB	EMORB	UMAFIC
All		0.67	0.15	0.10	0.73	0.48	0.62
Back Arc			0.13	0.16	0.43	0.71	0.74
MORB/SED				0.16	5.63E-03	3.60E-10	1.25E-05
MORB					0.56	0.11	0.34
N + EMORB						1.10E-02	0.11
EMORB							0.22
UMAFIC							

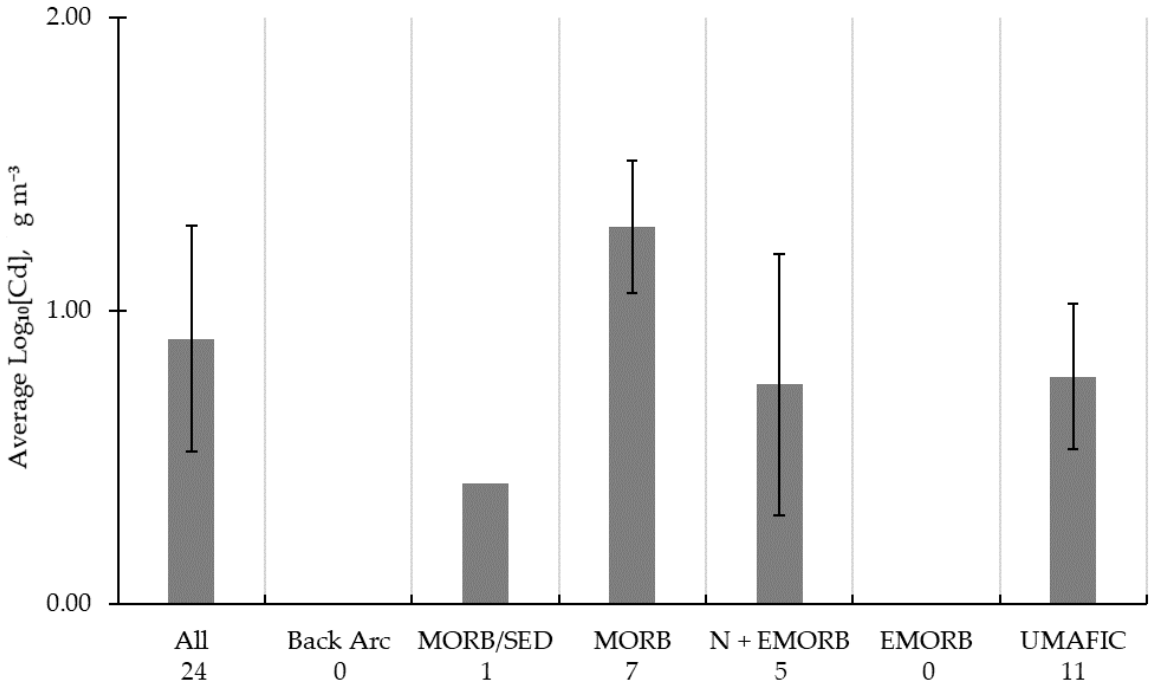

Figure S14: *Means and standard deviations of fluid endmember cadmium concentrations, as common logarithms of the concentration in grams per cubic metre, by host rock category.*

Table S16: *Matrix of t-test values between host rock categories for the common logarithm of cadmium concentration in fluid endmembers. The values coloured red indicate the corresponding categories are significantly different. Values in standard black indicate the difference between host categories is not significant. There are no significantly similar host rock types in terms of cadmium concentration.*

Cd	All	Back Arc	MORB/SED	MORB	N + EMORB	EMORB	UMAFIC
All				1.99E-02	0.43		0.34
Back Arc							
MORB/SED							
MORB					1.95E-02		1.08E-03
N + EMORB							0.89
EMORB							
UMAFIC							

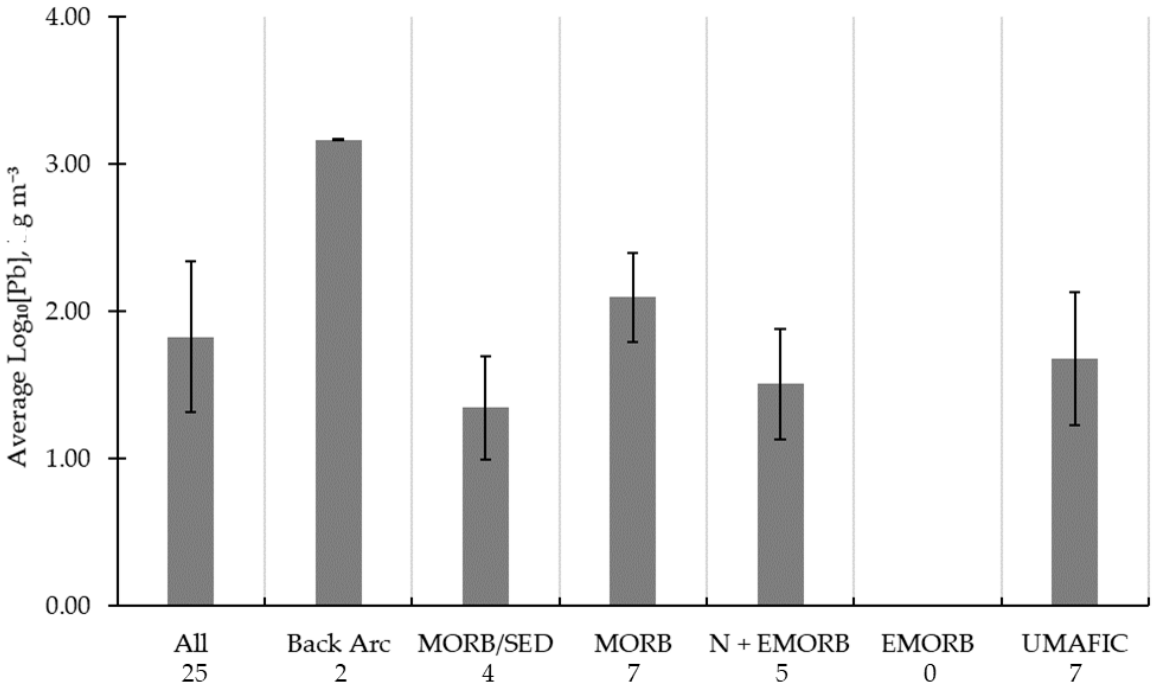

***Figure S15**: Means and standard deviations of fluid endmember lead concentrations, as common logarithms of the concentration in grams per cubic metre, by host rock category.*

***Table S17:** Matrix of t-test values between host rock categories for the common logarithm of lead concentration in fluid endmembers. The values coloured red indicate the corresponding categories are significantly different. Values in standard black indicate the difference between host categories is not significant. There are no significantly similar host rock types in terms of lead concentration.*

Pb	All	Back Arc	MORB/SED	MORB	N + EMORB	EMORB	UMAFIC
All		7.02E-03	0.15	0.29	0.29		0.59
Back Arc			2.23E-03	2.08E-03	2.01E-03		1.63E-02
MORB/SED				4.38E-03	0.53		0.36
MORB					1.29E-02		0.14
N + EMORB							0.60
EMORB							
UMAFIC							

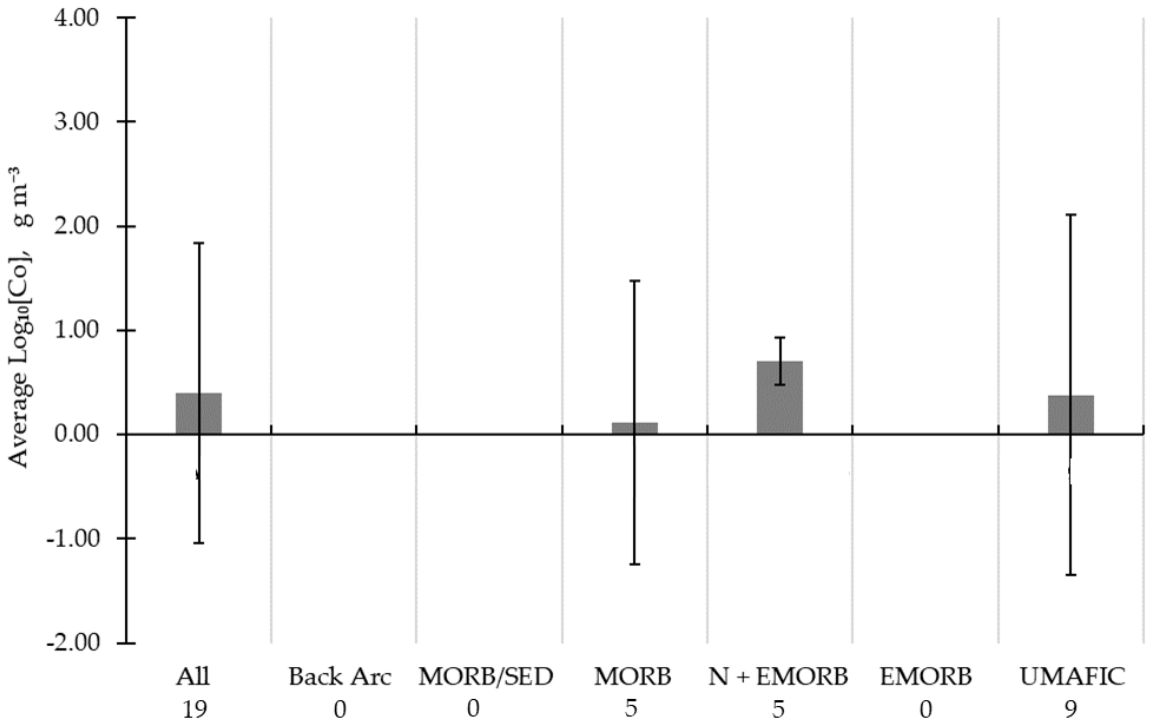

***Figure S16**: Means and standard deviations of fluid endmember cobalt concentrations, as common logarithms of the concentration in grams per cubic metre, by host rock category.*

***Table S18:** Matrix of t-test values between host rock categories for the common logarithm of cobalt concentration in fluid endmembers. There are no significantly different host rock types in terms of lithium concentration. Values in standard black indicate the difference between host categories is not significant. Significantly similar host rock types are indicated by bold black text.*

Co	All	Back Arc	MORB/SED	MORB	N + EMORB	EMORB	UMAFIC
All				0.70	0.64		**0.98**
Back Arc							
MORB/SED							
MORB					0.37		0.79
N + EMORB							0.71
EMORB							
UMAFIC							

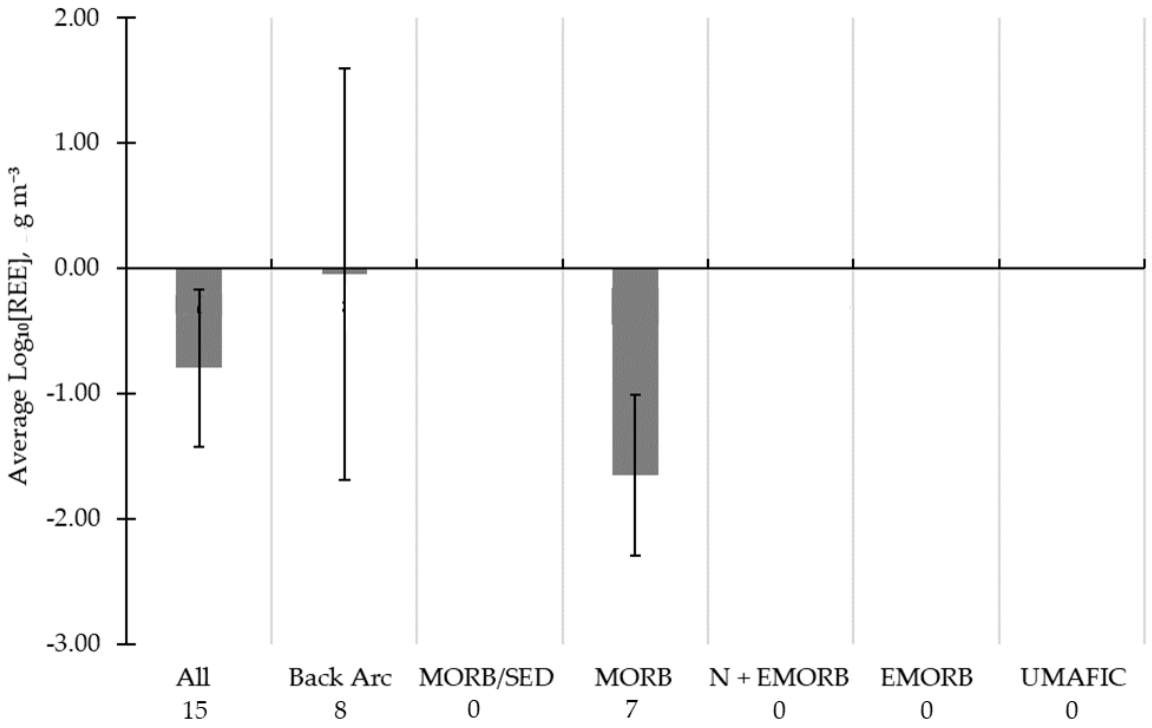

Figure S17: *Means and standard deviations of fluid endmember Rare Earth Element (REE) concentrations, as common logarithms of the concentration in grams per cubic metre, by host rock category.*

Table S19: *Matrix of t-test values between host rock categories for the common logarithm of Rare Earth Element (REE) concentration in fluid endmembers. The values coloured red indicate the corresponding categories are significantly different. Values in standard black indicate the difference between host categories is not significant. There are no significantly similar host rock types in terms of REE concentration.*

REE	All	Back Arc	MORB/SED	MORB	N + EMORB	EMORB	UMAFIC
All		0.28		0.16			
Back Arc				3.06E-02			
MORB/SED							
MORB							
N + EMORB							
EMORB							
UMAFIC							

THIS PAGE IS INTENTIONALLY BLANK

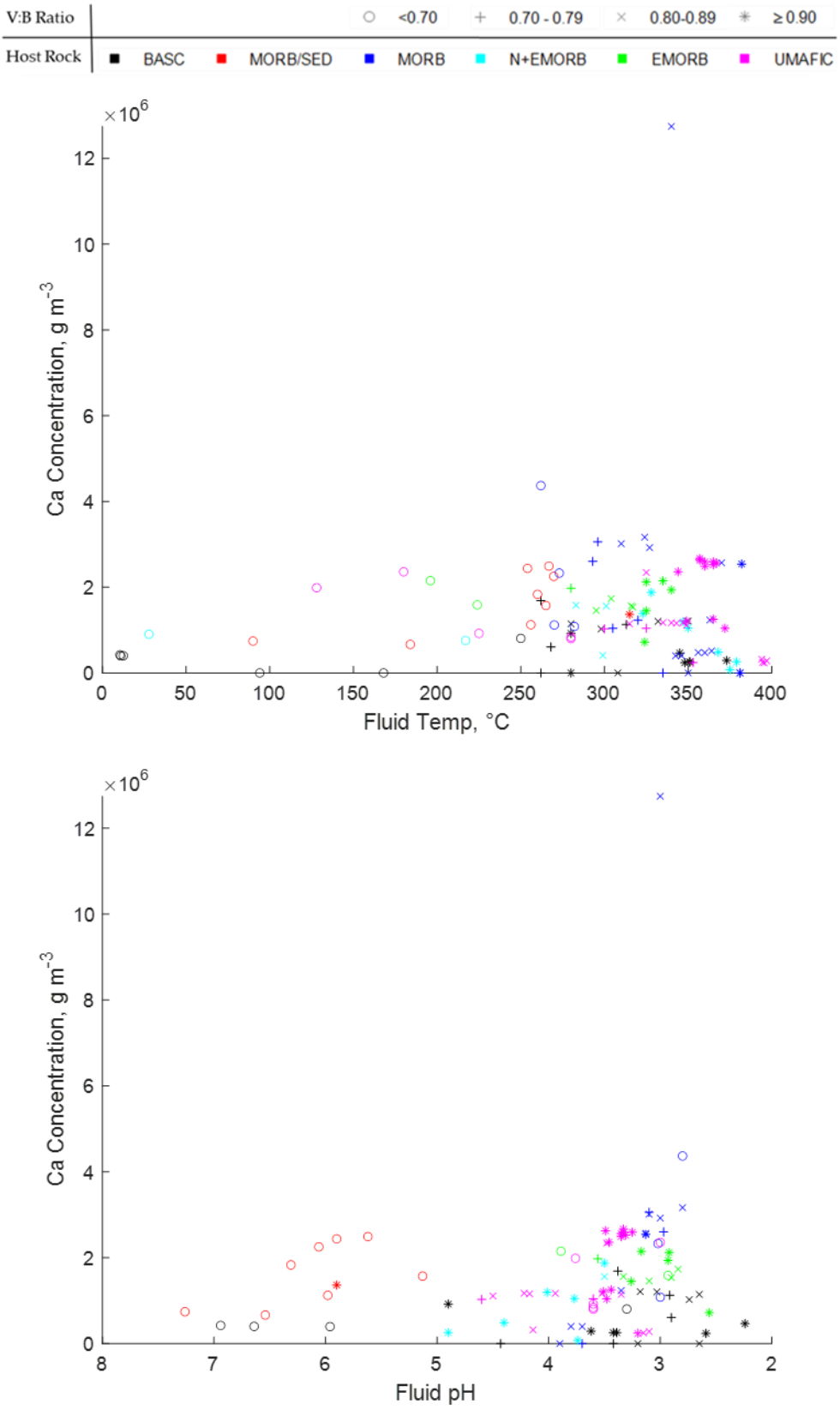

***Figure S18**: Distribution of calcium concentrations in hydrothermal fluids (as **Figure 21**), rotated to demonstrate distributions with temperature (top) and pH (bottom): V:B ratio interval indicated by marker type; Host Rock type indicated by marker colour*

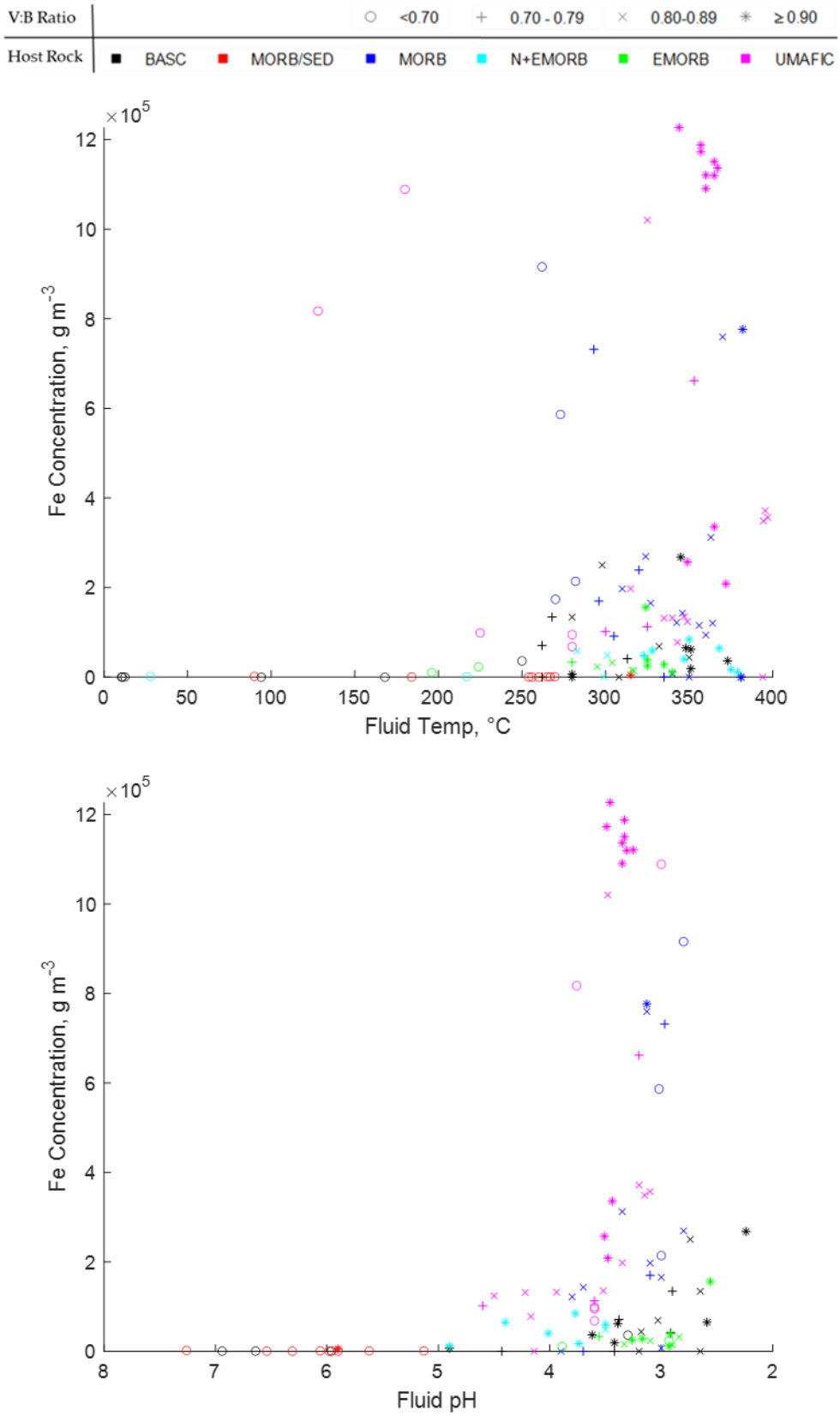

***Figure S19**: Distribution of iron concentrations in hydrothermal fluids (as **Figure 22**), rotated to demonstrate distributions with temperature (top) and pH (bottom): V:B ratio interval indicated by marker type; Host Rock type indicated by marker colour*

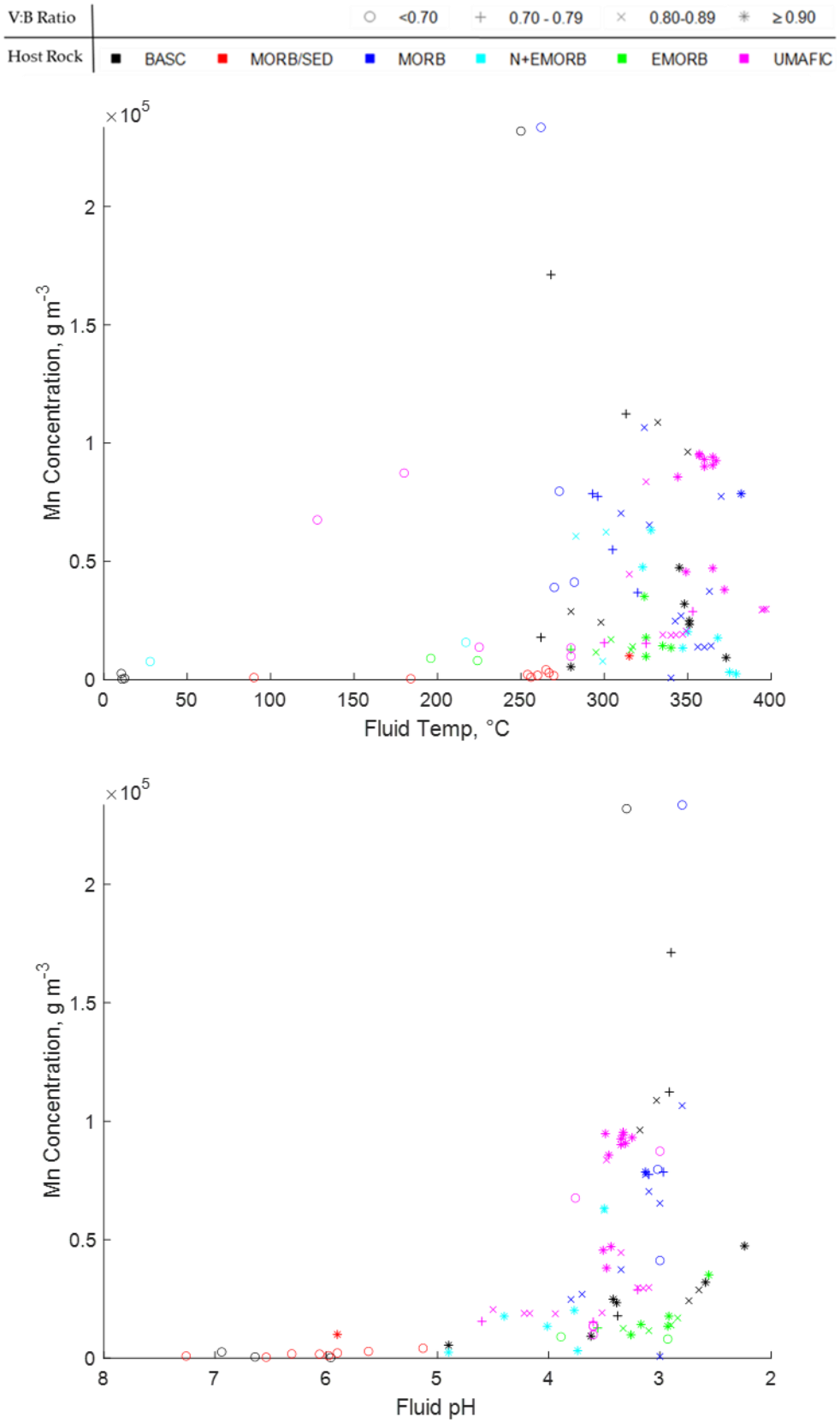

***Figure S20**: Distribution of manganese concentrations in hydrothermal fluids (as **Figure 23**), rotated to demonstrate distributions with temperature (top) and pH (bottom): V:B ratio interval indicated by marker type; Host Rock type indicated by marker colour*

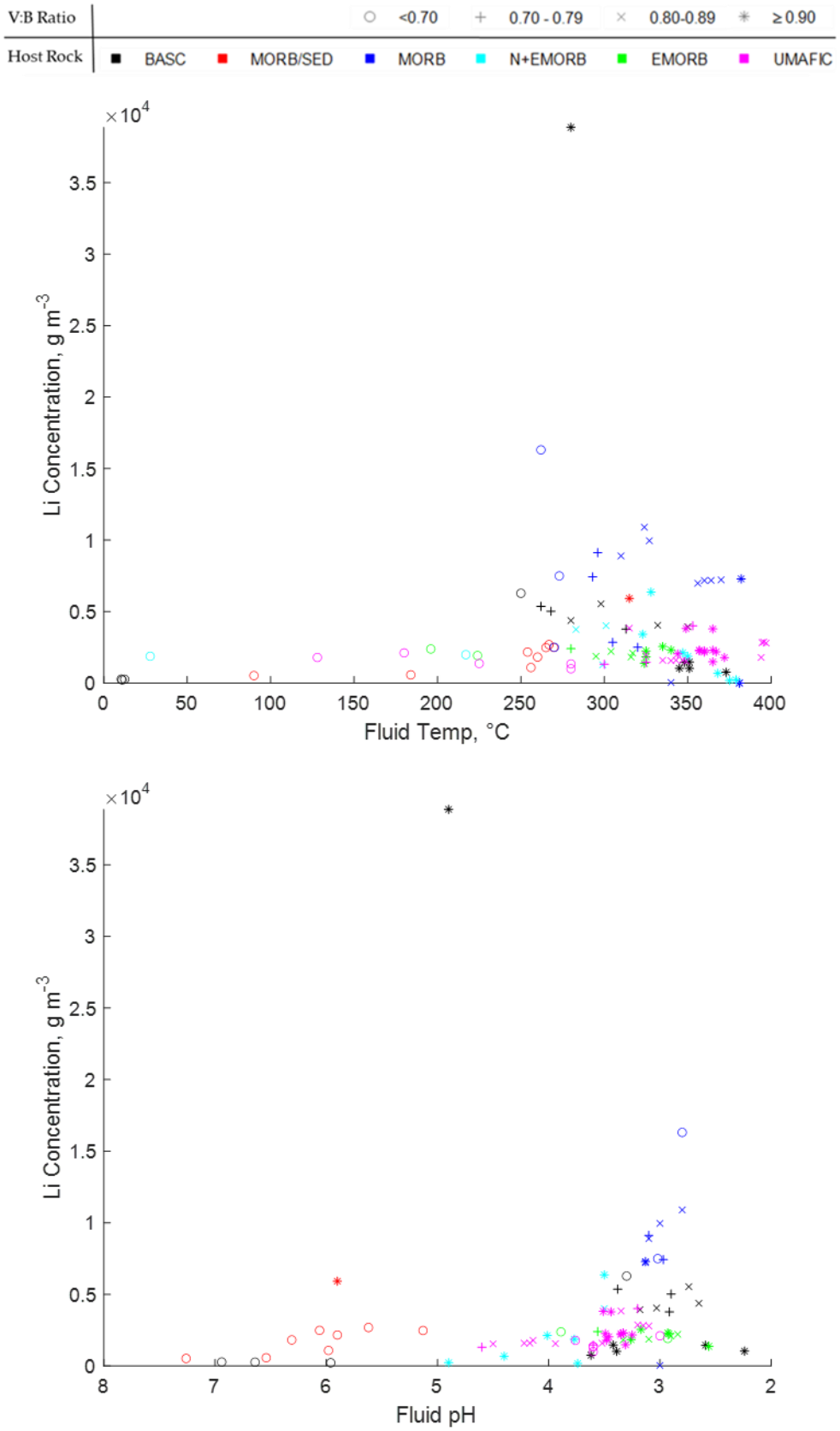

Figure S21: *Distribution of lithum concentrations in hydrothermal fluids (as* ***Figure 24****), rotated to demonstrate distributions with temperature (top) and pH (bottom): V:B ratio interval indicated by marker type; Host Rock type indicated by marker colour*

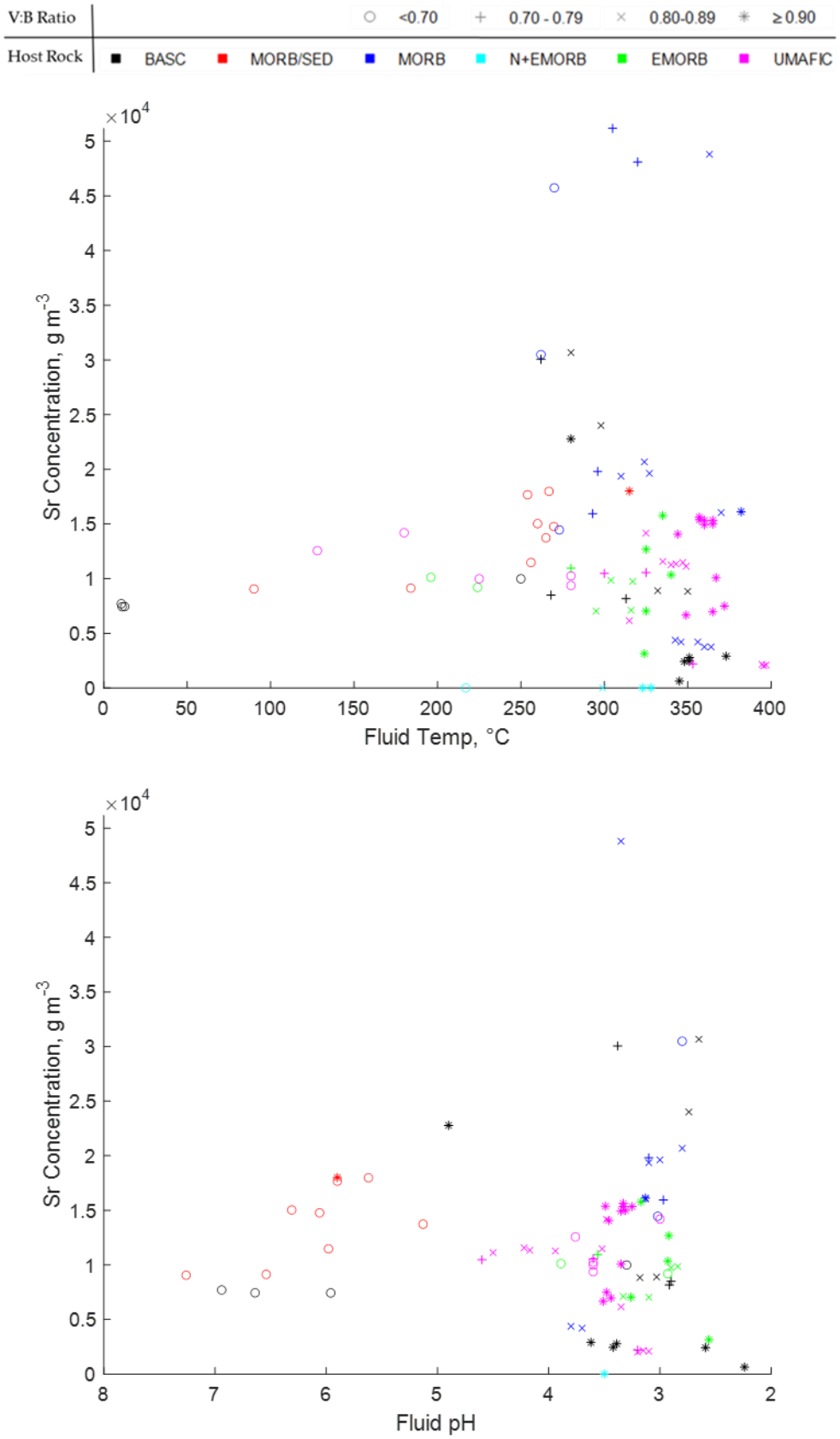

Figure S22: *Distribution of strontium concentrations in hydrothermal fluids (as* ***Fig. 25****), rotated to show distributions with temperature (top) and pH (bottom): V:B ratio interval indicated by marker type; Host Rock type indicated by marker colour*

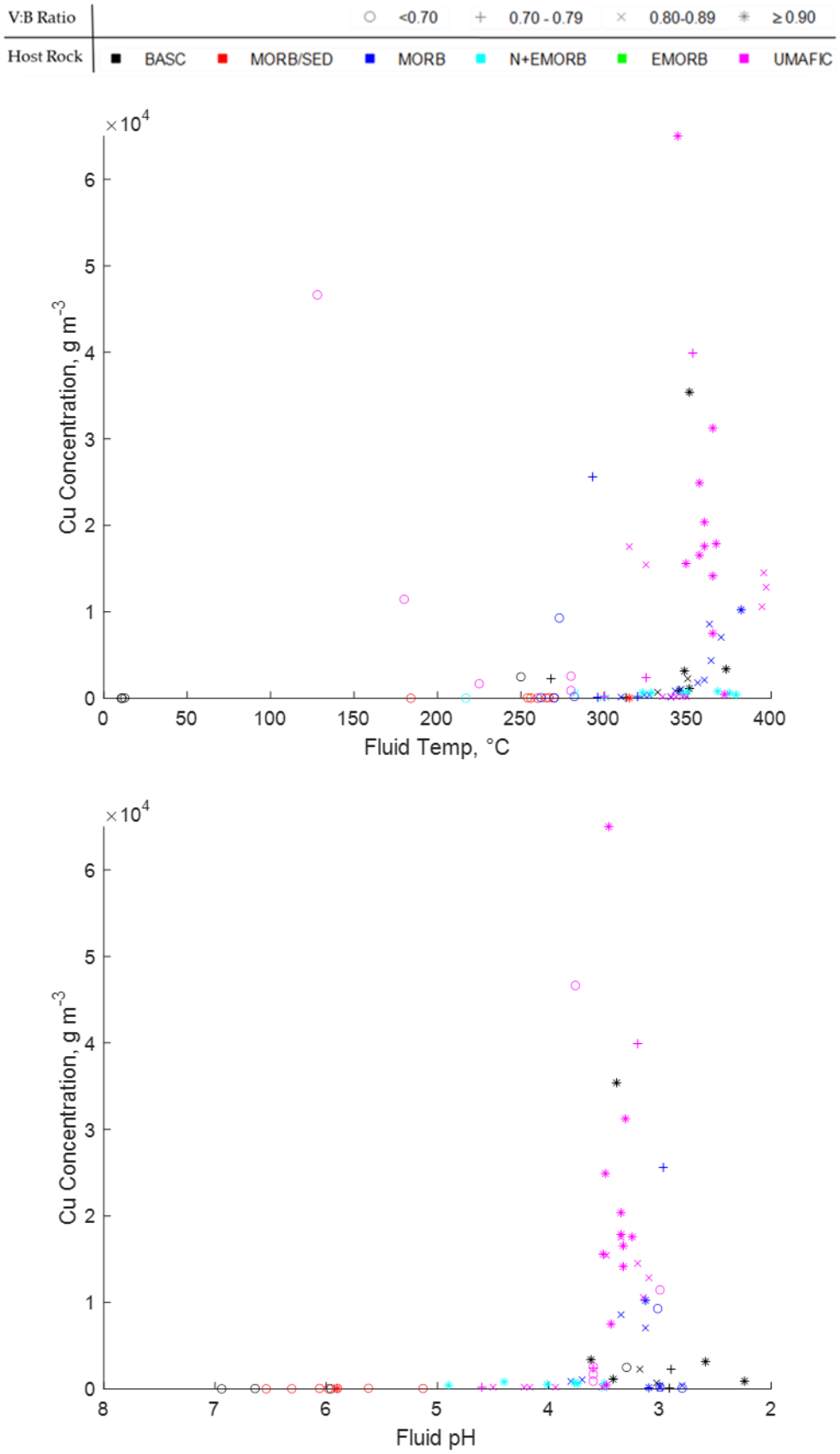

Figure S23: *Distribution of copper concentrations in hydrothermal fluids (as* ***Figure 26****), rotated to demonstrate distributions with temperature (top) and pH (bottom): V:B ratio interval indicated by marker type; Host Rock type indicated by marker colour*

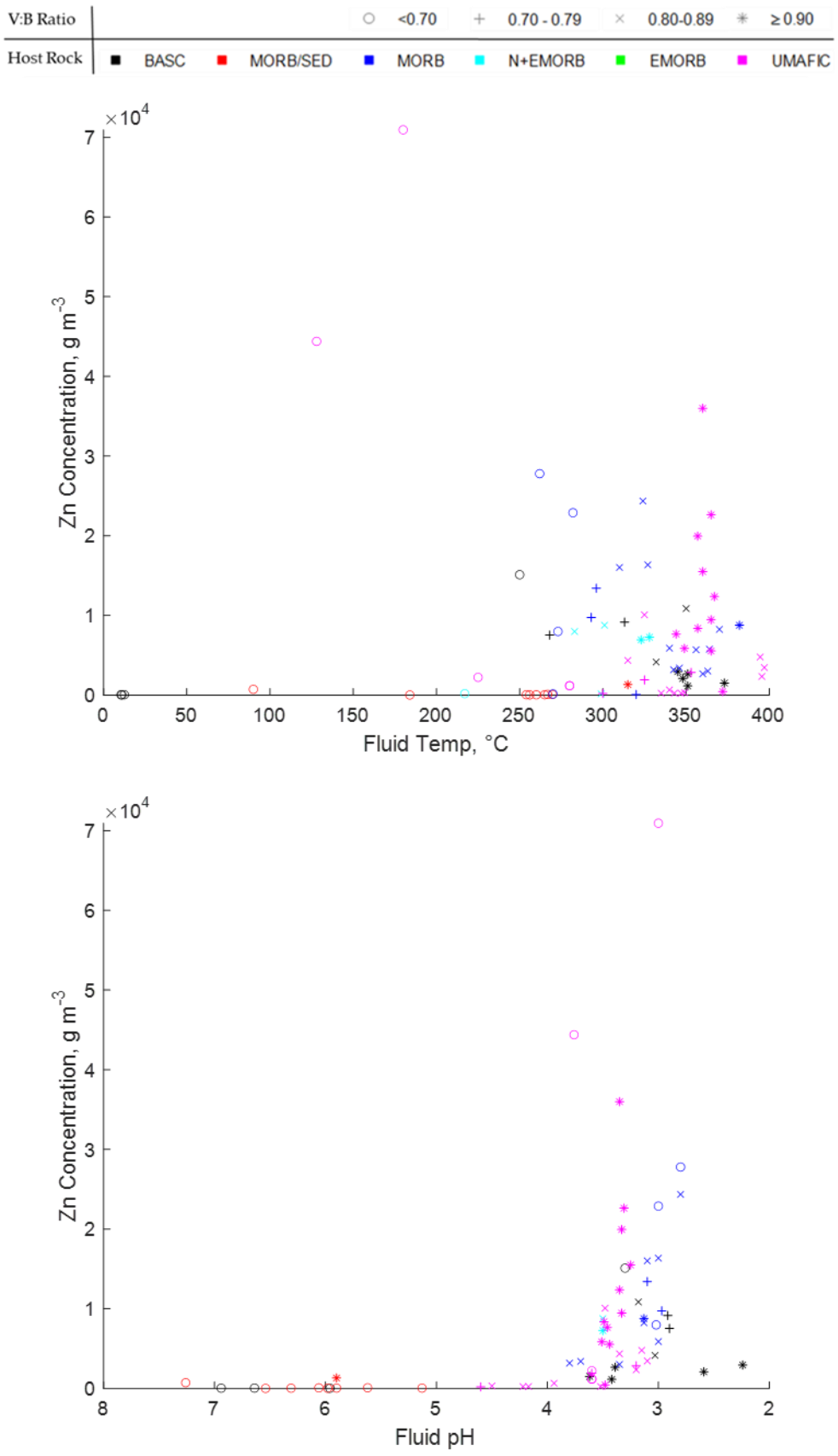

Figure S24: *Distribution of zinc concentrations in hydrothermal fluids (as* ***Figure 27****), rotated to demonstrate distributions with temperature (top) and pH (bottom): V:B ratio interval indicated by marker type; Host Rock type indicated by marker colour*

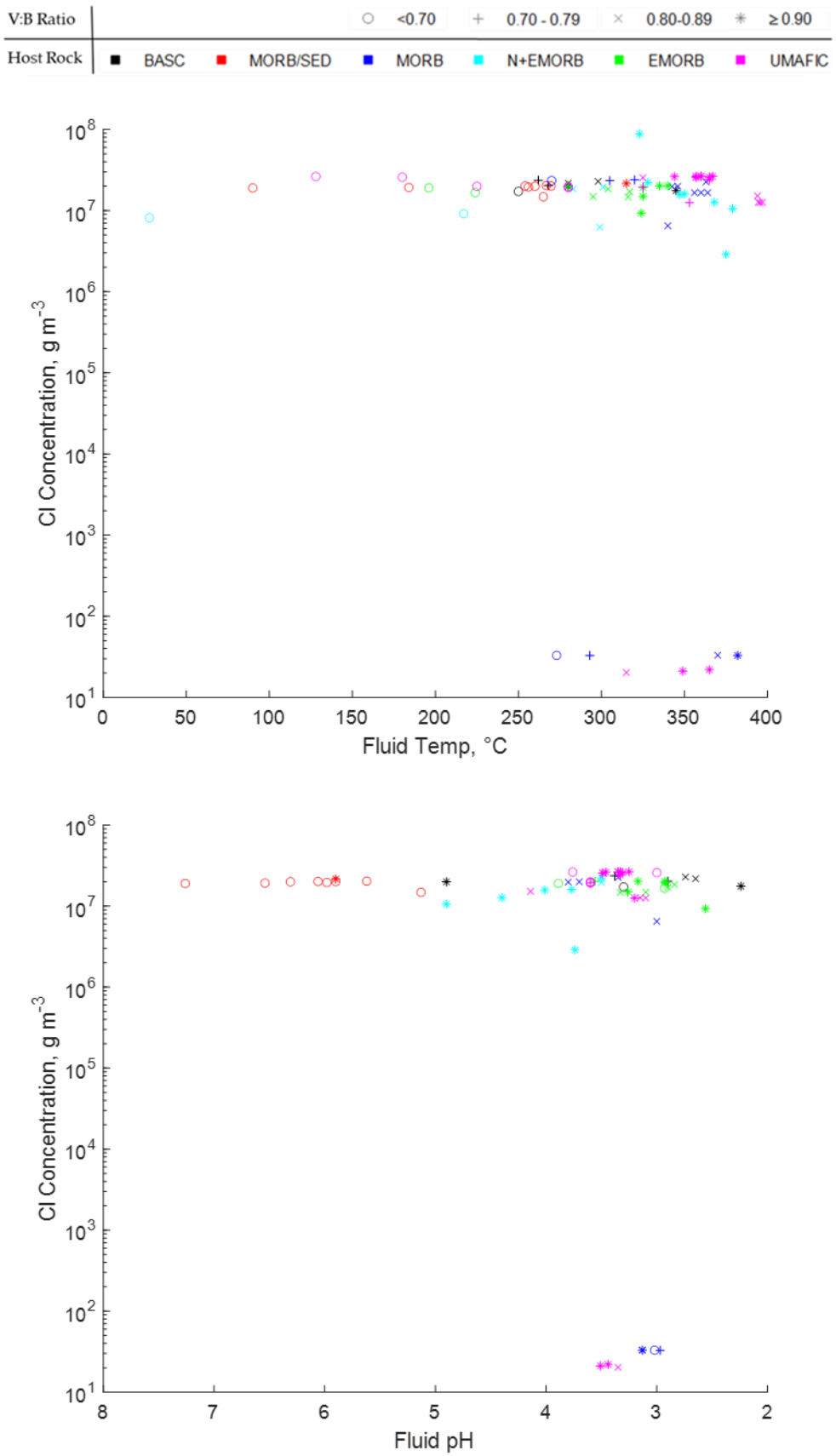

Figure S25: *Distribution of chlorine concentrations in hydrothermal fluids on a logarithmic axis (as* ***Figure 28*** *(bottom)), rotated to show distributions with temperature (top) and pH (bottom): V:B ratio interval indicated by marker type; Host Rock type indicated by marker colour*

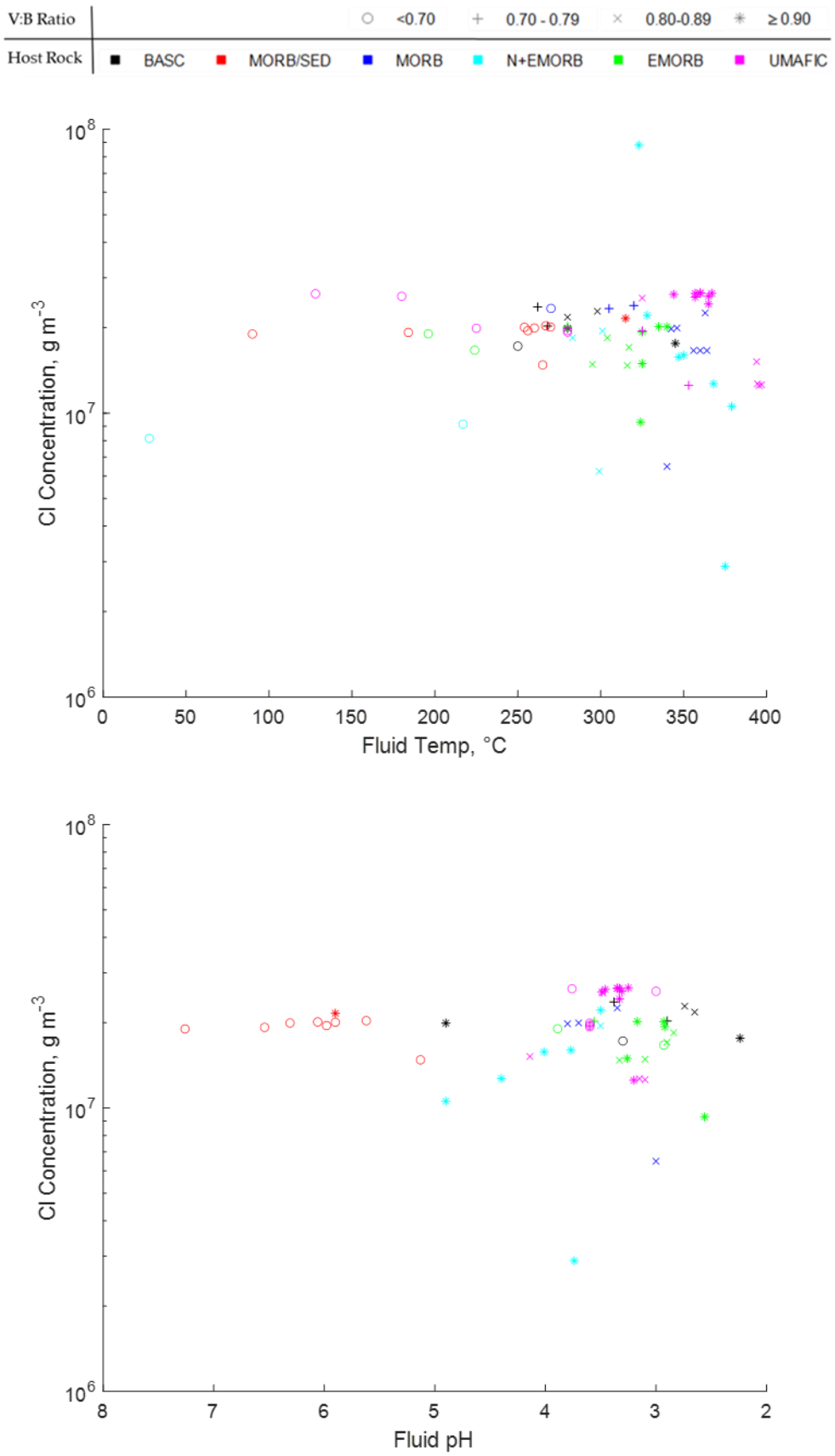

Figure S26: *Distribution of higher band chlorine concentrations in hydrothermal fluids on a logarithmic axis (as* ***Figure 29)*** *rotated to demonstrate distributions with temperature (top) and pH (bottom): V:B ratio interval indicated by marker type; Host Rock type indicated by marker colour*

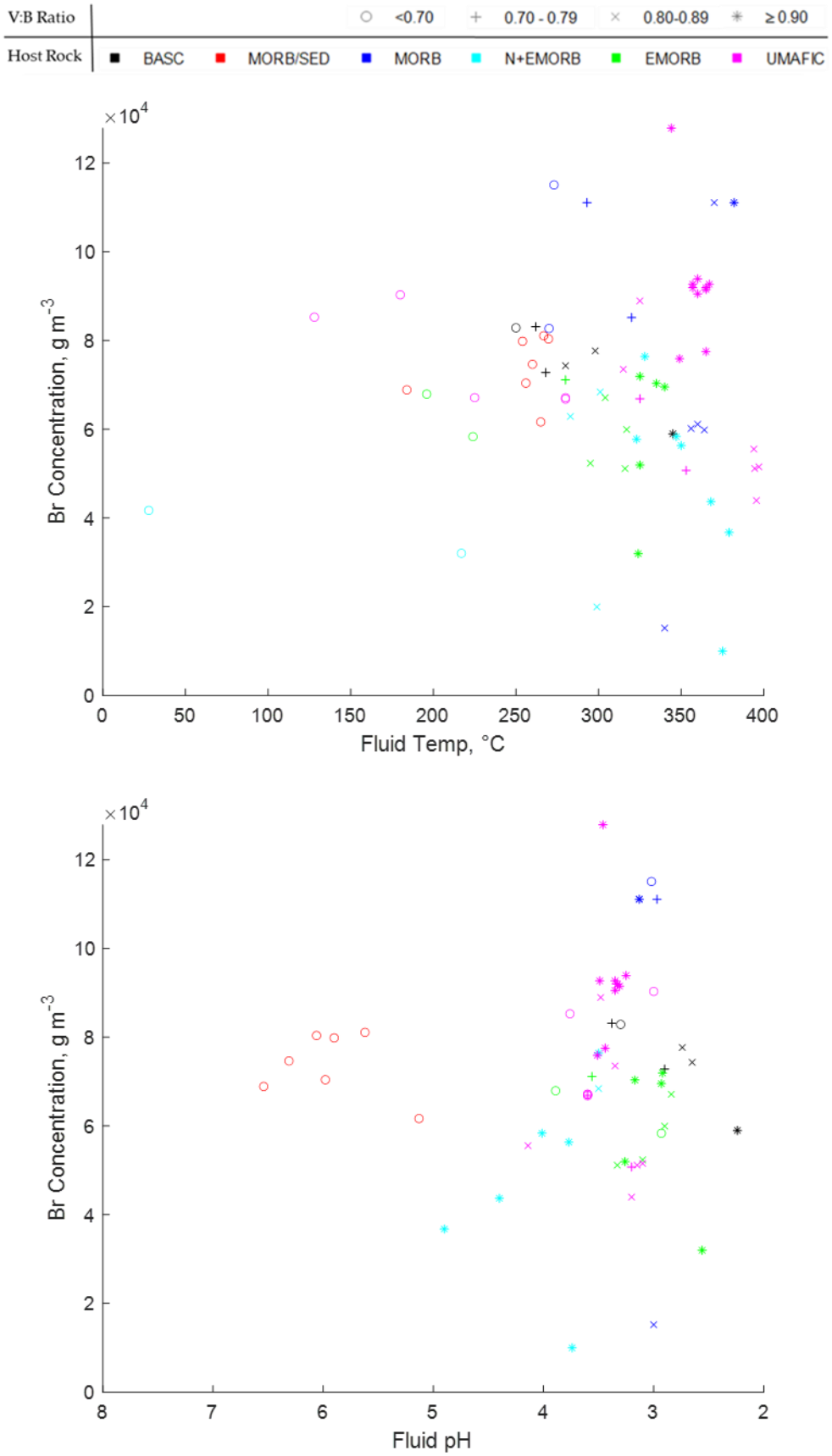

Figure S27: *Distribution of bromine concentrations in hydrothermal fluids (as* ***Figure 30****), rotated to demonstrate distributions with temperature (top) and pH (bottom): V:B ratio interval indicated by marker type; Host Rock type indicated by marker colour*

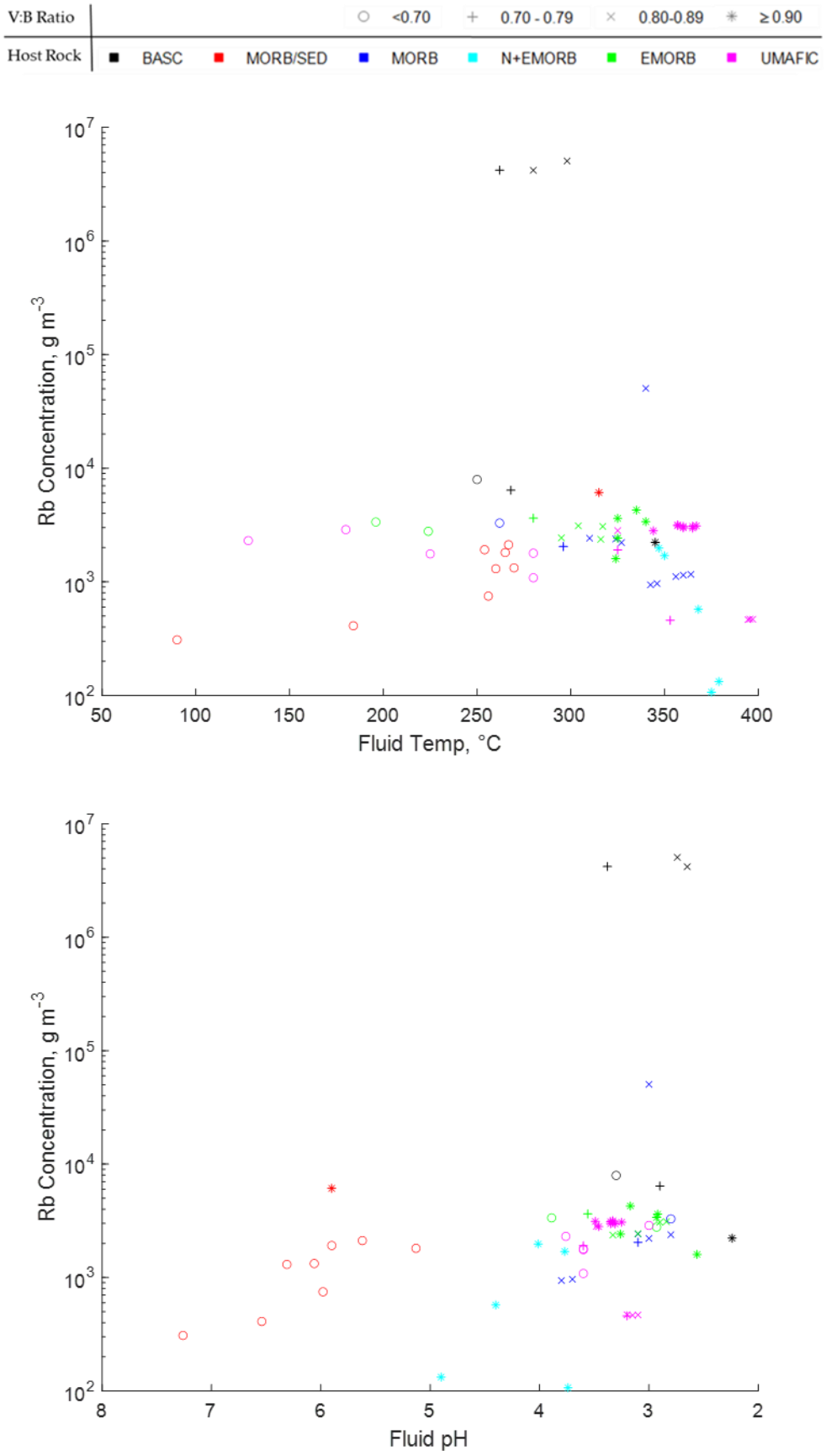

Figure S28: *Distribution of rubidium concentrations in hydrothermal fluids (as* ***Figure 31****), rotated to demonstrate distributions with temperature (top) and pH (bottom): V:B ratio interval indicated by marker type; Host Rock type indicated by marker colour*

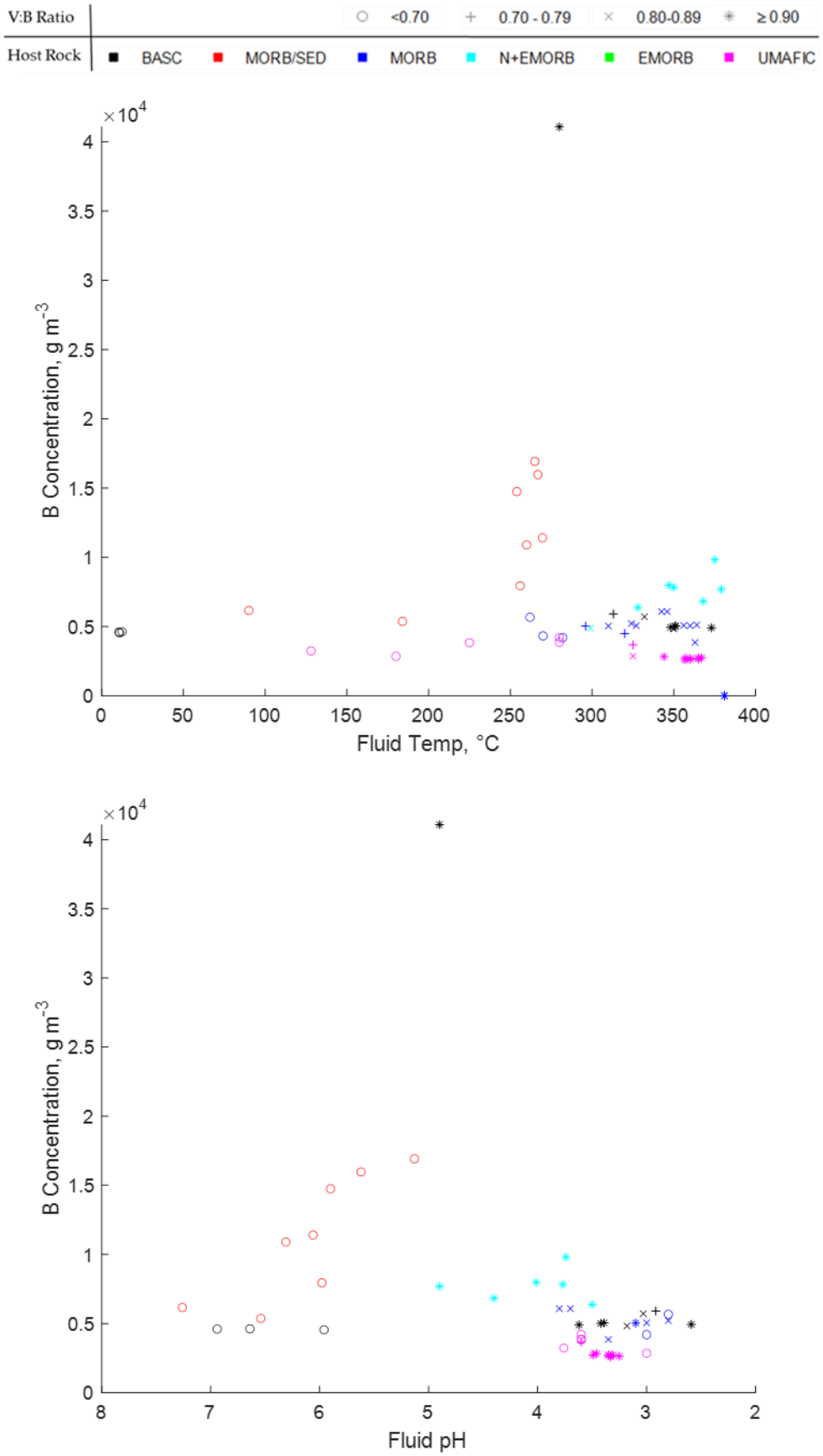

***Figure S6**: Distribution of boron concentrations in hydrothermal fluids (as **Figure 32**), rotated to demonstrate distributions with temperature (top) and pH (bottom): V:B ratio interval indicated by marker type; Host Rock type indicated by marker colour*

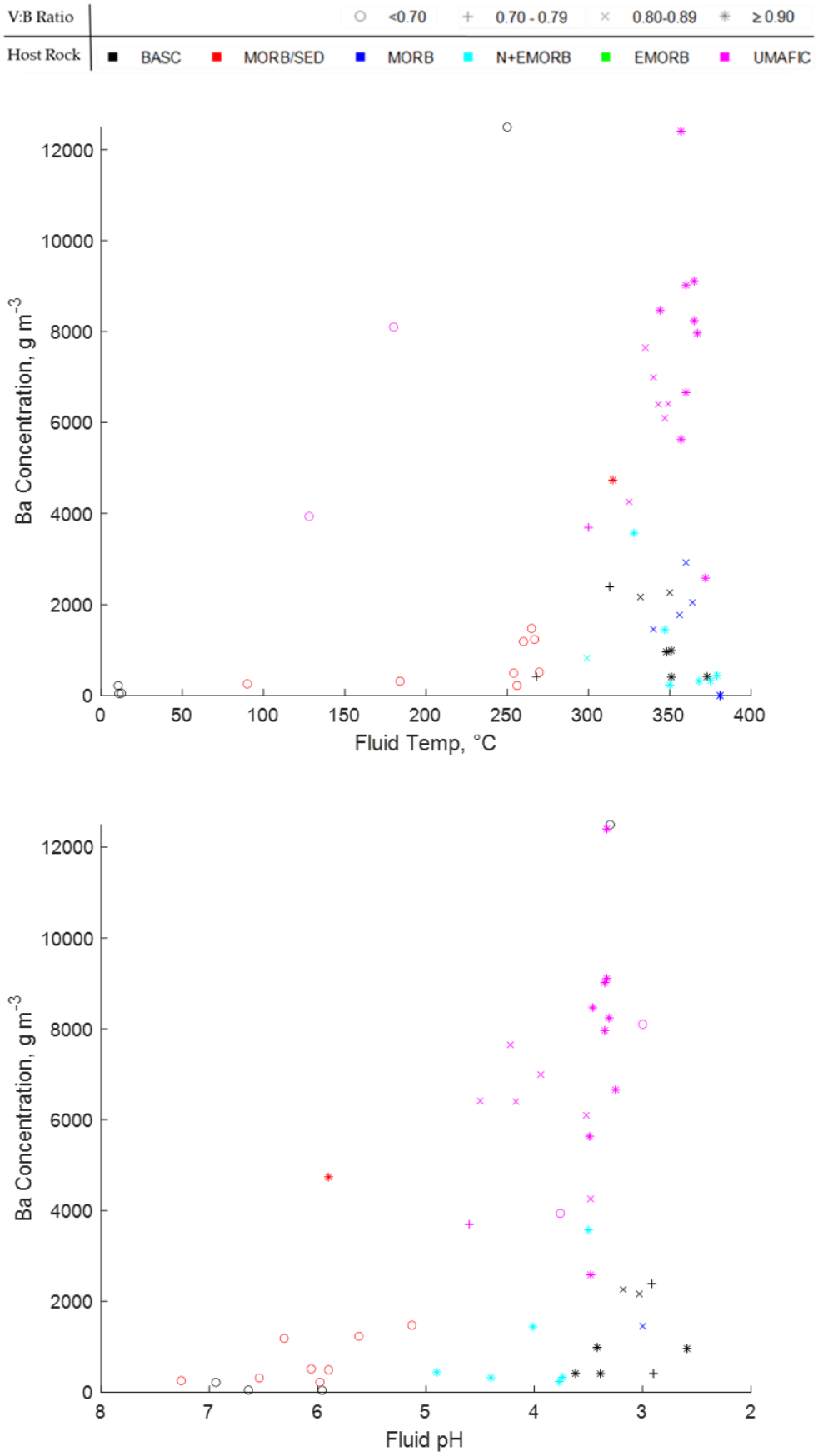

***Figure S30**: Distribution of barium concentrations in hydrothermal fluids (as **Figure 33**), rotated to demonstrate distributions with temperature (top) and pH (bottom): V:B ratio interval indicated by marker type; Host Rock type indicated by marker colour*

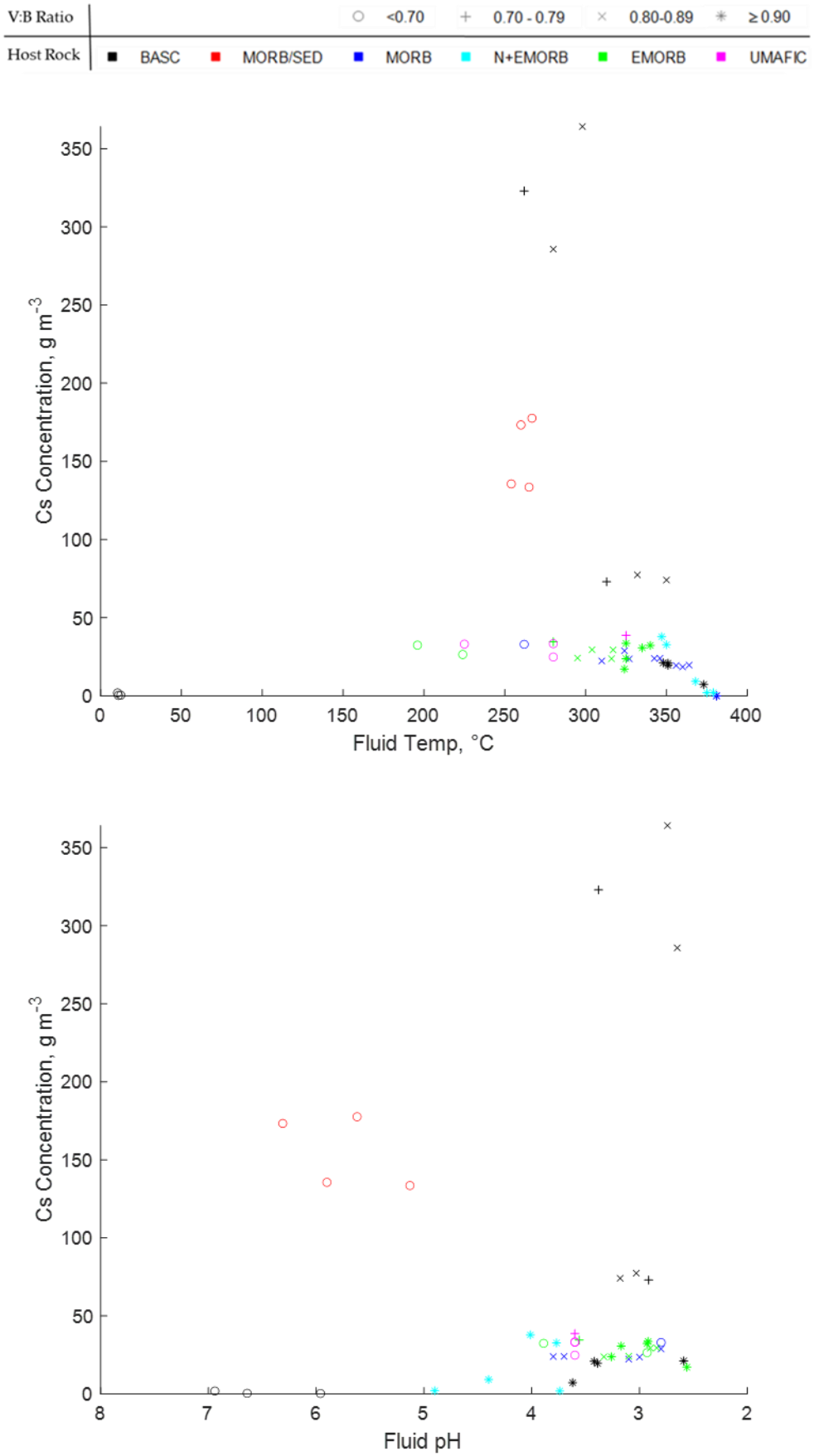

***Figure S31**: Distribution of caesium concentrations in hydrothermal fluids (as **Figure 34**), rotated to demonstrate distributions with temperature (top) and pH (bottom): V:B ratio interval indicated by marker type; Host Rock type indicated by marker colour*

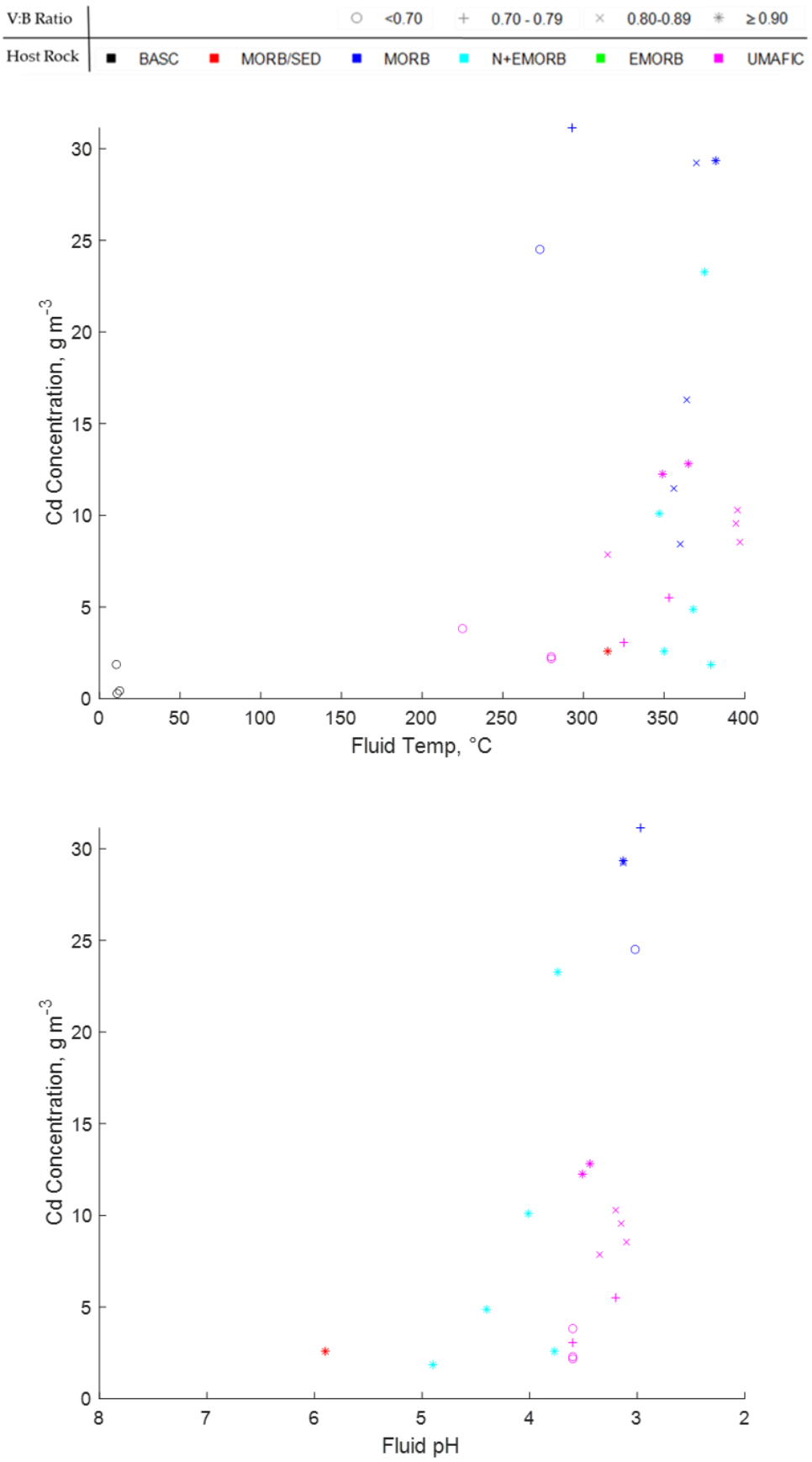

***Figure S32**: Distribution of cadmium concentrations in hydrothermal fluids (as **Figure 35**), rotated to show distributions with temperature (top) and pH (bottom): V:B ratio interval indicated by marker type; Host Rock type indicated by marker colour*

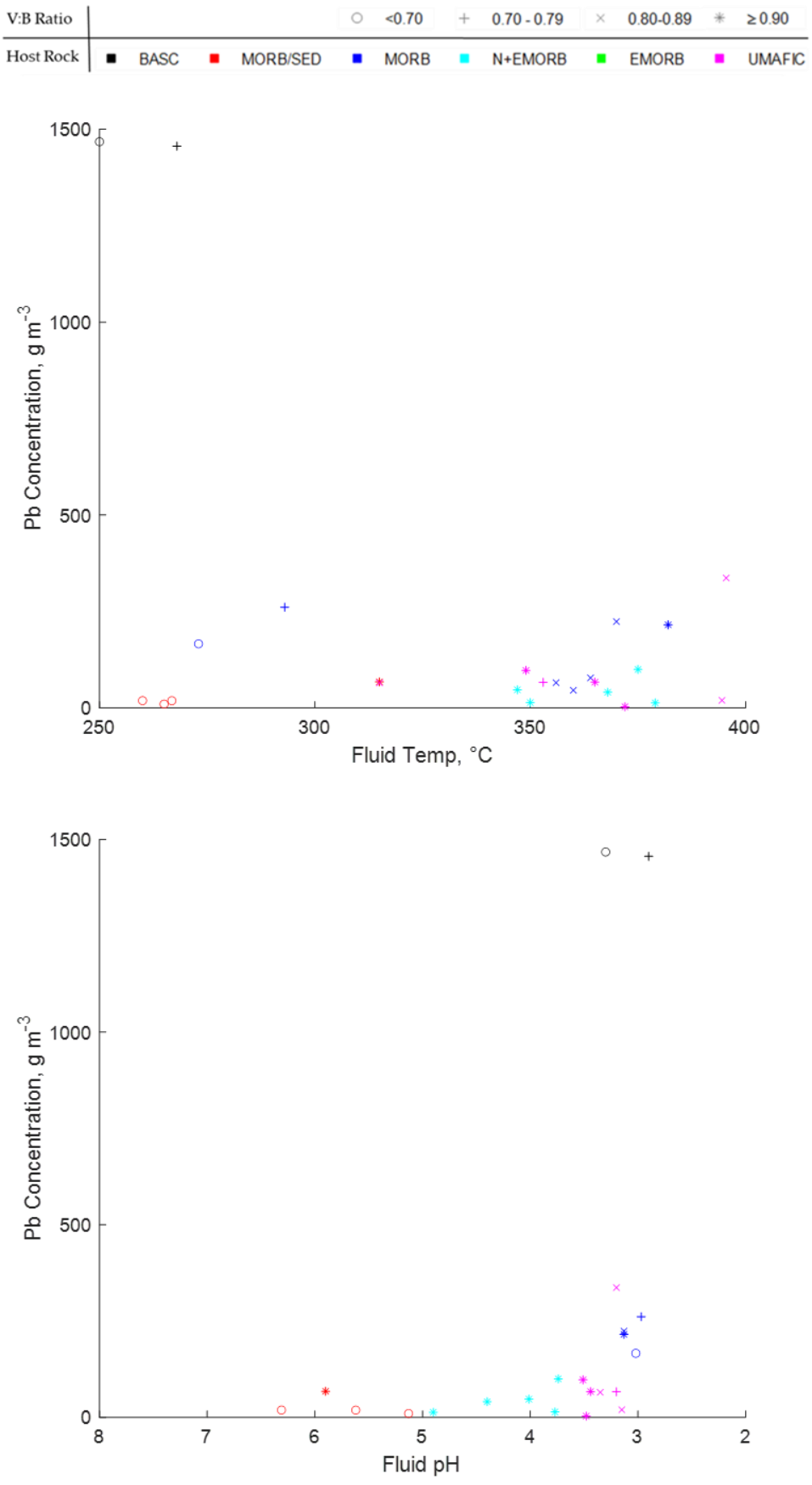

***Figure S7**: Distribution of lead concentrations in hydrothermal fluids (as **Figure 36**), rotated to demonstrate distributions with temperature (top) and pH (bottom): V:B ratio interval indicated by marker type; Host Rock type indicated by marker colour*

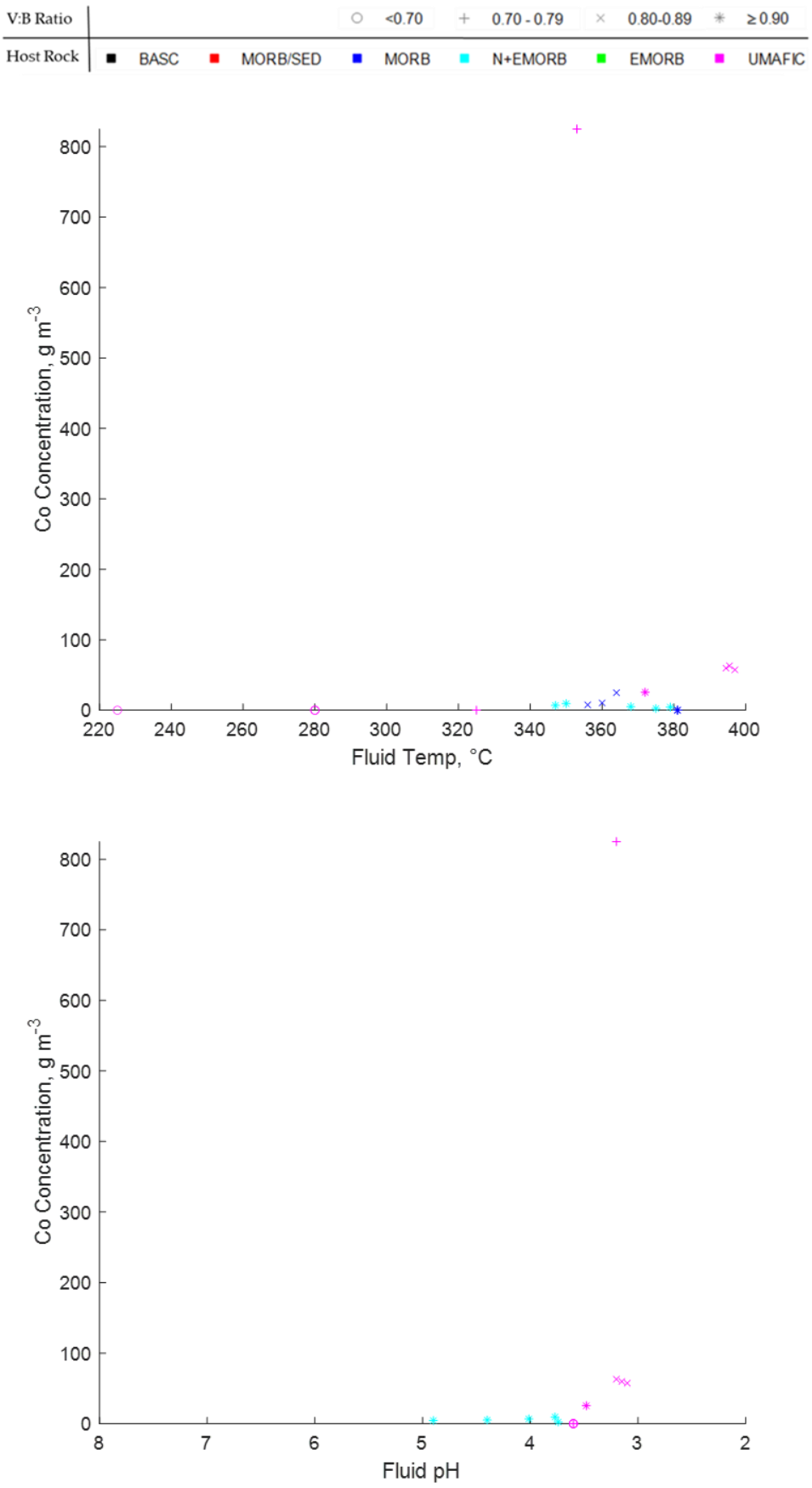

***Figure S34**: Distribution of cobalt concentrations in hydrothermal fluids (as **Figure 37**), rotated to demonstrate distributions with temperature (top) and pH (bottom): V:B ratio interval indicated by marker type; Host Rock type indicated by marker colour*

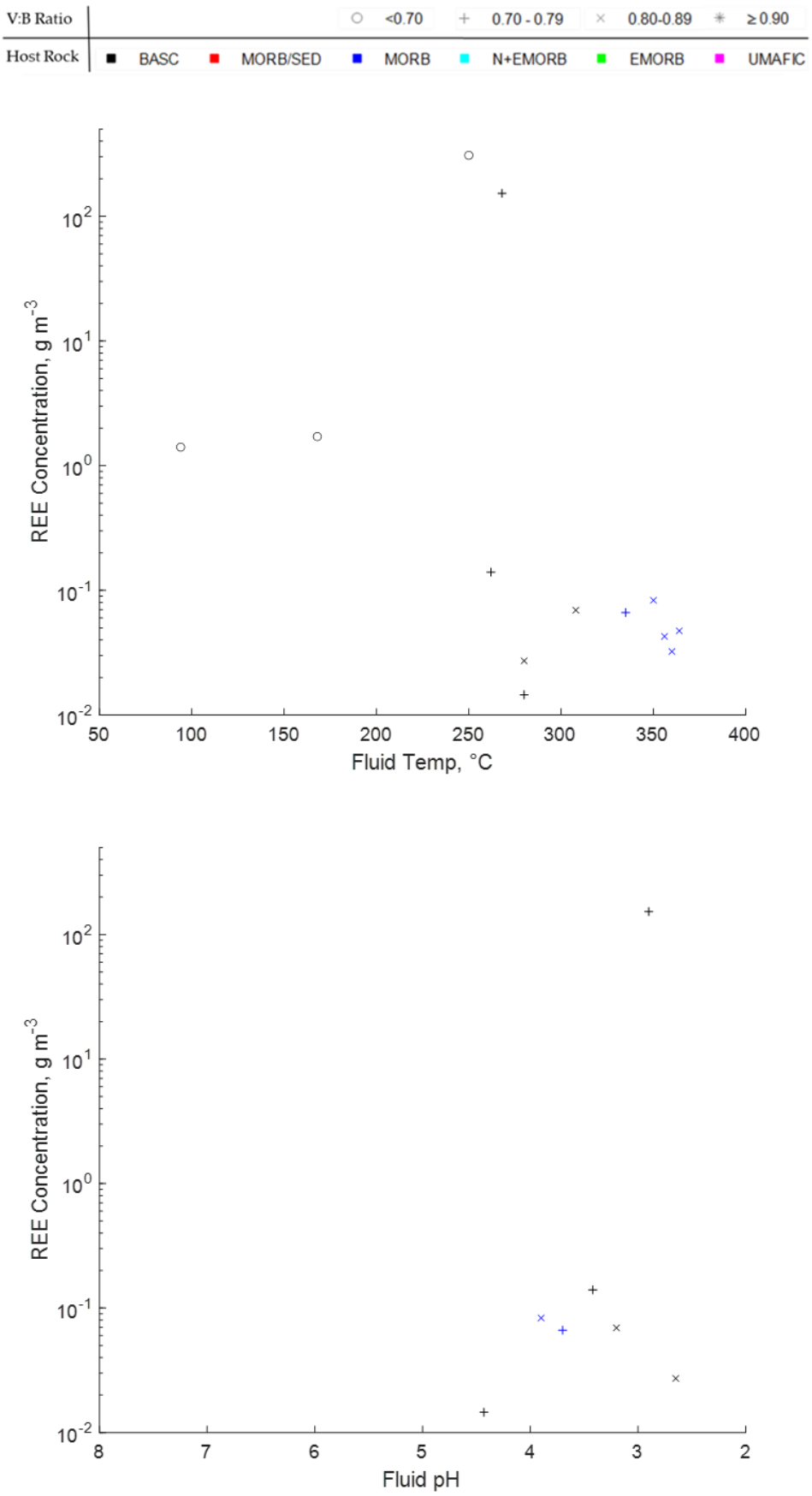

Figure S35: *Distribution of REE concentrations in hydrothermal fluids (as* ***Figure 38****), rotated to demonstrate distributions with temperature (top) and pH (bottom): V:B ratio interval indicated by marker type; Host Rock type indicated by marker colour*

THIS PAGE IS INTENTIONALLY BLANK

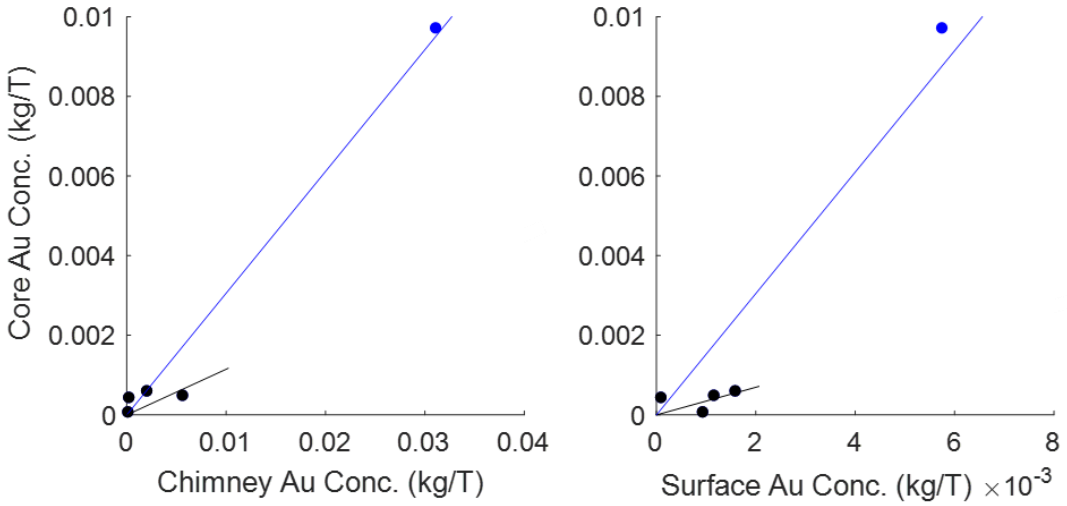

***Figure S36**: (left) Distribution of concentration of gold in core and chimney-type deposits. Data including Beebe (shown in blue) produces a line of best fit (blue), described as $y=0.3058x$, $R^2 = 0.9824$; Data excluding Beebe, is shown in the shorter black line, described as $y=0.1148x$, $R^2 = 0.5778$.*

(right) Distribution of concentration of gold in core and surface-type deposits. Data including Beebe (shown in blue) produces a line of best fit (blue), described as $y=1.5246x$, $R^2 = 0.9193$; Data excluding Beebe, is shown in the shorter black line, described as $y=0.3474x$, $R^2 = 0.703$.

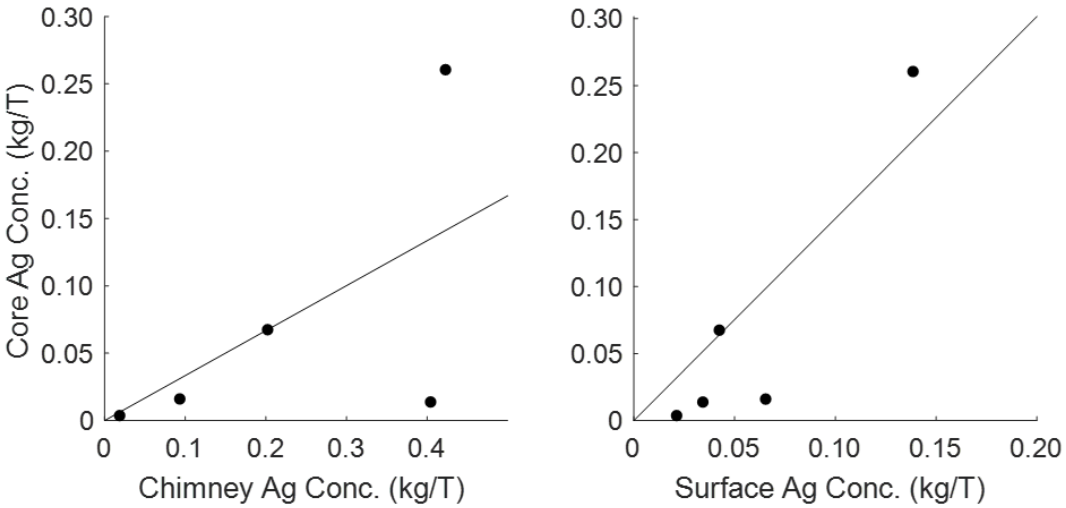

Figure S37: *(left) Distribution of concentration of silver in core and chimney-type deposits. A relationship is represented by line of best fit, following y = 0.3338x, with an R^2 value of 0.5997;*

(right) Distribution of concentration of silver in core and surface-type deposits. A relationship is represented by line of best fit, following y = 1.5078x, with an R^2 value of 0.8389

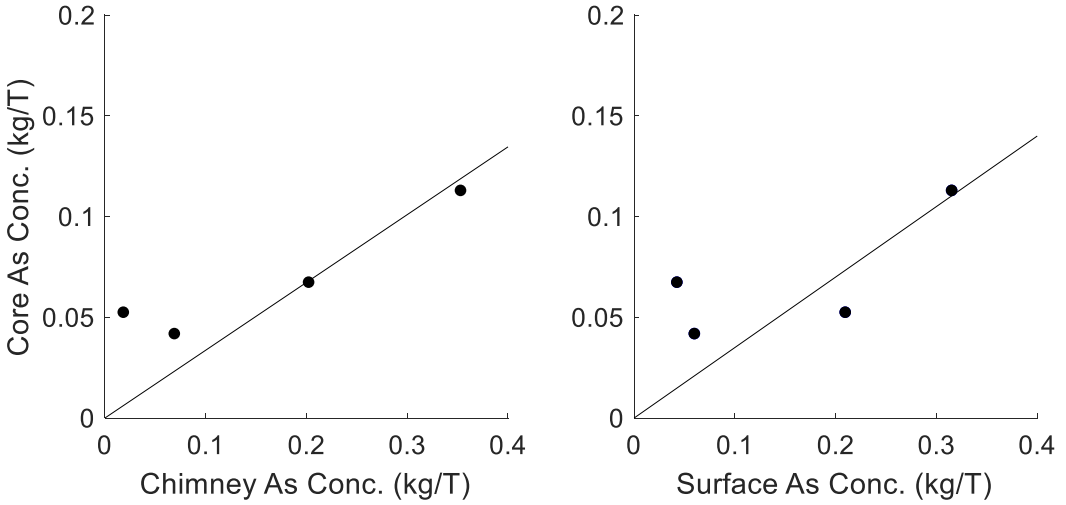

Figure S38*: (left) Distribution of concentration of arsenic in core and chimney-type deposits. A relationship is represented by line of best fit, following y = 1.3705x, with an R^2 value of 0.537.*

(right) Distribution of concentration of arsenic in core and surface-type deposits Relationship is represented by line of best fit, following y = 1.4618x, with an R^2 value of 0.5988 .

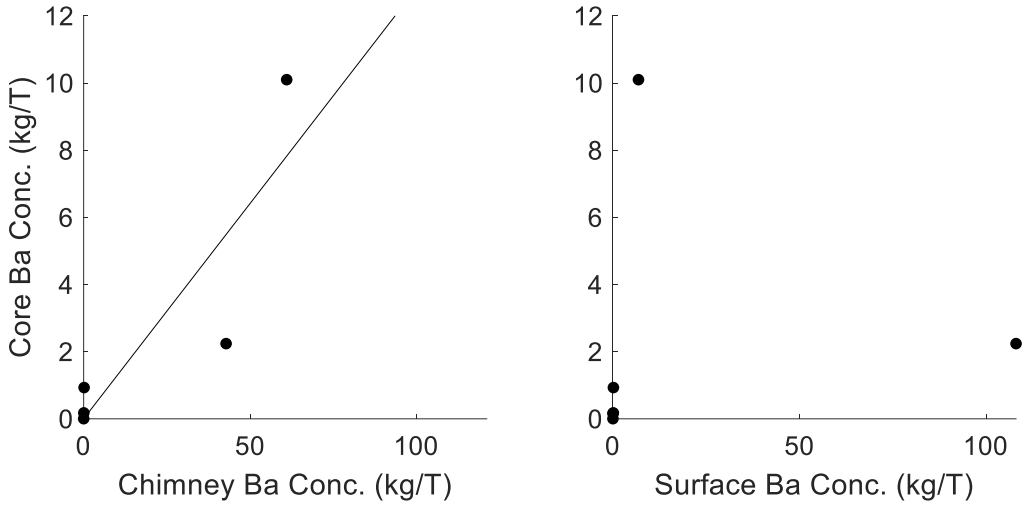

Figure S39: *(left) Distribution of concentration of barium in core and chimney-type deposits. A relationship is represented by line of best fit, following y = 0.1283x, with an R^2 value of 0.8462.*

(right) Distribution of concentration of barium in core and surface-type deposits. No relationship.

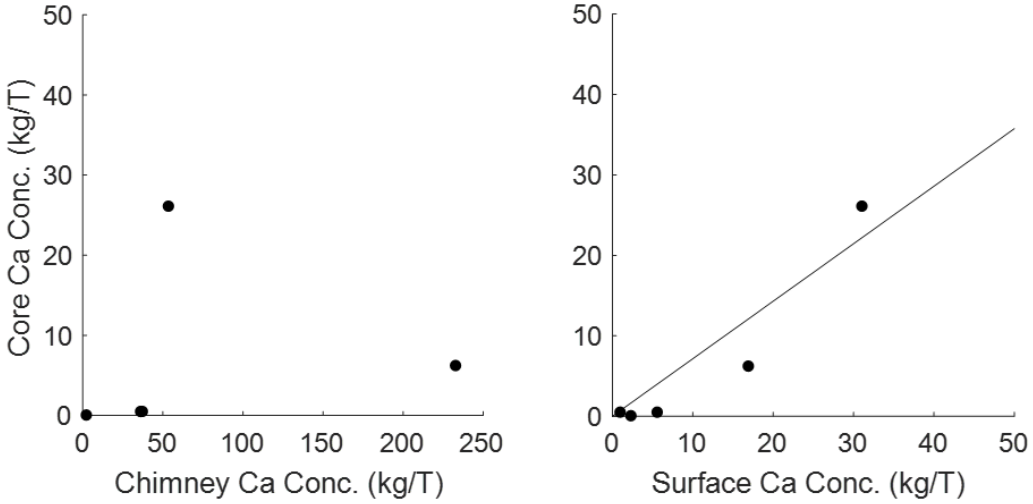

Figure S40: *(left) Distribution of concentration of calcium in core and chimney-type deposits. No relationship.*

(right) Distribution of concentration of calcium in core and surface-type deposits. A relationship is represented by line of best fit, following y = 0.715x, with an R^2 value of 0.9108.

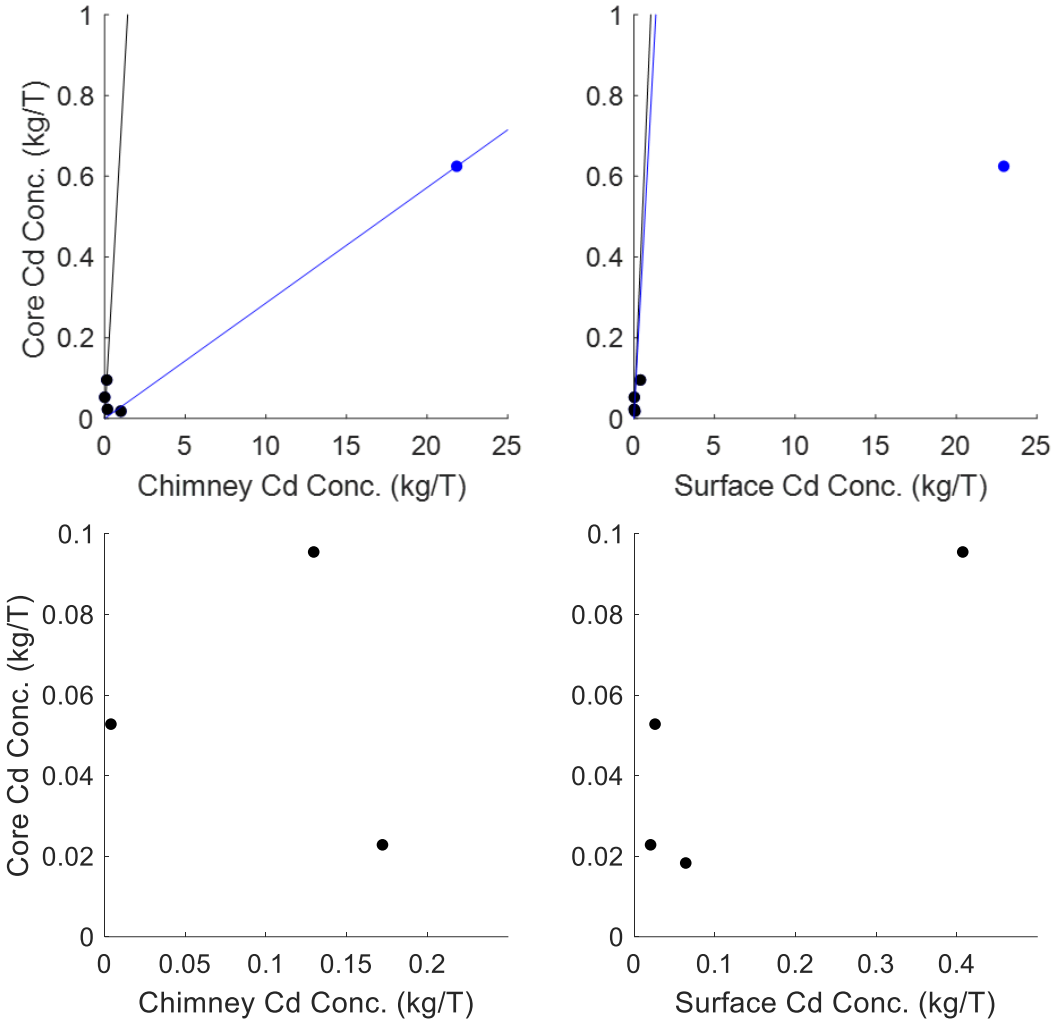

Figure S41*: (top) Distribution of concentration of cadmium in (left) core and chimney-type deposits and (right) in core and surface-type deposits. Snake pit, in blue, is clearly anomalous.*

No apparent relationships

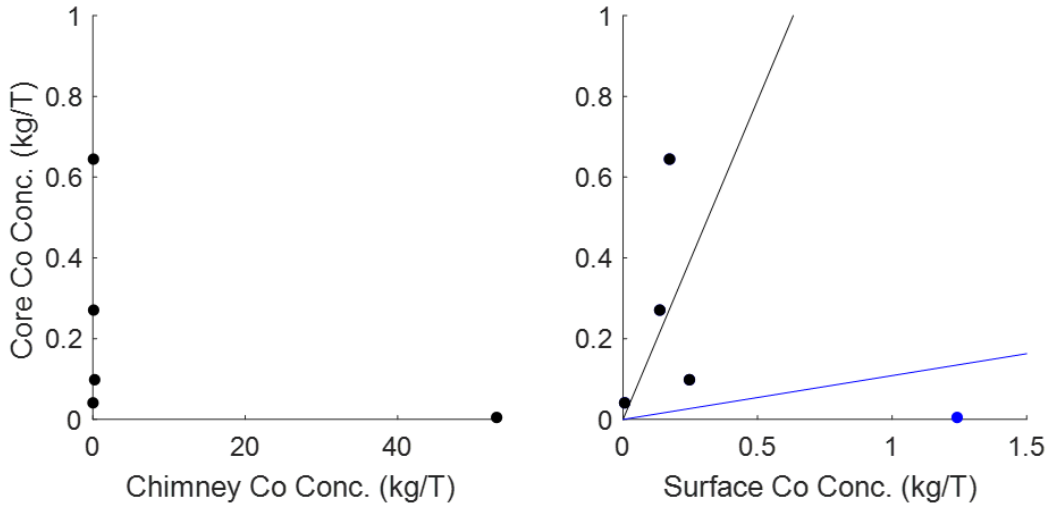

***Figure S42**: (left) Distribution of concentration of cobalt in core and chimney-type deposits. No relationship.*

(right) Distribution of concentration of cobalt in core and surface-type deposits. Disregarding Endeavor as an anomaly; a relationship is represented by line of best fit, following y = 1.5803x, with an R^2 value of 0.9079.

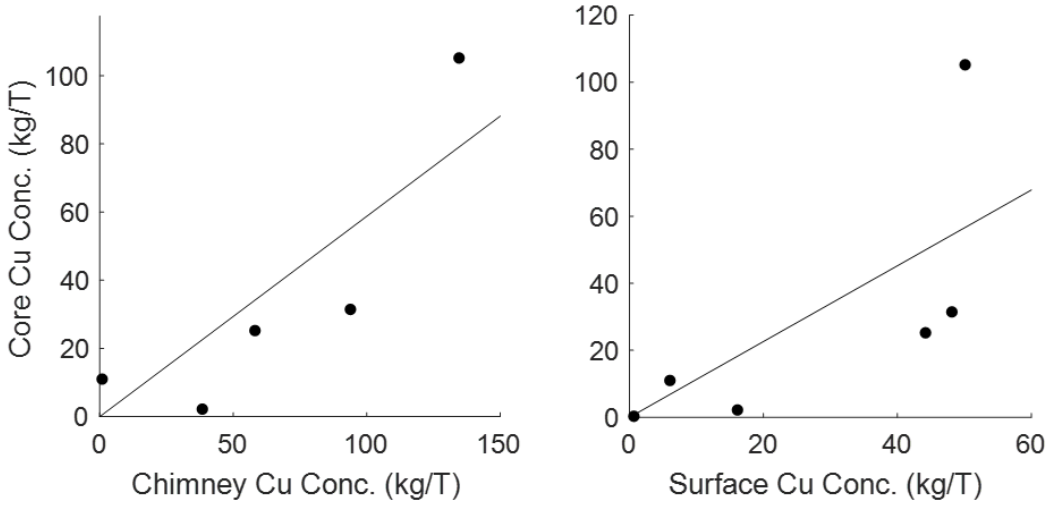

***Figure S48:** (left) Distribution of concentration of copper in core and chimney-type deposits. A relationship is represented by line of best fit, following y = 0.5877x, with an R^2 value of 0.8558.*

(right) Distribution of concentration of copper in core and surface-type deposits A relationship is represented by line of best fit, following y = 1.1307, with an R^2 value of 0.7058.

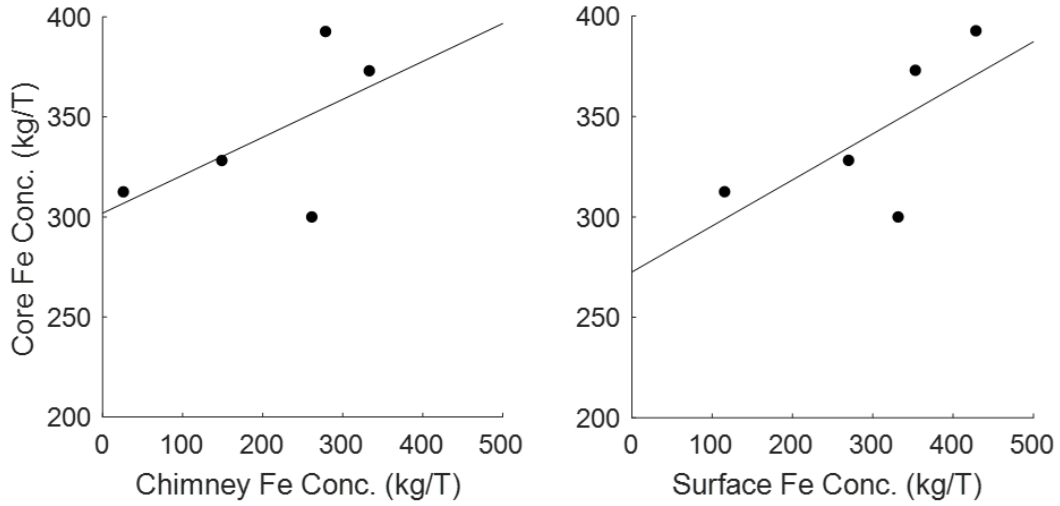

Figure S44: *(left) Distribution of concentration of iron in core and chimney-type deposits. A relationship is represented by line of best fit, following y = 0.1896x + 301.59, with an R^2 value of 0.3403.*

(right) Distribution of concentration of iron in core and surface-type deposits A relationship is represented by line of best fit, following y = 0.2294x + 272.57, with an R^2 value of 0.4579.

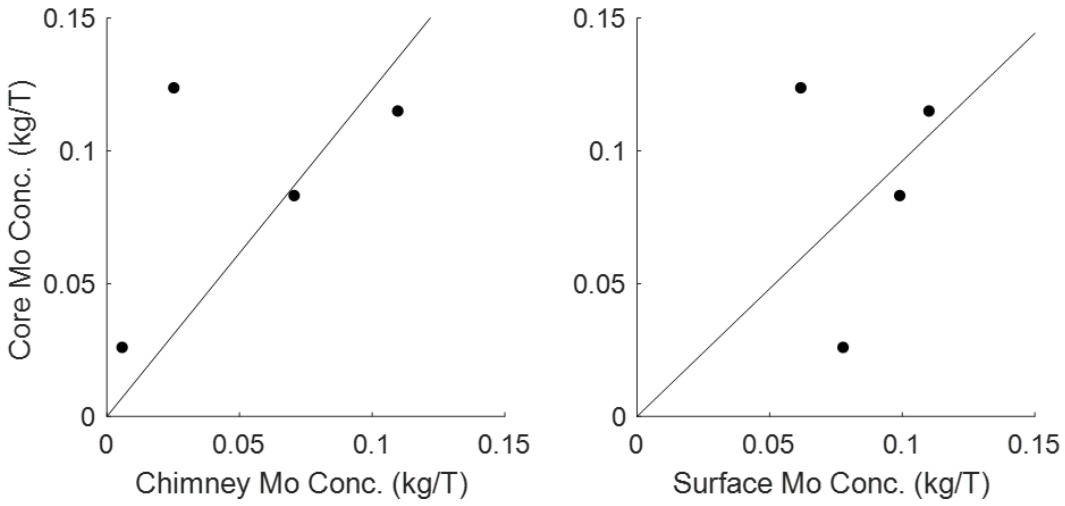

Figure S95*: (left) Distribution of concentration of molybdenum in core and chimney-type deposits. A relationship is represented by line of best fit, following y = 1.2307x, with an R^2 value of 0.7409.*

(right) Distribution of concentration of molybdenum in core and surface-type deposits A relationship is represented by line of best fit, following y = 0.9617x, with an R^2 value of 0.8134.

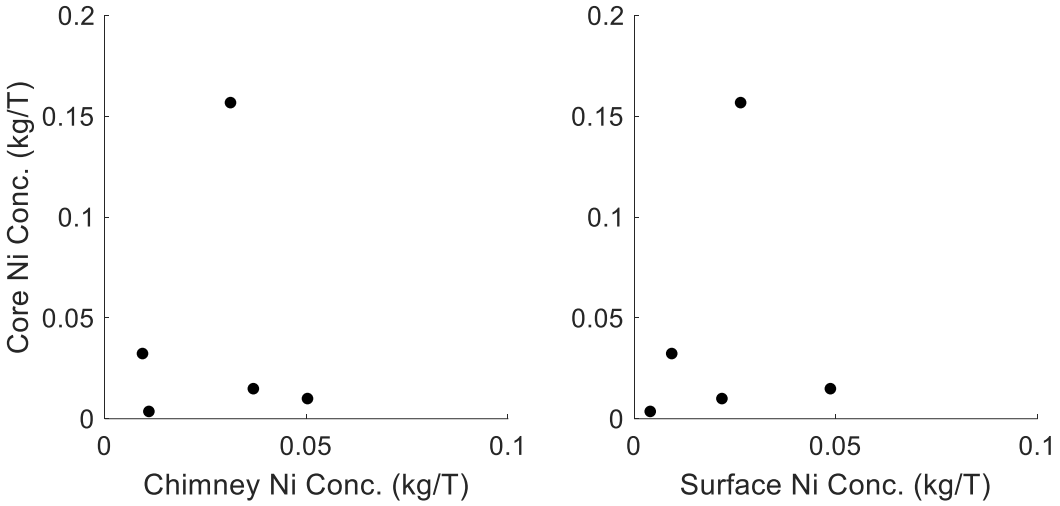

Figure S46: *(left) Distribution of concentration of nickel in core and chimney-type deposits. A weak positive relationship is noted.*

(right) Distribution of concentration of nickel in core and surface-type deposits A weak positive relationship is noted.

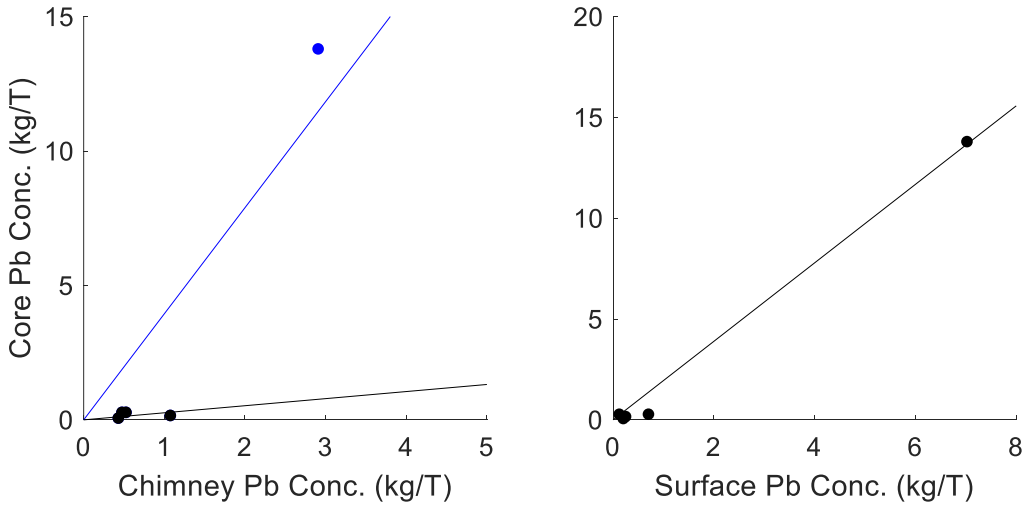

Figure S47*: (left) Distribution of concentration of lead in core and chimney-type deposits. Disregarding Endeavour (in blue), a relationship is represented by line of best fit, following y = 0.2633x, with an R^2 value of 0.679.*

(right) Distribution of concentration of lead in core and surface-type deposits A relationship is represented by line of best fit, following y = 1.9465x, with an R^2 value of 0.9926.

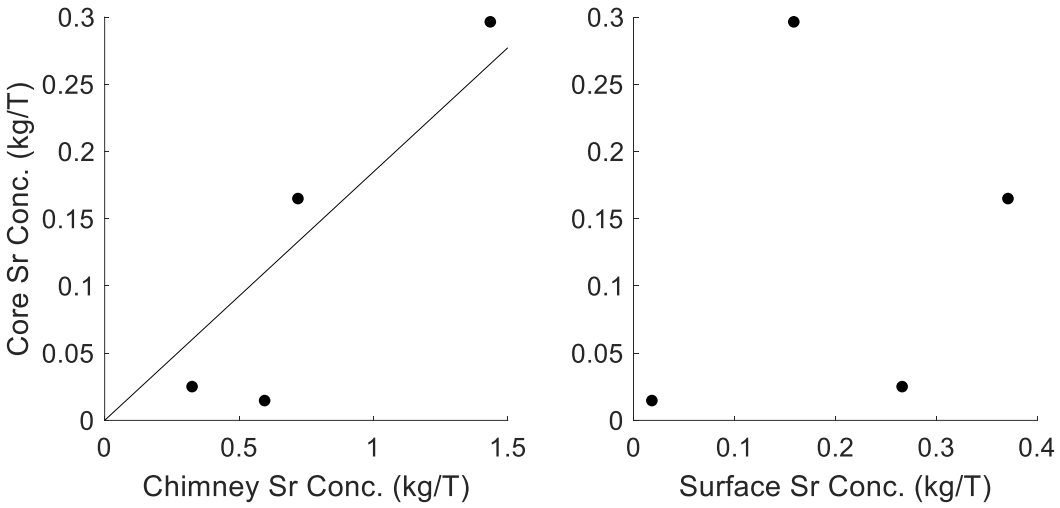

Figure S48: *(left) Distribution of concentration of strontium in core and chimney-type deposits. A relationship is represented by line of best fit, following y = 0.1848x, with an R^2 value of 0.8939.*

(right) Distribution of concentration of strontium in core and surface-type deposits. No relationship is observed.

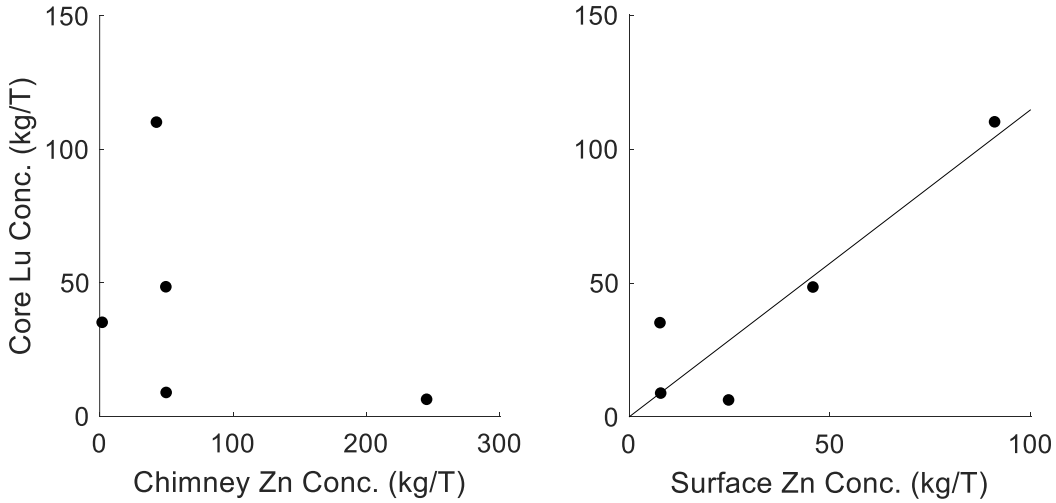

Figure S49: *(left) Distribution of concentration of zinc in core and chimney-type deposits. No relationship is observed.*

(right) Distribution of concentration of zinc in core and surface-type deposits. A relationship is represented by line of best fit, following y = 1.1472x, with an R^2 value of 0.9223.

***Table S20**: Inter-elemental correlation matrix of hydrothermal deposit concentrations excluding Rare Earth Elements. Red cells indicate a strong negative correlation blue cells, a strong positive correlation.*

	Au	Ag	As	B	Ba	Br	Ca	Cd	Ce	Cl	Co	Cs	Cu	Dy	Er	Eu	Fe	Gd	Hf	Hg
Au																				
Ag		0.11																		
As			0.08	-0.20	0.07	0.08	-0.08	-0.03		0.00	-0.03	-0.10	0.17				-0.15		-0.10	0.05
B			0.02	-0.15	0.24	0.01	-0.07	-0.02		0.03	-0.02	0.01	-0.05				-0.23		0.06	0.22
Ba				-0.32	0.06	0.01	-0.04	-0.01		0.04	-0.01	0.13	0.00				-0.10		0.08	0.10
Br					-0.24	0.54	-0.17	0.37		0.18	-0.18		-0.19				0.15		-0.11	-0.14
Ca						0.03	-0.09	-0.02		-0.32	-0.02	0.00	-0.09				-0.36		0.06	0.14
Cd							-0.10	-0.02		0.13	-0.05	0.07	-0.14				-0.14		0.06	-0.01
Ce								-0.04		-0.31	-0.03	0.02	-0.06				-0.37		-0.01	-0.13
Cl											0.31	0.69	0.07				0.35		0.76	-0.42
Co												0.00	0.02				0.09		0.06	-0.04
Cs													-0.03				0.06		0.22	-0.08
Cu																	0.01		-0.19	-0.05
Dy																				
Er																				
Eu																				
Fe																			0.11	-0.13
Gd																				
Hf																				0.02
Hg																				
Ho																				
La																				
Li																				
Lu																				
Mn																				
Mo																				
Nb																				
Nd																				
Ni																				
Pb																				
Pd																				
Pr																				
Rb																				
Sm																				
Sr																				
Ta																				
Tb																				
V																				
Y																				
Yb																				
Zn																				

Table S20: *(Continued)*

	Ho	La	Li	Lu	Mn	Mo	Nb	Nd	Ni	Pb	Pd	Pr	Rb	Sm	Sr	Ta	Tb	V	Y	Yb	Zn
Au			-0.20		-0.03	0.06	-0.09		-0.01	0.15			-0.16		-0.06	0.03		0.01			0.36
Ag			-0.14		-0.02	-0.05	-0.07		0.01	0.15			-0.12		0.22	-0.14		-0.01			0.24
As					-0.01	-0.01	-0.02		0.00	0.11			0.00		-0.02	-0.19		-0.01			0.07
B					0.68	-0.32	-0.77		-0.24	-0.16			-0.33		-0.16			0.41			-0.10
Ba			0.17		-0.02	-0.09	0.14		0.05	0.27			0.01		0.62	0.02		-0.01			0.17
Br					0.51	-0.25	0.62		-0.07	-0.01			-0.18		-0.14	0.02		0.28			0.07
Ca			0.03		-0.01	-0.11	0.10		0.01	-0.07			-0.10		0.35	0.04		-0.01			-0.16
Cd			-0.15		-0.01	-0.05	-0.09		0.01	-0.01			0.19		0.15	-0.03		-0.05			-0.03
Ce																					
Cl					-0.30	0.06	-0.40		-0.29	0.20			0.03		-0.33			0.11			0.18
Co			0.11		-0.01	0.09	-0.17		0.00	-0.02			0.00		-0.04	-0.01		0.00			-0.04
Cs			0.02		0.07	0.13	0.10		0.02	0.00			0.03		0.01	-0.04		-0.01			-0.02
Cu			0.03		-0.04	0.16	-0.15		-0.04	-0.04			0.15		-0.09	0.12		0.07			-0.12
Dy																					
Er																					
Eu																					
Fe			-0.12		-0.14	0.08	-0.12		-0.03	-0.24			0.26		-0.41	-0.06		-0.04			-0.39
Gd																					
Hf					0.03	-0.07	0.36		0.14	0.05			0.46		0.08	-0.07		0.04			0.03
Hg					-0.08	-0.11	-0.13		0.00	0.08			0.05		-0.03	0.00		0.09			0.15
Ho																					
La																					
Li					-0.04	0.26	0.88		0.09	-0.06			0.63		0.04			0.65			-0.13
Lu																					
Mn						0.35	0.72		0.31	-0.01			-0.17		-0.01	0.00		0.11			-0.04
Mo							-0.20		-0.02	-0.07			0.09		-0.09	0.00		0.12			-0.13
Nb									0.09	0.35			0.15		0.17	0.00		0.15			-0.14
Nd																					
Ni										0.12			0.36		0.04	-0.02		0.11			0.13
Pb													0.10		-0.01	-0.02		0.02			0.33
Pd																					
Pr																					
Rb															0.03	-0.06		-0.06			-0.05
Sm																					
Sr																-0.03		-0.06			-0.11
Ta																		0.06			-0.01
Tb																					
V																					0.16
Y																					
Yb																					
Zn																					

***Table S21**: Inter-elemental correlation matrix of deposit concentrations exclusively including Rare Earth Elements. Red cells indicate a strong negative correlation: blue cells, a strong positive correlation.*

	Au	Ag	As	B	Ba	Br	Ca	Cd	Ce	Cl	Co	Cs	Cu	Dy	Er	Eu	Fe	Gd	Hf	Hg
Au									-0.08					-0.02	-0.04	0.02		0.01		
Ag									-0.04					0.03	0.02	0.01		0.05		
As									-0.05					-0.03	-0.01	-0.05		-0.06		
B																				
Ba					-0.01									-0.14	-0.13	-0.02		-0.14		
Br						0.54								0.13	0.09	0.55		0.17		
Ca									0.00					0.26	0.25	-0.07		0.29		
Cd									-0.11					-0.09	-0.06	-0.06		-0.11		
Ce										0.00	-0.01	0.08	-0.21	0.96	0.96	0.14	-0.11	0.97	0.25	-0.03
Cl																				
Co														-0.26	-0.26	-0.04		-0.26		
Cs														0.28	0.28	0.09		0.28		
Cu														-0.23	-0.23	-0.11		-0.23		
Dy															1.00	0.63	-0.29	1.00	0.99	-0.12
Er																0.61	-0.30	0.99	0.99	-0.09
Eu																	0.09	0.66	0.29	-0.01
Fe																		-0.31		
Gd																			0.99	-0.14
Hf																				
Hg																				
Ho																				
La																				
Li																				
Lu																				
Mn																				
Mo																				
Nb																				
Nd																				
Ni																				
Pb																				
Pd																				
Pr																				
Rb																				
Sm																				
Sr																				
Ta																				
Tb																				
V																				
Y																				
Yb																				
Zn																				

Table S21: *(Continued)*

	Ho	La	Li	Lu	Mn	Mo	Nb	Nd	Ni	Pb	Pd	Pr	Rb	Sm	Sr	Ta	Tb	V	Y	Yb	Zn
Au	-0.02	-0.08		0.02				-0.05				0.02		-0.14			-0.02		-0.11	-0.01	
Ag	0.03	-0.10		0.03				-0.01				0.03		-0.10			0.06		0.00	0.08	
As	-0.01	-0.09		0.07				-0.02				-0.09		-0.12			0.13		-0.04	-0.06	
B																			-0.10	0.36	
Ba	-0.13	0.01		-0.01				0.00				-0.05		-0.01			-0.01		0.13	0.00	
Br	0.10	0.50		0.11				0.52				0.34		0.53			0.18		0.14	0.12	
Ca	0.26	-0.10		0.11				-0.01				0.53		0.00			-0.03		0.04	0.03	
Cd	-0.06	-0.04		-0.03				-0.05				-0.13		-0.17			-0.02		0.09	0.00	
Ce	0.96	0.08		0.25	0.13	-0.07	0.45	0.99	0.07	-0.01		0.45	0.15	0.33	-0.04	-0.12	0.08	0.03	0.94	0.32	-0.07
Cl		0.00																	-0.15	-0.32	
Co	-0.27	-0.03		-0.01				0.01				-0.09		-0.06			-0.01		0.02	-0.05	
Cs	0.28	-0.03		0.29				0.05				0.01		0.23			-0.01		0.28	0.24	
Cu	-0.23	-0.16		-0.18				-0.20				-0.08		-0.25			-0.04		-0.13	0.12	
Dy	1.00	0.88		1.00	-0.12	-0.14	0.97	0.97	0.75	-0.18		0.39	0.93	0.99	-0.03	-0.44	0.35	0.60	1.00	1.00	-0.14
Er	1.00	0.87		1.00	-0.15	-0.13	0.97	0.96	0.75	-0.18		0.39	0.92	0.98	-0.03	-0.45	0.34	0.58	1.00	1.00	-0.14
Eu	0.61	0.07		0.34	0.56	-0.18	0.69	0.08	0.04	-0.02		0.24	0.10	0.53	-0.09	0.01	0.12	0.40	0.36	0.33	-0.12
Fe	-0.30	0.14		-0.13				-0.17				-0.39		0.03			-0.01		-0.15	-0.11	
Gd	1.00	0.89		0.99	-0.09	-0.16	0.97	0.98	0.73	-0.19		0.40	0.93	0.99	-0.03	-0.43	0.35	0.64	1.00	0.99	-0.15
Hf	0.99	0.15		0.86				0.23				0.39		0.73			0.29		0.90	0.78	
Hg	-0.09	0.37		-0.05				-0.04				-0.18		0.04			-0.06		-0.05	0.06	
Ho		0.88		1.00	-0.15	-0.13	0.97	0.96	0.74	-0.17		0.39	0.93	0.98	-0.03	-0.44	0.35	0.59	1.00	1.00	-0.13
La				0.10	-0.05	-0.24	0.26	0.99	0.09	-0.05		0.43	0.35	0.35	-0.04	-0.04	-0.02	-0.13	0.42	0.17	-0.10
Li																			0.81		
Lu					0.03	-0.09	0.26	0.17	0.12	-0.02		0.41	0.06	0.92	-0.02	-0.31	0.34	0.33	0.98	0.94	-0.08
Mn								0.10				-0.08		0.21			0.10		0.04	0.14	
Mo								-0.02				-0.24		-0.30			-0.02		-0.02	-0.17	
Nb								0.37				0.48		0.44			0.10		0.37	0.25	
Nd									0.06	0.07		0.42	0.16	0.28	-0.02	-0.10	0.06	0.16	0.90	0.24	-0.03
Ni												0.00		0.15			0.04		0.13	0.12	
Pb												-0.07		-0.06			-0.01		0.01	0.21	
Pd																					
Pr													0.41	0.40	0.00	-0.09	0.01	0.66	0.39	0.40	-0.04
Rb														0.16			0.00		0.29	0.23	
Sm															-0.05	-0.14	0.29	0.13	0.91	0.84	-0.19
Sr																	0.00		0.09	0.03	
Ta																	-0.03		-0.07	-0.26	
Tb																		0.09	0.34	0.28	-0.03
V																			0.24	0.01	
Y																				0.69	0.05
Yb																					-0.06
Zn																					

CODE FOR 3D META ANALYSIS PLOTS

```
clc;close all;clear all;
%% load pH
pHbascA =
xlsread('Analysis3d.xlsx','bar','O5:O10');
pHbascB =
xlsread('Analysis3d.xlsx','bar','O12:O16');
pHbascC =
xlsread('Analysis3d.xlsx','bar','O18:O23');
pHbascD =
xlsread('Analysis3d.xlsx','bar','O25:O30');
pHmsedA =
xlsread('Analysis3d.xlsx','bar','O32:O39');
pHmsedD =
xlsread('Analysis3d.xlsx','bar','O41');
pHmorbA =
xlsread('Analysis3d.xlsx','bar','O43:O46');
pHmorbB =
xlsread('Analysis3d.xlsx','bar','O48:O52');
pHmorbC =
xlsread('Analysis3d.xlsx','bar','O54:O65');
pHmorbD =
xlsread('Analysis3d.xlsx','bar','O67:O69');
pHnemorbA =
xlsread('Analysis3d.xlsx','bar','O71:O72');
pHnemorbC =
xlsread('Analysis3d.xlsx','bar','O74:O76');
pHnemorbD =
xlsread('Analysis3d.xlsx','bar','O78:O84');
pHemorbA =
xlsread('Analysis3d.xlsx','bar','O86:O87');
pHemorbB =
xlsread('Analysis3d.xlsx','bar','O89');
```

```
pHemorbC =
xlsread('Analysis3d.xlsx','bar','O91:O94');
pHemorbD =
xlsread('Analysis3d.xlsx','bar','O96:O100');
pHumafA =
xlsread('Analysis3d.xlsx','bar','O102:O106');
pHumafB =
xlsread('Analysis3d.xlsx','bar','O108:O110');
pHumafC =
xlsread('Analysis3d.xlsx','bar','O112:O122');
pHumafD =
xlsread('Analysis3d.xlsx','bar','O124:O134');
%% load temp
TbascA =
xlsread('Analysis3d.xlsx','bar','P5:P10');
TbascB =
xlsread('Analysis3d.xlsx','bar','P12:P16');
TbascC =
xlsread('Analysis3d.xlsx','bar','P18:P23');
TbascD =
xlsread('Analysis3d.xlsx','bar','P25:P30');
TmsedA =
xlsread('Analysis3d.xlsx','bar','P32:P39');
TmsedD =
xlsread('Analysis3d.xlsx','bar','P41');
TmorbA =
xlsread('Analysis3d.xlsx','bar','P43:P46');
TmorbB =
xlsread('Analysis3d.xlsx','bar','P48:P52');
TmorbC =
xlsread('Analysis3d.xlsx','bar','P54:P65');
TmorbD =
xlsread('Analysis3d.xlsx','bar','P67:P69');
```

```
TnemorbA =
xlsread('Analysis3d.xlsx','bar','P71:P72');
TnemorbC =
xlsread('Analysis3d.xlsx','bar','P74:P76');
TnemorbD =
xlsread('Analysis3d.xlsx','bar','P78:P84');
TemorbA =
xlsread('Analysis3d.xlsx','bar','P86:P87');
TemorbB =
xlsread('Analysis3d.xlsx','bar','P89');
TemorbC =
xlsread('Analysis3d.xlsx','bar','P91:P94');
TemorbD =
xlsread('Analysis3d.xlsx','bar','P96:P100');
TumafA =
xlsread('Analysis3d.xlsx','bar','P102:P106');
TumafB =
xlsread('Analysis3d.xlsx','bar','P108:P110');
TumafC =
xlsread('Analysis3d.xlsx','bar','P112:P122');
TumafD =
xlsread('Analysis3d.xlsx','bar','P124:P134');
%% load Ca
CabascA =
xlsread('Analysis3d.xlsx','bar','AL5:AL10');
CabascB =
xlsread('Analysis3d.xlsx','bar','AL12:AL16');
CabascC =
xlsread('Analysis3d.xlsx','bar','AL18:AL23');
CabascD =
xlsread('Analysis3d.xlsx','bar','AL25:AL30');
CamsedA =
xlsread('Analysis3d.xlsx','bar','AL32:AL39');
```

```
CamsedD =
xlsread('Analysis3d.xlsx','bar','AL41');
CamorbA =
xlsread('Analysis3d.xlsx','bar','AL43:AL46');
CamorbB =
xlsread('Analysis3d.xlsx','bar','AL48:AL52');
CamorbC =
xlsread('Analysis3d.xlsx','bar','AL54:AL65');
CamorbD =
xlsread('Analysis3d.xlsx','bar','AL67:AL69');
CanemorbA =
xlsread('Analysis3d.xlsx','bar','AL71:AL72');
CanemorbC =
xlsread('Analysis3d.xlsx','bar','AL74:AL76');
CanemorbD =
xlsread('Analysis3d.xlsx','bar','AL78:AL84');
CaemorbA =
xlsread('Analysis3d.xlsx','bar','AL86:AL87');
CaemorbB =
xlsread('Analysis3d.xlsx','bar','AL89');
CaemorbC =
xlsread('Analysis3d.xlsx','bar','AL91:AL94');
CaemorbD =
xlsread('Analysis3d.xlsx','bar','AL96:AL100')
;
CaumafA =
xlsread('Analysis3d.xlsx','bar','AL102:AL106'
);
CaumafB =
xlsread('Analysis3d.xlsx','bar','AL108:AL110'
);
```

```
CaumafC =
xlsread('Analysis3d.xlsx','bar','AL112:AL122'
);
CaumafD =
xlsread('Analysis3d.xlsx','bar','AL124:AL134'
);
%% load Fe
FebascA =
xlsread('Analysis3d.xlsx','bar','T5:T10');
FebascB =
xlsread('Analysis3d.xlsx','bar','T12:T16');
FebascC =
xlsread('Analysis3d.xlsx','bar','T18:T23');
FebascD =
xlsread('Analysis3d.xlsx','bar','T25:T30');
FemsedA =
xlsread('Analysis3d.xlsx','bar','T32:T39');
FemsedD =
xlsread('Analysis3d.xlsx','bar','T41');
FemorbA =
xlsread('Analysis3d.xlsx','bar','T43:T46');
FemorbB =
xlsread('Analysis3d.xlsx','bar','T48:T52');
FemorbC =
xlsread('Analysis3d.xlsx','bar','T54:T65');
FemorbD =
xlsread('Analysis3d.xlsx','bar','T67:T69');
FenemorbA =
xlsread('Analysis3d.xlsx','bar','T71:T72');
FenemorbC =
xlsread('Analysis3d.xlsx','bar','T74:T76');
FenemorbD =
xlsread('Analysis3d.xlsx','bar','T78:T84');
```

```
FeemorbA =
xlsread('Analysis3d.xlsx','bar','T86:T87');
FeemorbB =
xlsread('Analysis3d.xlsx','bar','T89');
FeemorbC =
xlsread('Analysis3d.xlsx','bar','T91:T94');
FeemorbD =
xlsread('Analysis3d.xlsx','bar','T96:T100');
FeumafA =
xlsread('Analysis3d.xlsx','bar','T102:T106');
FeumafB =
xlsread('Analysis3d.xlsx','bar','T108:T110');
FeumafC =
xlsread('Analysis3d.xlsx','bar','T112:T122');
FeumafD =
xlsread('Analysis3d.xlsx','bar','T124:T134');
%% load Mn
MnbascA =
xlsread('Analysis3d.xlsx','bar','S5:S10');
MnbascB =
xlsread('Analysis3d.xlsx','bar','S12:S16');
MnbascC =
xlsread('Analysis3d.xlsx','bar','S18:S23');
MnbascD =
xlsread('Analysis3d.xlsx','bar','S25:S30');
MnmsedA =
xlsread('Analysis3d.xlsx','bar','S32:S39');
MnmsedD =
xlsread('Analysis3d.xlsx','bar','S41');
MnmorbA =
xlsread('Analysis3d.xlsx','bar','S43:S46');
MnmorbB =
xlsread('Analysis3d.xlsx','bar','S48:S52');
```

```
MnmorbC =
xlsread('Analysis3d.xlsx','bar','S54:S65');
MnmorbD =
xlsread('Analysis3d.xlsx','bar','S67:S69');
MnnemorbA =
xlsread('Analysis3d.xlsx','bar','S71:S72');
MnnemorbC =
xlsread('Analysis3d.xlsx','bar','S74:S76');
MnnemorbD =
xlsread('Analysis3d.xlsx','bar','S78:S84');
MnemorbA =
xlsread('Analysis3d.xlsx','bar','S86:S87');
MnemorbB =
xlsread('Analysis3d.xlsx','bar','S89');
MnemorbC =
xlsread('Analysis3d.xlsx','bar','S91:S94');
MnemorbD =
xlsread('Analysis3d.xlsx','bar','S96:S100');
MnumafA =
xlsread('Analysis3d.xlsx','bar','S102:S106');
MnumafB =
xlsread('Analysis3d.xlsx','bar','S108:S110');
MnumafC =
xlsread('Analysis3d.xlsx','bar','S112:S122');
MnumafD =
xlsread('Analysis3d.xlsx','bar','S124:S134');
%% load Li
LibascA =
xlsread('Analysis3d.xlsx','bar','AI5:AI10');
LibascB =
xlsread('Analysis3d.xlsx','bar','AI12:AI16');
LibascC =
xlsread('Analysis3d.xlsx','bar','AI18:AI23');
```

```
LibascD =
xlsread('Analysis3d.xlsx','bar','AI25:AI30');
LimsedA =
xlsread('Analysis3d.xlsx','bar','AI32:AI39');
LimsedD =
xlsread('Analysis3d.xlsx','bar','AI41');
LimorbA =
xlsread('Analysis3d.xlsx','bar','AI43:AI46');
LimorbB =
xlsread('Analysis3d.xlsx','bar','AI48:AI52');
LimorbC =
xlsread('Analysis3d.xlsx','bar','AI54:AI65');
LimorbD =
xlsread('Analysis3d.xlsx','bar','AI67:AI69');
LinemorbA =
xlsread('Analysis3d.xlsx','bar','AI71:AI72');
LinemorbC =
xlsread('Analysis3d.xlsx','bar','AI74:AI76');
LinemorbD =
xlsread('Analysis3d.xlsx','bar','AI78:AI84');
LiemorbA =
xlsread('Analysis3d.xlsx','bar','AI86:AI87');
LiemorbB =
xlsread('Analysis3d.xlsx','bar','AI89');
LiemorbC =
xlsread('Analysis3d.xlsx','bar','AI91:AI94');
LiemorbD =
xlsread('Analysis3d.xlsx','bar','AI96:AI100')
;
LiumafA =
xlsread('Analysis3d.xlsx','bar','AI102:AI106'
);
```

```
LiumafB =
xlsread('Analysis3d.xlsx','bar','AI108:AI110'
);
LiumafC =
xlsread('Analysis3d.xlsx','bar','AI112:AI122'
);
LiumafD =
xlsread('Analysis3d.xlsx','bar','AI124:AI134'
);
%% load Sr
SrbascA =
xlsread('Analysis3d.xlsx','bar','AP5:AP10');
SrbascB =
xlsread('Analysis3d.xlsx','bar','AP12:AP16');
SrbascC =
xlsread('Analysis3d.xlsx','bar','AP18:AP23');
SrbascD =
xlsread('Analysis3d.xlsx','bar','AP25:AP30');
SrmsedA =
xlsread('Analysis3d.xlsx','bar','AP32:AP39');
SrmsedD =
xlsread('Analysis3d.xlsx','bar','AP41');
SrmorbA =
xlsread('Analysis3d.xlsx','bar','AP43:AP46');
SrmorbB =
xlsread('Analysis3d.xlsx','bar','AP48:AP52');
SrmorbC =
xlsread('Analysis3d.xlsx','bar','AP54:AP65');
SrmorbD =
xlsread('Analysis3d.xlsx','bar','AP67:AP69');
SrnemorbA =
xlsread('Analysis3d.xlsx','bar','AP71:AP72');
```

```
SrnemorbC =
xlsread('Analysis3d.xlsx','bar','AP74:AP76');
SrnemorbD =
xlsread('Analysis3d.xlsx','bar','AP78:AP84');
SremorbA =
xlsread('Analysis3d.xlsx','bar','AP86:AP87');
SremorbB =
xlsread('Analysis3d.xlsx','bar','AP89');
SremorbC =
xlsread('Analysis3d.xlsx','bar','AP91:AP94');
SremorbD =
xlsread('Analysis3d.xlsx','bar','AP96:AP100')
;
SrumafA =
xlsread('Analysis3d.xlsx','bar','AP102:AP106'
);
SrumafB =
xlsread('Analysis3d.xlsx','bar','AP108:AP110'
);
SrumafC =
xlsread('Analysis3d.xlsx','bar','AP112:AP122'
);
SrumafD =
xlsread('Analysis3d.xlsx','bar','AP124:AP134'
);
%% load Cu
CubascA =
xlsread('Analysis3d.xlsx','bar','AA5:AA10');
CubascB =
xlsread('Analysis3d.xlsx','bar','AA12:AA16');
CubascC =
xlsread('Analysis3d.xlsx','bar','AA18:AA23');
```

```
CubascD =
xlsread('Analysis3d.xlsx','bar','AA25:AA30');
CumsedA =
xlsread('Analysis3d.xlsx','bar','AA32:AA39');
CumsedD =
xlsread('Analysis3d.xlsx','bar','AA41');
CumorbA =
xlsread('Analysis3d.xlsx','bar','AA43:AA46');
CumorbB =
xlsread('Analysis3d.xlsx','bar','AA48:AA52');
CumorbC =
xlsread('Analysis3d.xlsx','bar','AA54:AA65');
CumorbD =
xlsread('Analysis3d.xlsx','bar','AA67:AA69');
CunemorbA =
xlsread('Analysis3d.xlsx','bar','AA71:AA72');
CunemorbC =
xlsread('Analysis3d.xlsx','bar','AA74:AA76');
CunemorbD =
xlsread('Analysis3d.xlsx','bar','AA78:AA84');
CuemorbA =
xlsread('Analysis3d.xlsx','bar','AA86:AA87');
CuemorbB =
xlsread('Analysis3d.xlsx','bar','AA89');
CuemorbC =
xlsread('Analysis3d.xlsx','bar','AA91:AA94');
CuemorbD =
xlsread('Analysis3d.xlsx','bar','AA96:AA100')
;
CuumafA =
xlsread('Analysis3d.xlsx','bar','AA102:AA106'
);
```

```
CuumafB =
xlsread('Analysis3d.xlsx','bar','AA108:AA110'
);
CuumafC =
xlsread('Analysis3d.xlsx','bar','AA112:AA122'
);
CuumafD =
xlsread('Analysis3d.xlsx','bar','AA124:AA134'
);
%% load Zn
ZnbascA =
xlsread('Analysis3d.xlsx','bar','AB5:AB10');
ZnbascB =
xlsread('Analysis3d.xlsx','bar','AB12:AB16');
ZnbascC =
xlsread('Analysis3d.xlsx','bar','AB18:AB23');
ZnbascD =
xlsread('Analysis3d.xlsx','bar','AB25:AB30');
ZnmsedA =
xlsread('Analysis3d.xlsx','bar','AB32:AB39');
ZnmsedD =
xlsread('Analysis3d.xlsx','bar','AB41');
ZnmorbA =
xlsread('Analysis3d.xlsx','bar','AB43:AB46');
ZnmorbB =
xlsread('Analysis3d.xlsx','bar','AB48:AB52');
ZnmorbC =
xlsread('Analysis3d.xlsx','bar','AB54:AB65');
ZnmorbD =
xlsread('Analysis3d.xlsx','bar','AB67:AB69');
ZnnemorbA =
xlsread('Analysis3d.xlsx','bar','AB71:AB72');
```

```
ZnnemorbC =
xlsread('Analysis3d.xlsx','bar','AB74:AB76');
ZnnemorbD =
xlsread('Analysis3d.xlsx','bar','AB78:AB84');
ZnemorbA =
xlsread('Analysis3d.xlsx','bar','AB86:AB87');
ZnemorbB =
xlsread('Analysis3d.xlsx','bar','AB89');
ZnemorbC =
xlsread('Analysis3d.xlsx','bar','AB91:AB94');
ZnemorbD =
xlsread('Analysis3d.xlsx','bar','AB96:AB100')
;
ZnumafA =
xlsread('Analysis3d.xlsx','bar','AB102:AB106'
);
ZnumafB =
xlsread('Analysis3d.xlsx','bar','AB108:AB110'
);
ZnumafC =
xlsread('Analysis3d.xlsx','bar','AB112:AB122'
);
ZnumafD =
xlsread('Analysis3d.xlsx','bar','AB124:AB134'
);
%% load Cl
ClbascA =
xlsread('Analysis3d.xlsx','bar','AK5:AK10');
ClbascB =
xlsread('Analysis3d.xlsx','bar','AK12:AK16');
ClbascC =
xlsread('Analysis3d.xlsx','bar','AK18:AK23');
```

```
ClbascD =
xlsread('Analysis3d.xlsx','bar','AK25:AK30');
ClmsedA =
xlsread('Analysis3d.xlsx','bar','AK32:AK39');
ClmsedD =
xlsread('Analysis3d.xlsx','bar','AK41');
ClmorbA =
xlsread('Analysis3d.xlsx','bar','AK43:AK46');
ClmorbB =
xlsread('Analysis3d.xlsx','bar','AK48:AK52');
ClmorbC =
xlsread('Analysis3d.xlsx','bar','AK54:AK65');
ClmorbD =
xlsread('Analysis3d.xlsx','bar','AK67:AK69');
ClnemorbA =
xlsread('Analysis3d.xlsx','bar','AK71:AK72');
ClnemorbC =
xlsread('Analysis3d.xlsx','bar','AK74:AK76');
ClnemorbD =
xlsread('Analysis3d.xlsx','bar','AK78:AK84');
ClemorbA =
xlsread('Analysis3d.xlsx','bar','AK86:AK87');
ClemorbB =
xlsread('Analysis3d.xlsx','bar','AK89');
ClemorbC =
xlsread('Analysis3d.xlsx','bar','AK91:AK94');
ClemorbD =
xlsread('Analysis3d.xlsx','bar','AK96:AK100')
;
ClumafA =
xlsread('Analysis3d.xlsx','bar','AK102:AK106'
);
```

```
ClumafB =
xlsread('Analysis3d.xlsx','bar','AK108:AK110'
);
ClumafC =
xlsread('Analysis3d.xlsx','bar','AK112:AK122'
);
ClumafD =
xlsread('Analysis3d.xlsx','bar','AK124:AK134'
);
%% load Br
BrbascA =
xlsread('Analysis3d.xlsx','bar','AN5:AN10');
BrbascB =
xlsread('Analysis3d.xlsx','bar','AN12:AN16');
BrbascC =
xlsread('Analysis3d.xlsx','bar','AN18:AN23');
BrbascD =
xlsread('Analysis3d.xlsx','bar','AN25:AN30');
BrmsedA =
xlsread('Analysis3d.xlsx','bar','AN32:AN39');
BrmsedD =
xlsread('Analysis3d.xlsx','bar','AN41');
BrmorbA =
xlsread('Analysis3d.xlsx','bar','AN43:AN46');
BrmorbB =
xlsread('Analysis3d.xlsx','bar','AN48:AN52');
BrmorbC =
xlsread('Analysis3d.xlsx','bar','AN54:AN65');
BrmorbD =
xlsread('Analysis3d.xlsx','bar','AN67:AN69');
BrnemorbA =
xlsread('Analysis3d.xlsx','bar','AN71:AN72');
```

```
BrnemorbC =
xlsread('Analysis3d.xlsx','bar','AN74:AN76');
BrnemorbD =
xlsread('Analysis3d.xlsx','bar','AN78:AN84');
BremorbA =
xlsread('Analysis3d.xlsx','bar','AN86:AN87');
BremorbB =
xlsread('Analysis3d.xlsx','bar','AN89');
BremorbC =
xlsread('Analysis3d.xlsx','bar','AN91:AN94');
BremorbD =
xlsread('Analysis3d.xlsx','bar','AN96:AN100')
;
BrumafA =
xlsread('Analysis3d.xlsx','bar','AN102:AN106'
);
BrumafB =
xlsread('Analysis3d.xlsx','bar','AN108:AN110'
);
BrumafC =
xlsread('Analysis3d.xlsx','bar','AN112:AN122'
);
BrumafD =
xlsread('Analysis3d.xlsx','bar','AN124:AN134'
);
%% load Rb
RbbascA =
xlsread('Analysis3d.xlsx','bar','AO5:AO10');
RbbascB =
xlsread('Analysis3d.xlsx','bar','AO12:AO16');
RbbascC =
xlsread('Analysis3d.xlsx','bar','AO18:AO23');
```

```
RbbascD =
xlsread('Analysis3d.xlsx','bar','AO25:AO30');
RbmsedA =
xlsread('Analysis3d.xlsx','bar','AO32:AO39');
RbmsedD =
xlsread('Analysis3d.xlsx','bar','AO41');
RbmorbA =
xlsread('Analysis3d.xlsx','bar','AO43:AO46');
RbmorbB =
xlsread('Analysis3d.xlsx','bar','AO48:AO52');
RbmorbC =
xlsread('Analysis3d.xlsx','bar','AO54:AO65');
RbmorbD =
xlsread('Analysis3d.xlsx','bar','AO67:AO69');
RbnemorbA =
xlsread('Analysis3d.xlsx','bar','AO71:AO72');
RbnemorbC =
xlsread('Analysis3d.xlsx','bar','AO74:AO76');
RbnemorbD =
xlsread('Analysis3d.xlsx','bar','AO78:AO84');
RbemorbA =
xlsread('Analysis3d.xlsx','bar','AO86:AO87');
RbemorbB =
xlsread('Analysis3d.xlsx','bar','AO89');
RbemorbC =
xlsread('Analysis3d.xlsx','bar','AO91:AO94');
RbemorbD =
xlsread('Analysis3d.xlsx','bar','AO96:AO100')
;
RbumafA =
xlsread('Analysis3d.xlsx','bar','AO102:AO106'
);
```

```
RbumafB =
xlsread('Analysis3d.xlsx','bar','AO108:AO110'
);
RbumafC =
xlsread('Analysis3d.xlsx','bar','AO112:AO122'
);
RbumafD =
xlsread('Analysis3d.xlsx','bar','AO124:AO134'
);
%% load B
BbascA =
xlsread('Analysis3d.xlsx','bar','AJ5:AJ10');
BbascB =
xlsread('Analysis3d.xlsx','bar','AJ12:AJ16');
BbascC =
xlsread('Analysis3d.xlsx','bar','AJ18:AJ23');
BbascD =
xlsread('Analysis3d.xlsx','bar','AJ25:AJ30');
BmsedA =
xlsread('Analysis3d.xlsx','bar','AJ32:AJ39');
BmsedD =
xlsread('Analysis3d.xlsx','bar','AJ41');
BmorbA =
xlsread('Analysis3d.xlsx','bar','AJ43:AJ46');
BmorbB =
xlsread('Analysis3d.xlsx','bar','AJ48:AJ52');
BmorbC =
xlsread('Analysis3d.xlsx','bar','AJ54:AJ65');
BmorbD =
xlsread('Analysis3d.xlsx','bar','AJ67:AJ69');
BnemorbA =
xlsread('Analysis3d.xlsx','bar','AJ71:AJ72');
```

```
BnemorbC =
xlsread('Analysis3d.xlsx','bar','AJ74:AJ76');
BnemorbD =
xlsread('Analysis3d.xlsx','bar','AJ78:AJ84');
BemorbA =
xlsread('Analysis3d.xlsx','bar','AJ86:AJ87');
BemorbB =
xlsread('Analysis3d.xlsx','bar','AJ89');
BemorbC =
xlsread('Analysis3d.xlsx','bar','AJ91:AJ94');
BemorbD =
xlsread('Analysis3d.xlsx','bar','AJ96:AJ100')
;
BumafA =
xlsread('Analysis3d.xlsx','bar','AJ102:AJ106'
);
BumafB =
xlsread('Analysis3d.xlsx','bar','AJ108:AJ110'
);
BumafC =
xlsread('Analysis3d.xlsx','bar','AJ112:AJ122'
);
BumafD =
xlsread('Analysis3d.xlsx','bar','AJ124:AJ134'
);
%% load Ba
BabascA =
xlsread('Analysis3d.xlsx','bar','AT5:AT10');
BabascB =
xlsread('Analysis3d.xlsx','bar','AT12:AT16');
BabascC =
xlsread('Analysis3d.xlsx','bar','AT18:AT23');
```

```
BabascD =
xlsread('Analysis3d.xlsx','bar','AT25:AT30');
BamsedA =
xlsread('Analysis3d.xlsx','bar','AT32:AT39');
BamsedD =
xlsread('Analysis3d.xlsx','bar','AT41');
BamorbA =
xlsread('Analysis3d.xlsx','bar','AT43:AT46');
BamorbB =
xlsread('Analysis3d.xlsx','bar','AT48:AT52');
BamorbC =
xlsread('Analysis3d.xlsx','bar','AT54:AT65');
BamorbD =
xlsread('Analysis3d.xlsx','bar','AT67:AT69');
BanemorbA =
xlsread('Analysis3d.xlsx','bar','AT71:AT72');
BanemorbC =
xlsread('Analysis3d.xlsx','bar','AT74:AT76');
BanemorbD =
xlsread('Analysis3d.xlsx','bar','AT78:AT84');
BaemorbA =
xlsread('Analysis3d.xlsx','bar','AT86:AT87');
BaemorbB =
xlsread('Analysis3d.xlsx','bar','AT89');
BaemorbC =
xlsread('Analysis3d.xlsx','bar','AT91:AT94');
BaemorbD =
xlsread('Analysis3d.xlsx','bar','AT96:AT100')
;
BaumafA =
xlsread('Analysis3d.xlsx','bar','AT102:AT106'
);
```

```
BaumafB =
xlsread('Analysis3d.xlsx','bar','AT108:AT110'
);
BaumafC =
xlsread('Analysis3d.xlsx','bar','AT112:AT122'
);
BaumafD =
xlsread('Analysis3d.xlsx','bar','AT124:AT134'
);
%% load Cs
CsbascA =
xlsread('Analysis3d.xlsx','bar','AS5:AS10');
CsbascB =
xlsread('Analysis3d.xlsx','bar','AS12:AS16');
CsbascC =
xlsread('Analysis3d.xlsx','bar','AS18:AS23');
CsbascD =
xlsread('Analysis3d.xlsx','bar','AS25:AS30');
CsmsedA =
xlsread('Analysis3d.xlsx','bar','AS32:AS39');
CsmsedD =
xlsread('Analysis3d.xlsx','bar','AS41');
CsmorbA =
xlsread('Analysis3d.xlsx','bar','AS43:AS46');
CsmorbB =
xlsread('Analysis3d.xlsx','bar','AS48:AS52');
CsmorbC =
xlsread('Analysis3d.xlsx','bar','AS54:AS65');
CsmorbD =
xlsread('Analysis3d.xlsx','bar','AS67:AS69');
CsnemorbA =
xlsread('Analysis3d.xlsx','bar','AS71:AS72');
```

```
CsnemorbC =
xlsread('Analysis3d.xlsx','bar','AS74:AS76');
CsnemorbD =
xlsread('Analysis3d.xlsx','bar','AS78:AS84');
CsemorbA =
xlsread('Analysis3d.xlsx','bar','AS86:AS87');
CsemorbB =
xlsread('Analysis3d.xlsx','bar','AS89');
CsemorbC =
xlsread('Analysis3d.xlsx','bar','AS91:AS94');
CsemorbD =
xlsread('Analysis3d.xlsx','bar','AS96:AS100')
;
CsumafA =
xlsread('Analysis3d.xlsx','bar','AS102:AS106'
);
CsumafB =
xlsread('Analysis3d.xlsx','bar','AS108:AS110'
);
CsumafC =
xlsread('Analysis3d.xlsx','bar','AS112:AS122'
);
CsumafD =
xlsread('Analysis3d.xlsx','bar','AS124:AS134'
);
%% load Cd
CdbascA =
xlsread('Analysis3d.xlsx','bar','AE5:AE10');
CdbascB =
xlsread('Analysis3d.xlsx','bar','AE12:AE16');
CdbascC =
xlsread('Analysis3d.xlsx','bar','AE18:AE23');
```

```
CdbascD =
xlsread('Analysis3d.xlsx','bar','AE25:AE30');
CdmsedA =
xlsread('Analysis3d.xlsx','bar','AE32:AE39');
CdmsedD =
xlsread('Analysis3d.xlsx','bar','AE41');
CdmorbA =
xlsread('Analysis3d.xlsx','bar','AE43:AE46');
CdmorbB =
xlsread('Analysis3d.xlsx','bar','AE48:AE52');
CdmorbC =
xlsread('Analysis3d.xlsx','bar','AE54:AE65');
CdmorbD =
xlsread('Analysis3d.xlsx','bar','AE67:AE69');
CdnemorbA =
xlsread('Analysis3d.xlsx','bar','AE71:AE72');
CdnemorbC =
xlsread('Analysis3d.xlsx','bar','AE74:AE76');
CdnemorbD =
xlsread('Analysis3d.xlsx','bar','AE78:AE84');
CdemorbA =
xlsread('Analysis3d.xlsx','bar','AE86:AE87');
CdemorbB =
xlsread('Analysis3d.xlsx','bar','AE89');
CdemorbC =
xlsread('Analysis3d.xlsx','bar','AE91:AE94');
CdemorbD =
xlsread('Analysis3d.xlsx','bar','AE96:AE100')
;
CdumafA =
xlsread('Analysis3d.xlsx','bar','AE102:AE106'
);
```

```
CdumafB =
xlsread('Analysis3d.xlsx','bar','AE108:AE110'
);
CdumafC =
xlsread('Analysis3d.xlsx','bar','AE112:AE122'
);
CdumafD =
xlsread('Analysis3d.xlsx','bar','AE124:AE134'
);
%% load Pb
PbbascA =
xlsread('Analysis3d.xlsx','bar','AG5:AG10');
PbbascB =
xlsread('Analysis3d.xlsx','bar','AG12:AG16');
PbbascC =
xlsread('Analysis3d.xlsx','bar','AG18:AG23');
PbbascD =
xlsread('Analysis3d.xlsx','bar','AG25:AG30');
PbmsedA =
xlsread('Analysis3d.xlsx','bar','AG32:AG39');
PbmsedD =
xlsread('Analysis3d.xlsx','bar','AG41');
PbmorbA =
xlsread('Analysis3d.xlsx','bar','AG43:AG46');
PbmorbB =
xlsread('Analysis3d.xlsx','bar','AG48:AG52');
PbmorbC =
xlsread('Analysis3d.xlsx','bar','AG54:AG65');
PbmorbD =
xlsread('Analysis3d.xlsx','bar','AG67:AG69');
PbnemorbA =
xlsread('Analysis3d.xlsx','bar','AG71:AG72');
```

```
PbnemorbC =
xlsread('Analysis3d.xlsx','bar','AG74:AG76');
PbnemorbD =
xlsread('Analysis3d.xlsx','bar','AG78:AG84');
PbemorbA =
xlsread('Analysis3d.xlsx','bar','AG86:AG87');
PbemorbB =
xlsread('Analysis3d.xlsx','bar','AG89');
PbemorbC =
xlsread('Analysis3d.xlsx','bar','AG91:AG94');
PbemorbD =
xlsread('Analysis3d.xlsx','bar','AG96:AG100')
;
PbumafA =
xlsread('Analysis3d.xlsx','bar','AG102:AG106'
);
PbumafB =
xlsread('Analysis3d.xlsx','bar','AG108:AG110'
);
PbumafC =
xlsread('Analysis3d.xlsx','bar','AG112:AG122'
);
PbumafD =
xlsread('Analysis3d.xlsx','bar','AG124:AG134'
);
%% load Co
CobascA =
xlsread('Analysis3d.xlsx','bar','U5:U10');
CobascB =
xlsread('Analysis3d.xlsx','bar','U12:U16');
CobascC =
xlsread('Analysis3d.xlsx','bar','U18:U23');
```

```
CobascD =
xlsread('Analysis3d.xlsx','bar','U25:U30');
ComsedA =
xlsread('Analysis3d.xlsx','bar','U32:U39');
ComsedD =
xlsread('Analysis3d.xlsx','bar','U41');
ComorbA =
xlsread('Analysis3d.xlsx','bar','U43:U46');
ComorbB =
xlsread('Analysis3d.xlsx','bar','U48:U52');
ComorbC =
xlsread('Analysis3d.xlsx','bar','U54:U65');
ComorbD =
xlsread('Analysis3d.xlsx','bar','U67:U69');
ConemorbA =
xlsread('Analysis3d.xlsx','bar','U71:U72');
ConemorbC =
xlsread('Analysis3d.xlsx','bar','U74:U76');
ConemorbD =
xlsread('Analysis3d.xlsx','bar','U78:U84');
CoemorbA =
xlsread('Analysis3d.xlsx','bar','U86:U87');
CoemorbB =
xlsread('Analysis3d.xlsx','bar','U89');
CoemorbC =
xlsread('Analysis3d.xlsx','bar','U91:U94');
CoemorbD =
xlsread('Analysis3d.xlsx','bar','U96:U100');
CoumafA =
xlsread('Analysis3d.xlsx','bar','U102:U106');
CoumafB =
xlsread('Analysis3d.xlsx','bar','U108:U110');
```

```
CoumafC =
xlsread('Analysis3d.xlsx','bar','U112:U122');
CoumafD =
xlsread('Analysis3d.xlsx','bar','U124:U134');
%% load REE
REEbascA =
xlsread('Analysis3d.xlsx','bar','AU5:AU10');
REEbascB =
xlsread('Analysis3d.xlsx','bar','AU12:AU16');
REEbascC =
xlsread('Analysis3d.xlsx','bar','AU18:AU23');
REEbascD =
xlsread('Analysis3d.xlsx','bar','AU25:AU30');
REEmsedA =
xlsread('Analysis3d.xlsx','bar','AU32:AU39');
REEmsedD =
xlsread('Analysis3d.xlsx','bar','AU41');
REEmorbA =
xlsread('Analysis3d.xlsx','bar','AU43:AU46');
REEmorbB =
xlsread('Analysis3d.xlsx','bar','AU48:AU52');
REEmorbC =
xlsread('Analysis3d.xlsx','bar','AU54:AU65');
REEmorbD =
xlsread('Analysis3d.xlsx','bar','AU67:AU69');
REEnemorbA =
xlsread('Analysis3d.xlsx','bar','AU71:AU72');
REEnemorbC =
xlsread('Analysis3d.xlsx','bar','AU74:AU76');
REEnemorbD =
xlsread('Analysis3d.xlsx','bar','AU78:AU84');
REEemorbA =
xlsread('Analysis3d.xlsx','bar','AU86:AU87');
```

```
REEemorbB =
xlsread('Analysis3d.xlsx','bar','AU89');
REEemorbC =
xlsread('Analysis3d.xlsx','bar','AU91:AU94');
REEemorbD =
xlsread('Analysis3d.xlsx','bar','AU96:AU100')
;
REEumafA =
xlsread('Analysis3d.xlsx','bar','AU102:AU106'
);
REEumafB =
xlsread('Analysis3d.xlsx','bar','AU108:AU110'
);
REEumafC =
xlsread('Analysis3d.xlsx','bar','AU112:AU122'
);
REEumafD =
xlsread('Analysis3d.xlsx','bar','AU124:AU134'
);
%% Change Marker/font Size
set(groot,'defaultLineMarkerSize',8);
%% plot Ca
figure;
scatter3(pHbascA,TbascA,CabascA,'ko');
hold on
scatter3(pHbascB,TbascB,CabascB,'k+');
scatter3(pHbascC,TbascC,CabascC,'kx');
scatter3(pHbascD,TbascD,CabascD,'k*');
scatter3(pHmsedA,TmsedA,CamsedA,'ro');
scatter3(pHmsedD,TmsedD,CamsedD,'r*');
scatter3(pHmorbA,TmorbA,CamorbA,'bo');
scatter3(pHmorbB,TmorbB,CamorbB,'b+');
scatter3(pHmorbC,TmorbC,CamorbC,'bx');
```

```
scatter3(pHmorbD,TmorbD,CamorbD,'b*');
scatter3(pHnemorbA,TnemorbA,CanemorbA,'co');
scatter3(pHnemorbC,TnemorbC,CanemorbC,'cx');
scatter3(pHnemorbD,TnemorbD,CanemorbD,'c*');
scatter3(pHemorbA,TemorbA,CaemorbA,'go');
scatter3(pHemorbB,TemorbB,CaemorbB,'g+');
scatter3(pHemorbC,TemorbC,CaemorbC,'gx');
scatter3(pHemorbD,TemorbD,CaemorbD,'g*');
scatter3(pHumafA,TumafA,CaumafA,'mo');
scatter3(pHumafB,TumafB,CaumafB,'m+');
scatter3(pHumafC,TumafC,CaumafC,'mx');
scatter3(pHumafD,TumafD,CaumafD,'m*');
hold off
set (gca,'Xdir','reverse'); xlim([2 8]);
zlim([0 inf]);
xlabel('Fluid pH'); ylabel('Fluid Temp,
°C');zlabel('Ca Concentration, g m^-^3');
%ph
figure;
scatter(pHbascA,CabascA,'ko');
hold on
scatter(pHbascB,CabascB,'k+');
scatter(pHbascC,CabascC,'kx');
scatter(pHbascD,CabascD,'k*');
scatter(pHmsedA,CamsedA,'ro');
scatter(pHmsedD,CamsedD,'r*');
scatter(pHmorbA,CamorbA,'bo');
scatter(pHmorbB,CamorbB,'b+');
scatter(pHmorbC,CamorbC,'bx');
scatter(pHmorbD,CamorbD,'b*');
scatter(pHnemorbA,CanemorbA,'co');
scatter(pHnemorbC,CanemorbC,'cx');
scatter(pHnemorbD,CanemorbD,'c*');
```

```
scatter(pHemorbA,CaemorbA,'go');
scatter(pHemorbB,CaemorbB,'g+');
scatter(pHemorbC,CaemorbC,'gx');
scatter(pHemorbD,CaemorbD,'g*');
scatter(pHumafA,CaumafA,'mo');
scatter(pHumafB,CaumafB,'m+');
scatter(pHumafC,CaumafC,'mx');
scatter(pHumafD,CaumafD,'m*');
hold off
set (gca,'Xdir','reverse'); xlim([2 8]);
ylim([0 inf]);
xlabel('Fluid pH'); ylabel('Ca Concentration,
g m^-^3');
%temp
figure;
scatter(TbascA,CabascA,'ko');
hold on
scatter(TbascB,CabascB,'k+');
scatter(TbascC,CabascC,'kx');
scatter(TbascD,CabascD,'k*');
scatter(TmsedA,CamsedA,'ro');
scatter(TmsedD,CamsedD,'r*');
scatter(TmorbA,CamorbA,'bo');
scatter(TmorbB,CamorbB,'b+');
scatter(TmorbC,CamorbC,'bx');
scatter(TmorbD,CamorbD,'b*');
scatter(TnemorbA,CanemorbA,'co');
scatter(TnemorbC,CanemorbC,'cx');
scatter(TnemorbD,CanemorbD,'c*');
scatter(TemorbA,CaemorbA,'go');
scatter(TemorbB,CaemorbB,'g+');
scatter(TemorbC,CaemorbC,'gx');
scatter(TemorbD,CaemorbD,'g*');
```

```
scatter(TumafA,CaumafA,'mo');
scatter(TumafB,CaumafB,'m+');
scatter(TumafC,CaumafC,'mx');
scatter(TumafD,CaumafD,'m*');
hold off
xlabel('Fluid Temp, °C'); ylabel('Ca
Concentration, g m^-^3');ylim([0 inf]);
%% plot Fe
figure;
scatter3(pHbascA,TbascA,FebascA,'ko');
hold on
scatter3(pHbascB,TbascB,FebascB,'k+');
scatter3(pHbascC,TbascC,FebascC,'kx');
scatter3(pHbascD,TbascD,FebascD,'k*');
scatter3(pHmsedA,TmsedA,FemsedA,'ro');
scatter3(pHmsedD,TmsedD,FemsedD,'r*');
scatter3(pHmorbA,TmorbA,FemorbA,'bo');
scatter3(pHmorbB,TmorbB,FemorbB,'b+');
scatter3(pHmorbC,TmorbC,FemorbC,'bx');
scatter3(pHmorbD,TmorbD,FemorbD,'b*');
scatter3(pHnemorbA,TnemorbA,FenemorbA,'co');
scatter3(pHnemorbC,TnemorbC,FenemorbC,'cx');
scatter3(pHnemorbD,TnemorbD,FenemorbD,'c*');
scatter3(pHemorbA,TemorbA,FeemorbA,'go');
scatter3(pHemorbB,TemorbB,FeemorbB,'g+');
scatter3(pHemorbC,TemorbC,FeemorbC,'gx');
scatter3(pHemorbD,TemorbD,FeemorbD,'g*');
scatter3(pHumafA,TumafA,FeumafA,'mo');
scatter3(pHumafB,TumafB,FeumafB,'m+');
scatter3(pHumafC,TumafC,FeumafC,'mx');
scatter3(pHumafD,TumafD,FeumafD,'m*');
hold off
```

```
set (gca,'Xdir','reverse'); xlim([2
8]),zlim([0 inf]);
xlabel('Fluid pH'); ylabel('Fluid Temp,
°C');zlabel('Fe Concentration, g m^-^3');
%ph
figure;
scatter(pHbascA,FebascA,'ko');
hold on
scatter(pHbascB,FebascB,'k+');
scatter(pHbascC,FebascC,'kx');
scatter(pHbascD,FebascD,'k*');
scatter(pHmsedA,FemsedA,'ro');
scatter(pHmsedD,FemsedD,'r*');
scatter(pHmorbA,FemorbA,'bo');
scatter(pHmorbB,FemorbB,'b+');
scatter(pHmorbC,FemorbC,'bx');
scatter(pHmorbD,FemorbD,'b*');
scatter(pHnemorbA,FenemorbA,'co');
scatter(pHnemorbC,FenemorbC,'cx');
scatter(pHnemorbD,FenemorbD,'c*');
scatter(pHemorbA,FeemorbA,'go');
scatter(pHemorbB,FeemorbB,'g+');
scatter(pHemorbC,FeemorbC,'gx');
scatter(pHemorbD,FeemorbD,'g*');
scatter(pHumafA,FeumafA,'mo');
scatter(pHumafB,FeumafB,'m+');
scatter(pHumafC,FeumafC,'mx');
scatter(pHumafD,FeumafD,'m*');
hold off
set (gca,'Xdir','reverse'); xlim([2 8]);
ylim([0 inf]);
xlabel('Fluid pH'); ylabel('Fe Concentration,
g m^-^3');
```

```
%temp
figure;
scatter(TbascA,FebascA,'ko');
hold on
scatter(TbascB,FebascB,'k+');
scatter(TbascC,FebascC,'kx');
scatter(TbascD,FebascD,'k*');
scatter(TmsedA,FemsedA,'ro');
scatter(TmsedD,FemsedD,'r*');
scatter(TmorbA,FemorbA,'bo');
scatter(TmorbB,FemorbB,'b+');
scatter(TmorbC,FemorbC,'bx');
scatter(TmorbD,FemorbD,'b*');
scatter(TnemorbA,FenemorbA,'co');
scatter(TnemorbC,FenemorbC,'cx');
scatter(TnemorbD,FenemorbD,'c*');
scatter(TemorbA,FeemorbA,'go');
scatter(TemorbB,FeemorbB,'g+');
scatter(TemorbC,FeemorbC,'gx');
scatter(TemorbD,FeemorbD,'g*');
scatter(TumafA,FeumafA,'mo');
scatter(TumafB,FeumafB,'m+');
scatter(TumafC,FeumafC,'mx');
scatter(TumafD,FeumafD,'m*');
hold off
xlabel('Fluid Temp, °C'); ylabel('Fe
Concentration, g m^-^3');ylim([0 inf]);
%% plot Mn
figure;
scatter3(pHbascA,TbascA,MnbascA,'ko');
hold on
scatter3(pHbascB,TbascB,MnbascB,'k+');
scatter3(pHbascC,TbascC,MnbascC,'kx');
```

```
scatter3(pHbascD,TbascD,MnbascD,'k*');
scatter3(pHmsedA,TmsedA,MnmsedA,'ro');
scatter3(pHmsedD,TmsedD,MnmsedD,'r*');
scatter3(pHmorbA,TmorbA,MnmorbA,'bo');
scatter3(pHmorbB,TmorbB,MnmorbB,'b+');
scatter3(pHmorbC,TmorbC,MnmorbC,'bx');
scatter3(pHmorbD,TmorbD,MnmorbD,'b*');
scatter3(pHnemorbA,TnemorbA,MnnemorbA,'co');
scatter3(pHnemorbC,TnemorbC,MnnemorbC,'cx');
scatter3(pHnemorbD,TnemorbD,MnnemorbD,'c*');
scatter3(pHemorbA,TemorbA,MnemorbA,'go');
scatter3(pHemorbB,TemorbB,MnemorbB,'g+');
scatter3(pHemorbC,TemorbC,MnemorbC,'gx');
scatter3(pHemorbD,TemorbD,MnemorbD,'g*');
scatter3(pHumafA,TumafA,MnumafA,'mo');
scatter3(pHumafB,TumafB,MnumafB,'m+');
scatter3(pHumafC,TumafC,MnumafC,'mx');
scatter3(pHumafD,TumafD,MnumafD,'m*');
hold off
set (gca,'Xdir','reverse'); xlim([2 8]);
zlim([0 inf]);
xlabel('Fluid pH'); ylabel('Fluid Temp,
°C');zlabel('Mn Concentration, g m^-^3');
%ph
figure;
scatter(pHbascA,MnbascA,'ko');
hold on
scatter(pHbascB,MnbascB,'k+');
scatter(pHbascC,MnbascC,'kx');
scatter(pHbascD,MnbascD,'k*');
scatter(pHmsedA,MnmsedA,'ro');
scatter(pHmsedD,MnmsedD,'r*');
scatter(pHmorbA,MnmorbA,'bo');
```

```
scatter(pHmorbB,MnmorbB,'b+');
scatter(pHmorbC,MnmorbC,'bx');
scatter(pHmorbD,MnmorbD,'b*');
scatter(pHnemorbA,MnnemorbA,'co');
scatter(pHnemorbC,MnnemorbC,'cx');
scatter(pHnemorbD,MnnemorbD,'c*');
scatter(pHemorbA,MnemorbA,'go');
scatter(pHemorbB,MnemorbB,'g+');
scatter(pHemorbC,MnemorbC,'gx');
scatter(pHemorbD,MnemorbD,'g*');
scatter(pHumafA,MnumafA,'mo');
scatter(pHumafB,MnumafB,'m+');
scatter(pHumafC,MnumafC,'mx');
scatter(pHumafD,MnumafD,'m*');
hold off
set (gca,'Xdir','reverse'); xlim([2 8]);
ylim([0 inf]);
xlabel('Fluid pH'); ylabel('Mn Concentration,
g m^-^3');
%temp
figure;
scatter(TbascA,MnbascA,'ko');
hold on
scatter(TbascB,MnbascB,'k+');
scatter(TbascC,MnbascC,'kx');
scatter(TbascD,MnbascD,'k*');
scatter(TmsedA,MnmsedA,'ro');
scatter(TmsedD,MnmsedD,'r*');
scatter(TmorbA,MnmorbA,'bo');
scatter(TmorbB,MnmorbB,'b+');
scatter(TmorbC,MnmorbC,'bx');
scatter(TmorbD,MnmorbD,'b*');
scatter(TnemorbA,MnnemorbA,'co');
```

```
scatter(TnemorbC,MnnemorbC,'cx');
scatter(TnemorbD,MnnemorbD,'c*');
scatter(TemorbA,MnemorbA,'go');
scatter(TemorbB,MnemorbB,'g+');
scatter(TemorbC,MnemorbC,'gx');
scatter(TemorbD,MnemorbD,'g*');
scatter(TumafA,MnumafA,'mo');
scatter(TumafB,MnumafB,'m+');
scatter(TumafC,MnumafC,'mx');
scatter(TumafD,MnumafD,'m*');
hold off
xlabel('Fluid Temp, °C'); ylabel('Mn
Concentration, g m^-^3');ylim([0 inf]);
%% plot Li
figure;
scatter3(pHbascA,TbascA,LibascA,'ko');
hold on
scatter3(pHbascB,TbascB,LibascB,'k+');
scatter3(pHbascC,TbascC,LibascC,'kx');
scatter3(pHbascD,TbascD,LibascD,'k*');
scatter3(pHmsedA,TmsedA,LimsedA,'ro');
scatter3(pHmsedD,TmsedD,LimsedD,'r*');
scatter3(pHmorbA,TmorbA,LimorbA,'bo');
scatter3(pHmorbB,TmorbB,LimorbB,'b+');
scatter3(pHmorbC,TmorbC,LimorbC,'bx');
scatter3(pHmorbD,TmorbD,LimorbD,'b*');
scatter3(pHnemorbA,TnemorbA,LinemorbA,'co');
scatter3(pHnemorbC,TnemorbC,LinemorbC,'cx');
scatter3(pHnemorbD,TnemorbD,LinemorbD,'c*');
scatter3(pHemorbA,TemorbA,LiemorbA,'go');
scatter3(pHemorbB,TemorbB,LiemorbB,'g+');
scatter3(pHemorbC,TemorbC,LiemorbC,'gx');
scatter3(pHemorbD,TemorbD,LiemorbD,'g*');
```

```
scatter3(pHumafA,TumafA,LiumafA,'mo');
scatter3(pHumafB,TumafB,LiumafB,'m+');
scatter3(pHumafC,TumafC,LiumafC,'mx');
scatter3(pHumafD,TumafD,LiumafD,'m*');
hold off
set (gca,'Xdir','reverse'); xlim([2 8]);
zlim([0 inf]);
xlabel('Fluid pH'); ylabel('Fluid Temp,
°C');zlabel('Li Concentration, g m^-^3');
%ph
figure;
scatter(pHbascA,LibascA,'ko');
hold on
scatter(pHbascB,LibascB,'k+');
scatter(pHbascC,LibascC,'kx');
scatter(pHbascD,LibascD,'k*');
scatter(pHmsedA,LimsedA,'ro');
scatter(pHmsedD,LimsedD,'r*');
scatter(pHmorbA,LimorbA,'bo');
scatter(pHmorbB,LimorbB,'b+');
scatter(pHmorbC,LimorbC,'bx');
scatter(pHmorbD,LimorbD,'b*');
scatter(pHnemorbA,LinemorbA,'co');
scatter(pHnemorbC,LinemorbC,'cx');
scatter(pHnemorbD,LinemorbD,'c*');
scatter(pHemorbA,LiemorbA,'go');
scatter(pHemorbB,LiemorbB,'g+');
scatter(pHemorbC,LiemorbC,'gx');
scatter(pHemorbD,LiemorbD,'g*');
scatter(pHumafA,LiumafA,'mo');
scatter(pHumafB,LiumafB,'m+');
scatter(pHumafC,LiumafC,'mx');
scatter(pHumafD,LiumafD,'m*');
```

```
hold off
set (gca,'Xdir','reverse'); xlim([2 8]);
ylim([0 inf]);
xlabel('Fluid pH'); ylabel('Li Concentration,
g m^-^3');
%temp
figure;
scatter(TbascA,LibascA,'ko');
hold on
scatter(TbascB,LibascB,'k+');
scatter(TbascC,LibascC,'kx');
scatter(TbascD,LibascD,'k*');
scatter(TmsedA,LimsedA,'ro');
scatter(TmsedD,LimsedD,'r*');
scatter(TmorbA,LimorbA,'bo');
scatter(TmorbB,LimorbB,'b+');
scatter(TmorbC,LimorbC,'bx');
scatter(TmorbD,LimorbD,'b*');
scatter(TnemorbA,LinemorbA,'co');
scatter(TnemorbC,LinemorbC,'cx');
scatter(TnemorbD,LinemorbD,'c*');
scatter(TemorbA,LiemorbA,'go');
scatter(TemorbB,LiemorbB,'g+');
scatter(TemorbC,LiemorbC,'gx');
scatter(TemorbD,LiemorbD,'g*');
scatter(TumafA,LiumafA,'mo');
scatter(TumafB,LiumafB,'m+');
scatter(TumafC,LiumafC,'mx');
scatter(TumafD,LiumafD,'m*');
hold off
xlabel('Fluid Temp, °C'); ylabel('Li
Concentration, g m^-^3');ylim([0 inf]);
%% plot Sr
```

```
figure;
scatter3(pHbascA,TbascA,SrbascA,'ko');
hold on
scatter3(pHbascB,TbascB,SrbascB,'k+');
scatter3(pHbascC,TbascC,SrbascC,'kx');
scatter3(pHbascD,TbascD,SrbascD,'k*');
scatter3(pHmsedA,TmsedA,SrmsedA,'ro');
scatter3(pHmsedD,TmsedD,SrmsedD,'r*');
scatter3(pHmorbA,TmorbA,SrmorbA,'bo');
scatter3(pHmorbB,TmorbB,SrmorbB,'b+');
scatter3(pHmorbC,TmorbC,SrmorbC,'bx');
scatter3(pHmorbD,TmorbD,SrmorbD,'b*');
scatter3(pHnemorbA,TnemorbA,SrnemorbA,'co');
scatter3(pHnemorbC,TnemorbC,SrnemorbC,'cx');
scatter3(pHnemorbD,TnemorbD,SrnemorbD,'c*');
scatter3(pHemorbA,TemorbA,SremorbA,'go');
scatter3(pHemorbB,TemorbB,SremorbB,'g+');
scatter3(pHemorbC,TemorbC,SremorbC,'gx');
scatter3(pHemorbD,TemorbD,SremorbD,'g*');
scatter3(pHumafA,TumafA,SrumafA,'mo');
scatter3(pHumafB,TumafB,SrumafB,'m+');
scatter3(pHumafC,TumafC,SrumafC,'mx');
scatter3(pHumafD,TumafD,SrumafD,'m*');
hold off
set (gca,'Xdir','reverse'); xlim([2 8]);
zlim([0 inf]);
xlabel('Fluid pH'); ylabel('Fluid Temp,
°C');zlabel('Sr Concentration, g m^-^3');
%ph
figure;
scatter(pHbascA,SrbascA,'ko');
hold on
scatter(pHbascB,SrbascB,'k+');
```

```
scatter(pHbascC,SrbascC,'kx');
scatter(pHbascD,SrbascD,'k*');
scatter(pHmsedA,SrmsedA,'ro');
scatter(pHmsedD,SrmsedD,'r*');
scatter(pHmorbA,SrmorbA,'bo');
scatter(pHmorbB,SrmorbB,'b+');
scatter(pHmorbC,SrmorbC,'bx');
scatter(pHmorbD,SrmorbD,'b*');
scatter(pHnemorbA,SrnemorbA,'co');
scatter(pHnemorbC,SrnemorbC,'cx');
scatter(pHnemorbD,SrnemorbD,'c*');
scatter(pHemorbA,SremorbA,'go');
scatter(pHemorbB,SremorbB,'g+');
scatter(pHemorbC,SremorbC,'gx');
scatter(pHemorbD,SremorbD,'g*');
scatter(pHumafA,SrumafA,'mo');
scatter(pHumafB,SrumafB,'m+');
scatter(pHumafC,SrumafC,'mx');
scatter(pHumafD,SrumafD,'m*');
hold off
set (gca,'Xdir','reverse'); xlim([2 8]);
ylim([0 inf]);
xlabel('Fluid pH'); ylabel('Sr Concentration,
g m^-^3');
%temp
figure;
scatter(TbascA,SrbascA,'ko');
hold on
scatter(TbascB,SrbascB,'k+');
scatter(TbascC,SrbascC,'kx');
scatter(TbascD,SrbascD,'k*');
scatter(TmsedA,SrmsedA,'ro');
scatter(TmsedD,SrmsedD,'r*');
```

```
scatter(TmorbA,SrmorbA,'bo');
scatter(TmorbB,SrmorbB,'b+');
scatter(TmorbC,SrmorbC,'bx');
scatter(TmorbD,SrmorbD,'b*');
scatter(TnemorbA,SrnemorbA,'co');
scatter(TnemorbC,SrnemorbC,'cx');
scatter(TnemorbD,SrnemorbD,'c*');
scatter(TemorbA,SremorbA,'go');
scatter(TemorbB,SremorbB,'g+');
scatter(TemorbC,SremorbC,'gx');
scatter(TemorbD,SremorbD,'g*');
scatter(TumafA,SrumafA,'mo');
scatter(TumafB,SrumafB,'m+');
scatter(TumafC,SrumafC,'mx');
scatter(TumafD,SrumafD,'m*');
hold off
xlabel('Fluid Temp, °C'); ylabel('Sr
Concentration, g m^-^3');ylim([0 inf]);
%% plot Cu
figure;
scatter3(pHbascA,TbascA,CubascA,'ko');
hold on
scatter3(pHbascB,TbascB,CubascB,'k+');
scatter3(pHbascC,TbascC,CubascC,'kx');
scatter3(pHbascD,TbascD,CubascD,'k*');
scatter3(pHmsedA,TmsedA,CumsedA,'ro');
scatter3(pHmsedD,TmsedD,CumsedD,'r*');
scatter3(pHmorbA,TmorbA,CumorbA,'bo');
scatter3(pHmorbB,TmorbB,CumorbB,'b+');
scatter3(pHmorbC,TmorbC,CumorbC,'bx');
scatter3(pHmorbD,TmorbD,CumorbD,'b*');
scatter3(pHnemorbA,TnemorbA,CunemorbA,'co');
scatter3(pHnemorbC,TnemorbC,CunemorbC,'cx');
```

```
scatter3(pHnemorbD,TnemorbD,CunemorbD,'c*');
scatter3(pHemorbA,TemorbA,CuemorbA,'go');
scatter3(pHemorbB,TemorbB,CuemorbB,'g+');
scatter3(pHemorbC,TemorbC,CuemorbC,'gx');
scatter3(pHemorbD,TemorbD,CuemorbD,'g*');
scatter3(pHumafA,TumafA,CuumafA,'mo');
scatter3(pHumafB,TumafB,CuumafB,'m+');
scatter3(pHumafC,TumafC,CuumafC,'mx');
scatter3(pHumafD,TumafD,CuumafD,'m*');
hold off
set (gca,'Xdir','reverse'); xlim([2 8]);
zlim([0 inf]);
xlabel('Fluid pH'); ylabel('Fluid Temp,
°C');zlabel('Cu Concentration, g m^-^3');
%ph
figure;
scatter(pHbascA,CubascA,'ko');
hold on
scatter(pHbascB,CubascB,'k+');
scatter(pHbascC,CubascC,'kx');
scatter(pHbascD,CubascD,'k*');
scatter(pHmsedA,CumsedA,'ro');
scatter(pHmsedD,CumsedD,'r*');
scatter(pHmorbA,CumorbA,'bo');
scatter(pHmorbB,CumorbB,'b+');
scatter(pHmorbC,CumorbC,'bx');
scatter(pHmorbD,CumorbD,'b*');
scatter(pHnemorbA,CunemorbA,'co');
scatter(pHnemorbC,CunemorbC,'cx');
scatter(pHnemorbD,CunemorbD,'c*');
scatter(pHemorbA,CuemorbA,'go');
scatter(pHemorbB,CuemorbB,'g+');
scatter(pHemorbC,CuemorbC,'gx');
```

```
scatter(pHemorbD,CuemorbD,'g*');
scatter(pHumafA,CuumafA,'mo');
scatter(pHumafB,CuumafB,'m+');
scatter(pHumafC,CuumafC,'mx');
scatter(pHumafD,CuumafD,'m*');
hold off
set (gca,'Xdir','reverse'); xlim([2 8]);
ylim([0 inf]);
xlabel('Fluid pH'); ylabel('Cu Concentration,
g m^-^3');
%temp
figure;
scatter(TbascA,CubascA,'ko');
hold on
scatter(TbascB,CubascB,'k+');
scatter(TbascC,CubascC,'kx');
scatter(TbascD,CubascD,'k*');
scatter(TmsedA,CumsedA,'ro');
scatter(TmsedD,CumsedD,'r*');
scatter(TmorbA,CumorbA,'bo');
scatter(TmorbB,CumorbB,'b+');
scatter(TmorbC,CumorbC,'bx');
scatter(TmorbD,CumorbD,'b*');
scatter(TnemorbA,CunemorbA,'co');
scatter(TnemorbC,CunemorbC,'cx');
scatter(TnemorbD,CunemorbD,'c*');
scatter(TemorbA,CuemorbA,'go');
scatter(TemorbB,CuemorbB,'g+');
scatter(TemorbC,CuemorbC,'gx');
scatter(TemorbD,CuemorbD,'g*');
scatter(TumafA,CuumafA,'mo');
scatter(TumafB,CuumafB,'m+');
scatter(TumafC,CuumafC,'mx');
```

```
scatter(TumafD,CuumafD,'m*');
hold off
xlabel('Fluid Temp, °C'); ylabel('Cu
Concentration, g m^-^3');ylim([0 inf]);
%% plot Zn
figure;
scatter3(pHbascA,TbascA,ZnbascA,'ko');
hold on
scatter3(pHbascB,TbascB,ZnbascB,'k+');
scatter3(pHbascC,TbascC,ZnbascC,'kx');
scatter3(pHbascD,TbascD,ZnbascD,'k*');
scatter3(pHmsedA,TmsedA,ZnmsedA,'ro');
scatter3(pHmsedD,TmsedD,ZnmsedD,'r*');
scatter3(pHmorbA,TmorbA,ZnmorbA,'bo');
scatter3(pHmorbB,TmorbB,ZnmorbB,'b+');
scatter3(pHmorbC,TmorbC,ZnmorbC,'bx');
scatter3(pHmorbD,TmorbD,ZnmorbD,'b*');
scatter3(pHnemorbA,TnemorbA,ZnnemorbA,'co');
scatter3(pHnemorbC,TnemorbC,ZnnemorbC,'cx');
scatter3(pHnemorbD,TnemorbD,ZnnemorbD,'c*');
scatter3(pHemorbA,TemorbA,ZnemorbA,'go');
scatter3(pHemorbB,TemorbB,ZnemorbB,'g+');
scatter3(pHemorbC,TemorbC,ZnemorbC,'gx');
scatter3(pHemorbD,TemorbD,ZnemorbD,'g*');
scatter3(pHumafA,TumafA,ZnumafA,'mo');
scatter3(pHumafB,TumafB,ZnumafB,'m+');
scatter3(pHumafC,TumafC,ZnumafC,'mx');
scatter3(pHumafD,TumafD,ZnumafD,'m*');
hold off
set (gca,'Xdir','reverse'); xlim([2 8]);
zlim([0 inf]);
xlabel('Fluid pH'); ylabel('Fluid Temp,
°C');zlabel('Zn Concentration, g m^-^3');
```

```
%ph
figure;
scatter(pHbascA,ZnbascA,'ko');
hold on
scatter(pHbascB,ZnbascB,'k+');
scatter(pHbascC,ZnbascC,'kx');
scatter(pHbascD,ZnbascD,'k*');
scatter(pHmsedA,ZnmsedA,'ro');
scatter(pHmsedD,ZnmsedD,'r*');
scatter(pHmorbA,ZnmorbA,'bo');
scatter(pHmorbB,ZnmorbB,'b+');
scatter(pHmorbC,ZnmorbC,'bx');
scatter(pHmorbD,ZnmorbD,'b*');
scatter(pHnemorbA,ZnnemorbA,'co');
scatter(pHnemorbC,ZnnemorbC,'cx');
scatter(pHnemorbD,ZnnemorbD,'c*');
scatter(pHemorbA,ZnemorbA,'go');
scatter(pHemorbB,ZnemorbB,'g+');
scatter(pHemorbC,ZnemorbC,'gx');
scatter(pHemorbD,ZnemorbD,'g*');
scatter(pHumafA,ZnumafA,'mo');
scatter(pHumafB,ZnumafB,'m+');
scatter(pHumafC,ZnumafC,'mx');
scatter(pHumafD,ZnumafD,'m*');
hold off
set (gca,'Xdir','reverse'); xlim([2 8]);
ylim([0 inf]);
xlabel('Fluid pH'); ylabel('Zn Concentration,
g m^-^3');
%temp
figure;
scatter(TbascA,ZnbascA,'ko');
hold on
```

```
scatter(TbascB,ZnbascB,'k+');
scatter(TbascC,ZnbascC,'kx');
scatter(TbascD,ZnbascD,'k*');
scatter(TmsedA,ZnmsedA,'ro');
scatter(TmsedD,ZnmsedD,'r*');
scatter(TmorbA,ZnmorbA,'bo');
scatter(TmorbB,ZnmorbB,'b+');
scatter(TmorbC,ZnmorbC,'bx');
scatter(TmorbD,ZnmorbD,'b*');
scatter(TnemorbA,ZnnemorbA,'co');
scatter(TnemorbC,ZnnemorbC,'cx');
scatter(TnemorbD,ZnnemorbD,'c*');
scatter(TemorbA,ZnemorbA,'go');
scatter(TemorbB,ZnemorbB,'g+');
scatter(TemorbC,ZnemorbC,'gx');
scatter(TemorbD,ZnemorbD,'g*');
scatter(TumafA,ZnumafA,'mo');
scatter(TumafB,ZnumafB,'m+');
scatter(TumafC,ZnumafC,'mx');
scatter(TumafD,ZnumafD,'m*');
hold off
xlabel('Fluid Temp, °C'); ylabel('Zn
Concentration, g m^-^3');ylim([0 inf]);%here
%% plot Cl
figure;
scatter3(pHbascA,TbascA,ClbascA,'ko');
hold on
scatter3(pHbascB,TbascB,ClbascB,'k+');
scatter3(pHbascC,TbascC,ClbascC,'kx');
scatter3(pHbascD,TbascD,ClbascD,'k*');
scatter3(pHmsedA,TmsedA,ClmsedA,'ro');
scatter3(pHmsedD,TmsedD,ClmsedD,'r*');
scatter3(pHmorbA,TmorbA,ClmorbA,'bo');
```

```
scatter3(pHmorbB,TmorbB,ClmorbB,'b+');
scatter3(pHmorbC,TmorbC,ClmorbC,'bx');
scatter3(pHmorbD,TmorbD,ClmorbD,'b*');
scatter3(pHnemorbA,TnemorbA,ClnemorbA,'co');
scatter3(pHnemorbC,TnemorbC,ClnemorbC,'cx');
scatter3(pHnemorbD,TnemorbD,ClnemorbD,'c*');
scatter3(pHemorbA,TemorbA,ClemorbA,'go');
scatter3(pHemorbB,TemorbB,ClemorbB,'g+');
scatter3(pHemorbC,TemorbC,ClemorbC,'gx');
scatter3(pHemorbD,TemorbD,ClemorbD,'g*');
scatter3(pHumafA,TumafA,ClumafA,'mo');
scatter3(pHumafB,TumafB,ClumafB,'m+');
scatter3(pHumafC,TumafC,ClumafC,'mx');
scatter3(pHumafD,TumafD,ClumafD,'m*');
hold off
set (gca,'Xdir','reverse'); xlim([2 8]);
zlim([0 inf]);
xlabel('Fluid pH'); ylabel('Fluid Temp,
°C');zlabel('Cl Concentration, g m^-^3');
%ph
figure;
scatter(pHbascA,ClbascA,'ko');
hold on
scatter(pHbascB,ClbascB,'k+');
scatter(pHbascC,ClbascC,'kx');
scatter(pHbascD,ClbascD,'k*');
scatter(pHmsedA,ClmsedA,'ro');
scatter(pHmsedD,ClmsedD,'r*');
scatter(pHmorbA,ClmorbA,'bo');
scatter(pHmorbB,ClmorbB,'b+');
scatter(pHmorbC,ClmorbC,'bx');
scatter(pHmorbD,ClmorbD,'b*');
scatter(pHnemorbA,ClnemorbA,'co');
```

```
scatter(pHnemorbC,ClnemorbC,'cx');
scatter(pHnemorbD,ClnemorbD,'c*');
scatter(pHemorbA,ClemorbA,'go');
scatter(pHemorbB,ClemorbB,'g+');
scatter(pHemorbC,ClemorbC,'gx');
scatter(pHemorbD,ClemorbD,'g*');
scatter(pHumafA,ClumafA,'mo');
scatter(pHumafB,ClumafB,'m+');
scatter(pHumafC,ClumafC,'mx');
scatter(pHumafD,ClumafD,'m*');
hold off
set (gca,'Xdir','reverse'); xlim([2 8]);
ylim([0 inf]);
xlabel('Fluid pH'); ylabel('Cl Concentration,
g m^-^3');
%temp
figure;
scatter(TbascA,ClbascA,'ko');
hold on
scatter(TbascB,ClbascB,'k+');
scatter(TbascC,ClbascC,'kx');
scatter(TbascD,ClbascD,'k*');
scatter(TmsedA,ClmsedA,'ro');
scatter(TmsedD,ClmsedD,'r*');
scatter(TmorbA,ClmorbA,'bo');
scatter(TmorbB,ClmorbB,'b+');
scatter(TmorbC,ClmorbC,'bx');
scatter(TmorbD,ClmorbD,'b*');
scatter(TnemorbA,ClnemorbA,'co');
scatter(TnemorbC,ClnemorbC,'cx');
scatter(TnemorbD,ClnemorbD,'c*');
scatter(TemorbA,ClemorbA,'go');
scatter(TemorbB,ClemorbB,'g+');
```

```
scatter(TemorbC,ClemorbC,'gx');
scatter(TemorbD,ClemorbD,'g*');
scatter(TumafA,ClumafA,'mo');
scatter(TumafB,ClumafB,'m+');
scatter(TumafC,ClumafC,'mx');
scatter(TumafD,ClumafD,'m*');
hold off
xlabel('Fluid Temp, °C'); ylabel('Cl
Concentration, g m^-^3');ylim([0 inf]);
%% plot Br
figure;
scatter3(pHbascA,TbascA,BrbascA,'ko');
hold on
scatter3(pHbascB,TbascB,BrbascB,'k+');
scatter3(pHbascC,TbascC,BrbascC,'kx');
scatter3(pHbascD,TbascD,BrbascD,'k*');
scatter3(pHmsedA,TmsedA,BrmsedA,'ro');
scatter3(pHmsedD,TmsedD,BrmsedD,'r*');
scatter3(pHmorbA,TmorbA,BrmorbA,'bo');
scatter3(pHmorbB,TmorbB,BrmorbB,'b+');
scatter3(pHmorbC,TmorbC,BrmorbC,'bx');
scatter3(pHmorbD,TmorbD,BrmorbD,'b*');
scatter3(pHnemorbA,TnemorbA,BrnemorbA,'co');
scatter3(pHnemorbC,TnemorbC,BrnemorbC,'cx');
scatter3(pHnemorbD,TnemorbD,BrnemorbD,'c*');
scatter3(pHemorbA,TemorbA,BremorbA,'go');
scatter3(pHemorbB,TemorbB,BremorbB,'g+');
scatter3(pHemorbC,TemorbC,BremorbC,'gx');
scatter3(pHemorbD,TemorbD,BremorbD,'g*');
scatter3(pHumafA,TumafA,BrumafA,'mo');
scatter3(pHumafB,TumafB,BrumafB,'m+');
scatter3(pHumafC,TumafC,BrumafC,'mx');
scatter3(pHumafD,TumafD,BrumafD,'m*');
```

```
hold off
set (gca,'Xdir','reverse'); xlim([2 8]);
zlim([0 inf]);
xlabel('Fluid pH'); ylabel('Fluid Temp,
°C');zlabel('Br Concentration, g m^-^3');
%ph
figure;
scatter(pHbascA,BrbascA,'ko');
hold on
scatter(pHbascB,BrbascB,'k+');
scatter(pHbascC,BrbascC,'kx');
scatter(pHbascD,BrbascD,'k*');
scatter(pHmsedA,BrmsedA,'ro');
scatter(pHmsedD,BrmsedD,'r*');
scatter(pHmorbA,BrmorbA,'bo');
scatter(pHmorbB,BrmorbB,'b+');
scatter(pHmorbC,BrmorbC,'bx');
scatter(pHmorbD,BrmorbD,'b*');
scatter(pHnemorbA,BrnemorbA,'co');
scatter(pHnemorbC,BrnemorbC,'cx');
scatter(pHnemorbD,BrnemorbD,'c*');
scatter(pHemorbA,BremorbA,'go');
scatter(pHemorbB,BremorbB,'g+');
scatter(pHemorbC,BremorbC,'gx');
scatter(pHemorbD,BremorbD,'g*');
scatter(pHumafA,BrumafA,'mo');
scatter(pHumafB,BrumafB,'m+');
scatter(pHumafC,BrumafC,'mx');
scatter(pHumafD,BrumafD,'m*');
hold off
set (gca,'Xdir','reverse'); xlim([2 8]);
ylim([0 inf]);
```

```
xlabel('Fluid pH'); ylabel('Br Concentration,
g m^-^3');
%temp
figure;
scatter(TbascA,BrbascA,'ko');
hold on
scatter(TbascB,BrbascB,'k+');
scatter(TbascC,BrbascC,'kx');
scatter(TbascD,BrbascD,'k*');
scatter(TmsedA,BrmsedA,'ro');
scatter(TmsedD,BrmsedD,'r*');
scatter(TmorbA,BrmorbA,'bo');
scatter(TmorbB,BrmorbB,'b+');
scatter(TmorbC,BrmorbC,'bx');
scatter(TmorbD,BrmorbD,'b*');
scatter(TnemorbA,BrnemorbA,'co');
scatter(TnemorbC,BrnemorbC,'cx');
scatter(TnemorbD,BrnemorbD,'c*');
scatter(TemorbA,BremorbA,'go');
scatter(TemorbB,BremorbB,'g+');
scatter(TemorbC,BremorbC,'gx');
scatter(TemorbD,BremorbD,'g*');
scatter(TumafA,BrumafA,'mo');
scatter(TumafB,BrumafB,'m+');
scatter(TumafC,BrumafC,'mx');
scatter(TumafD,BrumafD,'m*');
hold off
xlabel('Fluid Temp, °C'); ylabel('Br
Concentration, g m^-^3');ylim([0 inf]);
%% plot Rb
figure;
scatter3(pHbascA,TbascA,RbbascA,'ko');
hold on
```

```
scatter3(pHbascB,TbascB,RbbascB,'k+');
scatter3(pHbascC,TbascC,RbbascC,'kx');
scatter3(pHbascD,TbascD,RbbascD,'k*');
scatter3(pHmsedA,TmsedA,RbmsedA,'ro');
scatter3(pHmsedD,TmsedD,RbmsedD,'r*');
scatter3(pHmorbA,TmorbA,RbmorbA,'bo');
scatter3(pHmorbB,TmorbB,RbmorbB,'b+');
scatter3(pHmorbC,TmorbC,RbmorbC,'bx');
scatter3(pHmorbD,TmorbD,RbmorbD,'b*');
scatter3(pHnemorbA,TnemorbA,RbnemorbA,'co');
scatter3(pHnemorbC,TnemorbC,RbnemorbC,'cx');
scatter3(pHnemorbD,TnemorbD,RbnemorbD,'c*');
scatter3(pHemorbA,TemorbA,RbemorbA,'go');
scatter3(pHemorbB,TemorbB,RbemorbB,'g+');
scatter3(pHemorbC,TemorbC,RbemorbC,'gx');
scatter3(pHemorbD,TemorbD,RbemorbD,'g*');
scatter3(pHumafA,TumafA,RbumafA,'mo');
scatter3(pHumafB,TumafB,RbumafB,'m+');
scatter3(pHumafC,TumafC,RbumafC,'mx');
scatter3(pHumafD,TumafD,RbumafD,'m*');
hold off
set (gca,'Xdir','reverse'); xlim([2 8]);
zlim([0 inf]);
xlabel('Fluid pH'); ylabel('Fluid Temp,
°C');zlabel('Rb Concentration, g m^-^3');
%ph
figure;
scatter(pHbascA,RbbascA,'ko');
hold on
scatter(pHbascB,RbbascB,'k+');
scatter(pHbascC,RbbascC,'kx');
scatter(pHbascD,RbbascD,'k*');
scatter(pHmsedA,RbmsedA,'ro');
```

```
scatter(pHmsedD,RbmsedD,'r*');
scatter(pHmorbA,RbmorbA,'bo');
scatter(pHmorbB,RbmorbB,'b+');
scatter(pHmorbC,RbmorbC,'bx');
scatter(pHmorbD,RbmorbD,'b*');
scatter(pHnemorbA,RbnemorbA,'co');
scatter(pHnemorbC,RbnemorbC,'cx');
scatter(pHnemorbD,RbnemorbD,'c*');
scatter(pHemorbA,RbemorbA,'go');
scatter(pHemorbB,RbemorbB,'g+');
scatter(pHemorbC,RbemorbC,'gx');
scatter(pHemorbD,RbemorbD,'g*');
scatter(pHumafA,RbumafA,'mo');
scatter(pHumafB,RbumafB,'m+');
scatter(pHumafC,RbumafC,'mx');
scatter(pHumafD,RbumafD,'m*');
hold off
set (gca,'Xdir','reverse'); xlim([2 8]);
ylim([0 inf]);
xlabel('Fluid pH'); ylabel('Rb Concentration,
g m^-^3');
%temp
figure;
scatter(TbascA,RbbascA,'ko');
hold on
scatter(TbascB,RbbascB,'k+');
scatter(TbascC,RbbascC,'kx');
scatter(TbascD,RbbascD,'k*');
scatter(TmsedA,RbmsedA,'ro');
scatter(TmsedD,RbmsedD,'r*');
scatter(TmorbA,RbmorbA,'bo');
scatter(TmorbB,RbmorbB,'b+');
scatter(TmorbC,RbmorbC,'bx');
```

```
scatter(TmorbD,RbmorbD,'b*');
scatter(TnemorbA,RbnemorbA,'co');
scatter(TnemorbC,RbnemorbC,'cx');
scatter(TnemorbD,RbnemorbD,'c*');
scatter(TemorbA,RbemorbA,'go');
scatter(TemorbB,RbemorbB,'g+');
scatter(TemorbC,RbemorbC,'gx');
scatter(TemorbD,RbemorbD,'g*');
scatter(TumafA,RbumafA,'mo');
scatter(TumafB,RbumafB,'m+');
scatter(TumafC,RbumafC,'mx');
scatter(TumafD,RbumafD,'m*');
hold off
xlabel('Fluid Temp, °C'); ylabel('Rb
Concentration, g m^-^3');ylim([0 inf]);%here
%% plot B
figure;
scatter3(pHbascA,TbascA,BbascA,'ko');
hold on
scatter3(pHbascB,TbascB,BbascB,'k+');
scatter3(pHbascC,TbascC,BbascC,'kx');
scatter3(pHbascD,TbascD,BbascD,'k*');
scatter3(pHmsedA,TmsedA,BmsedA,'ro');
scatter3(pHmsedD,TmsedD,BmsedD,'r*');
scatter3(pHmorbA,TmorbA,BmorbA,'bo');
scatter3(pHmorbB,TmorbB,BmorbB,'b+');
scatter3(pHmorbC,TmorbC,BmorbC,'bx');
scatter3(pHmorbD,TmorbD,BmorbD,'b*');
scatter3(pHnemorbA,TnemorbA,BnemorbA,'co');
scatter3(pHnemorbC,TnemorbC,BnemorbC,'cx');
scatter3(pHnemorbD,TnemorbD,BnemorbD,'c*');
scatter3(pHemorbA,TemorbA,BemorbA,'go');
scatter3(pHemorbB,TemorbB,BemorbB,'g+');
```

```
scatter3(pHemorbC,TemorbC,BemorbC,'gx');
scatter3(pHemorbD,TemorbD,BemorbD,'g*');
scatter3(pHumafA,TumafA,BumafA,'mo');
scatter3(pHumafB,TumafB,BumafB,'m+');
scatter3(pHumafC,TumafC,BumafC,'mx');
scatter3(pHumafD,TumafD,BumafD,'m*');
hold off
set (gca,'Xdir','reverse'); xlim([2 8]);
zlim([0 inf]);
xlabel('Fluid pH'); ylabel('Fluid Temp,
°C');zlabel('B Concentration, g m^-^3');
%ph
figure;
scatter(pHbascA,BbascA,'ko');
hold on
scatter(pHbascB,BbascB,'k+');
scatter(pHbascC,BbascC,'kx');
scatter(pHbascD,BbascD,'k*');
scatter(pHmsedA,BmsedA,'ro');
scatter(pHmsedD,BmsedD,'r*');
scatter(pHmorbA,BmorbA,'bo');
scatter(pHmorbB,BmorbB,'b+');
scatter(pHmorbC,BmorbC,'bx');
scatter(pHmorbD,BmorbD,'b*');
scatter(pHnemorbA,BnemorbA,'co');
scatter(pHnemorbC,BnemorbC,'cx');
scatter(pHnemorbD,BnemorbD,'c*');
scatter(pHemorbA,BemorbA,'go');
scatter(pHemorbB,BemorbB,'g+');
scatter(pHemorbC,BemorbC,'gx');
scatter(pHemorbD,BemorbD,'g*');
scatter(pHumafA,BumafA,'mo');
scatter(pHumafB,BumafB,'m+');
```

```
scatter(pHumafC,BumafC,'mx');
scatter(pHumafD,BumafD,'m*');
hold off
set (gca,'Xdir','reverse'); xlim([2 8]);
ylim([0 inf]);
xlabel('Fluid pH'); ylabel('B Concentration,
g m^-^3');
%temp
figure;
scatter(TbascA,BbascA,'ko');
hold on
scatter(TbascB,BbascB,'k+');
scatter(TbascC,BbascC,'kx');
scatter(TbascD,BbascD,'k*');
scatter(TmsedA,BmsedA,'ro');
scatter(TmsedD,BmsedD,'r*');
scatter(TmorbA,BmorbA,'bo');
scatter(TmorbB,BmorbB,'b+');
scatter(TmorbC,BmorbC,'bx');
scatter(TmorbD,BmorbD,'b*');
scatter(TnemorbA,BnemorbA,'co');
scatter(TnemorbC,BnemorbC,'cx');
scatter(TnemorbD,BnemorbD,'c*');
scatter(TemorbA,BemorbA,'go');
scatter(TemorbB,BemorbB,'g+');
scatter(TemorbC,BemorbC,'gx');
scatter(TemorbD,BemorbD,'g*');
scatter(TumafA,BumafA,'mo');
scatter(TumafB,BumafB,'m+');
scatter(TumafC,BumafC,'mx');
scatter(TumafD,BumafD,'m*');
hold off
```

```
xlabel('Fluid Temp, °C'); ylabel('B
Concentration, g m^-^3');ylim([0 inf]);
%% plot Ba
figure;
scatter3(pHbascA,TbascA,BabascA,'ko');
hold on
scatter3(pHbascB,TbascB,BabascB,'k+');
scatter3(pHbascC,TbascC,BabascC,'kx');
scatter3(pHbascD,TbascD,BabascD,'k*');
scatter3(pHmsedA,TmsedA,BamsedA,'ro');
scatter3(pHmsedD,TmsedD,BamsedD,'r*');
scatter3(pHmorbA,TmorbA,BamorbA,'bo');
scatter3(pHmorbB,TmorbB,BamorbB,'b+');
scatter3(pHmorbC,TmorbC,BamorbC,'bx');
scatter3(pHmorbD,TmorbD,BamorbD,'b*');
scatter3(pHnemorbA,TnemorbA,BanemorbA,'co');
scatter3(pHnemorbC,TnemorbC,BanemorbC,'cx');
scatter3(pHnemorbD,TnemorbD,BanemorbD,'c*');
scatter3(pHemorbA,TemorbA,BaemorbA,'go');
scatter3(pHemorbB,TemorbB,BaemorbB,'g+');
scatter3(pHemorbC,TemorbC,BaemorbC,'gx');
scatter3(pHemorbD,TemorbD,BaemorbD,'g*');
scatter3(pHumafA,TumafA,BaumafA,'mo');
scatter3(pHumafB,TumafB,BaumafB,'m+');
scatter3(pHumafC,TumafC,BaumafC,'mx');
scatter3(pHumafD,TumafD,BaumafD,'m*');
hold off
set (gca,'Xdir','reverse'); xlim([2 8]);
zlim([0 inf]);
xlabel('Fluid pH'); ylabel('Fluid Temp,
°C');zlabel('Ba Concentration, g m^-^3');
%ph
figure;
```

```
scatter(pHbascA,BabascA,'ko');
hold on
scatter(pHbascB,BabascB,'k+');
scatter(pHbascC,BabascC,'kx');
scatter(pHbascD,BabascD,'k*');
scatter(pHmsedA,BamsedA,'ro');
scatter(pHmsedD,BamsedD,'r*');
scatter(pHmorbA,BamorbA,'bo');
scatter(pHmorbB,BamorbB,'b+');
scatter(pHmorbC,BamorbC,'bx');
scatter(pHmorbD,BamorbD,'b*');
scatter(pHnemorbA,BanemorbA,'co');
scatter(pHnemorbC,BanemorbC,'cx');
scatter(pHnemorbD,BanemorbD,'c*');
scatter(pHemorbA,BaemorbA,'go');
scatter(pHemorbB,BaemorbB,'g+');
scatter(pHemorbC,BaemorbC,'gx');
scatter(pHemorbD,BaemorbD,'g*');
scatter(pHumafA,BaumafA,'mo');
scatter(pHumafB,BaumafB,'m+');
scatter(pHumafC,BaumafC,'mx');
scatter(pHumafD,BaumafD,'m*');
hold off
set (gca,'Xdir','reverse'); xlim([2 8]);
ylim([0 inf]);
xlabel('Fluid pH'); ylabel('Ba Concentration,
g m^-^3');
%temp
figure;
scatter(TbascA,BabascA,'ko');
hold on
scatter(TbascB,BabascB,'k+');
scatter(TbascC,BabascC,'kx');
```

```
scatter(TbascD,BabascD,'k*');
scatter(TmsedA,BamsedA,'ro');
scatter(TmsedD,BamsedD,'r*');
scatter(TmorbA,BamorbA,'bo');
scatter(TmorbB,BamorbB,'b+');
scatter(TmorbC,BamorbC,'bx');
scatter(TmorbD,BamorbD,'b*');
scatter(TnemorbA,BanemorbA,'co');
scatter(TnemorbC,BanemorbC,'cx');
scatter(TnemorbD,BanemorbD,'c*');
scatter(TemorbA,BaemorbA,'go');
scatter(TemorbB,BaemorbB,'g+');
scatter(TemorbC,BaemorbC,'gx');
scatter(TemorbD,BaemorbD,'g*');
scatter(TumafA,BaumafA,'mo');
scatter(TumafB,BaumafB,'m+');
scatter(TumafC,BaumafC,'mx');
scatter(TumafD,BaumafD,'m*');
hold off
xlabel('Fluid Temp, °C'); ylabel('Ba
Concentration, g m^-^3');ylim([0 inf]);
%% plot Cs
figure;
scatter3(pHbascA,TbascA,CsbascA,'ko');
hold on
scatter3(pHbascB,TbascB,CsbascB,'k+');
scatter3(pHbascC,TbascC,CsbascC,'kx');
scatter3(pHbascD,TbascD,CsbascD,'k*');
scatter3(pHmsedA,TmsedA,CsmsedA,'ro');
scatter3(pHmsedD,TmsedD,CsmsedD,'r*');
scatter3(pHmorbA,TmorbA,CsmorbA,'bo');
scatter3(pHmorbB,TmorbB,CsmorbB,'b+');
scatter3(pHmorbC,TmorbC,CsmorbC,'bx');
```

```
scatter3(pHmorbD,TmorbD,CsmorbD,'b*');
scatter3(pHnemorbA,TnemorbA,CsnemorbA,'co');
scatter3(pHnemorbC,TnemorbC,CsnemorbC,'cx');
scatter3(pHnemorbD,TnemorbD,CsnemorbD,'c*');
scatter3(pHemorbA,TemorbA,CsemorbA,'go');
scatter3(pHemorbB,TemorbB,CsemorbB,'g+');
scatter3(pHemorbC,TemorbC,CsemorbC,'gx');
scatter3(pHemorbD,TemorbD,CsemorbD,'g*');
scatter3(pHumafA,TumafA,CsumafA,'mo');
scatter3(pHumafB,TumafB,CsumafB,'m+');
scatter3(pHumafC,TumafC,CsumafC,'mx');
scatter3(pHumafD,TumafD,CsumafD,'m*');
hold off
set (gca,'Xdir','reverse'); xlim([2 8]);
zlim([0 inf]);
xlabel('Fluid pH'); ylabel('Fluid Temp,
°C');zlabel('Cs Concentration, g m^-^3');
%ph
figure;
scatter(pHbascA,CsbascA,'ko');
hold on
scatter(pHbascB,CsbascB,'k+');
scatter(pHbascC,CsbascC,'kx');
scatter(pHbascD,CsbascD,'k*');
scatter(pHmsedA,CsmsedA,'ro');
scatter(pHmsedD,CsmsedD,'r*');
scatter(pHmorbA,CsmorbA,'bo');
scatter(pHmorbB,CsmorbB,'b+');
scatter(pHmorbC,CsmorbC,'bx');
scatter(pHmorbD,CsmorbD,'b*');
scatter(pHnemorbA,CsnemorbA,'co');
scatter(pHnemorbC,CsnemorbC,'cx');
scatter(pHnemorbD,CsnemorbD,'c*');
```

```
scatter(pHemorbA,CsemorbA,'go');
scatter(pHemorbB,CsemorbB,'g+');
scatter(pHemorbC,CsemorbC,'gx');
scatter(pHemorbD,CsemorbD,'g*');
scatter(pHumafA,CsumafA,'mo');
scatter(pHumafB,CsumafB,'m+');
scatter(pHumafC,CsumafC,'mx');
scatter(pHumafD,CsumafD,'m*');
hold off
set (gca,'Xdir','reverse'); xlim([2 8]);
ylim([0 inf]);
xlabel('Fluid pH'); ylabel('Cs Concentration,
g m^-^3');
%temp
figure;
scatter(TbascA,CsbascA,'ko');
hold on
scatter(TbascB,CsbascB,'k+');
scatter(TbascC,CsbascC,'kx');
scatter(TbascD,CsbascD,'k*');
scatter(TmsedA,CsmsedA,'ro');
scatter(TmsedD,CsmsedD,'r*');
scatter(TmorbA,CsmorbA,'bo');
scatter(TmorbB,CsmorbB,'b+');
scatter(TmorbC,CsmorbC,'bx');
scatter(TmorbD,CsmorbD,'b*');
scatter(TnemorbA,CsnemorbA,'co');
scatter(TnemorbC,CsnemorbC,'cx');
scatter(TnemorbD,CsnemorbD,'c*');
scatter(TemorbA,CsemorbA,'go');
scatter(TemorbB,CsemorbB,'g+');
scatter(TemorbC,CsemorbC,'gx');
scatter(TemorbD,CsemorbD,'g*');
```

```
scatter(TumafA,CsumafA,'mo');
scatter(TumafB,CsumafB,'m+');
scatter(TumafC,CsumafC,'mx');
scatter(TumafD,CsumafD,'m*');
hold off
xlabel('Fluid Temp, °C'); ylabel('Cs
Concentration, g m^-^3');ylim([0 inf]);
%% plot Cd
figure;
scatter3(pHbascA,TbascA,CdbascA,'ko');
hold on
scatter3(pHbascB,TbascB,CdbascB,'k+');
scatter3(pHbascC,TbascC,CdbascC,'kx');
scatter3(pHbascD,TbascD,CdbascD,'k*');
scatter3(pHmsedA,TmsedA,CdmsedA,'ro');
scatter3(pHmsedD,TmsedD,CdmsedD,'r*');
scatter3(pHmorbA,TmorbA,CdmorbA,'bo');
scatter3(pHmorbB,TmorbB,CdmorbB,'b+');
scatter3(pHmorbC,TmorbC,CdmorbC,'bx');
scatter3(pHmorbD,TmorbD,CdmorbD,'b*');
scatter3(pHnemorbA,TnemorbA,CdnemorbA,'co');
scatter3(pHnemorbC,TnemorbC,CdnemorbC,'cx');
scatter3(pHnemorbD,TnemorbD,CdnemorbD,'c*');
scatter3(pHemorbA,TemorbA,CdemorbA,'go');
scatter3(pHemorbB,TemorbB,CdemorbB,'g+');
scatter3(pHemorbC,TemorbC,CdemorbC,'gx');
scatter3(pHemorbD,TemorbD,CdemorbD,'g*');
scatter3(pHumafA,TumafA,CdumafA,'mo');
scatter3(pHumafB,TumafB,CdumafB,'m+');
scatter3(pHumafC,TumafC,CdumafC,'mx');
scatter3(pHumafD,TumafD,CdumafD,'m*');
hold off
```

```
set (gca,'Xdir','reverse'); xlim([2 8]);
zlim([0 inf]);
xlabel('Fluid pH'); ylabel('Fluid Temp,
°C');zlabel('Cd Concentration, g m^-^3');
%ph
figure;
scatter(pHbascA,CdbascA,'ko');
hold on
scatter(pHbascB,CdbascB,'k+');
scatter(pHbascC,CdbascC,'kx');
scatter(pHbascD,CdbascD,'k*');
scatter(pHmsedA,CdmsedA,'ro');
scatter(pHmsedD,CdmsedD,'r*');
scatter(pHmorbA,CdmorbA,'bo');
scatter(pHmorbB,CdmorbB,'b+');
scatter(pHmorbC,CdmorbC,'bx');
scatter(pHmorbD,CdmorbD,'b*');
scatter(pHnemorbA,CdnemorbA,'co');
scatter(pHnemorbC,CdnemorbC,'cx');
scatter(pHnemorbD,CdnemorbD,'c*');
scatter(pHemorbA,CdemorbA,'go');
scatter(pHemorbB,CdemorbB,'g+');
scatter(pHemorbC,CdemorbC,'gx');
scatter(pHemorbD,CdemorbD,'g*');
scatter(pHumafA,CdumafA,'mo');
scatter(pHumafB,CdumafB,'m+');
scatter(pHumafC,CdumafC,'mx');
scatter(pHumafD,CdumafD,'m*');
hold off
set (gca,'Xdir','reverse'); xlim([2 8]);
ylim([0 inf]);
xlabel('Fluid pH'); ylabel('Cd Concentration,
g m^-^3');
```

```
%temp
figure;
scatter(TbascA,CsbascA,'ko');
hold on
scatter(TbascB,CdbascB,'k+');
scatter(TbascC,CdbascC,'kx');
scatter(TbascD,CdbascD,'k*');
scatter(TmsedA,CdmsedA,'ro');
scatter(TmsedD,CdmsedD,'r*');
scatter(TmorbA,CdmorbA,'bo');
scatter(TmorbB,CdmorbB,'b+');
scatter(TmorbC,CdmorbC,'bx');
scatter(TmorbD,CdmorbD,'b*');
scatter(TnemorbA,CdnemorbA,'co');
scatter(TnemorbC,CdnemorbC,'cx');
scatter(TnemorbD,CdnemorbD,'c*');
scatter(TemorbA,CdemorbA,'go');
scatter(TemorbB,CdemorbB,'g+');
scatter(TemorbC,CdemorbC,'gx');
scatter(TemorbD,CdemorbD,'g*');
scatter(TumafA,CdumafA,'mo');
scatter(TumafB,CdumafB,'m+');
scatter(TumafC,CdumafC,'mx');
scatter(TumafD,CdumafD,'m*');
hold off
xlabel('Fluid Temp, °C'); ylabel('Cd
Concentration, g m^-^3');ylim([0 inf]);
%% plot Pb
figure;
scatter3(pHbascA,TbascA,PbbascA,'ko');
hold on
scatter3(pHbascB,TbascB,PbbascB,'k+');
scatter3(pHbascC,TbascC,PbbascC,'kx');
```

```
scatter3(pHbascD,TbascD,PbbascD,'k*');
scatter3(pHmsedA,TmsedA,PbmsedA,'ro');
scatter3(pHmsedD,TmsedD,PbmsedD,'r*');
scatter3(pHmorbA,TmorbA,PbmorbA,'bo');
scatter3(pHmorbB,TmorbB,PbmorbB,'b+');
scatter3(pHmorbC,TmorbC,PbmorbC,'bx');
scatter3(pHmorbD,TmorbD,PbmorbD,'b*');
scatter3(pHnemorbA,TnemorbA,PbnemorbA,'co');
scatter3(pHnemorbC,TnemorbC,PbnemorbC,'cx');
scatter3(pHnemorbD,TnemorbD,PbnemorbD,'c*');
scatter3(pHemorbA,TemorbA,PbemorbA,'go');
scatter3(pHemorbB,TemorbB,PbemorbB,'g+');
scatter3(pHemorbC,TemorbC,PbemorbC,'gx');
scatter3(pHemorbD,TemorbD,PbemorbD,'g*');
scatter3(pHumafA,TumafA,PbumafA,'mo');
scatter3(pHumafB,TumafB,PbumafB,'m+');
scatter3(pHumafC,TumafC,PbumafC,'mx');
scatter3(pHumafD,TumafD,PbumafD,'m*');
hold off
set (gca,'Xdir','reverse'); xlim([2 8]);
zlim([0 inf]);
xlabel('Fluid pH'); ylabel('Fluid Temp,
°C');zlabel('Pb Concentration, g m^-^3');
%ph
figure;
scatter(pHbascA,PbbascA,'ko');
hold on
scatter(pHbascB,PbbascB,'k+');
scatter(pHbascC,PbbascC,'kx');
scatter(pHbascD,PbbascD,'k*');
scatter(pHmsedA,PbmsedA,'ro');
scatter(pHmsedD,PbmsedD,'r*');
scatter(pHmorbA,PbmorbA,'bo');
```

```
scatter(pHmorbB,PbmorbB,'b+');
scatter(pHmorbC,PbmorbC,'bx');
scatter(pHmorbD,PbmorbD,'b*');
scatter(pHnemorbA,PbnemorbA,'co');
scatter(pHnemorbC,PbnemorbC,'cx');
scatter(pHnemorbD,PbnemorbD,'c*');
scatter(pHemorbA,PbemorbA,'go');
scatter(pHemorbB,PbemorbB,'g+');
scatter(pHemorbC,PbemorbC,'gx');
scatter(pHemorbD,PbemorbD,'g*');
scatter(pHumafA,PbumafA,'mo');
scatter(pHumafB,PbumafB,'m+');
scatter(pHumafC,PbumafC,'mx');
scatter(pHumafD,PbumafD,'m*');
hold off
set (gca,'Xdir','reverse'); xlim([2 8]);
ylim([0 inf]);
xlabel('Fluid pH'); ylabel('Pb Concentration,
g m^-^3');
%temp
figure;
scatter(TbascA,PbbascA,'ko');
hold on
scatter(TbascB,PbbascB,'k+');
scatter(TbascC,PbbascC,'kx');
scatter(TbascD,PbbascD,'k*');
scatter(TmsedA,PbmsedA,'ro');
scatter(TmsedD,PbmsedD,'r*');
scatter(TmorbA,PbmorbA,'bo');
scatter(TmorbB,PbmorbB,'b+');
scatter(TmorbC,PbmorbC,'bx');
scatter(TmorbD,PbmorbD,'b*');
scatter(TnemorbA,PbnemorbA,'co');
```

```
scatter(TnemorbC,PbnemorbC,'cx');
scatter(TnemorbD,PbnemorbD,'c*');
scatter(TemorbA,PbemorbA,'go');
scatter(TemorbB,PbemorbB,'g+');
scatter(TemorbC,PbemorbC,'gx');
scatter(TemorbD,PbemorbD,'g*');
scatter(TumafA,PbumafA,'mo');
scatter(TumafB,PbumafB,'m+');
scatter(TumafC,PbumafC,'mx');
scatter(TumafD,PbumafD,'m*');
hold off
xlabel('Fluid Temp, °C'); ylabel('Pb
Concentration, g m^-^3');ylim([0 inf]);
%% plot Co
figure;
scatter3(pHbascA,TbascA,CobascA,'ko');
hold on
scatter3(pHbascB,TbascB,CobascB,'k+');
scatter3(pHbascC,TbascC,CobascC,'kx');
scatter3(pHbascD,TbascD,CobascD,'k*');
scatter3(pHmsedA,TmsedA,ComsedA,'ro');
scatter3(pHmsedD,TmsedD,ComsedD,'r*');
scatter3(pHmorbA,TmorbA,ComorbA,'bo');
scatter3(pHmorbB,TmorbB,ComorbB,'b+');
scatter3(pHmorbC,TmorbC,ComorbC,'bx');
scatter3(pHmorbD,TmorbD,ComorbD,'b*');
scatter3(pHnemorbA,TnemorbA,ConemorbA,'co');
scatter3(pHnemorbC,TnemorbC,ConemorbC,'cx');
scatter3(pHnemorbD,TnemorbD,ConemorbD,'c*');
scatter3(pHemorbA,TemorbA,CoemorbA,'go');
scatter3(pHemorbB,TemorbB,CoemorbB,'g+');
scatter3(pHemorbC,TemorbC,CoemorbC,'gx');
scatter3(pHemorbD,TemorbD,CoemorbD,'g*');
```

```
scatter3(pHumafA,TumafA,CoumafA,'mo');
scatter3(pHumafB,TumafB,CoumafB,'m+');
scatter3(pHumafC,TumafC,CoumafC,'mx');
scatter3(pHumafD,TumafD,CoumafD,'m*');
hold off
set (gca,'Xdir','reverse'); xlim([2 8]);
zlim([0 inf]);
xlabel('Fluid pH'); ylabel('Fluid Temp,
°C');zlabel('Co Concentration, g m^-^3');
%ph
figure;
scatter(pHbascA,CobascA,'ko');
hold on
scatter(pHbascB,CobascB,'k+');
scatter(pHbascC,CobascC,'kx');
scatter(pHbascD,CobascD,'k*');
scatter(pHmsedA,ComsedA,'ro');
scatter(pHmsedD,ComsedD,'r*');
scatter(pHmorbA,ComorbA,'bo');
scatter(pHmorbB,ComorbB,'b+');
scatter(pHmorbC,ComorbC,'bx');
scatter(pHmorbD,ComorbD,'b*');
scatter(pHnemorbA,ConemorbA,'co');
scatter(pHnemorbC,ConemorbC,'cx');
scatter(pHnemorbD,ConemorbD,'c*');
scatter(pHemorbA,CoemorbA,'go');
scatter(pHemorbB,CoemorbB,'g+');
scatter(pHemorbC,CoemorbC,'gx');
scatter(pHemorbD,CoemorbD,'g*');
scatter(pHumafA,CoumafA,'mo');
scatter(pHumafB,CoumafB,'m+');
scatter(pHumafC,CoumafC,'mx');
scatter(pHumafD,CoumafD,'m*');
```

```
hold off
set (gca,'Xdir','reverse'); xlim([2 8]);
ylim([0 inf]);
xlabel('Fluid pH'); ylabel('Co Concentration,
g m^-^3');
%temp
figure;
scatter(TbascA,CobascA,'ko');
hold on
scatter(TbascB,CobascB,'k+');
scatter(TbascC,CobascC,'kx');
scatter(TbascD,CobascD,'k*');
scatter(TmsedA,ComsedA,'ro');
scatter(TmsedD,ComsedD,'r*');
scatter(TmorbA,ComorbA,'bo');
scatter(TmorbB,ComorbB,'b+');
scatter(TmorbC,ComorbC,'bx');
scatter(TmorbD,ComorbD,'b*');
scatter(TnemorbA,ConemorbA,'co');
scatter(TnemorbC,ConemorbC,'cx');
scatter(TnemorbD,ConemorbD,'c*');
scatter(TemorbA,CoemorbA,'go');
scatter(TemorbB,CoemorbB,'g+');
scatter(TemorbC,CoemorbC,'gx');
scatter(TemorbD,CoemorbD,'g*');
scatter(TumafA,CoumafA,'mo');
scatter(TumafB,CoumafB,'m+');
scatter(TumafC,CoumafC,'mx');
scatter(TumafD,CoumafD,'m*');
hold off
xlabel('Fluid Temp, °C'); ylabel('Co
Concentration, g m^-^3');ylim([0 inf]);
%% plot REE
```

```
figure;
scatter3(pHbascA,TbascA,REEbascA,'ko');
hold on
scatter3(pHbascB,TbascB,REEbascB,'k+');
scatter3(pHbascC,TbascC,REEbascC,'kx');
scatter3(pHbascD,TbascD,REEbascD,'k*');
scatter3(pHmsedA,TmsedA,REEmsedA,'ro');
scatter3(pHmsedD,TmsedD,REEmsedD,'r*');
scatter3(pHmorbA,TmorbA,REEmorbA,'bo');
scatter3(pHmorbB,TmorbB,REEmorbB,'b+');
scatter3(pHmorbC,TmorbC,REEmorbC,'bx');
scatter3(pHmorbD,TmorbD,REEmorbD,'b*');
scatter3(pHnemorbA,TnemorbA,REEnemorbA,'co');
scatter3(pHnemorbC,TnemorbC,REEnemorbC,'cx');
scatter3(pHnemorbD,TnemorbD,REEnemorbD,'c*');
scatter3(pHemorbA,TemorbA,REEemorbA,'go');
scatter3(pHemorbB,TemorbB,REEemorbB,'g+');
scatter3(pHemorbC,TemorbC,REEemorbC,'gx');
scatter3(pHemorbD,TemorbD,REEemorbD,'g*');
scatter3(pHumafA,TumafA,REEumafA,'mo');
scatter3(pHumafB,TumafB,REEumafB,'m+');
scatter3(pHumafC,TumafC,REEumafC,'mx');
scatter3(pHumafD,TumafD,REEumafD,'m*');
hold off
set (gca,'Xdir','reverse'); xlim([2 8]);
zlim([0 inf]);
xlabel('Fluid pH'); ylabel('Fluid Temp,
°C');zlabel('REE concentration, g m^-^3');
%ph
figure;
scatter(pHbascA,CobascA,'ko');
hold on
scatter(pHbascB,REEbascB,'k+');
```

```
scatter(pHbascC,REEbascC,'kx');
scatter(pHbascD,REEbascD,'k*');
scatter(pHmsedA,REEmsedA,'ro');
scatter(pHmsedD,REEmsedD,'r*');
scatter(pHmorbA,REEmorbA,'bo');
scatter(pHmorbB,REEmorbB,'b+');
scatter(pHmorbC,REEmorbC,'bx');
scatter(pHmorbD,REEmorbD,'b*');
scatter(pHnemorbA,REEnemorbA,'co');
scatter(pHnemorbC,REEnemorbC,'cx');
scatter(pHnemorbD,REEnemorbD,'c*');
scatter(pHemorbA,REEemorbA,'go');
scatter(pHemorbB,REEemorbB,'g+');
scatter(pHemorbC,REEemorbC,'gx');
scatter(pHemorbD,REEemorbD,'g*');
scatter(pHumafA,REEumafA,'mo');
scatter(pHumafB,REEumafB,'m+');
scatter(pHumafC,REEumafC,'mx');
scatter(pHumafD,REEumafD,'m*');
hold off
set (gca,'Xdir','reverse'); xlim([2 8]);
ylim([0 inf]);
xlabel('Fluid pH'); ylabel('REE
Concentration, g m^-^3');
%temp
figure;
scatter(TbascA,REEbascA,'ko');
hold on
scatter(TbascB,REEbascB,'k+');
scatter(TbascC,REEbascC,'kx');
scatter(TbascD,REEbascD,'k*');
scatter(TmsedA,REEmsedA,'ro');
scatter(TmsedD,REEmsedD,'r*');
```

```
scatter(TmorbA,REEmorbA,'bo');
scatter(TmorbB,REEmorbB,'b+');
scatter(TmorbC,REEmorbC,'bx');
scatter(TmorbD,REEmorbD,'b*');
scatter(TnemorbA,REEnemorbA,'co');
scatter(TnemorbC,REEnemorbC,'cx');
scatter(TnemorbD,REEnemorbD,'c*');
scatter(TemorbA,REEemorbA,'go');
scatter(TemorbB,REEemorbB,'g+');
scatter(TemorbC,REEemorbC,'gx');
scatter(TemorbD,REEemorbD,'g*');
scatter(TumafA,REEumafA,'mo');
scatter(TumafB,REEumafB,'m+');
scatter(TumafC,REEumafC,'mx');
scatter(TumafD,REEumafD,'m*');
hold off
xlabel('Fluid Temp, °C'); ylabel('REE
Concentration, g m^-^3');ylim([0 inf]);
%% plot dist
figure;
scatter(TbascA,pHbascA,'ko');
hold on
scatter(TbascB,pHbascB,'k+');
scatter(TbascC,pHbascC,'kx');
scatter(TbascD,pHbascD,'k*');
scatter(TmsedA,pHmsedA,'ro');
scatter(TmsedD,pHmsedD,'r*');
scatter(TmorbA,pHmorbA,'bo');
scatter(TmorbB,pHmorbB,'b+');
scatter(TmorbC,pHmorbC,'bx');
scatter(TmorbD,pHmorbD,'b*');
scatter(TnemorbA,pHemorbA,'co');
scatter(TnemorbC,pHnemorbC,'cx');
```

```
scatter(TnemorbD,pHnemorbD,'c*');
scatter(TemorbA,pHemorbA,'go');
scatter(TemorbB,pHemorbB,'g+');
scatter(TemorbC,pHemorbC,'gx');
scatter(TemorbD,pHemorbD,'g*');
scatter(TumafA,pHumafA,'mo');
scatter(TumafB,pHumafB,'m+');
scatter(TumafC,pHumafC,'mx');
scatter(TumafD,pHmafD,'m*');
hold off
ylabel('Fluid pH'); xlabel('Fluid Temp, °C');
set (gca,'ydir','reverse'); ylim([2 8]);
%zlim
```

CODE FOR FLUID-DEPOSIT TREND PLOTS

```
clc;close all;clear all;
set(groot,'defaultLineMarkerSize',10);
%% load Au
%no Au Fluid data
%% load Ag
%no Ag fluid data
%% As
%no As fluid data
%% load B
%insuf
BA =
xlsread('graphrelchimn.xlsx','B','C3:C28');
BB =
xlsread('graphrelchimn.xlsx','B','D3:D28');
BC =
xlsread('graphrelchimn.xlsx','B','E3:E28');
BD =
xlsread('graphrelchimn.xlsx','B','F3:F28');
B0 =
xlsread('graphrelchimn.xlsx','B','I3:I28');
figure;
scatter(B0,BA,'filled','k');
hold on;
scatter(B0,BB,'filled','b');
scatter(B0,BC,'filled','r');
scatter(B0,BD,'filled','g');
hold off
pbaspect([1.5 1 1]);
xlim([0 inf]);ylim([0 inf]);
xlabel('Fluid B Concentration, g/T');
ylabel('Deposit B Concentation, kg/T');
%% load Ba
```

```
BaA =
xlsread('graphrelchimn.xlsx','Ba','C3:C28');
BaB =
xlsread('graphrelchimn.xlsx','Ba','D3:D28');
BaC =
xlsread('graphrelchimn.xlsx','Ba','E3:E28');
BaD =
xlsread('graphrelchimn.xlsx','Ba','F3:F28');
Ba0 =
xlsread('graphrelchimn.xlsx','Ba','I3:I28');
figure;
scatter(Ba0,BaA,'filled','k');
hold on;
%scatter(Ba0,BaB,'filled','b');
scatter(Ba0,BaC,'filled','r');
%scatter(Ba0,BaD,'filled','g');
hold off;
pbaspect([1.5 1 1]);
xlim([0 inf]);ylim([0 inf]);
xlabel('Fluid Ba Concentration, g/T');
ylabel('Deposit Ba Concentation, kg/T');
%% load Br
BrA =
xlsread('graphrelchimn.xlsx','Br','C3:C28');
BrB =
xlsread('graphrelchimn.xlsx','Br','D3:D28');
BrC =
xlsread('graphrelchimn.xlsx','Br','E3:E28');
BrD =
xlsread('graphrelchimn.xlsx','Br','F3:F28');
Br0 =
xlsread('graphrelchimn.xlsx','Br','I3:I28');
figure;
```

```
scatter(Br0,BrA,'filled','k');
hold on;
%scatter(Br0,BrB,'filled','b');
scatter(Br0,BrC,'filled','r');
%scatter(Br0,BrD,'filled','g');
brx=0:90;
bry1=(0.0003*(2.71828.^(0.0579*brx)));
bry2=(0.0018*(2.71828.^(0.0305*brx)));
bry3=0.0003*brx
plot(brx,bry1,'k-');
plot(brx,bry2,'r--');
plot(brx,bry3,'r--');
hold off;
pbaspect([1.5 1 1]);
xlim([0 inf]);ylim([0 inf]);
xlabel('Fluid Br Concentration, g/T');
ylabel('Deposit Br Concentation, kg/T');
%% load Ca
CaA =
xlsread('graphrelchimn.xlsx','Ca','C3:C28');
CaB =
xlsread('graphrelchimn.xlsx','Ca','D3:D28');
CaC =
xlsread('graphrelchimn.xlsx','Ca','E3:E28');
CaD =
xlsread('graphrelchimn.xlsx','Ca','F3:F28');
Ca0 =
xlsread('graphrelchimn.xlsx','Ca','I3:I28');
figure;
scatter(Ca0,CaA,'filled','k');
hold on;
scatter(Ca0,CaB,'filled','b');
scatter(Ca0,CaC,'filled','r');
```

```
%scatter(Ca0,CaD,'filled','g');
Cax = 0:3500
Ca1y = 0.051*Cax
Ca2y = 0.084*Cax
Ca3y = 0.0184*Cax
plot(Cax,Ca1y,'k-');
plot(Cax,Ca2y,'b-');
plot(Cax,Ca3y,'r-');
hold off
pbaspect([1.5 1 1]);
xlim([0 inf]);ylim([0 inf]);
xlabel('Fluid Ca Concentration, g/T');
ylabel('Deposit Ca Concentation, kg/T');
%% load Cd
CdA =
xlsread('graphrelchimn.xlsx','Cd','C3:C28');
CdB =
xlsread('graphrelchimn.xlsx','Cd','D3:D28');
CdC =
xlsread('graphrelchimn.xlsx','Cd','E3:E28');
CdD =
xlsread('graphrelchimn.xlsx','Cd','F3:F28');
Cd0 =
xlsread('graphrelchimn.xlsx','Cd','I3:I28');
figure;
scatter(Cd0,CdA,'filled','k');
hold on;
%scatter(Cd0,CdB,'filled','b');
scatter(Cd0,CdC,'filled','r');
%scatter(Cd0,CdD,'filled','g');
Cdx = 0:1;
Cdy = 9.5313*Cdx;
plot(Cdx,Cdy,'k-');
```

```
hold off;
pbaspect([1.5 1 1]);
xlim([0 inf]);ylim([0 inf]);
xlabel('Fluid Cd Concentration, g/T');
ylabel('Deposit Cd Concentation, kg/T');
%% load Ce
% one datapoint
%CeA =
xlsread('graphrelchimn.xlsx','Ce','C3:C28');
%CeB =
xlsread('graphrelchimn.xlsx','Ce','D3:D28');
%CeC =
xlsread('graphrelchimn.xlsx','Ce','E3:E28');
%CeD =
xlsread('graphrelchimn.xlsx','Ce','F3:F28');
%Ce0 =
xlsread('graphrelchimn.xlsx','Ce','I3:I28');
%figure;
%scatter(Ce0,CeA,'filled','k');
%hold on;
%scatter(Ce0,CeB,'filled','b');
%scatter(Ce0,CeC,'filled','r');
%scatter(Ce0,CeD,'filled','g');
%hold off
%xlim([0 inf]);ylim([0 inf]);
%xlabel('Fluid Ce Concentration, g/T');
ylabel('Deposit Ce Concentation, kg/T');
%% load Cl
ClA =
xlsread('graphrelchimn.xlsx','Cl','C3:C28');
ClB =
xlsread('graphrelchimn.xlsx','Cl','D3:D28');
```

```
ClC =
xlsread('graphrelchimn.xlsx','Cl','E3:E28');
ClD =
xlsread('graphrelchimn.xlsx','Cl','F3:F28');
Cl0 =
xlsread('graphrelchimn.xlsx','Cl','I3:I28');
figure;
scatter(Cl0,ClA,'filled','k');
hold on;
scatter(Cl0,ClB,'filled','b');
scatter(Cl0,ClC,'filled','r');
scatter(Cl0,ClD,'filled','g');
hold off;
pbaspect([1.5 1 1]);
xlim([0 inf]);ylim([0 inf]);
xlabel('Fluid Cl Concentration, g/T');
ylabel('Deposit Cl Concentation, kg/T');
%% load Co
CoA =
xlsread('graphrelchimn.xlsx','Co','C3:C28');
CoB =
xlsread('graphrelchimn.xlsx','Co','D3:D28');
CoC =
xlsread('graphrelchimn.xlsx','Co','E3:E28');
CoD =
xlsread('graphrelchimn.xlsx','Co','F3:F28');
Co0 =
xlsread('graphrelchimn.xlsx','Co','I3:I28');
figure;
scatter(Co0,CoA,'filled','k');
hold on;
%scatter(Co0,CoB,'filled','b');
scatter(Co0,CoC,'filled','r');
```

```
%scatter(Co0,CoD,'filled','g');
hold off;
pbaspect([1.5 1 1]);
xlim([0 inf]);ylim([0 inf]);
xlabel('Fluid Co Concentration, g/T');
ylabel('Deposit Co Concentation, kg/T');
%% load Cs
CsA =
xlsread('graphrelchimn.xlsx','Cs','C3:C28');
CsB =
xlsread('graphrelchimn.xlsx','Cs','D3:D28');
CsC =
xlsread('graphrelchimn.xlsx','Cs','E3:E28');
CsD =
xlsread('graphrelchimn.xlsx','Cs','F3:F28');
Cs0 =
xlsread('graphrelchimn.xlsx','Cs','I3:I28');
figure;
%scatter(Cs0,CsA,'filled','k');
%hold on;
%scatter(Cs0,CsB,'filled','b');
scatter(Cs0,CsC,'filled','r');
%scatter(Cs0,CsD,'filled','g');
hold off;
pbaspect([1.5 1 1]);
xlim([0 inf]);ylim([0 inf]);
xlabel('Fluid Cs Concentration, g/T');
ylabel('Deposit Cs Concentation, kg/T');
%% load Cu
CuA =
xlsread('graphrelchimn.xlsx','Cu','C3:C28');
CuB =
xlsread('graphrelchimn.xlsx','Cu','D3:D28');
```

```
CuC =
xlsread('graphrelchimn.xlsx','Cu','E3:E28');
CuD =
xlsread('graphrelchimn.xlsx','Cu','F3:F28');
Cu0 =
xlsread('graphrelchimn.xlsx','Cu','I3:I28');
figure;
scatter(Cu0,CuA,'filled','k');
hold on;
scatter(Cu0,CuB,'filled','b');
scatter(Cu0,CuC,'filled','r');
%scatter(Cu0,CuD,'filled','g');
Cux = 0:20;
Cuy1 = 6.7573*Cux;
Cuy2 = 41.10*Cux;
plot(Cux,Cuy1,'k-');
plot(Cux,Cuy2,'k--');
hold off;
pbaspect([1.5 1 1]);
xlim([0 inf]);ylim([0 inf]);
xlabel('Fluid Cu Concentration, g/T');
ylabel('Deposit Cu Concentation, kg/T');
%% load Dy
% no datapoints
%DyA =
xlsread('graphrelchimn.xlsx','Dy','C3:C28');
%DyB =
xlsread('graphrelchimn.xlsx','Dy','D3:D28');
%DyC =
xlsread('graphrelchimn.xlsx','Dy','E3:E28');
%DyD =
xlsread('graphrelchimn.xlsx','Dy','F3:F28');
```

```
%Dy0 =
xlsread('graphrelchimn.xlsx','Dy','I3:I28');
%figure;
%scatter(Dy0,DyA,'filled','k');
%hold on;
%scatter(Dy0,DyB,'filled','b');
%scatter(Dy0,DyC,'filled','r');
%scatter(Dy0,DyD,'filled','g');
%hold off
%xlim([0 inf]);ylim([0 inf]);
%xlabel('Fluid Dy Concentration, g/T');
ylabel('Deposit Dy Concentation, kg/T');
%% load Er
% no datapoints
%ErA =
xlsread('graphrelchimn.xlsx','Er','C3:C28');
%ErB =
xlsread('graphrelchimn.xlsx','Er','D3:D28');
%ErC =
xlsread('graphrelchimn.xlsx','Er','E3:E28');
%ErD =
xlsread('graphrelchimn.xlsx','Er','F3:F28');
%Er0 =
xlsread('graphrelchimn.xlsx','Er','I3:I28');
%figure;
%scatter(Er0,ErA,'filled','k');
%hold on;
%scatter(Er0,ErB,'filled','b');
%scatter(Er0,ErC,'filled','r');
%scatter(Er0,ErD,'filled','g');
%hold off
%xlim([0 inf]);ylim([0 inf]);
```

```
%xlabel('Fluid Er Concentration, g/T');
ylabel('Deposit Er Concentation, kg/T');
%% load Eu
% only one datapoint
%EuA =
xlsread('graphrelchimn.xlsx','Eu','C3:C28');
%EuB =
xlsread('graphrelchimn.xlsx','Eu','D3:D28');
%EuC =
xlsread('graphrelchimn.xlsx','Eu','E3:E28');
%EuD =
xlsread('graphrelchimn.xlsx','Eu','F3:F28');
%Eu0 =
xlsread('graphrelchimn.xlsx','Eu','I3:I28');
%figure;
%scatter(Eu0,EuA,'filled','k');
%hold on;
%scatter(Eu0,EuB,'filled','b');
%scatter(Eu0,EuC,'filled','r');
%scatter(Eu0,EuD,'filled','g');
%hold off
%xlim([0 inf]);ylim([0 inf]);
%xlabel('Fluid Eu Concentration, g/T');
ylabel('Deposit Eu Concentation, kg/T');
%% load Fe
FeA =
xlsread('graphrelchimn.xlsx','Fe','C3:C28');
FeB =
xlsread('graphrelchimn.xlsx','Fe','D3:D28');
FeC =
xlsread('graphrelchimn.xlsx','Fe','E3:E28');
FeD =
xlsread('graphrelchimn.xlsx','Fe','F3:F28');
```

```
Fe0 =
xlsread('graphrelchimn.xlsx','Fe','I3:I28');
figure;
scatter(Fe0,FeA,'filled','k');
hold on;
scatter(Fe0,FeB,'filled','b');
scatter(Fe0,FeC,'filled','r');
%scatter(Fe0,FeD,'filled','g');
Fex = 0:1000;
Fey = 0.9146*Fex;
plot(Fex,Fey,'k-');
hold off;
pbaspect([1.5 1 1]);
xlim([0 inf]);ylim([0 inf]);
xlabel('Fluid Fe Concentration, g/T');
ylabel('Deposit Fe Concentation, kg/T');
%% load Gd
% no data
% GdA =
xlsread('graphrelchimn.xlsx','Gd','C3:C28');
%GdB =
xlsread('graphrelchimn.xlsx','Gd','D3:D28');
%GdC =
xlsread('graphrelchimn.xlsx','Gd','E3:E28');
%GdD =
xlsread('graphrelchimn.xlsx','Gd','F3:F28');
%Gd0 =
xlsread('graphrelchimn.xlsx','Gd','I3:I28');
%figure;
%scatter(Gd0,GdA,'filled','k');
%hold on;
%scatter(Gd0,GdB,'filled','b');
%scatter(Gd0,GdC,'filled','r');
```

```
%scatter(Gd0,GdD,'filled','g');
%hold off
%xlim([0 inf]);ylim([0 inf]);
%xlabel('Fluid Gd Concentration, g/T');
ylabel('Deposit Gd Concentation, kg/T');
%% load Hf
% no data
%HfA =
xlsread('graphrelchimn.xlsx','Hf','C3:C28');
%HfB =
xlsread('graphrelchimn.xlsx','Hf','D3:D28');
%HfC =
xlsread('graphrelchimn.xlsx','Hf','E3:E28');
%HfD =
xlsread('graphrelchimn.xlsx','Hf','F3:F28');
%Hf0 =
xlsread('graphrelchimn.xlsx','Hf','I3:I28');
%figure;
%scatter(Hf0,HfA,'filled','k');
%hold on;
%scatter(Hf0,HfB,'filled','b');
%scatter(Hf0,HfC,'filled','r');
%scatter(Hf0,HfD,'filled','g');
%hold off
%xlim([0 inf]);ylim([0 inf]);
%xlabel('Fluid Hf Concentration, g/T');
ylabel('Deposit Hf Concentation, kg/T');
%% load Hg
% No data
% HgA =
xlsread('graphrelchimn.xlsx','Hg','C3:C28');
% HgB =
xlsread('graphrelchimn.xlsx','Hg','D3:D28');
```

```
% HgC =
xlsread('graphrelchimn.xlsx','Hg','E3:E28');
% HgD =
xlsread('graphrelchimn.xlsx','Hg','F3:F28');
% Hg0 =
xlsread('graphrelchimn.xlsx','Hg','I3:I28');
% figure;
% scatter(Hg0,HgA,'filled','k');
% hold on;
% scatter(Hg0,HgB,'filled','b');
% scatter(Hg0,HgC,'filled','r');
% scatter(Hg0,HgD,'filled','g');
% hold off
% xlim([0 inf]);ylim([0 inf]);
% xlabel('Fluid Hg Concentration, g/T');
ylabel('Deposit Hg Concentation, kg/T');
%% load Ho
% no data
% HoA =
xlsread('graphrelchimn.xlsx','Ho','C3:C28');
% HoB =
xlsread('graphrelchimn.xlsx','Ho','D3:D28');
% HoC =
xlsread('graphrelchimn.xlsx','Ho','E3:E28');
% HoD =
xlsread('graphrelchimn.xlsx','Ho','F3:F28');
%Ho0 =
xlsread('graphrelchimn.xlsx','Ho','I3:I28');
%figure;
%scatter(Ho0,HoA,'filled','k');
%hold on;
%scatter(Ho0,HoB,'filled','b');
%scatter(Ho0,HoC,'filled','r');
```

```
%scatter(Ho0,HoD,'filled','g');
%hold off
%xlim([0 inf]);ylim([0 inf]);
%xlabel('Fluid Ho Concentration, g/T');
ylabel('Deposit Ho Concentation, kg/T');
%% load La
% insufficent data
%LaA =
xlsread('graphrelchimn.xlsx','La','C3:C28');
%LaB =
xlsread('graphrelchimn.xlsx','La','D3:D28');
%LaC =
xlsread('graphrelchimn.xlsx','La','E3:E28');
%LaD =
xlsread('graphrelchimn.xlsx','La','F3:F28');
%La0 =
xlsread('graphrelchimn.xlsx','La','I3:I28');
%figure;
%scatter(La0,LaA,'filled','k');
%hold on;
%scatter(La0,LaB,'filled','b');
%scatter(La0,LaC,'filled','r');
%scatter(La0,LaD,'filled','g');
%hold off
%xlim([0 inf]);ylim([0 inf]);
%xlabel('Fluid La Concentration, g/T');
ylabel('Deposit La Concentation, kg/T');
%% load Li
LiA =
xlsread('graphrelchimn.xlsx','Li','C3:C28');
LiB =
xlsread('graphrelchimn.xlsx','Li','D3:D28');
```

```
LiC =
xlsread('graphrelchimn.xlsx','Li','E3:E28');
LiD =
xlsread('graphrelchimn.xlsx','Li','F3:F28');
Li0 =
xlsread('graphrelchimn.xlsx','Li','I3:I28');
figure;
scatter(Li0,LiA,'filled','k');
hold on;
scatter(Li0,LiB,'filled','b');
scatter(Li0,LiC,'filled','r');
scatter(Li0,LiD,'filled','g');
hold off
xlim([0 inf]);ylim([0 inf]);
xlabel('Fluid Li Concentration, g/T');
ylabel('Deposit Li Concentation, kg/T');
%% load Lu
LuA =
xlsread('graphrelchimn.xlsx','Lu','C3:C28');
LuB =
xlsread('graphrelchimn.xlsx','Lu','D3:D28');
LuC =
xlsread('graphrelchimn.xlsx','Lu','E3:E28');
LuD =
xlsread('graphrelchimn.xlsx','Lu','F3:F28');
Lu0 =
xlsread('graphrelchimn.xlsx','Lu','I3:I28');
figure;
scatter(Lu0,LuA,'filled','k');
hold on;
scatter(Lu0,LuB,'filled','b');
scatter(Lu0,LuC,'filled','r');
scatter(Lu0,LuD,'filled','g');
```

```
hold off
xlim([0 inf]);ylim([0 inf]);
xlabel('Fluid Lu Concentration, g/T');
ylabel('Deposit Lu Concentation, kg/T');
%% load Mn
MnA =
xlsread('graphrelchimn.xlsx','Mn','C3:C28');
MnB =
xlsread('graphrelchimn.xlsx','Mn','D3:D28');
MnC =
xlsread('graphrelchimn.xlsx','Mn','E3:E28');
MnD =
xlsread('graphrelchimn.xlsx','Mn','F3:F28');
Mn0 =
xlsread('graphrelchimn.xlsx','Mn','I3:I28');
figure;
scatter(Mn0,MnA,'filled','k');
hold on;
scatter(Mn0,MnB,'filled','b');
scatter(Mn0,MnC,'filled','r');
%scatter(Mn0,MnD,'filled','g');
hold off;
pbaspect([1.5 1 1]);
xlim([0 inf]);ylim([0 inf]);
xlabel('Fluid Mn Concentration, g/T');
ylabel('Deposit Mn Concentation, kg/T');
%% load Mo
MoA =
xlsread('graphrelchimn.xlsx','Mo','C3:C28');
MoB =
xlsread('graphrelchimn.xlsx','Mo','D3:D28');
MoC =
xlsread('graphrelchimn.xlsx','Mo','E3:E28');
```

```
MoD =
xlsread('graphrelchimn.xlsx','Mo','F3:F28');
Mo0 =
xlsread('graphrelchimn.xlsx','Mo','I3:I28');
figure;
scatter(Mo0,MoA,'filled','k');
hold on;
scatter(Mo0,MoB,'filled','b');
scatter(Mo0,MoC,'filled','r');
scatter(Mo0,MoD,'filled','g');
hold off
xlim([0 inf]);ylim([0 inf]);
xlabel('Fluid Mo Concentration, g/T');
ylabel('Deposit Mo Concentation, kg/T');
%% load Nb
% insuf data
NbA =
xlsread('graphrelchimn.xlsx','Nb','C3:C28');
NbB =
xlsread('graphrelchimn.xlsx','Nb','D3:D28');
NbC =
xlsread('graphrelchimn.xlsx','Nb','E3:E28');
NbD =
xlsread('graphrelchimn.xlsx','Nb','F3:F28');
Nb0 =
xlsread('graphrelchimn.xlsx','Nb','I3:I28');
figure;
scatter(Nb0,NbA,'filled','k');
hold on;
scatter(Nb0,NbB,'filled','b');
scatter(Nb0,NbC,'filled','r');
scatter(Nb0,NbD,'filled','g');
hold off
```

```
xlim([0 inf]);ylim([0 inf]);
xlabel('Fluid Nb Concentration, g/T');
ylabel('Deposit Nb Concentation, kg/T');
%% load Ni
%insuf data
NiA =
xlsread('graphrelchimn.xlsx','Ni','C3:C28');
NiB =
xlsread('graphrelchimn.xlsx','Ni','D3:D28');
NiC =
xlsread('graphrelchimn.xlsx','Ni','E3:E28');
NiD =
xlsread('graphrelchimn.xlsx','Ni','F3:F28');
Ni0 =
xlsread('graphrelchimn.xlsx','Ni','I3:I28');
figure;
scatter(Ni0,NiA,'filled','k');
hold on;
scatter(Ni0,NiB,'filled','b');
scatter(Ni0,NiC,'filled','r');
scatter(Ni0,NiD,'filled','g');
hold off
xlim([0 inf]);ylim([0 inf]);
xlabel('Fluid Ni Concentration, g/T');
ylabel('Deposit Ni Concentation, kg/T');
%% load Pb
PbA =
xlsread('graphrelchimn.xlsx','Pb','C3:C28');
PbB =
xlsread('graphrelchimn.xlsx','Pb','D3:D28');
PbC =
xlsread('graphrelchimn.xlsx','Pb','E3:E28');
```

```
PbD =
xlsread('graphrelchimn.xlsx','Pb','F3:F28');
Pb0 =
xlsread('graphrelchimn.xlsx','Pb','I3:I28');
figure;
scatter(Pb0,PbA,'filled','k');
hold on;
scatter(Pb0,PbB,'filled','b');
scatter(Pb0,PbC,'filled','r');
scatter(Pb0,PbD,'filled','g');
hold off
xlim([0 inf]);ylim([0 inf]);
xlabel('Fluid Pb Concentration, g/T');
ylabel('Deposit Pb Concentation, kg/T');
%% load Pd
%no data
PdA =
xlsread('graphrelchimn.xlsx','Pd','C3:C28');
PdB =
xlsread('graphrelchimn.xlsx','Pd','D3:D28');
PdC =
xlsread('graphrelchimn.xlsx','Pd','E3:E28');
PdD =
xlsread('graphrelchimn.xlsx','Pd','F3:F28');
Pd0 =
xlsread('graphrelchimn.xlsx','Pd','I3:I28');
figure;
scatter(Pd0,PdA,'filled','k');
hold on;
scatter(Pd0,PdB,'filled','b');
scatter(Pd0,PdC,'filled','r');
scatter(Pd0,PdD,'filled','g');
hold off
```

```
xlim([0 inf]);ylim([0 inf]);
xlabel('Fluid Pd Concentration, g/T');
ylabel('Deposit Pd Concentation, kg/T');
%% load Pr
%no data
PrA =
xlsread('graphrelchimn.xlsx','Pr','C3:C28');
PrB =
xlsread('graphrelchimn.xlsx','Pr','D3:D28');
PrC =
xlsread('graphrelchimn.xlsx','Pr','E3:E28');
PrD =
xlsread('graphrelchimn.xlsx','Pr','F3:F28');
Pr0 =
xlsread('graphrelchimn.xlsx','Pr','I3:I28');
figure;
scatter(Pr0,PrA,'filled','k');
hold on;
scatter(Pr0,PrB,'filled','b');
scatter(Pr0,PrC,'filled','r');
scatter(Pr0,PrD,'filled','g');
hold off
xlim([0 inf]);ylim([0 inf]);
xlabel('Fluid Pr Concentration, g/T');
ylabel('Deposit Pr Concentation, kg/T');
%% load Rb
RbA =
xlsread('graphrelchimn.xlsx','Rb','C3:C28');
RbB =
xlsread('graphrelchimn.xlsx','Rb','D3:D28');
RbC =
xlsread('graphrelchimn.xlsx','Rb','E3:E28');
```

```
RbD =
xlsread('graphrelchimn.xlsx','Rb','F3:F28');
Rb0 =
xlsread('graphrelchimn.xlsx','Rb','I3:I28');
figure;
scatter(Rb0,RbA,'filled','k');
hold on;
scatter(Rb0,RbB,'filled','b');
scatter(Rb0,RbC,'filled','r');
scatter(Rb0,RbD,'filled','g');
hold off
xlim([0 inf]);ylim([0 inf]);
xlabel('Fluid Rb Concentration, g/T');
ylabel('Deposit Rb Concentation, kg/T');
%% load Sm
%insuf data
SmA =
xlsread('graphrelchimn.xlsx','Sm','C3:C28');
SmB =
xlsread('graphrelchimn.xlsx','Sm','D3:D28');
SmC =
xlsread('graphrelchimn.xlsx','Sm','E3:E28');
SmD =
xlsread('graphrelchimn.xlsx','Sm','F3:F28');
Sm0 =
xlsread('graphrelchimn.xlsx','Sm','I3:I28');
figure;
scatter(Sm0,SmA,'filled','k');
hold on;
scatter(Sm0,SmB,'filled','b');
scatter(Sm0,SmC,'filled','r');
scatter(Sm0,SmD,'filled','g');
hold off
```

```
xlim([0 inf]);ylim([0 inf]);
xlabel('Fluid Sm Concentration, g/T');
ylabel('Deposit Sm Concentation, kg/T');
%% load Sr
SrA =
xlsread('graphrelchimn.xlsx','Sr','C3:C28');
SrB =
xlsread('graphrelchimn.xlsx','Sr','D3:D28');
SrC =
xlsread('graphrelchimn.xlsx','Sr','E3:E28');
SrD =
xlsread('graphrelchimn.xlsx','Sr','F3:F28');
Sr0 =
xlsread('graphrelchimn.xlsx','Sr','I3:I28');
figure;
scatter(Sr0,SrA,'filled','k');
hold on;
scatter(Sr0,SrB,'filled','b');
scatter(Sr0,SrC,'filled','r');
scatter(Sr0,SrD,'filled','g');
hold off
xlim([0 inf]);ylim([0 inf]);
xlabel('Fluid Sr Concentration, g/T');
ylabel('Deposit Sr Concentation, kg/T');
%% load Ta
%no data
TaA =
xlsread('graphrelchimn.xlsx','Ta','C3:C28');
TaB =
xlsread('graphrelchimn.xlsx','Ta','D3:D28');
TaC =
xlsread('graphrelchimn.xlsx','Ta','E3:E28');
```

```
TaD =
xlsread('graphrelchimn.xlsx','Ta','F3:F28');
Ta0 =
xlsread('graphrelchimn.xlsx','Ta','I3:I28');
figure;
scatter(Ta0,TaA,'filled','k');
hold on;
scatter(Ta0,TaB,'filled','b');
scatter(Ta0,TaC,'filled','r');
scatter(Ta0,TaD,'filled','g');
hold off
xlim([0 inf]);ylim([0 inf]);
xlabel('Fluid Ta Concentration, g/T');
ylabel('Deposit Ta Concentation, kg/T');
%% load Tb
% no data
TbA =
xlsread('graphrelchimn.xlsx','Tb','C3:C28');
TbB =
xlsread('graphrelchimn.xlsx','Tb','D3:D28');
TbC =
xlsread('graphrelchimn.xlsx','Tb','E3:E28');
TbD =
xlsread('graphrelchimn.xlsx','Tb','F3:F28');
Tb0 =
xlsread('graphrelchimn.xlsx','Tb','I3:I28');
figure;
scatter(Tb0,TbA,'filled','k');
hold on;
scatter(Tb0,TbB,'filled','b');
scatter(Tb0,TbC,'filled','r');
scatter(Tb0,TbD,'filled','g');
hold off
```

```
xlim([0 inf]);ylim([0 inf]);
xlabel('Fluid Tb Concentration, g/T');
ylabel('Deposit Tb Concentation, kg/T');
%% load V
%insuf data
VA =
xlsread('graphrelchimn.xlsx','V','C3:C28');
VB =
xlsread('graphrelchimn.xlsx','V','D3:D28');
VC =
xlsread('graphrelchimn.xlsx','V','E3:E28');
VD =
xlsread('graphrelchimn.xlsx','V','F3:F28');
V0 =
xlsread('graphrelchimn.xlsx','V','I3:I28');
figure;
scatter(V0,VA,'filled','k');
hold on;
scatter(V0,VB,'filled','b');
scatter(V0,VC,'filled','r');
scatter(V0,VD,'filled','g');
hold off
xlim([0 inf]);ylim([0 inf]);
xlabel('Fluid V Concentration, g/T');
ylabel('Deposit V Concentation, kg/T');
%% load Y
%insuf data
YA =
xlsread('graphrelchimn.xlsx','Y','C3:C28');
YB =
xlsread('graphrelchimn.xlsx','Y','D3:D28');
YC =
xlsread('graphrelchimn.xlsx','Y','E3:E28');
```

```
YD =
xlsread('graphrelchimn.xlsx','Y','F3:F28');
Y0 =
xlsread('graphrelchimn.xlsx','Y','I3:I28');
figure;
scatter(Y0,YA,'filled','k');
hold on;
scatter(Y0,YB,'filled','b');
scatter(Y0,YC,'filled','r');
scatter(Y0,YD,'filled','g');
hold off
xlim([0 inf]);ylim([0 inf]);
xlabel('Fluid Y Concentration, g/T');
ylabel('Deposit Y Concentation, kg/T');
%% load Yb
%insuf data
YbA =
xlsread('graphrelchimn.xlsx','Yb','C3:C28');
YbB =
xlsread('graphrelchimn.xlsx','Yb','D3:D28');
YbC =
xlsread('graphrelchimn.xlsx','Yb','E3:E28');
YbD =
xlsread('graphrelchimn.xlsx','Yb','F3:F28');
Yb0 =
xlsread('graphrelchimn.xlsx','Yb','I3:I28');
figure;
scatter(Yb0,YbA,'filled','k');
hold on;
scatter(Yb0,YbB,'filled','b');
scatter(Yb0,YbC,'filled','r');
scatter(Yb0,YbD,'filled','g');
hold off
```

```
xlim([0 inf]);ylim([0 inf]);
xlabel('Fluid Yb Concentration, g/T');
ylabel('Deposit Yb Concentation, kg/T');
%% load Zn
ZnA =
xlsread('graphrelchimn.xlsx','Zn','C3:C28');
ZnB =
xlsread('graphrelchimn.xlsx','Zn','D3:D28');
ZnC =
xlsread('graphrelchimn.xlsx','Zn','E3:E28');
ZnD =
xlsread('graphrelchimn.xlsx','Zn','F3:F28');
Zn0 =
xlsread('graphrelchimn.xlsx','Zn','I3:I28');
figure;
scatter(Zn0,ZnA,'filled','k');
hold on
scatter(Zn0,ZnB,'filled','b');
scatter(Zn0,ZnC,'filled','r');
%scatter(Zn0,ZnD,'filled','g');
Znx1 = 0:25;
Zny1 = 10.071*Znx1;
Znx2 = 0:10;
Zny2 = 36.483*Znx2
plot(Znx1,Zny1,'k-');
plot(Znx2,Zny2,'k--');
hold off
pbaspect([1.5 1 1]);
xlim([0 inf]);ylim([0 inf]);
xlabel('Fluid Zn Concentration, g/T');
ylabel('Deposit Zn Concentation, kg/T');
```

CODE FOR DEPOSIT-DEPOSIT TREND PLOTS

```
clc;close all;clear all;
set(groot,'defaultLineMarkerSize',10);
%% load Fe/Mn
FeMnA = xlsread('graphrelchimn.xlsx','FeMn
Ratio','C3:C28');
FeMnB = xlsread('graphrelchimn.xlsx','FeMn
Ratio','D3:D28');
FeMnC = xlsread('graphrelchimn.xlsx','FeMn
Ratio','E3:E28');
FeMnD = xlsread('graphrelchimn.xlsx','FeMn
Ratio','F3:F28');
% Plot Fe/Mn
figure;
subplot(1,2,1);
scatter(FeMnA,FeMnB);
subplot(1,2,2);
scatter(FeMnC,FeMnB);
%% load Au
AuA =
xlsread('graphrelchimn.xlsx','Au','C3:C28');
AuB =
xlsread('graphrelchimn.xlsx','Au','D3:D28');
AuC =
xlsread('graphrelchimn.xlsx','Au','E3:E28');
AuD =
xlsread('graphrelchimn.xlsx','Au','F3:F28');
Au0 =
xlsread('graphrelchimn.xlsx','Au','I3:I28');
AuAx =
xlsread('graphrelchimnexc.xlsx','Au','C3:C28'
);
```

```
AuBx =
xlsread('graphrelchimnexc.xlsx','Au','D3:D28'
);
AuCx =
xlsread('graphrelchimnexc.xlsx','Au','E3:E28'
);
AuDx =
xlsread('graphrelchimnexc.xlsx','Au','F3:F28'
);
x = 0:1;
YAu1 = 0.3058*x;
YAu2 = 0.1148*x;
YAu3 = 0.3474*x;
YAu4 = 1.5246*x;
figure;
subplot(1,2,1);
scatter(AuA,AuB,'blue','filled');
hold on;
scatter(AuAx,AuBx,'black','filled');
hold on;
plot(x,YAu1,'blue');
hold on;
plot(x,YAu2,'black');
xlim([0 inf]);ylim([0 inf]);
pbaspect([1 1 1]);
xlabel('Chimney Au Conc. (kg/T)');
ylabel('Core Au Conc. (kg/T)');
subplot(1,2,2);
scatter(AuC,AuB,'blue','filled');
hold on;
scatter(AuCx,AuBx,'black','filled');
plot(x,YAu3,'black');
xlim([0 inf]);ylim([0 inf]);
```

```
hold on
plot(x,YAu4,'blue');
pbaspect([1 1 1])
hold off;
xlabel('Surface Au Conc. (kg/T)');
figure;
scatter(AuA,AuC,10,FeMnA,'filled');
%% load Ag
AgA =
xlsread('graphrelchimn.xlsx','Ag','C3:C28');
AgB =
xlsread('graphrelchimn.xlsx','Ag','D3:D28');
AgC =
xlsread('graphrelchimn.xlsx','Ag','E3:E28');
AgD =
xlsread('graphrelchimn.xlsx','Ag','F3:F28');
Ag0 =
xlsread('graphrelchimn.xlsx','Ag','I3:I28');
YAg1 = 0.3338*x;
YAg2 = 1.5078*x;
figure;
subplot(1,2,1);
scatter(AgA,AgB,'black','filled');
hold on;
plot(x,YAg1,'black');
pbaspect([1 1 1]);
xlabel('Chimney Ag Conc. (kg/T)');
ylabel('Core Ag Conc. (kg/T)');
subplot(1,2,2);
scatter(AgC,AgB,'black','filled');
hold on
plot(x,YAg2,'black');
pbaspect([1 1 1]);
```

```
hold off;
xlabel('Surface Ag Conc. (kg/T)');
figure;
scatter(AgA,AgC);
%% As
AsA =
xlsread('graphrelchimn.xlsx','As','C3:C28');
AsB =
xlsread('graphrelchimn.xlsx','As','D3:D28');
AsC =
xlsread('graphrelchimn.xlsx','As','E3:E28');
AsD =
xlsread('graphrelchimn.xlsx','As','F3:F28');
As0 =
xlsread('graphrelchimn.xlsx','As','I3:I28');
AsAx =
xlsread('graphrelchimnexc.xlsx','As','C3:C28'
);
AsBx =
xlsread('graphrelchimnexc.xlsx','As','D3:D28'
);
AsCx =
xlsread('graphrelchimnexc.xlsx','As','E3:E28'
);
AsDx =
xlsread('graphrelchimnexc.xlsx','As','F3:F28'
);
x = 0:1;
YAs1 = 1.3705*x;
YAs2 = 0.3365*x;
YAs3 = 0.3499*x;
figure;
subplot(1,2,1);
```

```
%scatter(AsA,AsB,'blue','filled');
%hold on;
scatter(AsAx,AsBx,'black','filled');
hold on;
%plot(x,YAs1,'blue');
%hold on;
plot(x,YAs2,'black');
pbaspect([1 1 1]);
xlabel('Chimney As Conc. (kg/T)');
ylabel('Core As Conc. (kg/T)');
subplot(1,2,2);
scatter(AsC,AsB,'blue','filled');
hold on;
scatter(AsCx,AsBx,'black','filled');
plot(x,YAs3,'black');
pbaspect([1 1 1])
hold off;
xlabel('Surface As Conc. (kg/T)');
%% load B
% no data
%BA =
xlsread('graphrelchimn.xlsx','B','C3:C28');
%BB =
xlsread('graphrelchimn.xlsx','B','D3:D28');
%BC =
xlsread('graphrelchimn.xlsx','B','E3:E28');
%BD =
xlsread('graphrelchimn.xlsx','B','F3:F28');
%B0 =
xlsread('graphrelchimn.xlsx','B','I3:I28');
%x = 0:1;
%YAs1 = 1.3705*x;
%YAs2 = 0.3365*x;
```

```
%YAs3 = 0.3499*x;
%figure;
%subplot(1,2,1);
%scatter(BA,BB,'blue','filled');
%hold on;
%scatter(AsAx,AsBx,'black','filled');
%hold on;
%plot(x,YAs1,'blue');
%hold on;
%plot(x,YAs2,'black');
%pbaspect([1 1 1]);
%xlim([0 inf]);ylim([0 inf]);
%xlabel('Chimney B Conc. (kg/T)');
ylabel('Core B Conc. (kg/T)');
%subplot(1,2,2);
%scatter(BC,BB,'blue','filled');
%hold on;
%scatter(AsCx,AsBx,'black','filled');
%plot(x,YAs3,'black');
%pbaspect([1 1 1]);
%xlim([0 inf]);ylim([0 inf]);
%hold off;
%xlabel('Surface B Conc. (kg/T)');
%% load Ba
BaA =
xlsread('graphrelchimn.xlsx','Ba','C3:C28');
BaB =
xlsread('graphrelchimn.xlsx','Ba','D3:D28');
BaC =
xlsread('graphrelchimn.xlsx','Ba','E3:E28');
BaD =
xlsread('graphrelchimn.xlsx','Ba','F3:F28');
```

```
Ba0 =
xlsread('graphrelchimn.xlsx','Ba','I3:I28');
x = 0:100;
YBa1 = 0.1283*x
figure;
subplot(1,2,1);
scatter(BaA,BaB,'black','filled');
hold on;
plot(x,YBa1,'black');
pbaspect([1 1 1]);
xlim([0 inf]);ylim([0 inf]);
xlabel('Chimney Ba Conc. (kg/T)');
ylabel('Core Ba Conc. (kg/T)');
subplot(1,2,2);
scatter(BaC,BaB,'black','filled');
%hold on;
%scatter(AsCx,AsBx,'black','filled');
%plot(x,YAs3,'black');
pbaspect([1 1 1]);
xlim([0 inf]);ylim([0 inf]);
hold off;
xlabel('Surface Ba Conc. (kg/T)');
%% load Br
% insuf data
BrA =
xlsread('graphrelchimn.xlsx','Br','C3:C28');
BrB =
xlsread('graphrelchimn.xlsx','Br','D3:D28');
BrC =
xlsread('graphrelchimn.xlsx','Br','E3:E28');
BrD =
xlsread('graphrelchimn.xlsx','Br','F3:F28');
```

```
Br0 =
xlsread('graphrelchimn.xlsx','Br','I3:I28');
x = 0:1;
YBr2 = 1.159*x;
%YAs3 = 0.3499*x;
figure;
subplot(1,2,1);
scatter(BrA,BrB,'black','filled');
%hold on;
%scatter(AsAx,AsBx,'black','filled');
%hold on;
%plot(x,YAs1,'blue');
%hold on;
%plot(x,YAs2,'black');
pbaspect([1 1 1]);
xlim([0 inf]);ylim([0 inf]);
xlabel('Chimney Br Conc. (kg/T)');
ylabel('Core Br Conc. (kg/T)');
subplot(1,2,2);
scatter(BrC,BrB,'black','filled');
hold on;
%scatter(AsCx,AsBx,'black','filled');
plot(x,YBr2,'black');
pbaspect([1 1 1]);
xlim([0 inf]);ylim([0 inf]);
hold off;
xlabel('Surface Br Conc. (kg/T)');
%% load Ca
CaA =
xlsread('graphrelchimn.xlsx','Ca','C3:C28');
CaB =
xlsread('graphrelchimn.xlsx','Ca','D3:D28');
```

```
CaC =
xlsread('graphrelchimn.xlsx','Ca','E3:E28');
CaD =
xlsread('graphrelchimn.xlsx','Ca','F3:F28');
Ca0 =
xlsread('graphrelchimn.xlsx','Ca','I3:I28');
x = 0:50;
YCa1 = 0.715*x;
figure;
subplot(1,2,1);
scatter(CaA,CaB,'black','filled');
pbaspect([1 1 1]);
xlim([0 inf]);ylim([0 inf]);
xlabel('Chimney Ca Conc. (kg/T)');
ylabel('Core Ca Conc. (kg/T)');
subplot(1,2,2);
scatter(CaC,CaB,'black','filled');
hold on;
plot(x,YCa1,'black');
pbaspect([1 1 1]);
xlim([0 inf]);ylim([0 inf]);
hold off;
xlabel('Surface Ca Conc. (kg/T)');
%% load Cd
CdA =
xlsread('graphrelchimn.xlsx','Cd','C3:C28');
CdB =
xlsread('graphrelchimn.xlsx','Cd','D3:D28');
CdC =
xlsread('graphrelchimn.xlsx','Cd','E3:E28');
CdD =
xlsread('graphrelchimn.xlsx','Cd','F3:F28');
```

```
CdAx =
xlsread('graphrelchimnexc.xlsx','Cd','C3:C28'
);
CdBx =
xlsread('graphrelchimnexc.xlsx','Cd','D3:D28'
);
CdCx =
xlsread('graphrelchimnexc.xlsx','Cd','E3:E28'
);
CdDx =
xlsread('graphrelchimnexc.xlsx','Cd','F3:F28'
);
Cd0 =
xlsread('graphrelchimn.xlsx','Cd','I3:I28');
x = 0:25;
YCd1 = 0.0286*x;
YCd2 = 0.7003*x;
YCd3 = 0.9517*x;
YCd4 = 0.7333*x;
figure;
subplot(1,2,1);
%scatter(CdA,CdB,'blue','filled');
%hold on;
scatter(CdAx,CdBx,'black','filled');
%hold on;
%plot(x,YCd1,'blue');
hold on;
plot(x,YCd2,'black');
pbaspect([1 1 1]);
xlim([0 inf]);ylim([0 inf]);
xlabel('Chimney Cd Conc. (kg/T)');
ylabel('Core Cd Conc. (kg/T)');
subplot(1,2,2);
```

```
%scatter(CdC,CdB,'blue','filled');
scatter(CdCx,CdBx,'black','filled');
hold on;
plot(x,YCd3,'black');
%plot(x,YCd4,'blue');
pbaspect([1 1 1]);
xlim([0 inf]);ylim([0 inf]);
hold off;
xlabel('Surface Cd Conc. (kg/T)');
%% load Ce
%insuf data
CeA =
xlsread('graphrelchimn.xlsx','Ce','C3:C28');
CeB =
xlsread('graphrelchimn.xlsx','Ce','D3:D28');
CeC =
xlsread('graphrelchimn.xlsx','Ce','E3:E28');
CeD =
xlsread('graphrelchimn.xlsx','Ce','F3:F28');
Ce0 =
xlsread('graphrelchimn.xlsx','Ce','I3:I28');
x = 0:1;
%YAs1 = 1.3705*x;
%YAs2 = 0.3365*x;
%YAs3 = 0.3499*x;
figure;
subplot(1,2,1);
scatter(CeA,CeB,'black','filled');
%hold on;
%scatter(AsAx,AsBx,'black','filled');
%hold on;
%plot(x,YAs1,'blue');
%hold on;
```

```
%plot(x,YAs2,'black');
pbaspect([1 1 1]);
xlim([0 inf]);ylim([0 inf]);
xlabel('Chimney Ce Conc. (kg/T)');
ylabel('Core Ce Conc. (kg/T)');
subplot(1,2,2);
scatter(CeC,CeB,'black','filled');
%hold on;
%scatter(AsCx,AsBx,'black','filled');
%plot(x,YAs3,'black');
pbaspect([1 1 1]);
xlim([0 inf]);ylim([0 inf]);
hold off;
xlabel('Surface Ce Conc. (kg/T)');
%% load Cl
%insuf data
ClA =
xlsread('graphrelchimn.xlsx','Cl','C3:C28');
ClB =
xlsread('graphrelchimn.xlsx','Cl','D3:D28');
ClC =
xlsread('graphrelchimn.xlsx','Cl','E3:E28');
ClD =
xlsread('graphrelchimn.xlsx','Cl','F3:F28');
Cl0 =
xlsread('graphrelchimn.xlsx','Cl','I3:I28');
x = 0:1;
%YAs1 = 1.3705*x;
%YAs2 = 0.3365*x;
%YAs3 = 0.3499*x;
figure;
subplot(1,2,1);
scatter(ClA,ClB,'black','filled');
```

```
%hold on;
%scatter(AsAx,AsBx,'black','filled');
%hold on;
%plot(x,YAs1,'blue');
%hold on;
%plot(x,YAs2,'black');
pbaspect([1 1 1]);
xlim([0 inf]);ylim([0 inf]);
xlabel('Chimney Cl Conc. (kg/T)');
ylabel('Core Cl Conc. (kg/T)');
subplot(1,2,2);
scatter(ClC,ClB,'black','filled');
%hold on;
%scatter(AsCx,AsBx,'black','filled');
%plot(x,YAs3,'black');
pbaspect([1 1 1]);
xlim([0 inf]);ylim([0 inf]);
hold off;
xlabel('Surface Cl Conc. (kg/T)');
%% load Co
CoA =
xlsread('graphrelchimn.xlsx','Co','C3:C28');
CoB =
xlsread('graphrelchimn.xlsx','Co','D3:D28');
CoC =
xlsread('graphrelchimn.xlsx','Co','E3:E28');
CoD =
xlsread('graphrelchimn.xlsx','Co','F3:F28');
Co0 =
xlsread('graphrelchimn.xlsx','Co','I3:I28');
CoAx =
xlsread('graphrelchimnexc.xlsx','Co','C3:C28'
);
```

```
CoBx =
xlsread('graphrelchimnexc.xlsx','Co','D3:D28'
);
CoCx =
xlsread('graphrelchimnexc.xlsx','Co','E3:E28'
);
CoDx =
xlsread('graphrelchimnexc.xlsx','Co','F3:F28'
);
x = 0:2;
YCo4 = 0.1085*x;
YCo3 = 1.5803*x;
figure;
subplot(1,2,1);
scatter(CoA,CoB,'black','filled');
pbaspect([1 1 1]);
xlim([0 inf]);ylim([0 inf]);
xlabel('Chimney Co Conc. (kg/T)');
ylabel('Core Co Conc. (kg/T)');
subplot(1,2,2);
scatter(CoC,CoB,'blue','filled');
hold on;
scatter(CoCx,CoBx,'black','filled');
plot(x,YCo3,'black');
plot(x,YCo4,'blue');
pbaspect([1 1 1]);
xlim([0 inf]);ylim([0 inf]);
hold off;
xlabel('Surface Co Conc. (kg/T)');
%% load Cs
%insuf data
CsA =
xlsread('graphrelchimn.xlsx','Cs','C3:C28');
```

```
CsB =
xlsread('graphrelchimn.xlsx','Cs','D3:D28');
CsC =
xlsread('graphrelchimn.xlsx','Cs','E3:E28');
CsD =
xlsread('graphrelchimn.xlsx','Cs','F3:F28');
Cs0 =
xlsread('graphrelchimn.xlsx','Cs','I3:I28');
x = 0:1;
%YAs1 = 1.3705*x;
%YAs2 = 0.3365*x;
%YAs3 = 0.3499*x;
figure;
subplot(1,2,1);
scatter(CsA,CsB,'black','filled');
%hold on;
%scatter(AsAx,AsBx,'black','filled');
%hold on;
%plot(x,YAs1,'blue');
%hold on;
%plot(x,YAs2,'black');
pbaspect([1 1 1]);
xlim([0 inf]);ylim([0 inf]);
xlabel('Chimney Cs Conc. (kg/T)');
ylabel('Core Cs Conc. (kg/T)');
subplot(1,2,2);
scatter(CsC,CsB,'black','filled');
%hold on;
%scatter(AsCx,AsBx,'black','filled');
%plot(x,YAs3,'black');
pbaspect([1 1 1]);
xlim([0 inf]);ylim([0 inf]);
hold off;
```

```
xlabel('Surface Cs Conc. (kg/T)');
%% load Cu
CuA =
xlsread('graphrelchimn.xlsx','Cu','C3:C28');
CuB =
xlsread('graphrelchimn.xlsx','Cu','D3:D28');
CuC =
xlsread('graphrelchimn.xlsx','Cu','E3:E28');
CuD =
xlsread('graphrelchimn.xlsx','Cu','F3:F28');
Cu0 =
xlsread('graphrelchimn.xlsx','Cu','I3:I28');
x = 0:200;
YCu1 = 0.5877*x;
YCu2 = 1.1307*x;
figure;
subplot(1,2,1);
scatter(CuA,CuB,'black','filled');
hold on;
plot(x,YCu1,'black');
pbaspect([1 1 1]);
xlim([0 inf]);ylim([0 inf]);
xlabel('Chimney Cu Conc. (kg/T)');
ylabel('Core Cu Conc. (kg/T)');
subplot(1,2,2);
scatter(CuC,CuB,'black','filled');
hold on
plot(x,YCu2,'black');
pbaspect([1 1 1]);
xlim([0 inf]);ylim([0 inf]);
hold off;
xlabel('Surface Cu Conc. (kg/T)');
%% load Dy
```

```
% no data
DyA =
xlsread('graphrelchimn.xlsx','Dy','C3:C28');
DyB =
xlsread('graphrelchimn.xlsx','Dy','D3:D28');
DyC =
xlsread('graphrelchimn.xlsx','Dy','E3:E28');
DyD =
xlsread('graphrelchimn.xlsx','Dy','F3:F28');
Dy0 =
xlsread('graphrelchimn.xlsx','Dy','I3:I28');
x = 0:1;
%YAs1 = 1.3705*x;
%YAs2 = 0.3365*x;
%YAs3 = 0.3499*x;
figure;
subplot(1,2,1);
scatter(DyA,DyB,'black','filled');
%hold on;
%scatter(AsAx,AsBx,'black','filled');
%hold on;
%plot(x,YAs1,'blue');
%hold on;
%plot(x,YAs2,'black');
pbaspect([1 1 1]);
xlim([0 inf]);ylim([0 inf]);
xlabel('Chimney Dy Conc. (kg/T)');
ylabel('Core Dy Conc. (kg/T)');
subplot(1,2,2);
scatter(DyC,DyB,'black','filled');
%hold on;
%scatter(AsCx,AsBx,'black','filled');
%plot(x,YAs3,'black');
```

```
pbaspect([1 1 1]);
xlim([0 inf]);ylim([0 inf]);
hold off;
xlabel('Surface Dy Conc. (kg/T)');
%% load Er
% no data
ErA =
xlsread('graphrelchimn.xlsx','Er','C3:C28');
ErB =
xlsread('graphrelchimn.xlsx','Er','D3:D28');
ErC =
xlsread('graphrelchimn.xlsx','Er','E3:E28');
ErD =
xlsread('graphrelchimn.xlsx','Er','F3:F28');
Er0 =
xlsread('graphrelchimn.xlsx','Er','I3:I28');
x = 0:1;
%YAs1 = 1.3705*x;
%YAs2 = 0.3365*x;
%YAs3 = 0.3499*x;
figure;
subplot(1,2,1);
scatter(ErA,ErB,'black','filled');
%hold on;
%scatter(AsAx,AsBx,'black','filled');
%hold on;
%plot(x,YAs1,'blue');
%hold on;
%plot(x,YAs2,'black');
pbaspect([1 1 1]);
xlim([0 inf]);ylim([0 inf]);
xlabel('Chimney Er Conc. (kg/T)');
ylabel('Core Er Conc. (kg/T)');
```

```
subplot(1,2,2);
scatter(ErC,ErB,'black','filled');
%hold on;
%scatter(AsCx,AsBx,'black','filled');
%plot(x,YAs3,'black');
pbaspect([1 1 1]);
xlim([0 inf]);ylim([0 inf]);
hold off;
xlabel('Surface Er Conc. (kg/T)');
%% load Eu
%insuf data
EuA =
xlsread('graphrelchimn.xlsx','Eu','C3:C28');
EuB =
xlsread('graphrelchimn.xlsx','Eu','D3:D28');
EuC =
xlsread('graphrelchimn.xlsx','Eu','E3:E28');
EuD =
xlsread('graphrelchimn.xlsx','Eu','F3:F28');
Eu0 =
xlsread('graphrelchimn.xlsx','Eu','I3:I28');
x = 0:1;
%YAs1 = 1.3705*x;
%YAs2 = 0.3365*x;
%YAs3 = 0.3499*x;
figure;
subplot(1,2,1);
scatter(EuA,EuB,'black','filled');
%hold on;
%scatter(AsAx,AsBx,'black','filled');
%hold on;
%plot(x,YAs1,'blue');
%hold on;
```

```
%plot(x,YAs2,'black');
pbaspect([1 1 1]);
xlim([0 inf]);ylim([0 inf]);
xlabel('Chimney Eu Conc. (kg/T)');
ylabel('Core Eu Conc. (kg/T)');
subplot(1,2,2);
scatter(EuC,EuB,'black','filled');
%hold on;
%scatter(AsCx,AsBx,'black','filled');
%plot(x,YAs3,'black');
pbaspect([1 1 1]);
xlim([0 inf]);ylim([0 inf]);
hold off;
xlabel('Surface Eu Conc. (kg/T)');
%% load Fe
FeA =
xlsread('graphrelchimn.xlsx','Fe','C3:C28');
FeB =
xlsread('graphrelchimn.xlsx','Fe','D3:D28');
FeC =
xlsread('graphrelchimn.xlsx','Fe','E3:E28');
FeD =
xlsread('graphrelchimn.xlsx','Fe','F3:F28');
Fe0 =
xlsread('graphrelchimn.xlsx','Fe','I3:I28');
x = 0:500;
YFe1 = (0.1896*x)+301.9;
YFe2 = (0.2294*x)+272.57;
figure;
subplot(1,2,1);
scatter(FeA,FeB,'black','filled');
hold on
plot(x,YFe1,'black');
```

```
pbaspect([1 1 1]);
xlim([0 inf]);ylim([0 inf]);
xlabel('Chimney Fe Conc. (kg/T)');
ylabel('Core Fe Conc. (kg/T)');
subplot(1,2,2);
scatter(FeC,FeB,'black','filled');
hold on;
plot(x,YFe2,'black');
pbaspect([1 1 1]);
xlim([0 inf]);ylim([0 inf]);
hold off;
xlabel('Surface Fe Conc. (kg/T)');
%% load Gd
% no data
GdA =
xlsread('graphrelchimn.xlsx','Gd','C3:C28');
GdB =
xlsread('graphrelchimn.xlsx','Gd','D3:D28');
GdC =
xlsread('graphrelchimn.xlsx','Gd','E3:E28');
GdD =
xlsread('graphrelchimn.xlsx','Gd','F3:F28');
Gd0 =
xlsread('graphrelchimn.xlsx','Gd','I3:I28');
x = 0:1;
%YAs1 = 1.3705*x;
%YAs2 = 0.3365*x;
%YAs3 = 0.3499*x;
figure;
subplot(1,2,1);
scatter(GdA,GdB,'black','filled');
%hold on;
%scatter(AsAx,AsBx,'black','filled');
```

```
%hold on;
%plot(x,YAs1,'blue');
%hold on;
%plot(x,YAs2,'black');
pbaspect([1 1 1]);
xlim([0 inf]);ylim([0 inf]);
xlabel('Chimney Gd Conc. (kg/T)');
ylabel('Core Gd Conc. (kg/T)');
subplot(1,2,2);
scatter(GdC,GdB,'black','filled');
%hold on;
%scatter(AsCx,AsBx,'black','filled');
%plot(x,YAs3,'black');
pbaspect([1 1 1]);
xlim([0 inf]);ylim([0 inf]);
hold off;
xlabel('Surface Gd Conc. (kg/T)');
%% load Hf
%insuf data
HfA =
xlsread('graphrelchimn.xlsx','Hf','C3:C28');
HfB =
xlsread('graphrelchimn.xlsx','Hf','D3:D28');
HfC =
xlsread('graphrelchimn.xlsx','Hf','E3:E28');
HfD =
xlsread('graphrelchimn.xlsx','Hf','F3:F28');
Hf0 =
xlsread('graphrelchimn.xlsx','Hf','I3:I28');
x = 0:1;
%YAs1 = 1.3705*x;
%YAs2 = 0.3365*x;
%YAs3 = 0.3499*x;
```

```
figure;
subplot(1,2,1);
scatter(HfA,HfB,'black','filled');
%hold on;
%scatter(AsAx,AsBx,'black','filled');
%hold on;
%plot(x,YAs1,'blue');
%hold on;
%plot(x,YAs2,'black');
pbaspect([1 1 1]);
xlim([0 inf]);ylim([0 inf]);
xlabel('Chimney Hf Conc. (kg/T)');
ylabel('Core Hf Conc. (kg/T)');
subplot(1,2,2);
scatter(HfC,HfB,'black','filled');
%hold on;
%scatter(AsCx,AsBx,'black','filled');
%plot(x,YAs3,'black');
pbaspect([1 1 1]);
xlim([0 inf]);ylim([0 inf]);
hold off;
xlabel('Surface Hf Conc. (kg/T)');
%% load Hg
%insuf data
HgA =
xlsread('graphrelchimn.xlsx','Hg','C3:C28');
HgB =
xlsread('graphrelchimn.xlsx','Hg','D3:D28');
HgC =
xlsread('graphrelchimn.xlsx','Hg','E3:E28');
HgD =
xlsread('graphrelchimn.xlsx','Hg','F3:F28');
```

```
Hg0 =
xlsread('graphrelchimn.xlsx','Hg','I3:I28');
x = 0:1;
%YAs1 = 1.3705*x;
%YAs2 = 0.3365*x;
%YAs3 = 0.3499*x;
figure;
subplot(1,2,1);
scatter(HgA,HgB,'black','filled');
%hold on;
%scatter(AsAx,AsBx,'black','filled');
%hold on;
%plot(x,YAs1,'blue');
%hold on;
%plot(x,YAs2,'black');
pbaspect([1 1 1]);
xlim([0 inf]);ylim([0 inf]);
xlabel('Chimney Hg Conc. (kg/T)');
ylabel('Core Hg Conc. (kg/T)');
subplot(1,2,2);
scatter(HgC,HgB,'black','filled');
%hold on;
%scatter(AsCx,AsBx,'black','filled');
%plot(x,YAs3,'black');
pbaspect([1 1 1]);
xlim([0 inf]);ylim([0 inf]);
hold off;
xlabel('Surface Hg Conc. (kg/T)');
%% load Ho
% no data
HoA =
xlsread('graphrelchimn.xlsx','Ho','C3:C28');
```

```
HoB =
xlsread('graphrelchimn.xlsx','Ho','D3:D28');
HoC =
xlsread('graphrelchimn.xlsx','Ho','E3:E28');
HoD =
xlsread('graphrelchimn.xlsx','Ho','F3:F28');
Ho0 =
xlsread('graphrelchimn.xlsx','Ho','I3:I28');
x = 0:1;
%YAs1 = 1.3705*x;
%YAs2 = 0.3365*x;
%YAs3 = 0.3499*x;
figure;
subplot(1,2,1);
scatter(HoA,HoB,'black','filled');
%hold on;
%scatter(AsAx,AsBx,'black','filled');
%hold on;
%plot(x,YAs1,'blue');
%hold on;
%plot(x,YAs2,'black');
pbaspect([1 1 1]);
xlim([0 inf]);ylim([0 inf]);
xlabel('Chimney Ho Conc. (kg/T)');
ylabel('Core Ho Conc. (kg/T)');
subplot(1,2,2);
scatter(HoC,HoB,'black','filled');
%hold on;
%scatter(AsCx,AsBx,'black','filled');
%plot(x,YAs3,'black');
pbaspect([1 1 1]);
xlim([0 inf]);ylim([0 inf]);
hold off;
```

```
xlabel('Surface Ho Conc. (kg/T)');
%% load La
% insuf data
LaA =
xlsread('graphrelchimn.xlsx','La','C3:C28');
LaB =
xlsread('graphrelchimn.xlsx','La','D3:D28');
LaC =
xlsread('graphrelchimn.xlsx','La','E3:E28');
LaD =
xlsread('graphrelchimn.xlsx','La','F3:F28');
La0 =
xlsread('graphrelchimn.xlsx','La','I3:I28');
x = 0:1;
%YAs1 = 1.3705*x;
%YAs2 = 0.3365*x;
%YAs3 = 0.3499*x;
figure;
subplot(1,2,1);
scatter(LaA,LaB,'black','filled');
%hold on;
%scatter(AsAx,AsBx,'black','filled');
%hold on;
%plot(x,YAs1,'blue');
%hold on;
%plot(x,YAs2,'black');
pbaspect([1 1 1]);
xlim([0 inf]);ylim([0 inf]);
xlabel('Chimney La Conc. (kg/T)');
ylabel('Core La Conc. (kg/T)');
subplot(1,2,2);
scatter(LaC,LaB,'black','filled');
%hold on;
```

```
%scatter(AsCx,AsBx,'black','filled');
%plot(x,YAs3,'black');
pbaspect([1 1 1]);
xlim([0 inf]);ylim([0 inf]);
hold off;
xlabel('Surface La Conc. (kg/T)');
%% load Li
%insuf data
LiA =
xlsread('graphrelchimn.xlsx','Li','C3:C28');
LiB =
xlsread('graphrelchimn.xlsx','Li','D3:D28');
LiC =
xlsread('graphrelchimn.xlsx','Li','E3:E28');
LiD =
xlsread('graphrelchimn.xlsx','Li','F3:F28');
Li0 =
xlsread('graphrelchimn.xlsx','Li','I3:I28');
x = 0:1;
%YAs1 = 1.3705*x;
%YAs2 = 0.3365*x;
%YAs3 = 0.3499*x;
figure;
subplot(1,2,1);
scatter(LiA,LiB,'black','filled');
%hold on;
%scatter(AsAx,AsBx,'black','filled');
%hold on;
%plot(x,YAs1,'blue');
%hold on;
%plot(x,YAs2,'black');
pbaspect([1 1 1]);
xlim([0 inf]);ylim([0 inf]);
```

```
xlabel('Chimney Li Conc. (kg/T)');
ylabel('Core Li Conc. (kg/T)');
subplot(1,2,2);
scatter(LiC,LiB,'black','filled');
%hold on;
%scatter(AsCx,AsBx,'black','filled');
%plot(x,YAs3,'black');
pbaspect([1 1 1]);
xlim([0 inf]);ylim([0 inf]);
hold off;
xlabel('Surface Li Conc. (kg/T)');
%% load Lu
%insuf data
LuA =
xlsread('graphrelchimn.xlsx','Lu','C3:C28');
LuB =
xlsread('graphrelchimn.xlsx','Lu','D3:D28');
LuC =
xlsread('graphrelchimn.xlsx','Lu','E3:E28');
LuD =
xlsread('graphrelchimn.xlsx','Lu','F3:F28');
Lu0 =
xlsread('graphrelchimn.xlsx','Lu','I3:I28');
x = 0:1;
%YAs1 = 1.3705*x;
%YAs2 = 0.3365*x;
%YAs3 = 0.3499*x;
figure;
subplot(1,2,1);
scatter(LuA,LuB,'black','filled');
%hold on;
%scatter(AsAx,AsBx,'black','filled');
%hold on;
```

```
%plot(x,YAs1,'blue');
%hold on;
%plot(x,YAs2,'black');
pbaspect([1 1 1]);
xlim([0 inf]);ylim([0 inf]);
xlabel('Chimney Lu Conc. (kg/T)');
ylabel('Core Lu Conc. (kg/T)');
subplot(1,2,2);
scatter(LuC,LuB,'black','filled');
%hold on;
%scatter(AsCx,AsBx,'black','filled');
%plot(x,YAs3,'black');
pbaspect([1 1 1]);
xlim([0 inf]);ylim([0 inf]);
hold off;
xlabel('Surface Lu Conc. (kg/T)');
%% load Mn
%insuf data
MnA =
xlsread('graphrelchimn.xlsx','Mn','C3:C28');
MnB =
xlsread('graphrelchimn.xlsx','Mn','D3:D28');
MnC =
xlsread('graphrelchimn.xlsx','Mn','E3:E28');
MnD =
xlsread('graphrelchimn.xlsx','Mn','F3:F28');
Mn0 =
xlsread('graphrelchimn.xlsx','Mn','I3:I28');
MnAx =
xlsread('graphrelchimnexc.xlsx','Mn','C3:C28'
);
```

```
MnBx =
xlsread('graphrelchimnexc.xlsx','Mn','D3:D28'
);
MnCx =
xlsread('graphrelchimnexc.xlsx','Mn','E3:E28'
);
MnDx =
xlsread('graphrelchimnexc.xlsx','Mn','F3:F28'
);x = 0:1;
x=0:200000
YMn1 = 0.0041*x;
YMn2 = 1.19*x;
figure;
subplot(1,2,1);
scatter(MnA,MnB,'black','filled');
pbaspect([1 1 1]);
xlim([0 inf]);ylim([0 inf]);
xlabel('Chimney Mn Conc. (kg/T)');
ylabel('Core Mn Conc. (kg/T)');
subplot(1,2,2);
scatter(MnC,MnB,'blue','filled');
hold on;
scatter(MnCx,MnBx,'black','filled');
plot(x,YMn1,'blue');
plot(x,YMn2,'black');
pbaspect([1 1 1]);
xlim([0 inf]);ylim([0 inf]);
hold off;
xlabel('Surface Mn Conc. (kg/T)');
%% load Mo
MoA =
xlsread('graphrelchimn.xlsx','Mo','C3:C28');
```

```
MoB =
xlsread('graphrelchimn.xlsx','Mo','D3:D28');
MoC =
xlsread('graphrelchimn.xlsx','Mo','E3:E28');
MoD =
xlsread('graphrelchimn.xlsx','Mo','F3:F28');
Mo0 =
xlsread('graphrelchimn.xlsx','Mo','I3:I28');
x = 0:1;
YMo1 = 1.2307*x;
YMo2 = 0.9617*x;
figure;
subplot(1,2,1);
scatter(MoA,MoB,'black','filled');
hold on;
plot(x,YMo1,'black');
pbaspect([1 1 1]);
xlim([0 inf]);ylim([0 inf]);
xlabel('Chimney Mo Conc. (kg/T)');
ylabel('Core Mo Conc. (kg/T)');
subplot(1,2,2);
scatter(MoC,MoB,'black','filled');
hold on;
plot(x,YMo2,'black');
pbaspect([1 1 1]);
xlim([0 inf]);ylim([0 inf]);
hold off;
xlabel('Surface Mo Conc. (kg/T)');
%% load Nb
% few data
NbA =
xlsread('graphrelchimn.xlsx','Nb','C3:C28');
```

```
NbB =
xlsread('graphrelchimn.xlsx','Nb','D3:D28');
NbC =
xlsread('graphrelchimn.xlsx','Nb','E3:E28');
NbD =
xlsread('graphrelchimn.xlsx','Nb','F3:F28');
Nb0 =
xlsread('graphrelchimn.xlsx','Nb','I3:I28');
x = 0:1;
%YAs1 = 1.3705*x;
%YAs2 = 0.3365*x;
%YAs3 = 0.3499*x;
figure;
subplot(1,2,1);
scatter(NbA,NbB,'black','filled');
%hold on;
%scatter(AsAx,AsBx,'black','filled');
%hold on;
%plot(x,YAs1,'blue');
%hold on;
%plot(x,YAs2,'black');
pbaspect([1 1 1]);
xlim([0 inf]);ylim([0 inf]);
xlabel('Chimney Nb Conc. (kg/T)');
ylabel('Core Nb Conc. (kg/T)');
subplot(1,2,2);
scatter(NbC,NbB,'black','filled');
%hold on;
%scatter(AsCx,AsBx,'black','filled');
%plot(x,YAs3,'black');
pbaspect([1 1 1]);
xlim([0 inf]);ylim([0 inf]);
hold off;
```

```
xlabel('Surface Nb Conc. (kg/T)');
%% load Ni
%insuf
NiA =
xlsread('graphrelchimn.xlsx','Ni','C3:C28');
NiB =
xlsread('graphrelchimn.xlsx','Ni','D3:D28');
NiC =
xlsread('graphrelchimn.xlsx','Ni','E3:E28');
NiD =
xlsread('graphrelchimn.xlsx','Ni','F3:F28');
Ni0 =
xlsread('graphrelchimn.xlsx','Ni','I3:I28');
x = 0:1;
YNi1 = 1.2397*x;
YNi2 = 1.4814*x;
figure;
subplot(1,2,1);
scatter(NiA,NiB,'black','filled');
hold on
plot(x,YNi1,'black');
pbaspect([1 1 1]);
xlim([0 inf]);ylim([0 inf]);
xlabel('Chimney Ni Conc. (kg/T)');
ylabel('Core Ni Conc. (kg/T)');
subplot(1,2,2);
scatter(NiC,NiB,'black','filled');
hold on
plot(x,YNi2,'black');
pbaspect([1 1 1]);
xlim([0 inf]);ylim([0 inf]);
hold off;
xlabel('Surface Ni Conc. (kg/T)');
```

```
%% load Pb
% run blue
PbA =
xlsread('graphrelchimn.xlsx','Pb','C3:C28');
PbB =
xlsread('graphrelchimn.xlsx','Pb','D3:D28');
PbC =
xlsread('graphrelchimn.xlsx','Pb','E3:E28');
PbD =
xlsread('graphrelchimn.xlsx','Pb','F3:F28');
Pb0 =
xlsread('graphrelchimn.xlsx','Pb','I3:I28');
PbAx =
xlsread('graphrelchimnexc.xlsx','Pb','C3:C28'
);
PbBx =
xlsread('graphrelchimnexc.xlsx','Pb','D3:D28'
);
PbCx =
xlsread('graphrelchimnexc.xlsx','Pb','E3:E28'
);
Pb0 =
xlsread('graphrelchimn.xlsx','Pb','I3:I28');
x = 0:10;
YPb1 = 3.9452*x;
YPb2 = 0.2633*x;
YPb3 = 1.9465*x;
figure;
subplot(1,2,1);
scatter(PbA,PbB,'blue','filled');
hold on;
scatter(PbAx,PbBx,'black','filled');
plot(x,YPb1,'blue');
```

```
hold on;
plot(x,YPb2,'black');
pbaspect([1 1 1]);
xlim([0 inf]);ylim([0 inf]);
xlabel('Chimney Pb Conc. (kg/T)');
ylabel('Core Pb Conc. (kg/T)');
subplot(1,2,2);
scatter(PbC,PbB,'black','filled');
hold on;
plot(x,YPb3,'black');
pbaspect([1 1 1]);
xlim([0 inf]);ylim([0 inf]);
hold off;
xlabel('Surface Pb Conc. (kg/T)');
%% load Pd
%no data
PdA =
xlsread('graphrelchimn.xlsx','Pd','C3:C28');
PdB =
xlsread('graphrelchimn.xlsx','Pd','D3:D28');
PdC =
xlsread('graphrelchimn.xlsx','Pd','E3:E28');
PdD =
xlsread('graphrelchimn.xlsx','Pd','F3:F28');
Pd0 =
xlsread('graphrelchimn.xlsx','Pd','I3:I28');
x = 0:1;
%YAs1 = 1.3705*x;
%YAs2 = 0.3365*x;
%YAs3 = 0.3499*x;
figure;
subplot(1,2,1);
scatter(PdA,PdB,'black','filled');
```

```
%hold on;
%scatter(AsAx,AsBx,'black','filled');
%hold on;
%plot(x,YAs1,'blue');
%hold on;
%plot(x,YAs2,'black');
pbaspect([1 1 1]);
xlim([0 inf]);ylim([0 inf]);
xlabel('Chimney Pd Conc. (kg/T)');
ylabel('Core Pd Conc. (kg/T)');
subplot(1,2,2);
scatter(PdC,PdB,'black','filled');
%hold on;
%scatter(AsCx,AsBx,'black','filled');
%plot(x,YAs3,'black');
pbaspect([1 1 1]);
xlim([0 inf]);ylim([0 inf]);
hold off;
xlabel('Surface Pd Conc. (kg/T)');
%% load Pr
%no data
PrA =
xlsread('graphrelchimn.xlsx','Pr','C3:C28');
PrB =
xlsread('graphrelchimn.xlsx','Pr','D3:D28');
PrC =
xlsread('graphrelchimn.xlsx','Pr','E3:E28');
PrD =
xlsread('graphrelchimn.xlsx','Pr','F3:F28');
Pr0 =
xlsread('graphrelchimn.xlsx','Pr','I3:I28');
x = 0:1;
YPr1 = 1.7513*x;
```

```
figure;
subplot(1,2,1);
scatter(PrA,PrB,'black','filled');
pbaspect([1 1 1]);
xlim([0 inf]);ylim([0 inf]);
xlabel('Chimney Pr Conc. (kg/T)');
ylabel('Core Pr Conc. (kg/T)');
subplot(1,2,2);
scatter(PrC,PrB,'black','filled');
hold on;
plot(x,YPr1,'black');
pbaspect([1 1 1]);
xlim([0 inf]);ylim([0 inf]);
hold off;
xlabel('Surface Pr Conc. (kg/T)');
%% load Rb
%insuf data
RbA =
xlsread('graphrelchimn.xlsx','Rb','C3:C28');
RbB =
xlsread('graphrelchimn.xlsx','Rb','D3:D28');
RbC =
xlsread('graphrelchimn.xlsx','Rb','E3:E28');
RbD =
xlsread('graphrelchimn.xlsx','Rb','F3:F28');
x = 0:1;
%YAs1 = 1.3705*x;
%YAs2 = 0.3365*x;
%YAs3 = 0.3499*x;
figure;
subplot(1,2,1);
scatter(RbA,RbB,'black','filled');
%hold on;
```

```
%scatter(AsAx,AsBx,'black','filled');
%hold on;
%plot(x,YAs1,'blue');
%hold on;
%plot(x,YAs2,'black');
pbaspect([1 1 1]);
xlim([0 inf]);ylim([0 inf]);
xlabel('Chimney Rb Conc. (kg/T)');
ylabel('Core Rb Conc. (kg/T)');
subplot(1,2,2);
scatter(RbC,RbB,'black','filled');
%hold on;
%scatter(AsCx,AsBx,'black','filled');
%plot(x,YAs3,'black');
pbaspect([1 1 1]);
xlim([0 inf]);ylim([0 inf]);
hold off;
xlabel('Surface Rb Conc. (kg/T)');
%% load Sm
%insuf data
SmA =
xlsread('graphrelchimn.xlsx','Sm','C3:C28');
SmB =
xlsread('graphrelchimn.xlsx','Sm','D3:D28');
SmC =
xlsread('graphrelchimn.xlsx','Sm','E3:E28');
SmD =
xlsread('graphrelchimn.xlsx','Sm','F3:F28');
Sm0 =
xlsread('graphrelchimn.xlsx','Sm','I3:I28');
x = 0:1;
%YAs1 = 1.3705*x;
%YAs2 = 0.3365*x;
```

```
%YAs3 = 0.3499*x;
figure;
subplot(1,2,1);
scatter(SmA,SmB,'black','filled');
%hold on;
%scatter(AsAx,AsBx,'black','filled');
%hold on;
%plot(x,YAs1,'blue');
%hold on;
%plot(x,YAs2,'black');
pbaspect([1 1 1]);
xlim([0 inf]);ylim([0 inf]);
xlabel('Chimney Sm Conc. (kg/T)');
ylabel('Core Sm Conc. (kg/T)');
subplot(1,2,2);
scatter(SmC,SmB,'black','filled');
%hold on;
%scatter(AsCx,AsBx,'black','filled');
%plot(x,YAs3,'black');
pbaspect([1 1 1]);
xlim([0 inf]);ylim([0 inf]);
hold off;
xlabel('Surface Sm Conc. (kg/T)');
%% load Sr
SrA =
xlsread('graphrelchimn.xlsx','Sr','C3:C28');
SrB =
xlsread('graphrelchimn.xlsx','Sr','D3:D28');
SrC =
xlsread('graphrelchimn.xlsx','Sr','E3:E28');
SrD =
xlsread('graphrelchimn.xlsx','Sr','F3:F28');
```

```
Sr0 =
xlsread('graphrelchimn.xlsx','Sr','I3:I28');
x = 0:2;
YSr1 = 0.1848*x;
YSr2 = 1.3451*x;
figure;
subplot(1,2,1);
scatter(SrA,SrB,'black','filled');
hold on;
plot(x,YSr1,'black');
pbaspect([1 1 1]);
xlim([0 inf]);ylim([0 inf]);
xlabel('Chimney Sr Conc. (kg/T)');
ylabel('Core Sr Conc. (kg/T)');
subplot(1,2,2);
scatter(SrC,SrB,'black','filled');
%hold on;
%plot(x,YSr2,'black');
pbaspect([1 1 1]);
xlim([0 inf]);ylim([0 inf]);
hold off;
xlabel('Surface Sr Conc. (kg/T)');
%% load Ta
%insuf data
TaA =
xlsread('graphrelchimn.xlsx','Ta','C3:C28');
TaB =
xlsread('graphrelchimn.xlsx','Ta','D3:D28');
TaC =
xlsread('graphrelchimn.xlsx','Ta','E3:E28');
TaD =
xlsread('graphrelchimn.xlsx','Ta','F3:F28');
```

```
Ta0 =
xlsread('graphrelchimn.xlsx','Ta','I3:I28');
x = 0:1;
%YAs1 = 1.3705*x;
%YAs2 = 0.3365*x;
%YAs3 = 0.3499*x;
figure;
subplot(1,2,1);
scatter(TaA,TaB,'black','filled');
%hold on;
%scatter(AsAx,AsBx,'black','filled');
%hold on;
%plot(x,YAs1,'blue');
%hold on;
%plot(x,YAs2,'black');
pbaspect([1 1 1]);
xlim([0 inf]);ylim([0 inf]);
xlabel('Chimney Ta Conc. (kg/T)');
ylabel('Core Ta Conc. (kg/T)');
subplot(1,2,2);
scatter(TaC,TaB,'black','filled');
%hold on;
%scatter(AsCx,AsBx,'black','filled');
%plot(x,YAs3,'black');
pbaspect([1 1 1]);
xlim([0 inf]);ylim([0 inf]);
hold off;
xlabel('Surface Ta Conc. (kg/T)');
%% load Tb
% insuf data
TbA =
xlsread('graphrelchimn.xlsx','Tb','C3:C28');
```

```
TbB =
xlsread('graphrelchimn.xlsx','Tb','D3:D28');
TbC =
xlsread('graphrelchimn.xlsx','Tb','E3:E28');
TbD =
xlsread('graphrelchimn.xlsx','Tb','F3:F28');
Tb0 =
xlsread('graphrelchimn.xlsx','Tb','I3:I28');
x = 0:1;
%YAs1 = 1.3705*x;
%YAs2 = 0.3365*x;
%YAs3 = 0.3499*x;
figure;
subplot(1,2,1);
scatter(TbA,TbB,'black','filled');
%hold on;
%scatter(AsAx,AsBx,'black','filled');
%hold on;
%plot(x,YAs1,'blue');
%hold on;
%plot(x,YAs2,'black');
pbaspect([1 1 1]);
xlim([0 inf]);ylim([0 inf]);
xlabel('Chimney Tb Conc. (kg/T)');
ylabel('Core Tb Conc. (kg/T)');
subplot(1,2,2);
scatter(TbC,TbB,'black','filled');
%hold on;
%scatter(AsCx,AsBx,'black','filled');
%plot(x,YAs3,'black');
pbaspect([1 1 1]);
xlim([0 inf]);ylim([0 inf]);
hold off;
```

```
xlabel('Surface Tb Conc. (kg/T)');
%% load V
VA =
xlsread('graphrelchimn.xlsx','V','C3:C28');
VB =
xlsread('graphrelchimn.xlsx','V','D3:D28');
VC =
xlsread('graphrelchimn.xlsx','V','E3:E28');
VD =
xlsread('graphrelchimn.xlsx','V','F3:F28');
V0 =
xlsread('graphrelchimn.xlsx','V','I3:I28');
x = 0:1;
%YAs1 = 1.3705*x;
%YAs2 = 0.3365*x;
%YAs3 = 0.3499*x;
figure;
subplot(1,2,1);
scatter(VA,VB,'black','filled');
%hold on;
%scatter(AsAx,AsBx,'black','filled');
%hold on;
%plot(x,YAs1,'blue');
%hold on;
%plot(x,YAs2,'black');
pbaspect([1 1 1]);
xlim([0 inf]);ylim([0 inf]);
xlabel('Chimney V Conc. (kg/T)');
ylabel('Core V Conc. (kg/T)');
subplot(1,2,2);
scatter(VC,VB,'black','filled');
%hold on;
%scatter(AsCx,AsBx,'black','filled');
```

```
%plot(x,YAs3,'black');
pbaspect([1 1 1]);
xlim([0 inf]);ylim([0 inf]);
hold off;
xlabel('Surface V Conc. (kg/T)');
%% load Y
%few data
YA =
xlsread('graphrelchimn.xlsx','Y','C3:C28');
YB =
xlsread('graphrelchimn.xlsx','Y','D3:D28');
YC =
xlsread('graphrelchimn.xlsx','Y','E3:E28');
YD =
xlsread('graphrelchimn.xlsx','Y','F3:F28');
Y0 =
xlsread('graphrelchimn.xlsx','Y','I3:I28');
x = 0:1;
%YAs1 = 1.3705*x;
%YAs2 = 0.3365*x;
%YAs3 = 0.3499*x;
figure;
subplot(1,2,1);
scatter(YA,YB,'black','filled');
%hold on;
%scatter(AsAx,AsBx,'black','filled');
%hold on;
%plot(x,YAs1,'blue');
%hold on;
%plot(x,YAs2,'black');
pbaspect([1 1 1]);
xlim([0 inf]);ylim([0 inf]);
```

```
xlabel('Chimney Y Conc. (kg/T)');
ylabel('Core Y Conc. (kg/T)');
subplot(1,2,2);
scatter(YC,YB,'black','filled');
%hold on;
%scatter(AsCx,AsBx,'black','filled');
%plot(x,YAs3,'black');
pbaspect([1 1 1]);
xlim([0 inf]);ylim([0 inf]);
hold off;
xlabel('Surface Y Conc. (kg/T)');
%% load Yb
%insuf data
YbA =
xlsread('graphrelchimn.xlsx','Yb','C3:C28');
YbB =
xlsread('graphrelchimn.xlsx','Yb','D3:D28');
YbC =
xlsread('graphrelchimn.xlsx','Yb','E3:E28');
YbD =
xlsread('graphrelchimn.xlsx','Yb','F3:F28');
Yb0 =
xlsread('graphrelchimn.xlsx','Yb','I3:I28');
x = 0:1;
%YAs1 = 1.3705*x;
%YAs2 = 0.3365*x;
%YAs3 = 0.3499*x;
figure;
subplot(1,2,1);
scatter(YbA,YbB,'black','filled');
%hold on;
%scatter(AsAx,AsBx,'black','filled');
%hold on;
```

```
%plot(x,YAs1,'blue');
%hold on;
%plot(x,YAs2,'black');
pbaspect([1 1 1]);
xlim([0 inf]);ylim([0 inf]);
xlabel('Chimney Yb Conc. (kg/T)');
ylabel('Core Lu Conc. (kg/T)');
subplot(1,2,2);
scatter(YbC,YbB,'black','filled');
%hold on;
%scatter(AsCx,AsBx,'black','filled');
%plot(x,YAs3,'black');
pbaspect([1 1 1]);
xlim([0 inf]);ylim([0 inf]);
hold off;
xlabel('Surface Yb Conc. (kg/T)');
%% load Zn
ZnA =
xlsread('graphrelchimn.xlsx','Zn','C3:C28');
ZnB =
xlsread('graphrelchimn.xlsx','Zn','D3:D28');
ZnC =
xlsread('graphrelchimn.xlsx','Zn','E3:E28');
ZnD =
xlsread('graphrelchimn.xlsx','Zn','F3:F28');
Zn0 =
xlsread('graphrelchimn.xlsx','Zn','I3:I28');
x = 0:400;
YZn1 = (0.1945*x)+56.966;
YZn2 = 1.1472*x
figure;
subplot(1,2,1);
scatter(ZnA,ZnB,'black','filled');
```

```
hold on;
plot(x,YZn1,'black');
pbaspect([1 1 1]);
xlim([0 inf]);ylim([0 inf]);
xlabel('Chimney Zn Conc. (kg/T)');
ylabel('Core Lu Conc. (kg/T)');
subplot(1,2,2);
scatter(ZnC,ZnB,'black','filled');
hold on;
plot(x,YZn2,'black');
pbaspect([1 1 1]);
xlim([0 inf]);ylim([0 inf]);
hold off;
xlabel('Surface Zn Conc. (kg/T)');
```

Included Documents:

Graphrelchimn.xlsx

Analysis3D.xlsx

Excel_Database.xlsx